Preclinical models and IgA anti-GD2 antibody therapy for neuroblastoma

Marjolein Stip

Preclinical models and IgA anti-GD2 antibody therapy for neuroblastoma
Thesis with a summary in Dutch, Utrecht University

ISBN: 978-94-6483-964-7
DOI: https://doi.org/10.33540/2289

Research in this thesis was financially supported by the Villa Joep foundation
Printing of this thesis was financially supported by the UMC Utrecht & Infection and Immunity Utrecht.

Cover design, layout and printing by Ridderprint | www.ridderprint.nl

Preclinical models and IgA anti-GD2 antibody therapy for neuroblastoma

Preklinische modellen en IgA anti-GD2 antistoftherapie voor neuroblastoom
(met een samenvatting in het Nederlands)

Proefschrift

ter verkrijging van de graad van doctor aan de
Universiteit Utrecht
op gezag van de
rector magnificus, prof. dr. H.R.B.M. Kummeling,
ingevolge het besluit van het college voor promoties
in het openbaar te verdedigen op

woensdag 12 juni 2024 des middags te 12.15 uur

door

Maria Cornelia Stip

geboren op 28 juli 1994
te Sliedrecht

Promotor:

Prof. dr. J.H.W. Leusen

Copromotor:

Dr. F.A.G. Meyer-Wentrup

Beoordelingscommissie:

Prof. dr. R.R. de Krijger
Prof. dr. J.J. Molenaar (voorzitter)
Dr. G.A.M. Tytgat
Prof. dr. G. Vidarsson
Prof. dr. K.E. de Visser

TABLE OF CONTENTS

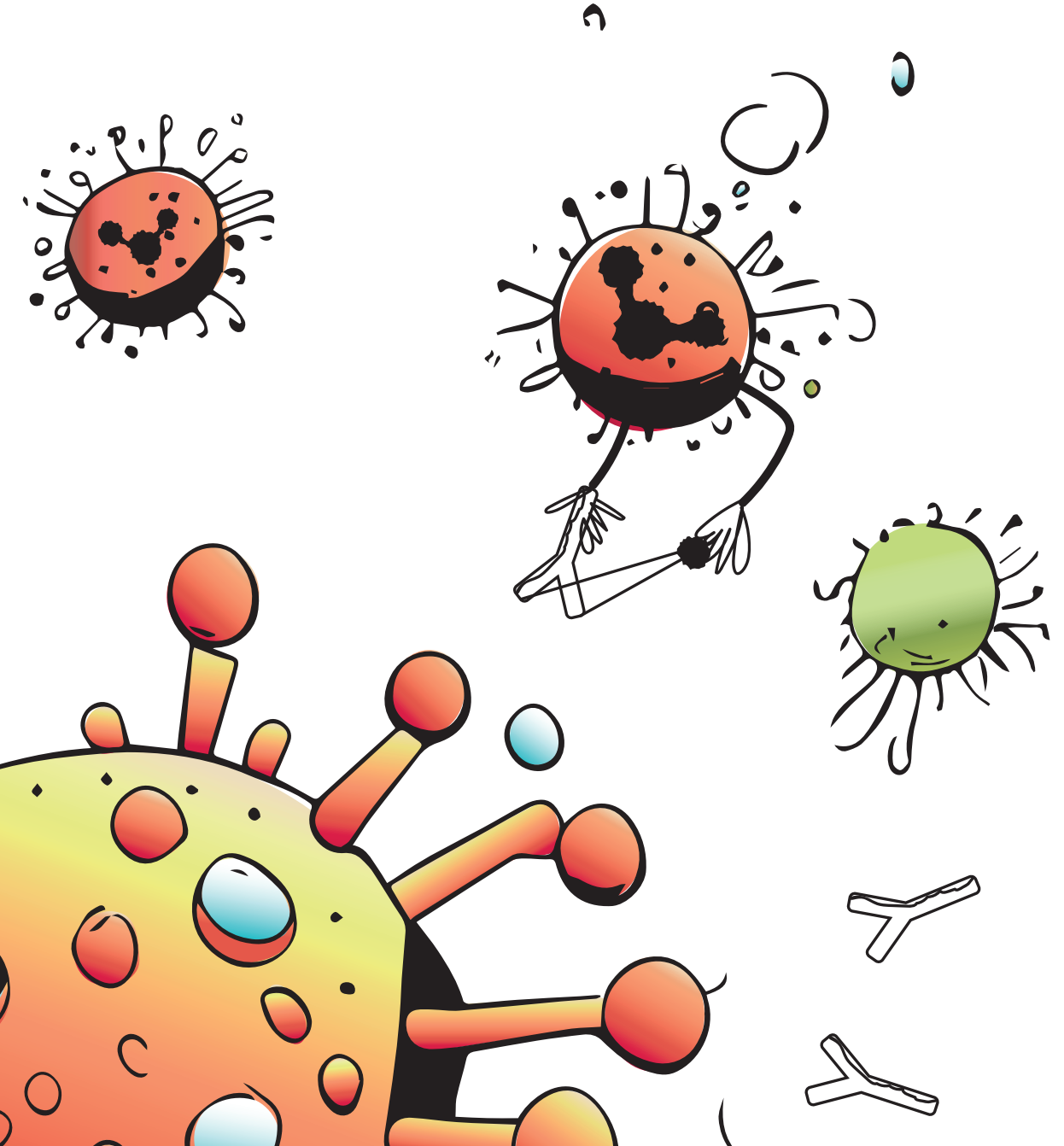

Chapter 1.

Introduction

NEUROBLASTOMA

Neuroblastoma is one of the most common tumors in children and responsible for about 15% of pediatric cancer deaths. Despite the preposition *neuro*, this tumor does not originate in the brain, but in the sympathoadrenal lineage of neural crest cells during embryonal development[1]. Hence, primary tumors often present in the adrenal gland or in the sympathetic neural ganglia in the abdomen. Other common tumor sites include the neck, thorax and pelvis. In Europe, risk stratification is currently based on the International Neuroblastoma Risk Group (INRG) classification system, in which patients can be classified as very low-, low-, intermediate- or high-risk. In this system, the risk group is determined by the age at diagnosis, tumor histology (grade), the presence of *MYCN* amplification or chromosome 11q aberrations and DNA ploidy[2]. In low-risk patients, tumors can regress spontaneously and otherwise surgery alone is often curative[3,4]. However, up to 50% of neuroblastoma patients presents with high-risk disease, for which the 5-year survival rate is only 45%[5].

High-risk neuroblastoma patients first receive induction therapy, composed of chemotherapy and surgery of the primary tumor. Subsequently, patients receive high-dose chemotherapy (COJEC protocol) in combination with tandem autologous stem cell transplantation and radiotherapy as consolidation therapy[6,7]. Since 2015, high-risk patients receive anti-disialoganglioside (GD2) antibody immunotherapy as maintenance therapy, which has increased event-free and overall survival of high-risk neuroblastoma patients significantly[8,9]. Anti-GD2 antibodies mainly exert their efficacy by inducing tumor cell killing by natural killer (NK) cells, macrophages and neutrophils. Anti-GD2 antibody therapy is combined with *13-cis* retinoic acid (isotretinoin) to differentiate tumor cells rendering them more susceptible to antibody therapy. In North America, therapy is further supplemented by granulocyte-macrophage colony-stimulating factor (GM-CSF), but not in Europe and other parts of the world, due to limited availability. GM-CSF increases numbers of myeloid cells, such as neutrophils, monocytes, and eosinophils and stimulates neutrophil-mediated antigen-dependent cellular cytotoxicity (ADCC) against tumor cells[10]. Although efficient, anti-GD2 antibody therapy induces severe, dose-limiting neuropathic pain, which is at least partially evoked through complement activation on GD2-expressing sensory neurons[11,12]. The introduction of long-term infusion strategies reduced this toxicity, but still 37.7% of the patients experience grade ≥3 neuropathic pain[13].

Currently, two anti-GD2 antibodies are clinically approved: dinutuximab (beta) and naxitamab[14,15]. Dinutuximab (ch14.18) was the first anti-GD2 antibody receiving clinical approval and is a chimeric IgG1 antibody. Naxitamab is a humanized version of the murine 3F8 antibody and is of the IgG1 isotype as well. A third antibody, hu14.18K322A is based on dinutuximab and is currently in phase II clinical trials[16]. This antibody is a humanized version of ch14.18 and additionally contains the K322A mutation, which reduces complement

activation. Though these anti-GD2 formats have never been compared, they appear to be similar in therapeutic efficacy.

High-risk neuroblastoma cells orchestrate a complex immunosuppressive microenvironment, which is maintained by regulatory T cells and immunosuppressive myeloid cells, such as tumor- associated macrophages (TAM) and myeloid-derived suppressor cells (MDSC). These immunosuppressive cells and their cytokines prevent elimination of tumor cells by the immune system and hamper the development and efficacy of novel T cell-based immunotherapies, such as checkpoint inhibitors and chimeric antigen receptor (CAR) T cells. The tumor microenvironment of neuroblastoma is further described in **Chapter 4**, with a special focus on the role of myeloid cells in development of neuroblastoma as well as in immunotherapy.

ANTIBODY IMMUNOTHERAPY

Nowadays, antibody immunotherapy is an important pillar of anti-cancer treatment. Antibodies are composed of 2 heavy chains (HC) and 2 kappa or lambda light chains (LC). The *N*-terminal end of the HC and LC form the antigen binding fragment (Fab), mediating antigen recognition and the *C*-terminal or constant part of the HC forms the crystallizable fragment (Fc), mediating effector function by binding Fc receptors.

To obtain monoclonal, target-specific antibodies, for example against GD2, George Köhler and César Milstein developed the hybridoma technology[17]. Using this method, mice are immunized with the target of interest to generate antigen-specific B cells, which are then fused with myeloma cells to generate hybridomas. These hybridomas are cloned and selected for the desired antibody. However, soon it was discovered that the murine antibodies isolated from these hybridomas elicit human anti-mouse antibodies (HAMAs), which neutralized the monoclonal antibodies, limiting their therapeutic efficacy[18]. From then on, antibodies were 'chimerized' by combining a murine Fab domain with a human constant domain and this paved the way for the first successful antibody therapy in cancer: rituximab[19]. Dinutuximab is another example of a chimerized antibody, composed of the variable domain from the murine 14.G2a clone and a human IgG1 constant domain. Currently, the variable domain of antibodies is usually humanized, reducing immunogenicity even more. Humanizing antibodies can be done by substituting immunogenic sequences in the Fab part by human sequences, based on *in silico* prediction methods[20]. Naxitamab and hu14.18K322A are both humanized antibodies, based on the murine 3F8 and 14.G2a clones respectively.

Antibodies are classified into 5 isotypes (IgM, IgD, IgG, IgE and IgA), which all have their specific role in the humoral immune response and follow each other up during class switching in B cells[21]. However, thus far only IgG antibody therapeutics have been applied

in the clinic, since they have a comprehensive set of effector functions, a long half-life (due to recycling by the neonatal Fc receptor (FcRn)) and a simple glycosylation profile. There are four IgG isotypes (IgG1, IgG2, IgG3 and IgG4), which all have different affinities for activating, inhibiting and decoy Fc gamma receptors (FcγRs) (**Table 1**). All four IgG isotypes have been employed as antibody therapy, but they can have completely different modes of action, partially due to their difference in affinity for the different FcγRs. The currently approved anti-GD2 antibodies are of the IgG1 isotype and therefore efficacy is mostly based on inducing antigen-dependent cellular cytotoxicity (ADCC) against tumor cells by effector cells upon engagement of activating FcγRs[14]. IgG3 antibodies have similar effector functions, since their affinity for FcγRs is comparable to IgG1. While IgG1 and IgG3 mostly rely on Fc-mediated effects, the efficacy IgG2 and IgG4 is mostly based on Fab-mediated effects, due to a lower affinity for FcγRs. Therefore, these isotypes are generally used when blocking/neutralizing antibodies or agonists are desired, examples of which are the anti-PD1 checkpoint inhibitor nivolumab[22] or anti-CD40 agonists, respectively[23]. However, recently it was discovered that anti-GD2 antibodies have an important Fab-mediated effect as well, since they block the interaction between GD2 and Siglec 7, a myeloid immune checkpoint axis[24].

	IgG receptors						IgA receptor
Structure							
Name	**FcγRI** CD64	**FcγRIIa** CD32a	**FcγRIIb** CD32b	**FcγRIIc** CD32c	**FcγRIIIa** CD16a	**FcγRIIIb** CD16b	**FcαRI** CD89
Affinity	High	Low-Medium	Low-Medium	Low-Medium	Low-Medium	Low-Medium	High
Affinity per isotype	IgG1=IgG3 > IgG4	IgG1>IgG3> IgG2=IgG4	IgG1=IgG3 =IgG4>IgG2	IgG1=IgG3 =IgG4>IgG2	IgG3>IgG1> IgG4=IgG2	IgG3>IgG1	IgA1 = IgA2
Function	Activating	Activating	Inhibitory	Activating	Activating	No signaling	Activating

Table 1 | Human Fc alpha and gamma receptors, their affinity for antibody isotypes and their function[29,47,48]. Activating and inhibiting Fc receptors signal through immunoreceptor tyrosine-based activation and inhibition motifs (ITAM and ITIM), respectively. The motif can be located on the cytoplasmic tail of the ligand binding α-chain (FcγRIIa, b and c) or on the associated FcR γ-chain (FcγRI, FcγRIIIa and FcαRI). FcγRIIIb does not convey intracellular signaling. Created with BioRender.com.

IgG isotypes do not only differ in FcγR affinity, but in their ability to induce complement-dependent cytotoxicity (CDC) as well. IgG1 and IgG3 can efficiently trigger the classical complement pathway via the C1q-binding domain in the Fc part of the antibody, but IgG2 and IgG4 barely activate the complement system[25,26]. In accordance with this, dinutuximab and naxitamab can induce complement-mediated lysis of neuroblastoma cells. However, this effector mechanism appears less important than ADCC, since the K322A mutation reducing C1q-binding present in the hu14.18K322A antibody does not compromise

therapeutic efficacy in patients[27]. Unfortunately, though the K322A mutation decreased the induction of pain in rats[11], it still induced grade 3-4 neuropathic pain in 68% of patients, which was dose-limiting in 11% of patients[28]. Hence, it is still not completely clear how exactly anti-GD2 antibodies induce neuropathic pain. Current hypotheses are that the K322A mutation is only partially inhibiting complement deposition, that neuropathic pain is induced by other complement pathways or that it is not induced by complement at all. Besides the induction of this severe side effect, there are other limitations to IgG anti-GD2 antibody therapy. Even though the introduction of IgG anti-GD2 antibody therapy was a big leap forward in the treatment of high-risk neuroblastoma, still 50% of the patients will eventually relapse and succumb to the disease. IgG antibodies mostly engage NK cells and macrophages, but other myeloid cells such as neutrophils, as well as immune cells from the adaptive immune system are not fully activated against the tumor by IgG. This lack of efficacy of IgG anti-GD2 antibodies can further be explained by the fact that IgG does not only bind to activating FcγRs, but to the inhibiting (FcγRIIb) and decoy (FcγRIIIb) receptors as well (**Table 1**), which is known to limit therapeutic efficacy[29]. To improve this and prevent neuropathic pain induced by IgG anti-GD2 antibody therapy, we developed anti-GD2 antibody therapy of the IgA isotype (described in **Chapter 5-7**). We expected IgA anti-GD2 therapy to 1) not induce complement-mediated pain, 2) to directly activate neutrophils and 3) to only bind to an activating Fc receptor: the Fc alpha receptor I (FcαRI or CD89).

IGA ANTIBODY THERAPY

Whereas monomeric IgG antibodies are most prevalent in serum, IgA antibodies are most abundant at mucosal surfaces, where they form dimeric and polymeric complexes through interaction with the joining chain[30]. In the circulation, IgA is mostly present as a monomeric antibody and has the second highest serum concentration of all isotypes. For the development of IgA antibody therapy, we have focused on monomeric IgA, which will more easily distribute through the body and penetrate the tumor due to the lower molecular weight. Two isotypes exist for human IgA - IgA1 and IgA2 - with three possible allotypes for IgA2 (IgA2m(1), IgA2m(2), and IgA2n)[31,32]. IgA1 and IgA2 molecules contain 2 and 4–5 *N*-glycosylation sites respectively, whereas IgG1 only has one[33]. Additionally, IgA1 is *O*-glycosylated in the hinge region - a trait associated with Berger's disease - making IgA2 the superior candidate for application in antibody therapy.

Fc-mediated effects of IgA antibody therapy are initiated by the activating FcαRI, which is expressed exclusively on myeloid cells. Neutrophils and macrophages are the most important effector cells for IgA antibody therapy, but the FcαRI is also expressed (or inducible) on eosinophils, monocytes, subsets of dendritic cells (DCs) and Kupffer cells[34,35].

Upon antigen binding, IgA can crosslink the FcαRI and trigger specific effector functions in myeloid cells, such as ADCC, phagocytosis, antigen presentation and neutrophil extracellular trap (NET) formation[36–38]. IgA lacks the C1q-binding domain required for activation of the classical complement pathway by IgG antibodies, which led us to hypothesize that IgA anti-GD2 antibodies would not induce neuropathic pain (see **Chapter 5**).

However, clinical application of IgA antibody therapy has been hampered by several properties of the IgA format. First of all, the heavy glycosylation of IgA renders the molecule susceptible to degradation by the asialoglycoprotein (ASGPR) and mannose receptors, thus limiting its half-life[39,40]. Additionally, the presence of extensive glycosylation would introduce large batch-to-batch variation in future clinical batches. Finally, the purification of heavily glycosylated IgA antibodies is difficult, due to the formation of aggregates and the need to perform size-exclusion chromatography as an additional step to obtain pure monomeric IgA. These three problems were already partially solved in the past by the introduction of several mutations in the so-called IgA2.0 molecule, as developed by the research group of Thomas Valerius[41]. In this thesis we will build further upon this format with IgA3.0, which among others eliminates 3 out of 4 glycosylation sites and introduces stabilizing bonds between HC and LC (described in detail in **Chapter 6**). Finally, it has been difficult to study IgA antibody therapy *in vivo*, since mice do not naturally express a homolog of human FcαRI[42]. Hence, several FcαRI transgenic mice were generated in the past, among others the model used in this thesis, which was generated by transducing the endogenous human promoter and regulatory elements along with the sequence encoding human FcαRI[43].

THESIS OUTLINE

Before focusing on the development of IgA anti-GD2 antibody therapy for neuroblastoma in *part II*, we describe two important *in vivo* tools required for these studies in *part I*. In **Chapter 2** we describe the development and characteristics of human CD89 (hCD89) transgenic mice that we use for *in vivo* studies. We localized the integration site of the hCD89 transgene and compared the immune cell composition and phenotype of wildtype and hCD89 transgenic mice. Thereafter, we compared IgA/CD89-mediated ADCC capacity of myeloid cells derived from several mouse strains and studied CD89 expression in tumor models. In **Chapter 3** we develop a novel method for long-term neutrophil depletion, in order to use this later to study the mechanism of action of IgA anti-GD2 antibody therapy. Before, rat anti-Ly-6G or rat anti-Gr-1 depleting antibodies were frequently used to deplete neutrophils, but these approaches are limited by efficacy problems, among others by depleting neutrophils only partially or transiently, or by lacking specificity for neutrophils

only[44,45]. Therefore, we designed a depletion strategy using a murinized anti-Ly-6G (clone 1A8) antibody, which efficiently and specifically depleted neutrophils in all mouse strains studied.

In *part II* of this thesis, the stage is set for IgA antibody therapy in neuroblastoma. **Chapter 4** first describes the tumor microenvironment of neuroblastoma extensively, especially focusing on the role of myeloid cells. In the second part of this chapter, we summarize currently existing strategies to engage, deplete or reprogram myeloid cells in neuroblastoma. In **Chapter 5**, we switch the isotype of the anti-GD2 antibody dinutuximab to IgA1. This chapter first describes the production and purification of IgA anti-GD2, the assessment of GD2 binding and the mechanism of action of IgA anti-GD2. Next, complement deposition and the induction of neuropathic pain by IgG1 and IgA anti-GD2 antibodies are compared. **Chapter 6** delineates the preclinical development of IgA anti-GD2 antibody therapy and the engineering of IgA3.0. Characteristics of this format, such as thermostability, glycosylation pattern and half-life are investigated and efficacy is evaluated using immune cells from cynomolgus monkeys and patients as well as in long-term *in vivo* neuroblastoma models. In **Chapter 7** we investigate the additional effect of blocking CD47, known as the 'don't eat me' signal, on the efficacy of IgA3.0 anti-GD2 antibody therapy in neuroblastoma. CD47 is often overexpressed in neuroblastoma and can bind to signal regulatory protein alpha (SIRPα), a myeloid immune checkpoint, thereby inhibiting myeloid cell-mediated tumor killing[46]. **Chapter 8** summarizes the most important findings in this thesis and places these in the perspective of the current literature in the field of neuroblastoma and antibody therapy.

REFERENCES

1. Preter, K. De *et al.* Human fetal neuroblast and neuroblastoma transcriptome analysis confirms neuroblast origin and highlights neuroblastoma candidate genes. *Genome Biol.* **7**, R84-r84. (2006).

2. Cohn, S. L. *et al.* The International Neuroblastoma Risk Group (INRG) classification system: an INRG Task Force report. *J. Clin. Oncol. Off. J. Am. Soc. Clin. Oncol.* **27**, 289–297 (2009).

3. De Bernardi, B. *et al.* Treatment of localised resectable neuroblastoma. Results of the LNESG1 study by the SIOP Europe Neuroblastoma Group. *Br. J. Cancer* **99**, 1027–1033 (2008).

4. Strother, D. R. *et al.* Outcome after surgery alone or with restricted use of chemotherapy for patients with low-risk neuroblastoma: results of Children's Oncology Group study P9641. *J. Clin. Oncol. Off. J. Am. Soc. Clin. Oncol.* **30**, 1842–1848 (2012).

5. Neuroblastoma - Childhood: Statistics. vol. 2020 (2019).

6. Maris, J. M. Recent advances in neuroblastoma. *N. Engl. J. Med.* **362**, 2202–2211 (2010).

7. Park, J. R. *et al.* Effect of Tandem Autologous Stem Cell Transplant vs Single Transplant on Event-Free Survival in Patients With High-Risk Neuroblastoma: A Randomized Clinical Trial. *JAMA* **322**, 746–755 (2019).

8. Yu, A. L. *et al.* Anti-GD2 antibody with GM-CSF, interleukin-2, and isotretinoin for neuroblastoma. *N. Engl. J. Med.* **363**, 1324–1334 (2010).

9. Cheung, N. K. *et al.* Murine anti-GD2 monoclonal antibody 3F8 combined with granulocyte-macrophage colony-stimulating factor and 13-cis-retinoic acid in high-risk patients with stage 4 neuroblastoma in first remission. *J. Clin. Oncol.* **30**, 3264–3270 (2012).

10. Cheung, N. K. *et al.* Key role for myeloid cells: phase II results of anti-G(D2) antibody 3F8 plus granulocyte-macrophage colony-stimulating factor for chemoresistant osteomedullary neuroblastoma. *Int. J. cancer* **135**, 2199–2205 (2014).

11. Sorkin, L. S. *et al.* Anti-GD(2) with an FC point mutation reduces complement fixation and decreases antibody-induced allodynia. *Cancer Res.* **149**, 362–367 (2010).

12. Evers, M. *et al.* Anti-GD2 IgA kills tumors by neutrophils without antibody-associated pain in the preclinical treatment of high-risk neuroblastoma. *J. Immunother. cancer* **9**, (2021).

13. Mueller, I. *et al.* Tolerability, response and outcome of high-risk neuroblastoma patients treated with long-term infusion of anti-GD(2) antibody ch14.18/CHO. *MAbs* **10**, 55–61 (2018).

14. Sait, S. & Modak, S. Anti-GD2 immunotherapy for neuroblastoma. *Expert Rev. Anticancer Ther.* **17**, 889–904 (2017).

15. Chan, G. C.-F. & Chan, C. M. Anti-GD2 Directed Immunotherapy for High-Risk and Metastatic Neuroblastoma. *Biomolecules* **12**, (2022).

16. Furman, W. L. *et al.* Improved Outcome in Children With Newly Diagnosed High-Risk Neuroblastoma Treated With Chemoimmunotherapy: Updated Results of a Phase II Study Using hu14.18K322A. *J. Clin. Oncol. Off. J. Am. Soc. Clin. Oncol.* **40**, 335–344 (2022).

17. Köhler, G. & Milstein, C. Continuous cultures of fused cells secreting antibody of predefined specificity. *Nature* **256**, 495–497 (1975).

18. Tjandra, J. J., Ramadi, L. & McKenzie, I. F. Development of human anti-murine antibody (HAMA) response in patients. *Immunol. Cell Biol.* **68 (Pt 6)**, 367–376 (1990).

19. Maloney, D. G. *et al.* IDEC-C2B8 (Rituximab) anti-CD20 monoclonal antibody therapy in patients with relapsed low-grade non-Hodgkin's lymphoma. *Blood* **90**, 2188–2195 (1997).

20. Kurella, V. B. & Gali, R. Antibody Design and Humanization via In Silico Modeling. *Methods Mol. Biol.* **1827**, 3–14 (2018).

21. Spiegelberg, H. L. Biological role of different antibody classes. *Int. Arch. Allergy Appl. Immunol.* **90 Suppl 1**, 22–27 (1989).

22. Wang, C. *et al.* In vitro characterization of the anti-PD-1 antibody nivolumab, BMS-936558, and in vivo toxicology in non-human primates. *Cancer Immunol. Res.* **2**, 846–856 (2014).

23. White, A. L. *et al.* Conformation of the human immunoglobulin G2 hinge imparts superagonistic properties to immunostimulatory anticancer antibodies. *Cancer Cell* **27**, 138–148 (2015).

24. Theruvath, J. *et al.* Anti-GD2 synergizes with CD47 blockade to mediate tumor eradication. *Nat. Med.* **28**, 333–344 (2022).

25. Vidarsson, G., Dekkers, G. & Rispens, T. IgG subclasses and allotypes: from structure to effector functions. *Front. Immunol.* **5**, 520 (2014).

26. Bindon, C. I., Hale, G., Brüggemann, M. & Waldmann, H. Human monoclonal IgG isotypes differ in complement activating function at the level of C4 as well as C1q. *J. Exp. Med.* **168**, 127–142 (1988).

27. Furman, W. L. *et al.* A Phase II Trial of Hu14.18K322A in Combination with Induction Chemotherapy in Children with Newly Diagnosed High-Risk Neuroblastoma. *Clin. cancer Res. an Off. J. Am. Assoc. Cancer Res.* **25**, 6320–6328 (2019).

28. Navid, F. *et al.* Phase I trial of a novel anti-GD2 monoclonal antibody, hu14.18K322A, designed to decrease toxicity in children with refractory or recurrent neuroblastoma. *J. Clin. Oncol.* **32**, 1445–1452 (2014).

29. Treffers, L. W. *et al.* FcγRIIIb Restricts Antibody-Dependent Destruction of Cancer Cells by Human Neutrophils. *Front. Immunol.* **9**, 3124 (2018).

30. Gutzeit, C., Magri, G. & Cerutti, A. Intestinal IgA production and its role in host-microbe interaction. *Immunol. Rev.* **260**, 76–85 (2014).

31. Tsuzukida, Y., Wang, C. C. & Putnam, F. W. Structure of the A2m(1) allotype of human IgA--a recombinant molecule. *Proc. Natl. Acad. Sci. U. S. A.* **76**, 1104–1108 (1979).

32. Chintalacharuvu, K. R., Raines, M. & Morrison, S. L. Divergence of human alpha-chain constant region gene sequences. A novel recombinant alpha 2 gene. *J. Immunol.* **152**, 5299–5304 (1994).

33. Mattu, T. S. *et al.* The glycosylation and structure of human serum IgA1, Fab, and Fc regions and the role of N-glycosylation on Fcα receptor interactions. *J. Biol. Chem.* **273**, 2260–2272 (1998).

34. Monteiro, R. C. & Van De Winkel, J. G. J. IgA Fc receptors. *Annu. Rev. Immunol.* **21**, 177–204 (2003).

35. van Egmond, M. *et al.* FcalphaRI-positive liver Kupffer cells: reappraisal of the function of immunoglobulin A in immunity. *Nat. Med.* **6**, 680–685 (2000).

36. Lowell, G. H., Smith, L. F., Griffiss, J. M. & Brandt, B. L. IgA-dependent, monocyte-mediated, antibacterial activity. *J. Exp. Med.* **152**, 452–457 (1980).

37. Shen, L. *et al.* Presentation of ovalbumin internalized via the immunoglobulin-A Fc receptor is enhanced through Fc receptor gamma-chain signaling. *Blood* **97**, 205–213 (2001).

38. Gimpel, A.-K. *et al.* IgA Complexes Induce Neutrophil Extracellular Trap Formation More Potently Than IgG Complexes. *Front. Immunol.* **12**, 761816 (2021).

39. Boross, P. *et al.* IgA EGFR antibodies mediate tumour killing in vivo. 1213–1226 (2013) doi:10.1002/emmm.201201929.

40. Goetze, A. M. *et al.* High-mannose glycans on the Fc region of therapeutic IgG antibodies increase serum clearance in humans. *Glycobiology* **21**, 949–959 (2011).

41. Lohse, S. *et al.* An Anti-EGFR IgA That Displays Improved Pharmacokinetics and Myeloid Effector Cell Engagement In Vivo. *Cancer Res.* **76**, 403–417 (2016).

42. Abi-Rached, L., Dorighi, K., Norman, P. J., Yawata, M. & Parham, P. Episodes of natural selection shaped the interactions of IgA-Fc with FcalphaRI and bacterial decoy proteins. *J. Immunol.* **178**, 7943–7954 (2007).

43. van Egmond, M. *et al.* Human immunoglobulin A receptor (FcalphaRI, CD89) function in transgenic mice requires both FcR gamma chain and CR3 (CD11b/CD18). *Blood* **93**, 4387–4394 (1999).

44. Fleming, T. J., Fleming, M. L. & Malek, T. R. Selective expression of Ly-6G on myeloid lineage cells in mouse bone marrow. RB6-8C5 mAb to granulocyte-differentiation antigen (Gr-1) detects members of the Ly-6 family. *J. Immunol.* **151**, 2399–2408 (1993).

45. Moses, K. *et al.* Survival of residual neutrophils and accelerated myelopoiesis limit the efficacy of antibody-mediated depletion of Ly-6G+ cells in tumor-bearing mice. *J. Leukoc. Biol.* **99**, 811–823 (2016).

46. Martínez-Sanz, P. *et al.* CD47-SIRPα Checkpoint Inhibition Enhances Neutrophil-Mediated Killing of Dinutuximab-Opsonized Neuroblastoma Cells. *Cancers (Basel).* **13**, (2021).

47. Nimmerjahn, F. & Ravetch, J. V. Fcgamma receptors as regulators of immune responses. *Nat. Rev. Immunol.* **8**, 34–47 (2008).

48. Patel, K. R., Roberts, J. T. & Barb, A. W. Multiple Variables at the Leukocyte Cell Surface Impact Fc γ Receptor-Dependent Mechanisms. *Front. Immunol.* **10**, 223 (2019).

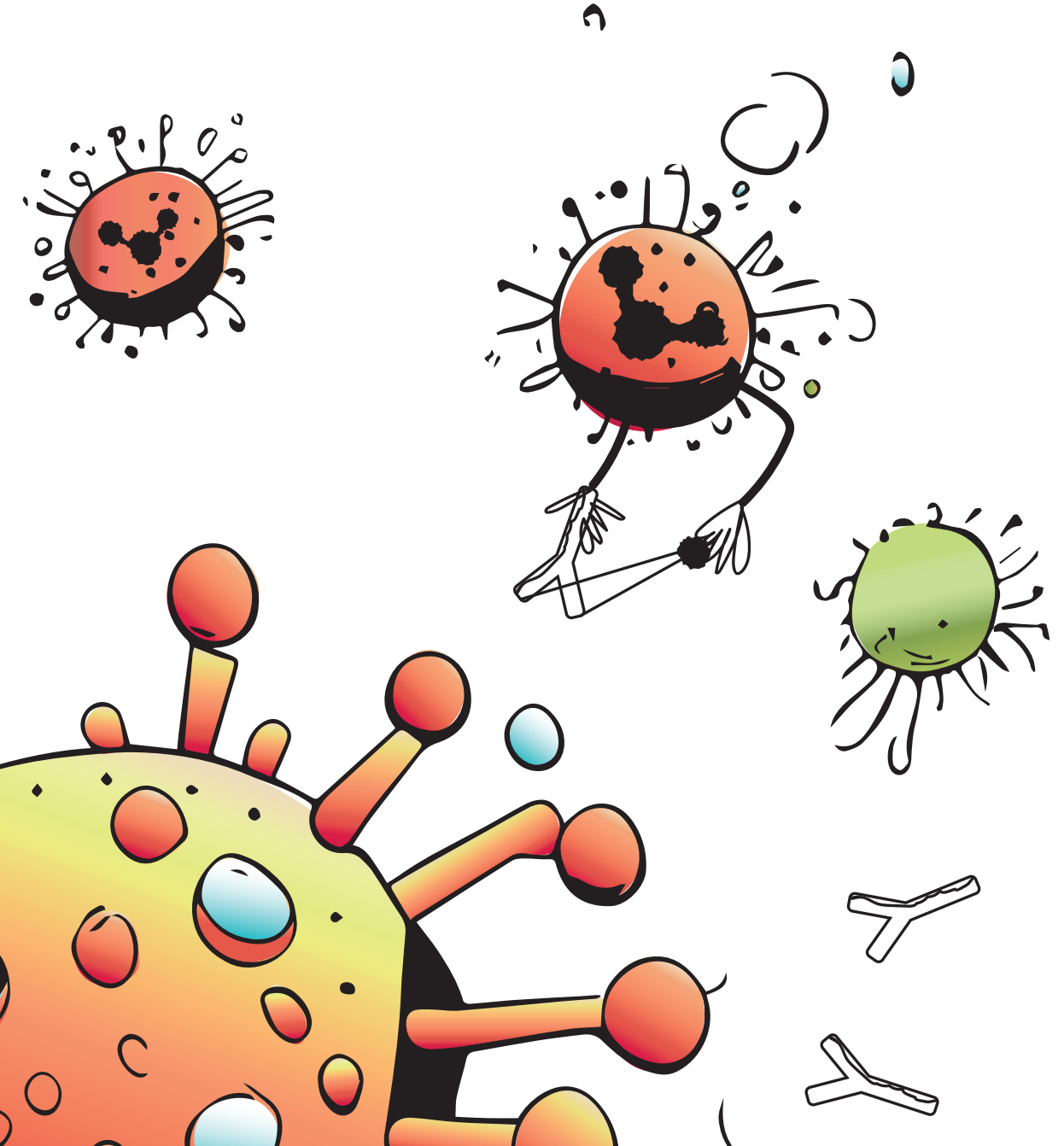

PART I

Developing mouse models to study IgA antibody therapy

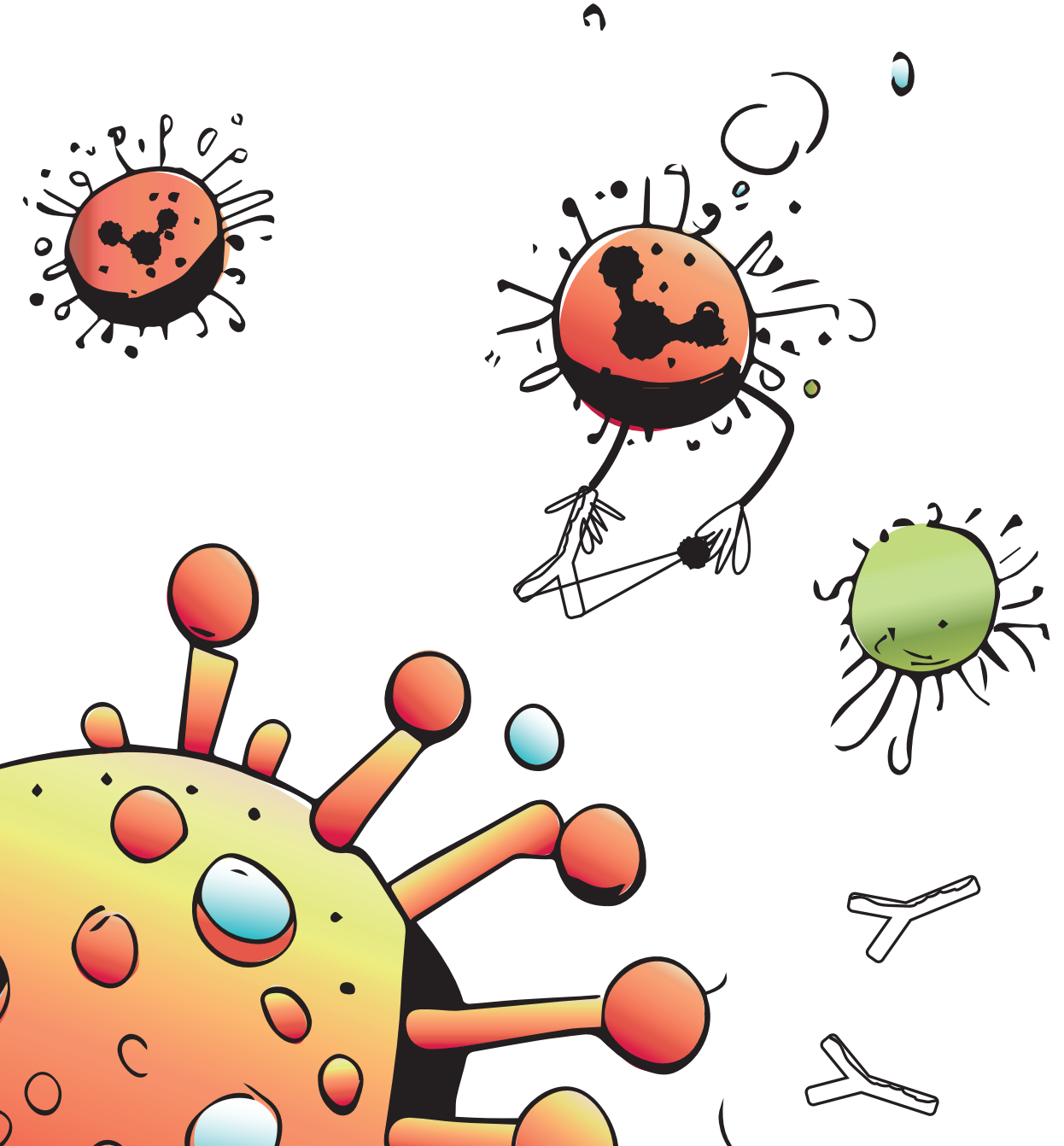

Chapter 2.

Characterization of human Fc alpha receptor transgenic mice: comparison of CD89 expression and antibody-dependent tumor killing between mouse strains

Marjolein C. Stip[1], J.H. Marco Jansen[1], Maaike Nederend[1], Maria Tsioumpekou[1], Mitchell Evers[1], Patricia A. Olofsen[1], Friederike Meyer-Wentrup[2], Jeanette H.W. Leusen[1]

Affiliations

1. Center for Translational Immunology, UMC Utrecht, Heidelberglaan 100, 3584 CX Utrecht, The Netherlands.
2. Princess Máxima Center for Pediatric Oncology, Heidelberglaan 25, 3584 CS Utrecht, The Netherlands.

Published in Cancer Immunology Immunotherapy, 2023

ABSTRACT

Since mice do not express a homologue of the human Fc alpha receptor (FcαRI or CD89), a transgenic mouse model was generated in four different backgrounds (C57BL/6, BALB/c, SCID and NXG) expressing the FcαRI under the endogenous human promoter. In this study, we describe previously unknown characteristics of this model, such as the integration site of the *FCAR* gene, the CD89 expression pattern in healthy male and female mice and in tumor-bearing mice, expression of myeloid activation markers and FcγRs and IgA/CD89-mediated tumor killing capacity. In all mouse strains, CD89 expression is highest in neutrophils, intermediate on other myeloid cells such as eosinophils and DC subsets and inducible on, among others, monocytes, macrophages and Kupffer cells. CD89 expression levels are highest in BALB/c and SCID, lower in C57BL/6 and lowest in NXG mice. Additionally, CD89 expression on myeloid cells is increased in tumor-bearing mice across all mouse strains. Using Targeted Locus Amplification, we determined that the hCD89 transgene has integrated in chromosome 4. Furthermore, we established that wildtype and hCD89 transgenic mice have a similar composition and phenotype of immune cells. Finally, IgA-mediated killing of tumor cells is most potent with neutrophils from BALB/c and C57BL/6 and less with neutrophils from SCID and NXG mice. However, when effector cells from whole blood are used, SCID and BALB/c are most efficient, since these strains have a much higher number of neutrophils. Overall, hCD89 transgenic mice provide a very powerful model to test the efficacy of IgA immunotherapy against infectious diseases and cancer.

Keywords

Fc alpha receptor, Immunoglobulin A, Neutrophils, Genetically engineered mouse model, Immunotherapy

INTRODUCTION

During the last two decades, interest in IgA antibodies and their receptor—the Fc alpha receptor I (FcαRI) or CD89—has increased significantly. Initially, most antibody research was devoted to the four IgG isotypes and their Fc gamma receptors (FcγRs) and currently IgG is still the only isotype used in antibodies for therapeutic applications. However, lately many studies have highlighted the potential of IgA/FcαRI immunotherapy as a treatment for both infectious diseases[1,2] and cancer[3–6] (reviewed in[7,8]).

The FcαRI is a member of the immunoglobulin (Ig) gene superfamily, but has only 20% homology to other Fc receptors and in contrast to all other Fc receptor genes, it is not located on chromosome 1 (1q23.3)[9]. The *FCAR* gene encoding FcαRI is located

on chromosome 19 (19q13.4) and its promoter is positioned between 59 and 197 bp downstream of the major transcription start site[10,11]. FcαRI is expressed exclusively on myeloid cells, such as neutrophils, eosinophils, monocytes, macrophages and subsets of dendritic cells (DCs)[12] and can be induced on Kupffer cells as well[13]. Monomeric IgA in complex with antigen or IgA-opsonized target cells can crosslink FcαRI and trigger specific effector functions in myeloid cells, such as antibody-dependent cellular cytotoxicity (ADCC) or phagocytosis (ADCP), antigen presentation and neutrophil extracellular trap (NET) formation[14–16]. In many other species, such as rats and chimpanzees, a homologue of the human FcαRI was found, but not in mice and canines[17–19]. The expression of IgA is different among species as well. Humans and primates express two isotypes, IgA1 and IgA2, and most other mammals (including mice) have only one isotype[20]. Rabbits have the most complex IgA system with up to 15 IgA isotypes[21–23].

Though mice express IgA, they do not express an FcαRI. The FcαRI was lost during evolution in mice due to competition with bacterial decoy proteins for IgA[24,25]. The absence of a mouse equivalent of human FcαRI has hampered research exploring the potential of IgA immunotherapy *in vivo*. To study IgA immunotherapy *in vivo*, several genetic mouse models have been generated to establish expression of human FcαRI in mice. The group of Jianmin Fang developed human CD89 (hCD89) transgenic mice under the murine CD14 promoter, thereby achieving CD89 expression in monocytes, but not in other myeloid cells[26]. Though this model was suitable to answer their research question, it does not reflect the human situation, where other myeloid cell subsets express CD89 as well. The group of Renato Monteiro described a transgenic model with hCD89 under the mouse CD11b promoter, while the group of Adrian Zuercher developed a model using the cre-lox system to insert hCD89 under the mouse Lysozyme M (LysM) promoter[27,28]. These models are more representative of the human CD89 expression pattern, as CD89 expression is present in multiple myeloid subsets. Additionally, in the model of Adrian Zuercher CD89 expression was highest in neutrophils and low in monocytes, corresponding to both the human and non-human primate expression pattern[27]. However, CD89 expression in murine eosinophils was absent, while it is present on human eosinophils. Finally, a hCD89 transgenic mouse model was developed in the lab of Jan van de Winkel, in which the endogenous human promoter and regulatory elements were transduced along with the sequence encoding hCD89[29,30]. The hCD89 promoter is regulated by the highly conserved transcription factors C/EBPα and Ets protein family members[31], which are widely expressed in mice as well. Therefore, this model was expected to result in a CD89 expression pattern more similar to the one found in humans.

Research using this human promoter-regulated CD89 transgenic mouse model has indeed established that CD89 expression in this model is very similar to the human pattern. First, it was confirmed that CD89 expression was present in neutrophils and subsets of monocytes and DCs, but also in activated Kupffer cells[13,30,32]. Interestingly, CD89 could be upregulated

in neutrophils and macrophages by cytokines such as GM-CSF and TNF-α, which are known to upregulate CD89 expression in human myeloid cells as well. Additionally, hCD89 transgenic mouse neutrophils and macrophages were able to perform phagocytosis and ADCC mediated by IgA and the FcαRI[4]. Many other—sometimes new—characteristics and mechanisms of IgA and the FcαRI were uncovered in these mice, such as an increase in intracellular free calcium levels upon FcαRI crosslinking and the requirement of Mac-1 (CD11b in complex with CD18) for secretory IgA binding to FcαRI[33,34]. Finally, the *in vivo* efficacy of IgA immunotherapy has been established for multiple tumor models in hCD89 transgenic mice, for example by targeting EGFR in intraperitoneal and metastatic A431 (epidermoid carcinoma) tumors, GD2 in neuroblastoma mouse models and CD20 in B cell malignancies (unpublished data and [3,4,35,36]).

However, many characteristics of this human promoter-regulated hCD89 transgenic mouse model are not fully elucidated. For instance, in this study we sought an explanation for the fact that homozygous breeding of these transgenic mice is lethal. Therefore, we first determined the integration site of the transgene. Next, as the introduction of CD89 (signaling) could potentially impact immune cell numbers or phenotype, we compared the immune cell composition and phenotype of WT and hCD89 transgenic mice in various strains. Furthermore, most characteristics of this model were previously described for hCD89 mice on the FVB/N background[30] and not within more commonly used strains, such as C57BL/6, BALB/c, SCID and NXG. Since it is known for more than half a century that immune cell composition and phenotype is different between mouse strains and genders[37,38], we assessed the hCD89 model in these four strains and in both male and female mice. Finally, we compared efficacy of IgA/CD89-mediated ADCC for each mouse strain and studied CD89 expression in tumor models.

METHODS

Animal experiments

Mice were housed and bred at the animal facility of the Utrecht University (GDL) from 2001 to 2019. From 2019 onwards they were kept at Janvier Labs (France) and transported to the GDL at least 1 week prior to each experiment. Food and water were provided ad libitum and mice were housed in groups under a 12:12 light–dark cycle. Mice were sacrificed by cervical dislocation. Both male and female mice from C57BL/6JRj, BALB/cByJ, CB17-SCID and NXG (NOD.Cg-*Prkdc*^{scid} *Il2rg*^{tm1}Wjl/Rj) or NSG (NOD.Cg-*Prkdc*^{scid} *Il2rg*^{tm1}Wjl/SzJ) strains were used. Mice in experimental groups were randomized based on weight, age and cage and researchers were single-blinded. Immune composition and CD89 expression data was generated with mice from Charles River (before 2019) and for the remaining experiments mice from Janvier were used (2019 onwards). All mouse experimental procedures were

approved by the institute's animal ethics committee and by the Dutch Central Authority for Scientific Procedures on Animals (CCD, AVD115002016410 and AVD11500202115442).

Generation of human FcαRI transgenic mice and cross-breeding

A 41-kb cosmid clone (R31931) insert of chromosome 19 carrying the 12-kb human FCAR gene in a 5.2 kb LAWRIST16 vector was provided by Dr L.K. Ashworth (Human Genome Center, Livermore, CA)[39,40] The genomic insert was linearized upon digestion with SfiI restriction enzymes, isolated by electro-elution and injected into fertilized FVB/N oocytes to generate the first generation of transgenic mice[30]. hCD89 transgenic FVB/N mice (founder GG2126) were bred with BALB/c and C57BL/6 mice for at least 40 generations to introduce hCD89 on these backgrounds (**Figure 1A**). Subsequently, hCD89 BALB/c mice were bred with SCID and NXG mice for at least 24 and 15 generations respectively. The hCD89 breeding was maintained hemizygously.

Targeted Locus Amplification, sequencing and alignment

Bone marrow (BM) of hCD89 transgenic BALB/c and NXG mice was isolated by flushing femurs and tibiae with full RPMI medium (RPMI 1640 medium, GlutaMAX (Gibco) supplemented with 10% Fetal Calf Serum (FCS, Bodinco) and 1% penicillin/streptomycin (Gibco)). BM cells were passed through a 70 µm cell strainer, frozen in freezing medium (50% RPMI medium, 40% FCS and 10% dimethyl sulfoxide (DMSO, Sigma)) and transferred to Cergentis for Targeted Locus Amplification (TLA) analysis.

Preparation of the samples and TLA was performed as described by De Vree and colleagues[41]. In short, BM cells were crosslinked using formaldehyde, then DNA was digested with NlaIII. The sample was ligated, crosslinks were reversed and the DNA was purified. To obtain circular chimeric DNA molecules for PCR amplification, DNA molecules were trimmed with NspI and ligated at a DNA concentration of 5 ng/µl to promote intramolecular ligation. As a consequence, a subset of NlaIII (CATG) sites were (re-)digested, generating DNA fragments of approximately 2 kb and allowing the amplification of entire restriction fragments. Primers are listed in **Supplemental Table 1**. Illumina NGS library was established from the PCR products according to the Nextera DNA Flex Library Prep (Illumina) protocol and libraries were sequenced (paired-end, 2 × 151 bases) on an Illumina sequencer.

Base calling and demultiplexing was performed using The Illumina System, together with the bcl2fastq Conversion Software (Illumina). Using the barcode information, paired-end FASTQ files were generated for each individual amplification of a TLA sample. Reads were mapped to the vector sequences (in this case chromosome 19, human genome hg38 and the LAWRIST16 vector) and host genome (mouse mm10) using BWA-MEM, version 0.7.15-r1140 (settings bwa mem -M -t 4 -B 7 -w 33 -O 5 -E 2 -T 33 -Y)[42]. The resulting mapped BAM files were analyzed using IGV software.

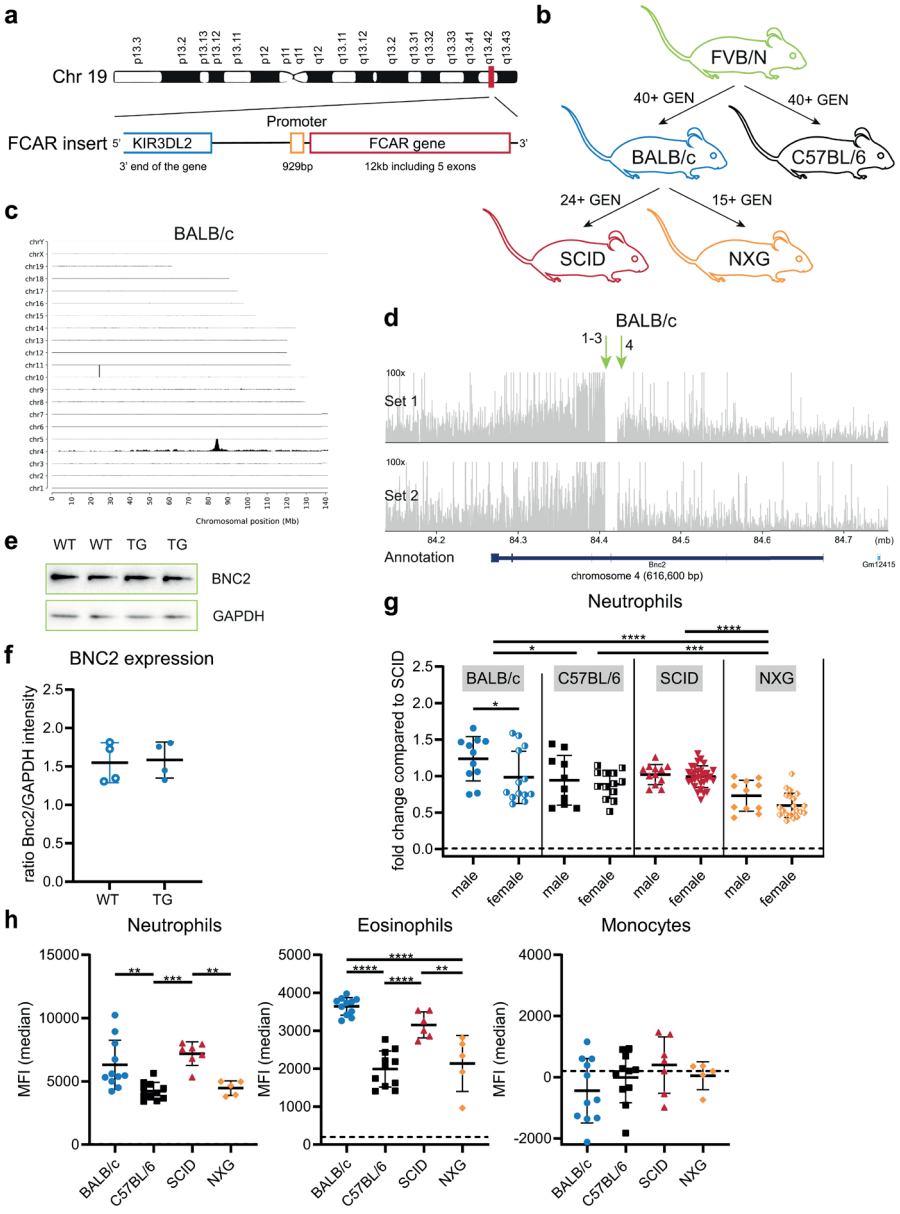

Figure 1 | Gene integration site and evaluation of hCD89 expression in circulating myeloid cells. (**A**) Detail of the genomic insert containing the *FCAR* gene that was used to generate the hCD89 mice (**B**) Schematic overview of the order in which hCD89 transgenic mice were generated on 4 different backgrounds. (**C**) Coverage of TLA sequence across the whole mouse genome with primer set 1 in the BALB/c sample. (**D**) Coverage of TLA sequence across the vector integration site in the BALB/c sample. Green arrows indicate the location of breakpoint sequences and genomic rearrangement. (**E**) Representative immunoblot for BNC2 in liver samples from BALB/c mice. Two independent experiments were performed and GAPDH was used as a loading control. (**F**) Normalized values of BNC2 expression in liver samples from BALB/c mice from 2 experiments. (**G**) CD89 expression on circulating neutrophils of both WT and hCD89 TG mice was determined by flow cytometry. Pooled data from at least 9 experiments: data from SCID

mice were standardized and data from other strains were related to SCID mice. Means were compared using Two-Way ANOVA with Tukey's post-hoc test. (**H**) CD89 expression on neutrophils, eosinophils and monocytes from hCD89 TG male mice. Representative experiment of at least 9 other experiments is shown. Means were compared using One-Way ANOVA with Tukey's post-hoc test. Dotted lines are WT background signal. Data as shown are mean ± SD. GEN = Generations

Western Blot

Liquid nitrogen frozen livers from BALB/c mice were grinded with mortar and pestle. Liver samples were lysed for 60 minutes (min) in RIPA buffer (Sigma) containing a protease/phosphatase inhibitor cocktail (Cell Signaling) and sonicated 3 times for 8 seconds. Lysates were centrifuged twice at 4 °C for 1 hour at 16,000 × *g* and supernatants were collected and stored at -80 °C. Protein concentration was determined using a Pierce BCA protein assay kit (ThermoFisher). 40 µg protein was boiled for 5 min in Laemmli sample buffer (Biorad) containing 10 mM dithiothreitol (DTT) and subjected to SDS-PAGE, followed by immunoblotting.

Specifically, proteins were separated by gel electrophoresis using 20% Tris–Glycine gels (ThermoFisher) and electro-transferred to a nitrocellulose membrane using the High MW program on a Trans-Blot Turbo Transfer System (Biorad). Membranes were blocked in 5% skim milk powder diluted in PBS, 0.1% Tween-20 (PBS-T) and incubated over-night at 4 °C with primary antibodies (rabbit anti-mouse BNC2 polyclonal antibody, 1:500 or mouse anti-GAPDH, 1:5,000 (ThermoFisher)). The next day, membranes were washed three times with PBS-T and incubated for 1 hour at room temperature (RT) with horseradish peroxidase-conjugated anti-rabbit or anti-mouse IgG antibodies (ThermoFisher) in PBS-T. Protein bands were visualized using enhanced chemiluminescence (ECL) detection (ThermoFisher) on a charge-coupled device (CCD) camera and Image Lab software was used for analysis and quantification.

Mouse tumor models

For the Ba/F3 tumor model, $2.5*10^6$ cells Ba/F3 cells were injected subcutaneously on the right flank of BALB/c mice. 9464D-GD2-luc2 cells were generated as described previously[43]. 9464D-GD2 cells were collected in PBS and $0.5*10^6$ cells were injected intraperitoneally in C57BL/6 mice. IMR32 cells were dissolved in a 1:1 mixture of PBS and high concentration matrigel (Corning) and $2.5*10^6$ cells were injected subcutaneously on the right flank of both SCID and NXG mice. After 14 days (Ba/F3 model), 27 days (9464D-GD2-luc2 model) or 51 days (IMR23 model) tumor and blood samples were collected for analysis.

Mouse tumors were carefully excised and collected in ice cold PBS. Tumors were cut and digested using the mouse tumor dissociation kit from Miltenyi. Up to 1 gram of tumor tissue was transferred to C tubes (Miltenyi) containing enzyme mix (DMEM culture medium, 100 µL Enzyme D, 50 µL Enzyme R, and 10 µL Enzyme A) and the 37C_m_TDK_1 program was run on a gentleMACS Octo Dissociator. Following dissociation, tumor cells were filtered using a 100 µm cell strainer and then used for further applications.

Patient PMN isolation and CD89 staining

Blood was obtained from patients in the UNICIT cohort of the UMC Utrecht. Blood was added on a Ficoll (GE Healthcare)/Histopaque 1119 (Sigma) layer and centrifuged for 20 min at 1500 RPM. Afterwards, low-density polymorphonuclear leukocytes (PMN) and high-density PMN were collected from the interphase between serum and Ficoll or in the Histopaque layer, respectively.

Antibody staining and flow cytometry

Blood was sampled from the submandibular vein in lithium-heparin tubes (Sarstedt). 30 µL of blood was stained with 30 µL of antibody solution and incubated for 15 min on RT (antibody panels described in **Supplemental Tables 2–4**). Next, samples were fixated and erythrocytes were lysed using the BD FACS lysing solution for 5–10 min on RT. After washing with PBS, latex beads were added to quantify cell numbers on a Canto II flow cytometer (BD). Dissociated tumor cells were stained with antibodies for 45 min on 4 °C as in **Supplemental Table 5** as well as with TO-PRO3 (1:50,000 ThermoFisher) and analyzed on the LSRFortessa (BD).

Patient PMN were washed in PBS, stained with PE anti-CD89 (BD, clone A59) for 30 min on 4 °C, followed by an additional PBS wash. Patient PMN were analyzed on a Canto II flow cytometer (BD).

Cell culture

A431, SKBR3, Ba/F3 and 9464D-GD2-luc2 cells were cultured in RMPI-1640, whereas IMR32 cells were cultured in DMEM medium. Both culture media were supplemented with HEPES, Glutamax, 10% heat-inactivated fetal calf serum (FCS, Bodinco) and 100 U/mL penicillin–streptomycin (p/s, Gibco). Neuroblastoma cells (IMR32 and 9464D-GD2-luc2) were additionally supplemented with 2% non-essential amino acids (ThermoFisher) and Ba/F3 cells with 0.1 ng/mL murine IL-3 (Immunotools). All cells were cultured at 37 °C in a humidified incubator containing 5% CO_2. Cells were not cultured past 20 passages and they were tested every 6 weeks for mycoplasma using a Mycoalert mycoplasma detection kit (Lonza).

^{51}Cr-release assays

Mice were injected subcutaneously with 20 µg recombinant human PEGylated G-CSF and after 4 days blood was collected in lithium-heparin tubes under terminal anesthesia. Murine neutrophils were isolated from blood by performing erythrocyte lysis (Biolegend) twice for 4 min at 4 °C, followed by magnetic separation using anti-Ly-6G Microbeads (Miltenyi) according to manufacturer's instructions. Neutrophils were added in an effector-target (E:T) ratio of 40:1 and for Whole Blood (WB) assays 25 µL of whole blood was added per condition.

Target cells were labeled with radioactive chromium-51 (Na251CrO4, PerkinElmer) for 2 h and washed three times. Antibodies against EGFR (A431), GD2 (IMR32) or HER-2 (SKBR3) were added in concentrations as indicated per experiment. The killing assays were incubated for 4 h at 37 °C in a humidified incubator containing 5% CO_2. Plates were centrifuged and supernatant was transferred to lumaplates (PerkinElmer) to assess radioactivity induced scintillation (in counts per minute, cpm) on a beta-gamma counter (PerkinElmer). Specific lysis was calculated using the formula: ((Experimental cpm—basal cpm)/(maximal cpm—basal cpm))*100, with maximal lysis determined by incubating target cells with 1.25% triton and minimal lysis determined by chromium release of target cells in the absence of antibodies and effector cells.

Analysis, statistics and software

Flow cytometry analysis was done in FlowJo (TreeStar). Marker expression and immune cell composition data were pooled from different experiments conducted over a period of approximately 1 year. To compensate for day-to-day variation, data points from SCID mice were first standardized for each experiment and thereafter data from other strains were related to SCID mice.

Statistical analysis was conducted using GraphPad Prism software (version 9.3.0). Means are represented with SD values. Immune cell composition and marker expression were evaluated using Two-Way ANOVAs, first to compare between wildtype and transgenic mice within a strain (when applicable) and next to compare between strains. ADCC assays were compared using Two-Way ANOVAs (or Mixed-Effects model in case of missing data). For all analyses Tukey's post-hoc test was used. Significance is indicated by * as $p < 0.05$, ** as $p < 0.01$, *** as $p < 0.001$ and **** as $p < 0.0001$.

RESULTS

Breeding and integration site

We first determined the size of the transgene (part of chromosome 19 containing the *FCAR* gene, **Figure 1A**) that was integrated in hCD89 transgenic (TG) mice, as well as the integration site and vector copy number using the TLA protocol of Cergentis[41]. We performed the analysis with BALB/c and NXG mice, since they were the first and last strain respectively to be generated (**Figure 1B**). In both mice the sequence of interest was integrated in chromosome 4, accompanied by a complex rearrangement, including the co-integration of a 146 kb genomic fragment from chromosome 10 (**Figure 1C**, **D** and **Supplemental Figure 1A–C**). Additionally, 220 bp of the LAWRIST16 vector sequence was integrated at the same site. Because of the complexity of the rearrangements and the multiple breakpoint sequences, the exact sequence at the integration site could not be

established (**Supplemental Table 6**). Coverage on the vector-side is 2–5 times higher than on the genome-side of the integration side, hence it is estimated that the copy number of the insert is 2–5. TLA sequencing showed that the *FCAR* gene is the only complete gene on the chromosome 19 insert (**Supplemental Figure 1D**). Furthermore, a part of the *KIR3DL2* gene is present, but this gene will not be functional.

Alignment in RefSeq of the vector integration site revealed that vector integration disrupted the mouse basonuclin 2 (*bnc2*) gene. In the past it was noted that homozygous hCD89 transgenic mice were unable to survive beyond 24 h, which corresponds to the phenotype described for *bnc2*$^{-/-}$ mice in literature[44]. To assess BNC2 expression levels in hemizygous hCD89 mice, we performed western blots for BNC2 on liver samples of wildtype (WT) and hCD89 TG mice. Interestingly, both WT and TG mice expressed similar levels of BNC2 in the liver (**Figure 1E**, **F**), indicating that expression of one allele is sufficient to induce normal levels of BNC2.

In healthy transgenic mice CD89 is expressed by neutrophils and eosinophils, but not monocytes.

Next, we characterized CD89 expression in circulating neutrophils and other immune subsets from different mouse strains by analyzing blood samples from healthy male and female, WT and hCD89 TG mice using flow cytometry. CD89 was expressed by neutrophils from all 4 strains, but interestingly CD89 expression levels were highest in BALB/c and SCID, lower in C57BL/6 and lowest in NXG mice (**Figure 1G**). Additionally, we observed that CD89 expression was significantly higher in neutrophils from male compared to female BALB/c mice and a similar trend was present in other mouse strains (**Figure 1G**).

CD89 expression on eosinophils was generally lower compared to neutrophils (**Figure 1H**), corresponding to the human situation. Similar to neutrophils, CD89 expression was highest on eosinophils from BALB/c and SCID and lower on C57BL/6 and NXG eosinophils (**Figure 1H**). Surprisingly, CD89 was not detected on circulating monocytes, although it is known to be expressed on healthy human monocytes (**Figure 1H**). As expected, CD89 was not expressed on T and B lymphocytes (data not shown).

Immune cell composition in the circulation is similar between WT and hCD89 TG mice but differs among mouse strains

Since we often use both WT and hCD89 TG mice in experiments, we evaluated whether the integration of the transgene affects the circulating leukocyte composition of hCD89 TG mice. Flow cytometry analysis of blood samples from healthy male and female, WT and hCD89 TG mice revealed that there were no differences in total leukocyte, neutrophil, eosinophil, monocyte and T and B cell numbers between WT and hCD89 TG mice in any of the 4 mouse strains (**Figure 2A–C** and **Supplemental Figure 2A–C**).

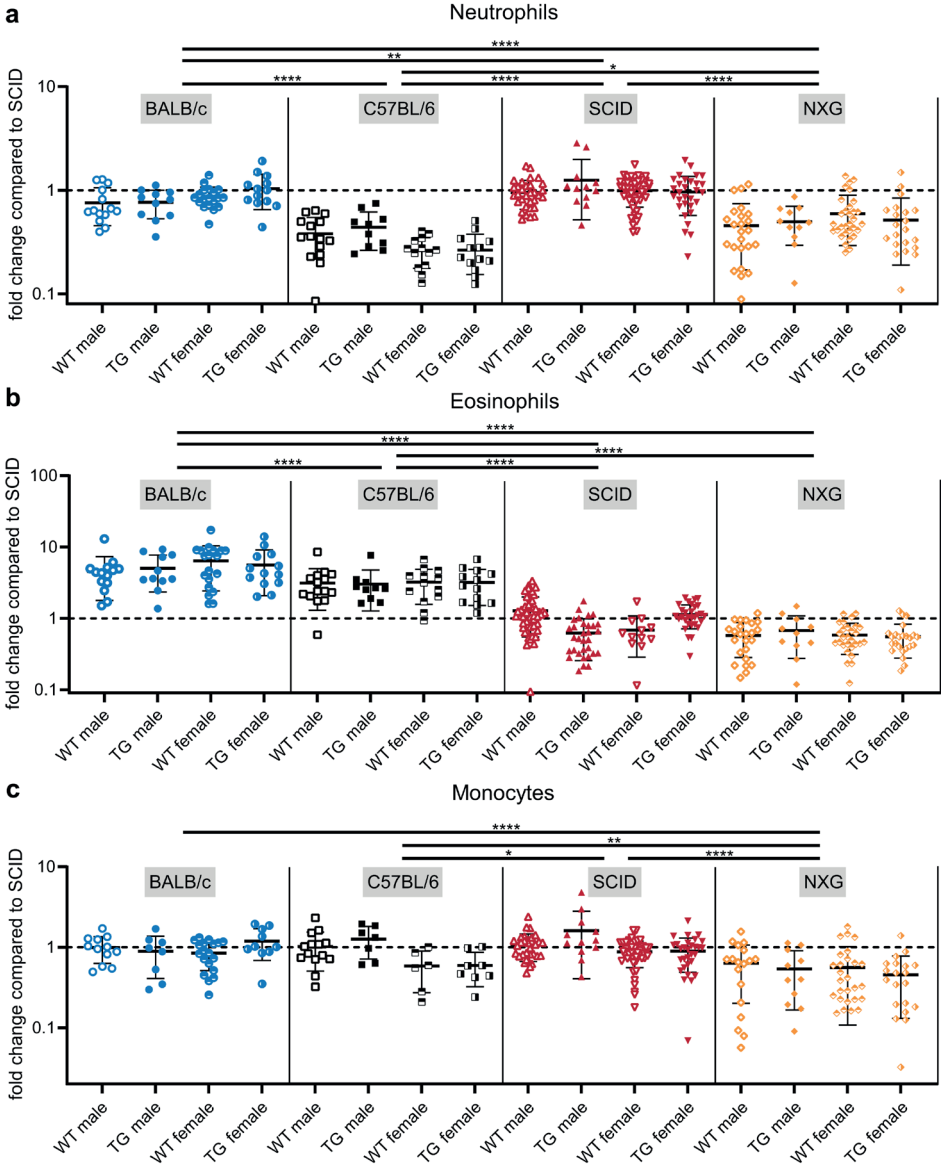

Figure 2 | Comparison of myeloid cell numbers in the circulation of WT and hCD89 TG mice. Blood was obtained from both female and male, WT and TG mice from all 4 strains. Antibody staining and subsequent flow cytometry analyses were performed to determine the number of (**A**) neutrophils, (**B**) eosinophils and (**C**) monocytes. Pooled data from at least 9 experiments: data from SCID mice were standardized and data from other strains were related to SCID mice. First, means of mice within a strain were compared and secondly all mice from each strain were pooled and compared using Two-Way ANOVA with Tukey's post-hoc test

However, we did observe many differences in leukocyte composition between mouse strains. As expected, overall leukocyte numbers were higher in immunocompetent BALB/c and C57BL/6 mice compared to immunocompromised SCID and NXG (**Supplemental Figure 2A**). Neutrophil numbers were higher in BALB/c and SCID mice compared to C57BL/6 and NXG mice (**Figure 2A**). BALB/c mice had more eosinophils compared to C57BL/6 mice, but both of these strains had much more eosinophils compared to immunocompromised mouse strains (**Figure 2B**). Monocyte numbers were relatively comparable among strains, only NXG mice had significantly less monocytes (**Figure 2C**). Additionally, neutrophil and monocyte numbers appeared to be lower in female compared to male C57BL/6 mice, though not significantly (**Figure 2A, C**). Finally, T and B cell numbers in BALB/c and C57BL/6 mice were inverted, BALB/c mice had higher T cell and C57BL/6 higher B cell numbers (**Supplemental Figure 1B, C**).

Phenotype of circulating myeloid cells is not affected by the hCD89 insert but differs among mouse strains

Although we did not observe differences in the number of circulating leukocytes between WT and hCD89 TG mice, we wanted to study effects of hCD89 transgene integration on the immune cell phenotype as well. Therefore, we first analyzed expression of myeloid activation marker CD11b using flow cytometry. Since it recently became clear that IgA immunotherapy can be significantly enhanced by blocking the CD47/signal-regulatory protein alpha (SIRPα) axis (a myeloid immune checkpoint)[45–47], we studied expression of SIRPα in the hCD89 TG mice as well. Again, no significant differences in CD11b or SIRPα were observed between WT and hCD89 TG mice in any of the 4 strains, except for a small decrease in CD11b expression on C57BL/6 neutrophils (**Figure 3A, B**). Interestingly, CD11b expression on NXG neutrophils was rather low compared to neutrophils from other strains, suggesting a low activation status of NXG neutrophils in healthy conditions (**Figure 3A**). On the other hand, CD11b expression on monocytes was highest in SCID and NXG, lower in BALB/c and lowest in C57BL/6 mice (**Figure 3A**). SIRPα expression on both neutrophils and monocytes from C57BL/6 mice was low compared to other strains, whereas SIRPα in NXG mice was only low on neutrophils, but not on monocytes (**Figure 3B**).

When studying the efficacy of IgA antibodies in mouse models, it is often performed in comparison to IgG antibodies. Hence, we studied the expression of receptors for IgG (FcγRs) on circulating myeloid cells of hCD89 TG mice as well. No changes in FcγR expression were found between WT and hCD89 TG mice, aside from a small decrease in FcγRII/FcγRIII expression on NXG monocytes (**Figure 3C–E**). In accordance with literature[48], expression of the high affinity, activating IgG receptor FcγRI was absent on neutrophils and monocytes (**Figure 3C**), whereas FcγRII and FcγRIII (inhibitory and activating receptors respectively) were modestly expressed (**Figure 3D**). Compared to the other strains, FcγRII/FcγRIII was less expressed in neutrophils and monocytes from C57BL/6 mice and in neutrophils from

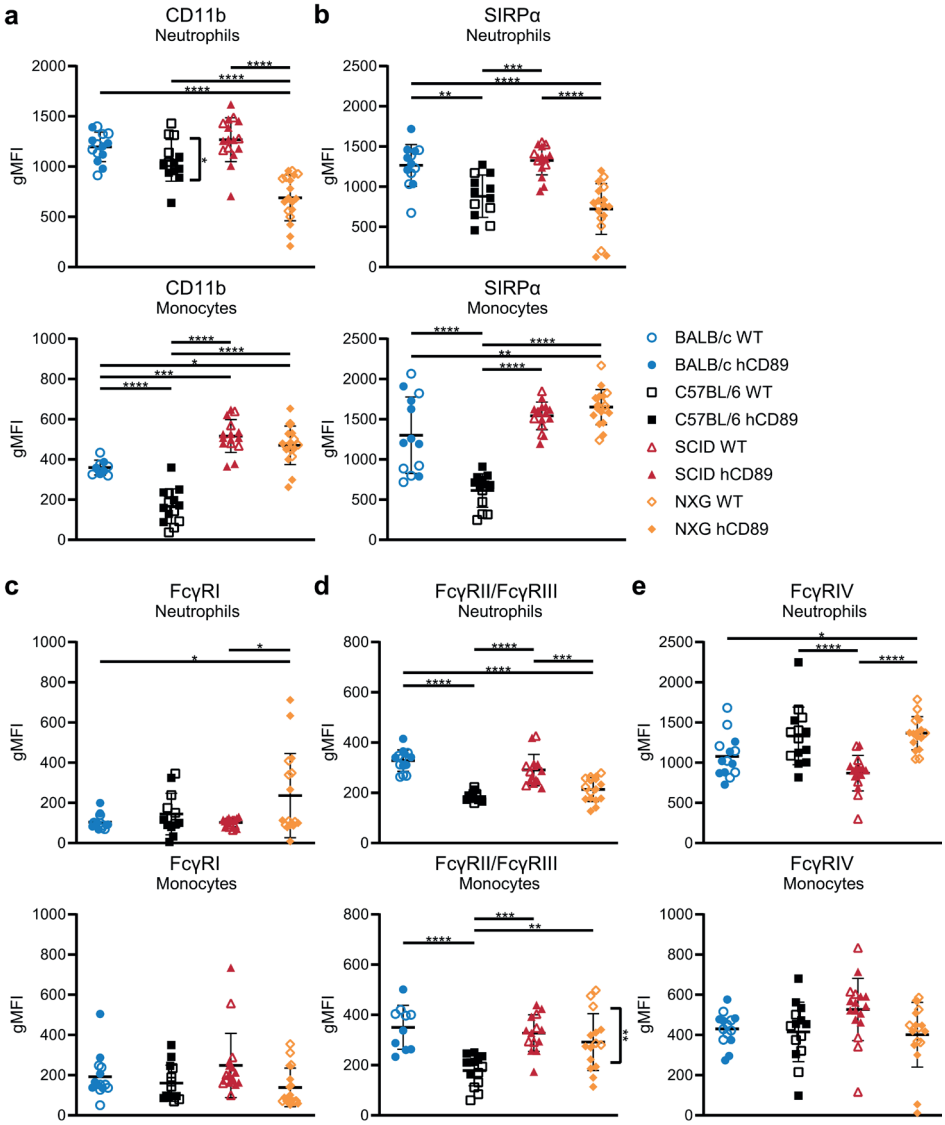

Figure 3 | Expression of activation markers and Fc gamma receptors. Blood was obtained from male WT and hCD89 TG mice from all 4 strains. Antibody staining and subsequent flow cytometry analyses were performed to determine expression of (**A**) CD11b, (**B**) SIRPα, (**C**) FcγRI, (**D**) FcγRII/FcγRIII and (**E**) FcγRIV on neutrophils and monocytes. Pooled data from at least 3 experiments: data from SCID mice were standardized and data from other strains were related to SCID mice. First, means of WT and hCD89 TG mice within a strain were compared and secondly all mice from each strain were pooled and compared using Two-Way ANOVA with Tukey's post-hoc test

NXG mice. FcγRIV was highly expressed in neutrophils from all strains, though expression was highest in C57BL/6 and NXG mice (**Figure 3E**). We did not observe high FcγRIV

expression in monocytes, since we only selected Ly6C^{high} monocytes and FcγRIV is known to be mostly expressed in Ly6C^{int} CD115^{+} instead of Ly6C^{high} monocytes.
Subsequentially, we analyzed these surface markers in G-CSF stimulated mice, since G-CSF is often administered in mouse models to activate neutrophils and other myeloid cells and to recruit them to the circulation. Four days after G-CSF stimulation CD89 expression in BM-derived neutrophils was increased, but not in circulating neutrophils (**Supplemental Figure 3A**). CD11b expression was reduced in neutrophils and SIRPα expression was unchanged after G-CSF stimulation (**Supplemental Figure 3B, C**). Additionally, G-CSF influenced FcγR expression (**Supplemental Figure 4A–C**), since FcγRII/FcγRIII expression was enhanced in all myeloid cells. FcγRIV expression was elevated in neutrophils and circulating eosinophils and monocytes.

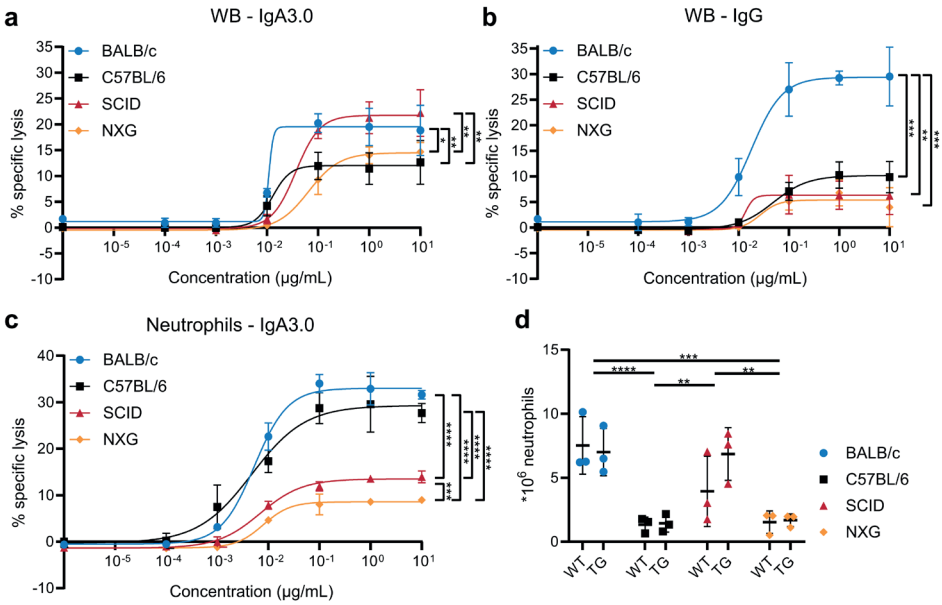

Figure 4 | Comparison of IgA- and IgG-mediated ADCC capacity of 4 different mouse strains. ^{51}Cr-release assays against EGFR-expressing A431 cells comparing (**A**) IgA3.0- or (**B**) IgG-mediated ADCC with whole blood from 4 different TG mouse strains. (**C**) ^{51}Cr-release assays showing concentration-dependent ADCC of EGFR-expressing A431 cells after binding of anti-EGFR IgA antibodies by isolated neutrophils from 4 different hCD89 TG mouse strains. ADCC capacity of strains was compared using a RM Two-Way ANOVA with Tukey's post-hoc test. (**D**) Total number of neutrophils per mouse after Ly-6G MACS isolation. Means were compared using Two-Way ANOVA with Tukey's post-hoc test. Graphs are representative data of at least 3 different experiments. WB = Whole Blood, WT = wildtype, TG = transgenic

Comparison of ADCC capability between strains

Besides the phenotypic characterization of hCD89 transgenic mice, we compared the functionality of CD89 expressed in different mouse strains by performing antigen-

dependent cellular cytotoxicity (ADCC) assays. Since neutrophil numbers are very low in the circulation (**Supplemental Figure 5A**), mice were injected with G-CSF 4 days prior to the experiment to mobilize myeloid cells from the bone marrow. Using effector cells from whole blood (WB), IgA-mediated killing of A431 cells, an epidermoid carcinoma cell line, was most efficient by SCID and BALB/c, but less efficient by NXG and C57BL/6 effector cells (**Figure 4A**). WB effector cells from BALB/c mice were able to adequately eliminate A431 tumor cells upon IgG stimulation, whereas WB effector cells from other strains did not achieve more than 10% specific lysis (**Figure 4B**).

Thereafter, we isolated neutrophils using magnetic-activated cell sorting (MACS) (**Supplemental Figure 5B**) to perform ADCC assays with pure neutrophils as effector cells. Interestingly, neutrophils from immunocompetent mouse strains (BALB/c and C57BL/6) induced more tumor cell lysis compared to neutrophils from immunocompromised mice (SCID and NXG) and NXG neutrophils performed even worse than neutrophils from SCID mice (**Figure 4C**). A similar pattern was observed when other tumor cells such as SKBR3 (breast cancer) and IMR32 (neuroblastoma) were used as target cells, though these cell lines were more resistant to killing in general (**Supplemental Figure 5C**). IgG-mediated killing of these tumor cells by neutrophils was lower than IgA-mediated killing (**Supplemental Figure 5C**). Similar to IgA, IgG antibodies induced more tumor cell lysis with neutrophils from immunocompetent strains. When neutrophils from wildtype mice were used as effector cells, only IgG induced tumor cell killing and not IgA, indicating that IgA-mediated ADCC is dependent on the expression of FcαRI (**Supplemental Figure 5D, E**). In both unstimulated (**Figure 1G**) as well as G-CSF stimulated mice (**Figure 4D**), neutrophil numbers are highest in BALB/c and SCID mice. This is consistent with the higher killing percentages observed in these strains, when equal volumes of whole blood are used in ADCC assays. However, in ADCC assays with equal numbers of neutrophils, neutrophils from immunocompetent mice induce most tumor cell lysis, suggesting that neutrophils from BALB/c and C57BL/6 mice are more potent.

CD89 expression is elevated in tumor-bearing mice and in PMN-MDSC from cancer patients

Finally, we studied CD89 expression in tumor-bearing mice, since IgA research is often performed in the context of mouse tumor models and not in healthy mice. Both WT and hCD89 TG BALB/c mice were injected subcutaneously with $2.5*10^6$ Ba/F3 cells, a murine pro-B cell line, and blood and tumor samples were analyzed after 14 days by flow cytometry. In these tumor-bearing mice, CD89 expression was more than doubled on intratumoral neutrophils compared to circulating neutrophils (**Figure 5A**). However, for intratumoral eosinophils we observed the opposite effect: they had lower CD89 expression compared to circulating eosinophils (**Figure 5B**). Additionally, CD89 was expressed on

monocytes and macrophages in the tumor microenvironment (**Figure 5C-D**). Circulating monocytes in tumor-bearing mice started to express CD89 as well (**Figure 5C**), whereas circulating monocytes in healthy mice were generally negative for CD89 (**Figure 1H**).

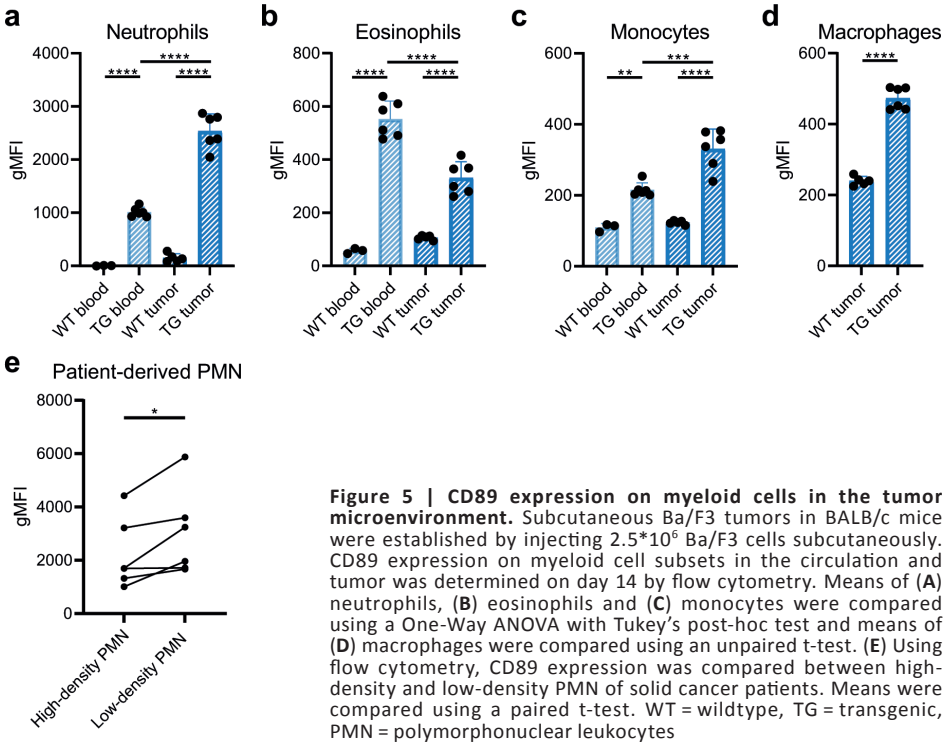

Figure 5 | CD89 expression on myeloid cells in the tumor microenvironment. Subcutaneous Ba/F3 tumors in BALB/c mice were established by injecting $2.5*10^6$ Ba/F3 cells subcutaneously. CD89 expression on myeloid cell subsets in the circulation and tumor was determined on day 14 by flow cytometry. Means of (**A**) neutrophils, (**B**) eosinophils and (**C**) monocytes were compared using a One-Way ANOVA with Tukey's post-hoc test and means of (**D**) macrophages were compared using an unpaired t-test. (**E**) Using flow cytometry, CD89 expression was compared between high-density and low-density PMN of solid cancer patients. Means were compared using a paired t-test. WT = wildtype, TG = transgenic, PMN = polymorphonuclear leukocytes

Mouse tumor models were established as well for the other mouse strains. Specifically, C57BL/6 mice were injected intraperitoneally with 9464D-GD2 neuroblastoma cells and subcutaneous IMR32 human neuroblastoma xenograft tumors were established in both SCID and NXG mice. In agreement with our data from the BALB/c tumor-bearing mice, in all three models CD89 expression was increased on intratumoral neutrophils, monocytes and macrophages, but decreased on intratumoral eosinophils (**Supplemental Figure 6**). Finally, we related these mouse CD89 expression data to CD89 expression in high-density and low-density neutrophils from solid cancer patients. High-density neutrophils are considered 'regular' neutrophils and low-density neutrophils are considered myeloid-derived suppressor cells (PMN-MDSC) that are educated by tumor cells[49]. Using antibody staining and flow cytometry we observed that CD89 expression is higher on low-density compared to high-density neutrophils (**Figure 5E**), supporting the findings in mice that CD89 expression is generally increased on tumor-associated myeloid cells.

DISCUSSION

In this study we thoroughly characterized a hCD89 transgenic mouse model regulated by the endogenous human promoter. Our results, along with previous studies, indicate that CD89 expression and function in this model highly resemble the human situation[12,50]. We and others observed that CD89 expression is highest in neutrophils, intermediate on other myeloid cells such as eosinophils and DC subsets and inducible on monocytes and Kupffer cells, among others. Interestingly, CD89 expression was increased in all myeloid cells except eosinophils in both blood and tumor samples of tumor-bearing hCD89 transgenic mice. We recently observed that PMN myeloid-derived suppressor cells (PMN-MDSCs) from several solid cancer patients (**Figure 5E**), such as melanoma and colorectal cancer, have elevated CD89 expression as well (unpublished data). This highlights again the similarity of CD89 regulation between humans and our hCD89 transgenic mice. Furthermore, the fact that CD89 expression is increased on tumor-infiltrating myeloid cells is promising for IgA immunotherapy and remains an interesting topic for future investigation.

Currently, the mice from our hCD89 transgenic model under the endogenous promoter are bred hemizygously. In the past, homozygous breeding of the hCD89 transgenic mice was attempted, but was never successful. We now show that this is caused by the integration site of the *FCAR* gene in our model, leading to disruption of the *bnc2* gene and not due to the introduction of hCD89 itself. BNC2 is an extremely conserved zinc finger protein and is required during embryonal development and the development of germ cells. *Bnc2*$^{-/-}$ mice are born with a cleft palate and abnormalities of craniofacial bones and tongue and most of these mice die within 24 h after birth[44,51]. This phenotype corresponds to the one observed when homozygous breeding of our hCD89 mice was attempted. However, when maintained hemizygously, hCD89 transgenic mice are fully healthy, able to reproduce and expressing equal levels of BNC2 in the liver as WT mice, indicating that one allele of *bnc2* is sufficient. Furthermore, we compared the immune cell composition and expression of CD11b, SIRPα and several FcγRs between WT and hCD89 TG mice, and did not find any differences. Hence, we believe that we can use WT littermates as control mice for hCD89 transgenic mice in the future, to reduce unnecessary breeding. On the other hand, we did find major differences in immune cell composition, marker expression and ADCC capacity between mouse strains (**Table 1**). In the future, these differences between mouse models should be taken into consideration when choosing a model for (IgA) research. For example, when BALB/c mice are chosen, IgA efficacy could be higher compared to C57BL/6, SCID and NXG mice, since BALB/c mice have higher neutrophil numbers and higher CD89 expression, resulting in more ADCC. Additionally, neutrophil infiltration and activation in C57BL/6 has been reported to be limited compared to BALB/c mice in for example lung inflammation models[52]. In many studies, IgA immunotherapy is compared to IgG immunotherapy, since IgG is currently the gold standard. IgA immunotherapy could be relatively more favorable

than IgG in BALB/c and SCID mice compared to C57BL/6 and NXG, mice, since the latter two have higher FcγRIV expression, required for IgG effector function. These examples highlight that depending on the mouse model, IgA studies could have different outcomes.

	BALB/c	C57BL/6	SCID	NXG
CD89 expression	++++	++	+++	+
Neutrophil numbers	++++	+	+++	+
Eosinophil numbers	+++	+++	+	+
Monocyte numbers	++	++	++	++
Whole blood ADCC – IgA	++++	+++	+++	+
Whole blood ADCC – IgG	+++	+	+	+
Neutrophil ADCC – IgA	++++	++++	++	+

Table 1 | Comparison of different mouse strains for CD89 expression, myeloid cell numbers and ADCC efficacy.

Additionally, we observed that male hCD89 transgenic mice tend to have higher CD89 expression than females. To our knowledge it is not well described how this translates to the human situation. However, it is known that there are major gender differences in for example neutrophil activation by type I interferons or immunoglobulin levels, including IgA[53–55]. It will be interesting to investigate gender differences in IgA and CD89 expression further in the human setting, but this is beyond the scope of this paper.

In this study, we found that neutrophils in SCID, but especially in NXG mice are much less activated than neutrophils from immunocompetent strains. It has been described that other innate cells such as macrophages and dendritic cells are dysfunctional in NXG (or NSG) mice, even though they are not directly modified by the strain's specific null mutations (*Prkdc*, *Il2rg*)[56]. Neutrophils from NXG mice could possibly be inactive due to the lack of signaling via IL-2 receptor gamma chain (IL-2rγ) as well, although this has not been described previously. Another possible explanation could lie in the fact that NXG mice have a SIRPα polymorphism, resulting in higher affinity for its target, CD47[57]. Since the SIRPα/CD47 axis is a myeloid checkpoint, this could explain why IgA-stimulated neutrophils from NXG mice are not able to kill tumor cells properly. Furthermore, we observed that in general neutrophils from all mouse strains induce less ADCC upon IgA stimulation than human neutrophils. Additionally, it is known that neutrophil numbers are lower in mice (~ 10% of circulating leukocytes) than in humans (~ 50–70%). BALB/c mice might yet be the most representative model of the human situation in this regard, since they have the highest neutrophil numbers and most activated neutrophils of all strains evaluated. Possibly the difference between mice and humans is the result of housing under germ-free conditions, resulting in less priming by cytokines and therefore less neutrophil activation in mice. For example, it was established that the gut microbiome is involved in neutrophil

aging and activation[58], indicating a relationship between exposure to microorganisms and neutrophil activation. Additionally, it is known that ADCC by mouse neutrophils can be enhanced by activating cytokines such as GM-CSF and TNF-α, further supporting the hypothesis that mouse neutrophils are less activated than human neutrophils in general[30]. Overall, the hCD89 transgenic mouse model provides a very powerful tool to test the efficacy of IgA immunotherapy against infectious diseases and cancer. In this study we thoroughly characterized previously unknown features of this model, such as the integration site of the *FCAR* gene, CD89 expression in healthy and tumor-bearing mice, expression of myeloid activation markers and FcγRs and tumor killing capacity. These data will form a solid base for deciding which model and which mouse strain to choose for *in vivo* experiments evaluating IgA immunotherapy.

Acknowledgements

We thank the flow cytometry facility in the UMCU for their service and the GDL laboratory for excellent care of the laboratory animals. We thank Cergentis for performing the TLA analysis, Craig Morton of the Institute of Marine Research in Bergen for his help determining the FCAR insert, and Thomas Valerius of the University of Kiel for encouraging us to breed the FcαRI transgenic mice in the NXG background. We would like to thank Mick van Eijs, Rik Verheijden, Karijn Suijkerbuijk and the UNICIT consortium for kindly providing patient material for this study.

Author contributions

Conceptualization MCS, JHMJ, and JHWL; Methodology MCS, JHMJ, MN, MT, ME and PAO; Formal Analysis MCS, JHMJ, MN and MT; Investigation MCS, JHMJ, MN, MT, ME and PAO; Resources MCS, JHMJ, MN, MT and JHWL; Writing—Original Draft MCS; Writing—Review & Editing MCS, JHMJ, MN, MT, PAO, FMW and JHWL; Supervision and Funding Acquisition JHWL and FMW.

Funding

MCS and MN were funded by Villa Joep (project 17 IgA and anti-GD2). JHMJ, MN, MT and PAO were funded by the KWF Dutch Cancer Society: Grant number 9038 / 2021-PPS.

Competing interests

JHWL is co-founder of TigaTx and inventor on patent applications WO2019059771 and WO2020197400.

Ethical approval

All mouse experimental procedures were approved by the institute's animal ethics committee and by the Dutch Central Authority for Scientific Procedures on Animals (CCD,

AVD115002016410 and AVD11500202115442). The UNICIT patient cohort was established according to the declaration of Helsinki and approved by the UMC Utrecht ethics committee (biobank approval TCBio 18–123).

Consent to participate

All human research participants provided informed consent for publication of the data in **Figure 5E**.

REFERENCES

1. Hellwig, S. M., van Spriel, A. B., Schellekens, J. F., Mooi, F. R. & van de Winkel, J. G. Immunoglobulin A-mediated protection against Bordetella pertussis infection. *Infect. Immun.* **69**, 4846–4850 (2001).

2. Balu, S. *et al.* A novel human IgA monoclonal antibody protects against tuberculosis. *J. Immunol.* **186**, 3113–3119 (2011).

3. Lohse, S. *et al.* An Anti-EGFR IgA That Displays Improved Pharmacokinetics and Myeloid Effector Cell Engagement In Vivo. *Cancer Res.* **76**, 403–417 (2016).

4. Boross, P. *et al.* IgA EGFR antibodies mediate tumour killing in vivo. 1213–1226 (2013) doi:10.1002/emmm.201201929.

5. Brandsma, A. M. *et al.* Potent Fc Receptor Signaling by IgA Leads to Superior Killing of Cancer Cells by Neutrophils Compared to IgG. *Front. Immunol.* **10**, 704 (2019).

6. Heemskerk, N. *et al.* Augmented antibody-based anticancer therapeutics boost neutrophil cytotoxicity. *J. Clin. Invest.* **131**, (2021).

7. Leusen, J. H. W. IgA as therapeutic antibody. *Mol. Immunol.* **68**, 35–39 (2015).

8. Sterlin, D. & Gorochov, G. When Therapeutic IgA Antibodies Might Come of Age. *Pharmacology* **106**, 9–19 (2021).

9. Wines, B. D. *et al.* Identification of residues in the first domain of human Fc alpha receptor essential for interaction with IgA. *J. Immunol.* **162**, 2146–2153 (1999).

10. Kremer, E. J. *et al.* The gene for the human IgA Fc receptor maps to 19q13.4. *Hum. Genet.* **89**, 107–108 (1992).

11. Shimokawa, T., Tsuge, T., Okumura, K. & Ra, C. Identification and characterization of the promoter for the gene encoding the human myeloid IgA Fc receptor (FcalphaR, CD89). *Immunogenetics* **51**, 945–954 (2000).

12. Monteiro, R. C. & Van De Winkel, J. G. J. IgA Fc receptors. *Annu. Rev. Immunol.* **21**, 177–204 (2003).

13. van Egmond, M. *et al.* FcalphaRI-positive liver Kupffer cells: reappraisal of the function of immunoglobulin A in immunity. *Nat. Med.* **6**, 680–685 (2000).

14. Lowell, G. H., Smith, L. F., Griffiss, J. M. & Brandt, B. L. IgA-dependent, monocyte-mediated, antibacterial activity. *J. Exp. Med.* **152**, 452–457 (1980).

15. Shen, L. *et al.* Presentation of ovalbumin internalized via the immunoglobulin-A Fc receptor is enhanced through Fc receptor gamma-chain signaling. *Blood* **97**, 205–213 (2001).

16. Gimpel, A.-K. *et al.* IgA Complexes Induce Neutrophil Extracellular Trap Formation More Potently Than IgG Complexes. *Front. Immunol.* **12**, 761816 (2021).

17. Maruoka, T., Nagata, T. & Kasahara, M. Identification of the rat IgA Fc receptor encoded in the leukocyte receptor complex. *Immunogenetics* **55**, 712–716 (2004).

18. Morton, H. C., Pleass, R. J., Storset, A. K., Brandtzaeg, P. & Woof, J. M. Cloning and characterization of equine CD89 and identification of the CD89 gene in chimpanzees and rhesus macaques. *Immunology* **115**, 74–84 (2005).

19. Ellis, J. A. Canine IgA and IgA deficiency: Implications for immunization against respiratory pathogens. *Can. Vet. J. = La Rev. Vet. Can.* **60**, 1305–1311 (2019).

20. Auffray, C., Nageotte, R., Sikorav, J. L., Heidmann, O. & Rougeon, F. Mouse immunoglobulin A: nucleotide sequence of the structural gene for the alpha heavy chain derived from cloned cDNAs. *Gene* **13**, 365–374 (1981).

21. Burnett, R. C., Hanly, W. C., Zhai, S. K. & Knight, K. L. The IgA heavy-chain gene family in rabbit: cloning and sequence analysis of 13 C alpha genes. *EMBO J.* **8**, 4041–4047 (1989).

22. Volgina, V. V, Kingzette, M., Zhai, S. K. & Knight, K. L. A single 3' alpha hs1,2 enhancer in the rabbit IgH locus. *J. Immunol.* **165**, 6400–6405 (2000).

23. Pinheiro, A. *et al.* Identification of a new European rabbit IgA with a serine-rich hinge region. *PLoS One* **13**, e0201567 (2018).

24. Reljic, R. In search of the elusive mouse macrophage Fc-alpha receptor. *Immunology letters* vol. 107 80–81 (2006).

25. Abi-Rached, L., Dorighi, K., Norman, P. J., Yawata, M. & Parham, P. Episodes of natural selection shaped the interactions of IgA-Fc with FcalphaRI and bacterial decoy proteins. *J. Immunol.* **178**, 7943–7954 (2007).

26. Xu, L. *et al.* Critical Role of Kupffer Cell CD89 Expression in Experimental IgA Nephropathy. *PLoS One* **11**, e0159426 (2016).

27. Koernig, S. *et al.* Topical application of human-derived Ig isotypes for the control of acute respiratory infection evaluated in a human CD89-expressing mouse model. *Mucosal Immunol.* **12**, 1013–1024 (2019).

28. Launay, P. *et al.* Fcalpha receptor (CD89) mediates the development of immunoglobulin A (IgA) nephropathy (Berger's disease). Evidence for pathogenic soluble receptor-Iga complexes in patients and CD89 transgenic mice. *J. Exp. Med.* **191**, 1999–2009 (2000).

29. van Egmond, M., Hanneke van Vuuren, A. J. & van de Winkel, J. G. The human Fc receptor for IgA (Fc alpha RI, CD89) on transgenic peritoneal macrophages triggers phagocytosis and tumor cell lysis. *Immunol. Lett.* **68**, 83–87 (1999).

30. van Egmond, M. *et al.* Human immunoglobulin A receptor (FcalphaRI, CD89) function in transgenic mice requires both FcR gamma chain and CR3 (CD11b/CD18). *Blood* **93**, 4387–4394 (1999).

31. Shimokawa, T. & Ra, C. C/EBP alpha and Ets protein family members regulate the human myeloid IgA Fc receptor (Fc alpha R, CD89) promoter. *J. Immunol.* **170**, 2564–2572 (2003).

32. Otten, M. A., Groenveld, I., van de Winkel, J. G. J. & van Egmond, M. Inefficient antigen presentation via the IgA Fc receptor (FcalphaRI) on dendritic cells. *Immunobiology* **211**, 503–510 (2006).

33. Stockmeyer, B. *et al.* Triggering Fc alpha-receptor I (CD89) recruits neutrophils as effector cells for CD20-directed antibody therapy. *J. Immunol.* **165**, 5954–5961 (2000).

34. Van Spriel, A. B., Leusen, J. H. W., Vilé, H. & Van De Winkel, J. G. J. Mac-1 (CD11b/CD18) as accessory molecule for Fc alpha R (CD89) binding of IgA. *J. Immunol.* **169**, 3831–3836 (2002).

35. Evers, M. *et al.* Novel chimerized IgA CD20 antibodies: Improving neutrophil activation against CD20-positive malignancies. *MAbs* **12**, 1795505 (2020).

36. Evers, M. *et al.* Anti-GD2 IgA kills tumors by neutrophils without antibody-associated pain in the preclinical treatment of high-risk neuroblastoma. *J. Immunother. cancer* **9**, (2021).

37. Chai, C. K. Selection for leukocyte counts in mice. *Genet. Res.* **8**, 125–142 (1966).

38. Hensel, J. A., Khattar, V., Ashton, R. & Ponnazhagan, S. Characterization of immune cell subtypes in three commonly used mouse strains reveals gender and strain-specific variations. *Lab. Invest.* **99**, 93–106 (2019).

39. Ashworth, L. K. *et al.* An integrated metric physical map of human chromosome 19. *Nat. Genet.* **11**, 422–427 (1995).

40. van Vuuren, A. J., van Egmond, M., Coenen, M. J., Morton, H. C. & van de Winkel, J. G. Characterization of the human myeloid IgA Fc receptor I (CD89) gene in a cosmid clone. *Immunogenetics* **49**, 586–589 (1999).

41. de Vree, P. J. P. *et al.* Targeted sequencing by proximity ligation for comprehensive variant detection and local haplotyping. *Nat. Biotechnol.* **32**, 1019–1025 (2014).

42. Li, H. & Durbin, R. Fast and accurate short read alignment with Burrows-Wheeler transform. *Bioinformatics* **25**, 1754–1760 (2009).

43. Stip, M. C. *et al.* IgA antibody immunotherapy targeting GD2 is effective in preclinical neuroblastoma models. *J. Immunother. cancer.* **11**, e006948 (2023).

44. Vanhoutteghem, A. *et al.* Basonuclin 2 has a function in the multiplication of embryonic craniofacial mesenchymal cells and is orthologous to disco proteins. *Proc. Natl. Acad. Sci. U. S. A.* **106**, 14432–14437 (2009).

45. Treffers, L. W. *et al.* IgA-Mediated Killing of Tumor Cells by Neutrophils Is Enhanced by CD47-SIRPα Checkpoint Inhibition. *Cancer Immunol. Res.* **8**, 120–130 (2020).

46. Baumann, N. *et al.* Myeloid checkpoint blockade improves killing of T-acute lymphoblastic leukemia cells by an IgA2 variant of daratumumab. *Front. Immunol.* **13**, 949140 (2022).

47. Chan, C. *et al.* Targeting Myeloid Checkpoint Molecules in Combination With Antibody Therapy: A Novel Anti-Cancer Strategy With IgA Antibodies? *Front. Immunol.* **13**, 932155 (2022).

48. Bruhns, P. & Jönsson, F. Mouse and human FcR effector functions. *Immunol. Rev.* **268**, 25–51 (2015).

49. Sagiv, J. Y. *et al.* Phenotypic diversity and plasticity in circulating neutrophil subpopulations in cancer. *Cell Rep.* **10**, 562–573 (2015).

50. Aleyd, E., Heineke, M. H. & van Egmond, M. The era of the immunoglobulin A Fc receptor FcαRI; its function and potential as target in disease. *Immunol. Rev.* **268**, 123–138 (2015).

51. Vanhoutteghem, A. *et al.* The importance of basonuclin 2 in adult mice and its relation to basonuclin 1. *Mech. Dev.* **140**, 53–73 (2016).

52. Corteling, R., Wyss, D. & Trifilieff, A. In vivo models of lung neutrophil activation. Comparison of mice and hamsters. *BMC Pharmacol.* **2**, 1 (2002).

53. Lorenzo, M. E. *et al.* Antibody responses and cross protection against lethal influenza A viruses differ between the sexes in C57BL/6 mice. *Vaccine* **29**, 9246–9255 (2011).

54. Klein, S. L. & Flanagan, K. L. Sex differences in immune responses. *Nat. Rev. Immunol.* **16**, 626–638 (2016).

55. Gupta, S. *et al.* Sex differences in neutrophil biology modulate response to type I interferons and immunometabolism. *Proc. Natl. Acad. Sci. U. S. A.* **117**, 16481–16491 (2020).

56. Shultz, L. D. *et al.* Multiple defects in innate and adaptive immunologic function in NOD/LtSz-scid mice. *J. Immunol.* **154**, 180–191 (1995).

57. Takenaka, K. *et al.* Polymorphism in Sirpa modulates engraftment of human hematopoietic stem cells. *Nat. Immunol.* **8**, 1313–1323 (2007).

58. Zhang, D. *et al.* Neutrophil ageing is regulated by the microbiome. *Nature* **525**, 528–532 (2015).

SUPPLEMENTAL INFORMATION

Primer set	Name/VP	Direction	Binding position		Sequence
			FCAR-chr19	*LAWRIST16*	
1	set1	RV	2,357	-	ATTCCAGCCTCTAAGTCTCT
	set1	FW	2,713	-	GATCACAAGGTCAGGAGATC
2	set2	RV	13,021	-	GGACTCGATTTGGCAGATAT
	set2	FW	13,172	-	CTGATCCTGAGTTCGTCATT

Table S1 | Primers used in TLA analysis

Marker	Fluorochrome	Clone	Dilution	Company
Human CD89	PE	A59	1:50	BD
CD45	BV510	30-F11	1:200	Biolegend
Ly6C	APC-Cy7	HK1.4	1:200	Biolegend
Ly6G	PE-Cy7	1A8	1:400	Biolegend
Siglec F (CD170)	BV421	S17007L	1:100	Biolegend
CD3e	APC	145-2C11	1:200	eBioscience
B220	FITC	RA3-6B2	1:100	Biolegend

Table S2 | Panel of fluorophore-conjugated antibodies for analysis of CD89 expression and phenotyping of circulating immune cells with flow cytometry

Marker	Fluorochrome	Clone	Dilution	Company
CD45	BV510	30F11	1:200	Biolegend
CD11b	FITC	M1/70	1:50	BD
Ly6C	APC-Cy7	HK1.4	1:200	Biolegend
Ly6G	PE	1A8	1:400	Biolegend
Siglec F (CD170)	BV421	S17007L	1:100	Biolegend
SIRPα (CD172a)	PerCP/Cy5.5	P84	1:50	Biolegend

Table S3 | Panel of fluorophore-conjugated antibodies for analysis of CD11b and SIRPα expression with flow cytometry

Marker	Fluorochrome	Clone	Dilution	Company
CD45	BV711	30F11	1:200	Biolegend
Ly6C	PerCP-Cy5.5	HK1.4	1:100	Biolegend
Ly6G	PE-Cy7	1A8	1:400	Biolegend
Siglec F (CD170)	BV421	S17007L	1:100	Biolegend
mFcγRI	PE	X54-5/7.1	1:50	Biolegend
mFcγRII/III	FITC	2.4G2	1:100	BD
mFcγRIV	BV511	9E9	1:100	Biolegend

Table S4 | Panel of fluorophore-conjugated antibodies for analysis of FcγR expression with flow cytometry

Marker	Fluorochrome	Clone	Dilution	Company
CD45	BV510	30F11	1:200	Biolegend
CD11b	FITC	M1/70	1:50	BD
F4/80	BV781	BM8	1:200	Biolegend
Human CD89	PE	A59	1:50	BD
Ly6C	PerCP-Cy5.5	HK1.4	1:100	Biolegend
Ly6G	PE-Cy7	1A8	1:200	Biolegend
Siglec F (CD170)	BV421	S17007L	1:50	Biolegend

Table S5 | Panel of fluorophore-conjugated antibodies for tumor analysis with flow cytometry

Breakpoint	Order	Sequence
1	chr10:24,031,978 (head) fused to hg38 chr19:54,852,450-54,852,551, fused to chr4:84,405,464 (head)	AAAGGAAAAATCTACCAAGAAGAGTTCTCAGTTCTGAACATCTATGCTTCAA ATGCAAGGGCACCCACATTCATAAAAGAAACTTAACTAAAGCTCAAAGCAC ACAATGATGGCTACATTGTAAACCCTGGAGCCTGTGACTATTTATGTTATAG GGCAGGGGACTGAAGGGGAAGGTGGAGCTCAGGTTGTTGATGAGTTGAC CTTGATACAACTTTAGAAATTTTTCTTAGATCTAACAGAGATGCTGGTATGTA ACTAGACAGAATACTTCTTACTGATAATTTTACAACCTAGTTTTTTTTAAGAC AGGCTCTCCAAAAT
2	chr4:84,406,787 (tail) fused to LAWRIST16-vector Vector:544-615 fused to FCAR-chr19 Vector: 19,982 (tail)	CACAGCCAAGATAAACCGGTACAAAACTCCACTCTGAAGCACACCCCCTTCC ACACTGCACTTTGAAAGACTCTGTTTTTGTCTCTGAGATGGGGTCTCAAGTA TTCCAGGCTGTGCTCAAACTCACCATTAAGCGGGCTAATTCGCCTCGAGGTG GCTTATCGAAATTAATACGACTCACTATAGGGAGACCCAAGCTTAGGATCAC CCTGAGGTCAGAAGTTTGTGACCAGCTTGGCCAACATGGCGAAACCCGTC
3	chr4:84,404,993 (tail) fused to hg38 chr19:54,852,578 (head)	TGTCCCCTCCTGGCTCCCTGGCACAGTAGGAGGGTGGCTTCACAGGGAG ACTTGCCTCCTGTAGGAGACACTCAGTGGGGAATTGCTCCTCAGGCATG AACAGGGTCCTGCTGGGCTCAGTGTAATCACAAGGGTCCGCGTGAGAG GTGGAGGAAGAGGGGAGTGGGGATTAGAGCAGTGTAGTGGGAGGGA GACGCTATCAGCCACTGTGGGCTTTGAAGG
4	chr10:24,031,972 (tail) fused to chr4:84,405,000-84,405,416 fused to chr4:84,422,506 (head)	GTTAGATCCATTTGGTTCATAACTTCTGTTAATTTCACAGTGTCTCTGTTT AGTTTCTGTTTCTATGATCTGTCCATTGCTGAGAGTGGGATGTTGAAGT CTCCCAATATTATTGTGTGGGGTGCACAGGAAAGGCCACACAAGTCCC ATACTGTGGAAATGCTACAATGGGAAGCTCTAGGGAGACTTCACAGTG ACCAAAGAGAGACTAGAGCCTGAACTGAGGCTTTCTGGTTGTCCGATC AGTTCTAACCACTCTGCTAGTAATCCATTTTCAACCTAAGACTGGGTTAT CTAAGTTTATGTTATGCACAGATAGCCTATCACAGCATGGCTATAGAAA GAGGATTCTAGAGTTTGGCCTTGAACTAACTATGAGAGGAAGGATGAC CTTGAACAATCGATCCTCCAGCTTCTACCTCCTGAGCACAGGAATTGTA GACTTGCCCTGCTTTATGTGGTGTTGGGGAATCTAGTACTTTGTGCAGG GCAAGCAAGACCAGTACCAGCTGAACTACAGCCCCAGGCCTCAACATA CTTTTTAAAAAAAACTACTTCAGTCTAGAAACTAATTAAGTGTGGGGGA GGAAGCAAAGAGAGAAGCCCCTAAACTTACGGGTGTATCATTATACAT GACTCTGAATATTCCTATGTCTGTGTGAATACCTAAACAGGGAG

Table S6 | Breakpoint sequences found in BALB/c and NXG mice using TLA analysis. Sequences of human chromosome 19 (including the hCD89 insert) are depicted in red, LAWRIST16 vector sequences in orange, mouse chromosome 4 in blue, mouse chromosome 10 in green and homologous bases are in purple.

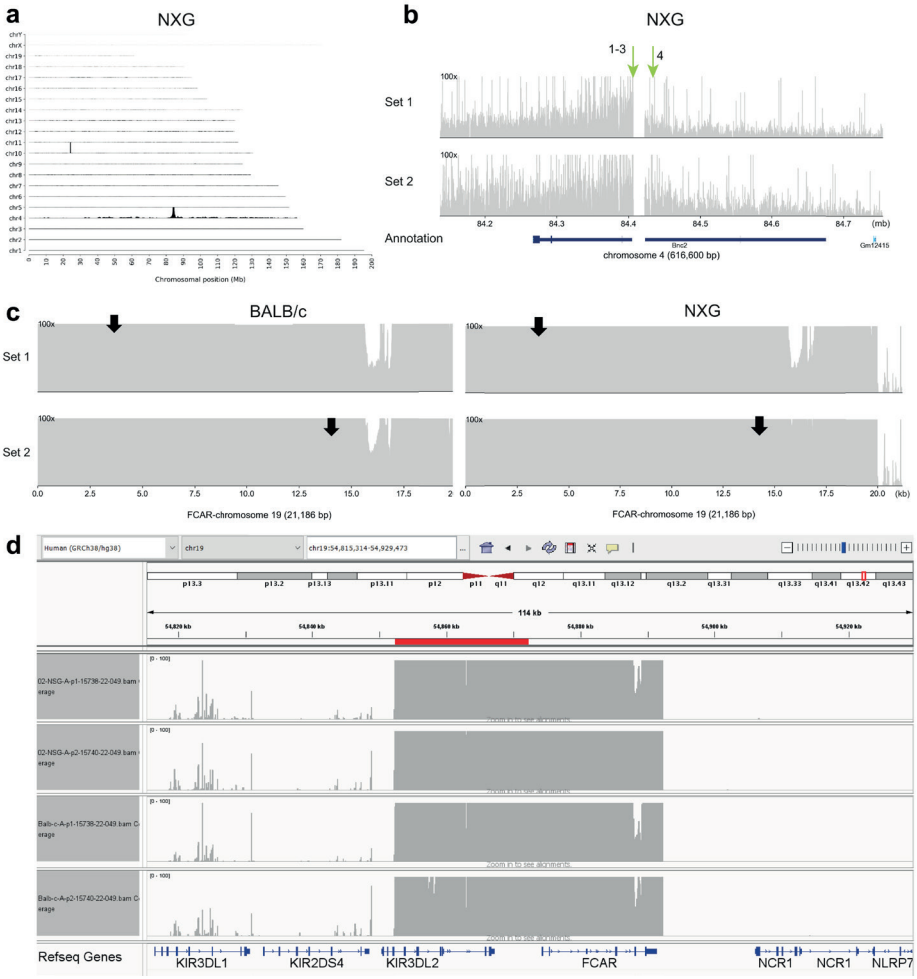

Figure S1 Determination of gene integration site and copy number (**A**) Coverage of TLA sequence across the whole mouse genome with primer set 1 in the NXG sample. (**B**) Coverage of TLA sequence across the vector integration site in the NXG sample. Green arrows indicate the location of breakpoint sequences and genomic rearrangement. (**C**) Coverage of Next Generation Sequencing across the hCD89 insert for both BALB/c and NXG samples. (**D**) TLA sequence coverage across the human chromosome 19. The green bar represents the human *FCAR* gene, the red bar additional integrated sequences of chromosome 19. The orange arrow indicates the breakpoint with the LAWRIST16 vector.

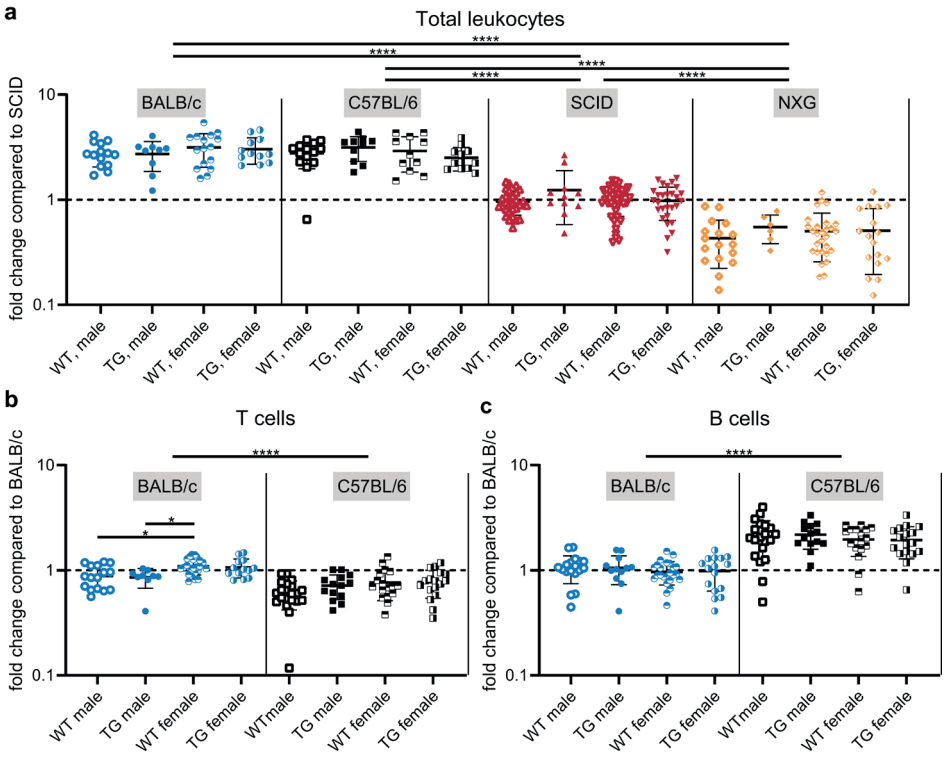

Figure S2 | Comparison of total leukocyte and T and B cell numbers in the circulation of WT and hCD89 TG mice Blood was obtained from both female and male, WT and hCD89 TG mice from all 4 strains. Antibody staining and subsequent flow cytometry analyses were performed to determine the number of (**A**) total leukocytes, (**B**) T cells and (**C**) B cells. Pooled data from at least 9 experiments. For total leukocytes, data from SCID mice were standardized and data from other strains was related to SCID mice. For T and B cells data was related to BALB/c mice. First, means of mice within a strain were compared and secondly all mice from each strain were pooled and compared using Two-Way ANOVA with Tukey's post-hoc test.

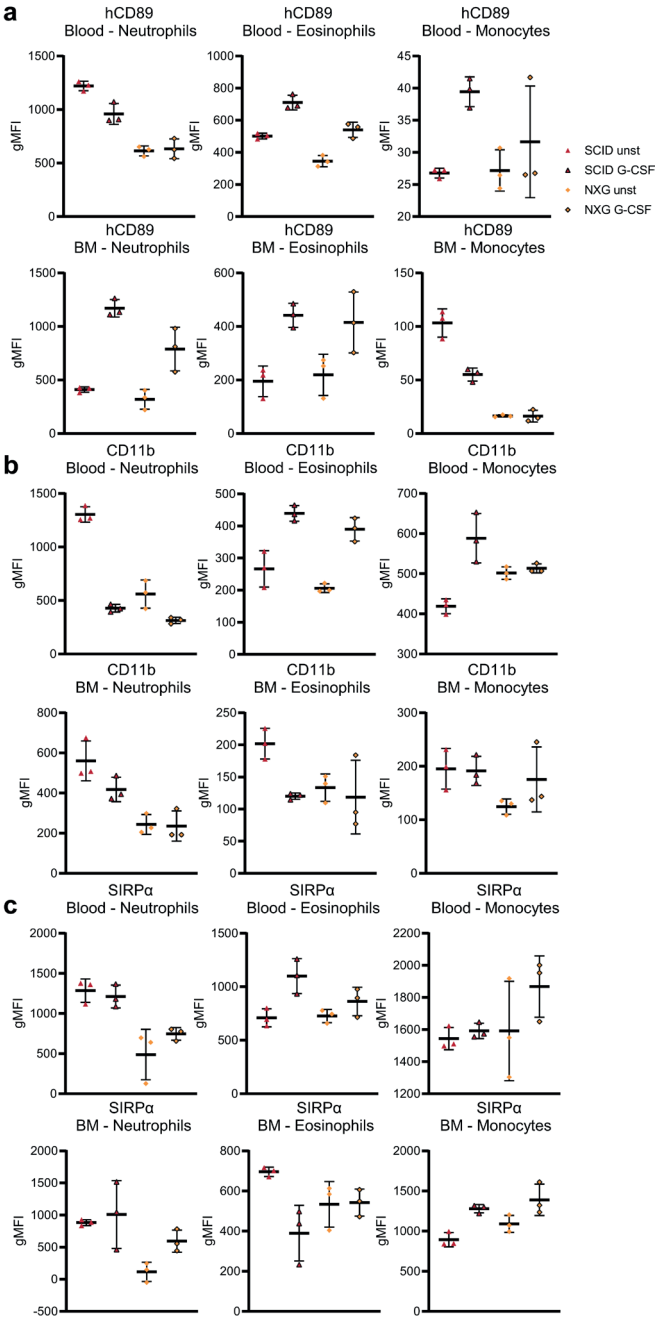

Figure S3 | CD89, CD11b and SIRPα expression in myeloid cells in peripheral blood and bone marrow
Blood and bone marrow was obtained from either PEG-G-CSF or unstimulated male hCD89 TG mice from 4 mouse strains. Antibody staining and subsequent flow cytometry analyses were performed to determine expression of (**A**) CD89, (**B**) CD11b and (**C**) SIRPα on neutrophils, eosinophils and monocytes. Unst = unstimulated.

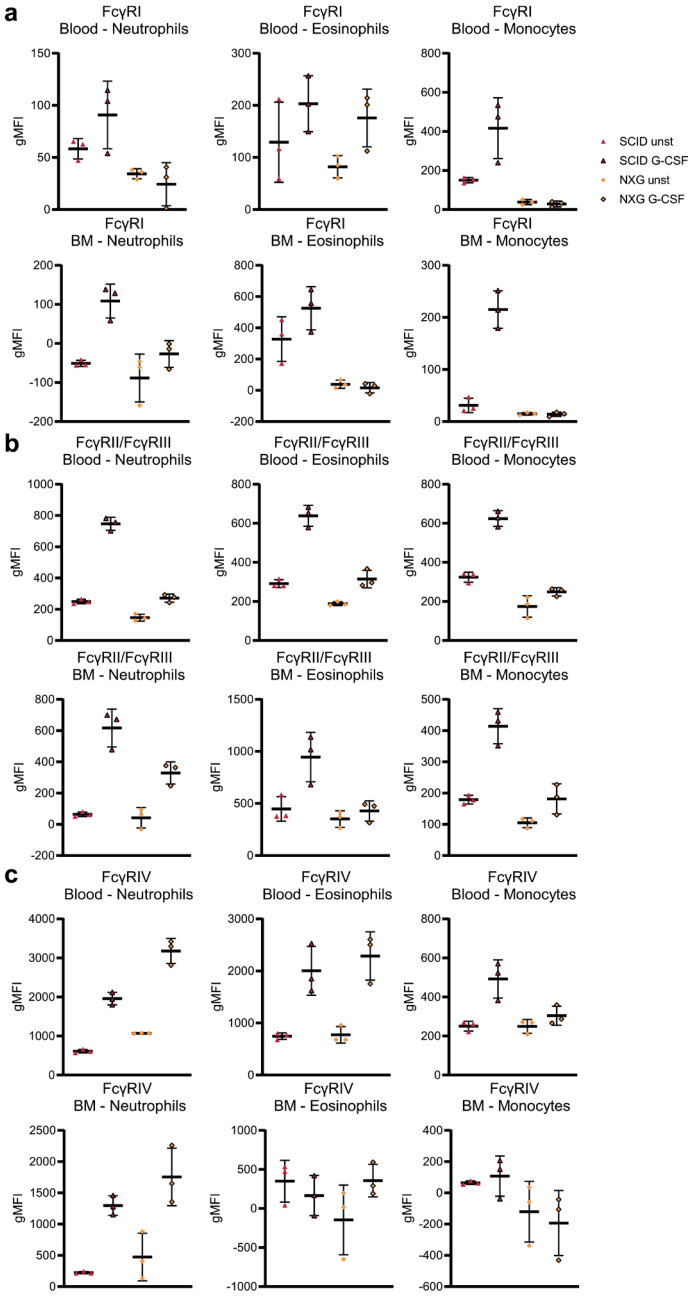

Figure S4 | FcγR expression in peripheral blood and bone marrow-derived myeloid cells Blood and bone marrow was obtained from either PEG-G-CSF or unstimulated male hCD89 TG mice from 4 mouse strains. Antibody staining and subsequent flow cytometry analyses were performed to determine expression of (**A**) FcγRI, (**B**) FcγRII/FcγRIII and (**C**) FcγRIV on neutrophils, eosinophils and monocytes. Unst = unstimulated.

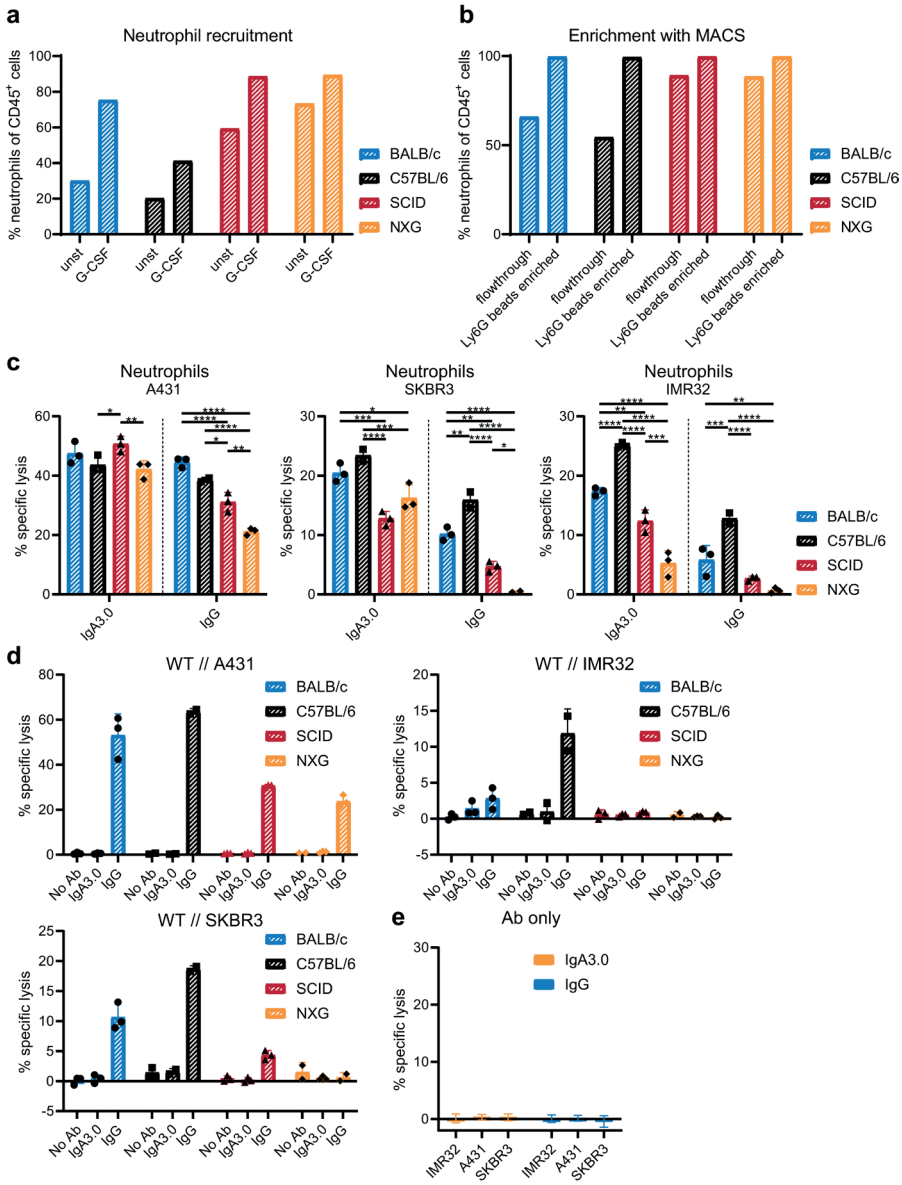

Figure S5 | Validation of neutrophil isolation and comparison of neutrophil ADCC between strains (**A**) Blood from PEG-G-CSF and unstimulated mice was collected and antibody staining and subsequent flow cytometry analyses were performed to determine the number of neutrophils in the circulation. (**B**) Cells in the flowthrough and enriched fraction after Ly6G MACS isolation were stained and analyzed by flow cytometry to validate neutrophil purity. (**C**) ^{51}Cr-release assays against 3 different targets/cell lines comparing IgA3.0- or IgG-mediated ADCC of isolated neutrophils from (**D**) 4 different hCD89 TG mouse strains and (**D**) WT mice. (**E**) IgA3.0 and IgG antibody only control in ^{51}Cr-release assays against 3 different targets/cell lines.

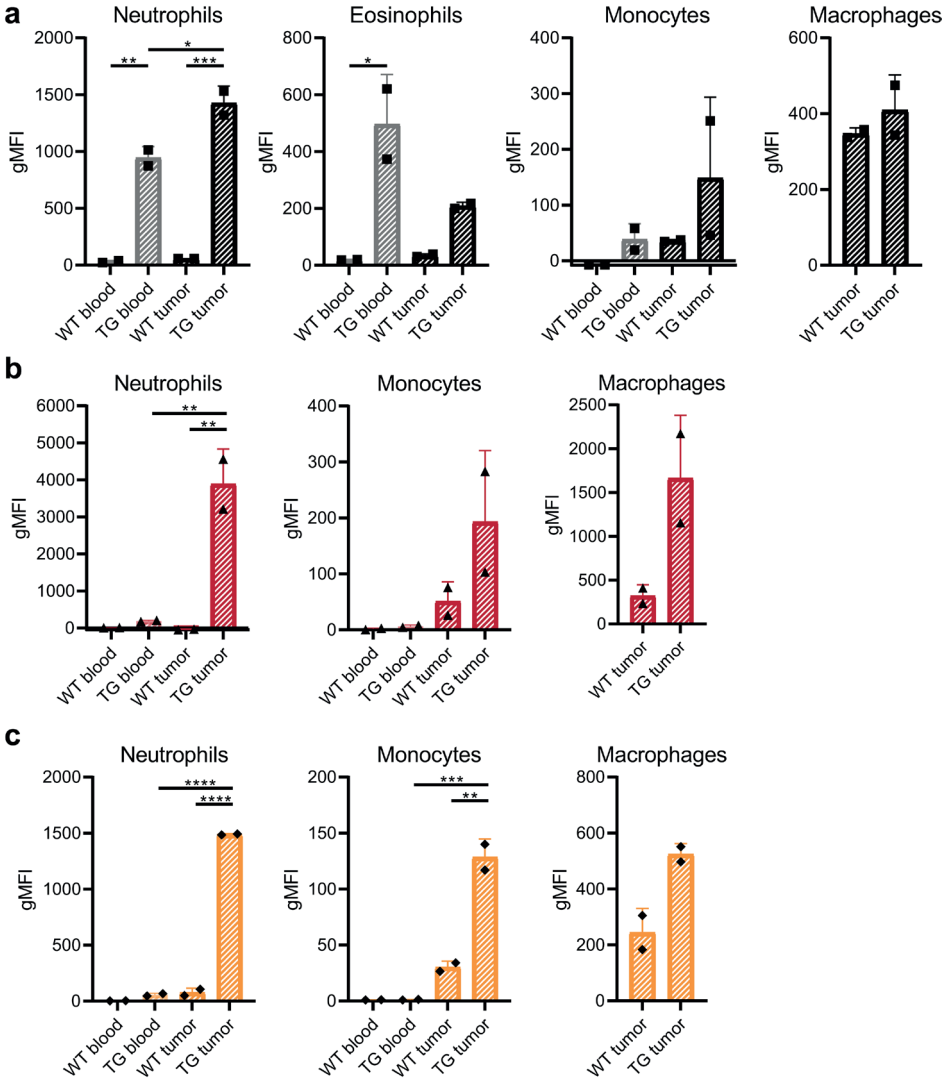

Figure S6 | CD89 expression on myeloid cells in the tumor microenvironment (**A**) Intraperitoneal 9464D-GD2 neuroblastoma in C57BL/6 mice was established by injecting $0.5*10^6$ 9464D-GD2 cells intraperitoneally. CD89 expression on myeloid cell subsets in the circulation and tumor was determined on day 27 by flow cytometry. Subcutaneous IMR32 human xenograft tumors were established in both (**B**) SCID and (**C**) NXG mice by injecting $2.5*10^6$ IMR32 cells subcutaneously. CD89 expression on myeloid cell subsets in the circulation and tumor was determined on day 51 by flow cytometry. Means of neutrophils, eosinophils and monocytes were compared using a One-Way ANOVA with Tukey's post-hoc test and means of macrophages were compared using an unpaired t-test. WT = wildtype, TG = transgenic.


2

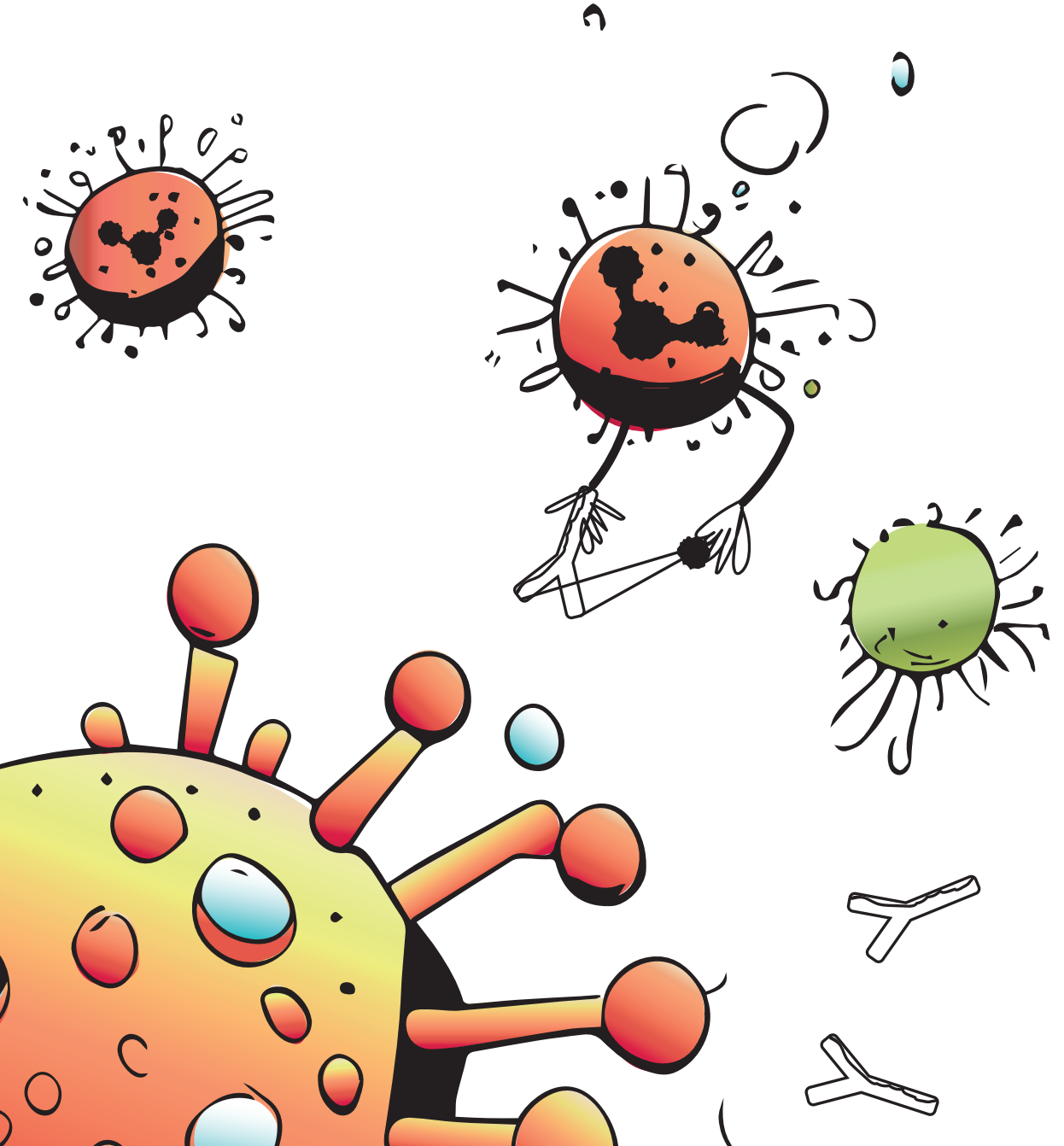

Chapter 3.

Effective, long-term, neutrophil depletion using a murinized anti-Ly-6G 1A8 antibody

Patricia A. Olofsen[1], Marjolein C. Stip[1], J. H. Marco Jansen[1], Chilam Chan[1], Maaike Nederend[1], Ralph G. Tieland[1], Maria Tsioumpekou[1] and Jeanette H. W. Leusen[1]

Affiliations

1. Center for Translational Immunology, UMC Utrecht, Heidelberglaan 100, 3584 CX Utrecht, The Netherlands

Published in Cells, 2022

ABSTRACT

Neutrophils are crucial innate immune cells but also play key roles in various diseases, such as cancer, where they can perform both pro- and anti-tumorigenic functions. To study the function of neutrophils *in vivo*, these cells are often depleted using Ly-6G or Gr-1 depleting antibodies or genetic "knockout" models. However, these methods have several limitations, being only partially effective, effective for a short term, and lacking specificity or the ability to conditionally deplete neutrophils. Here, we describe the use of a novel murinized Ly-6G (1A8) antibody. The murinized Ly-6G antibody is of the mouse IgG2a isotype, which is the only isotype that can bind all murine Fcγ receptors and C1q and is, therefore, able to activate antibody-dependent cellular cytotoxicity (ADCC), antibody-dependent phagocytosis (ADCP) and complement-dependent cytotoxicity (CDC) pathways. We show that this mouse-Ly-6G antibody shows efficient, long-term, and near-complete (>90%) neutrophil depletion in the peripheral blood of C57Bl6/J, Balb/c, NXG and SCID mice for up to at least four weeks, using a standardized neutrophil depletion strategy. In addition, we show that neutrophils are efficiently depleted in the blood and tumor tissue of IMR32 tumor-bearing SCID mice, analyzed six weeks after the start of the treatment.

Keywords

Neutrophils, Neutrophil depletion, *In vivo* neutrophil targeting, Immunotherapy, Cancer

INTRODUCTION

Neutrophils are the most abundant immune cells in the human body, comprising 50–70% of the white blood cell population in the circulation. They are essential for innate immune reactions but also play key roles in tumorigenesis, where they can perform both pro- and anti-tumorigenic functions[1–4]. To study the *in vivo* function of neutrophils, Ly-6G (clone 1A8) or Gr-1 (clone RB6-8C5) depleting antibodies are frequently used. Over the years, it has become clear that both these antibodies show efficacy problems, with depletion being only partially effective, transient, or lacking specificity[5–7]. The misinterpretation of results is observed in many studies due to the usage of the same antibody clone for both depletion and detection, thereby blocking the epitope for staining, resulting in false-negative results. In addition, whereas Ly-6G is only present on neutrophils, Ly-6C, the other receptor recognized by the Gr-1 antibody, can also be found on subsets of monocytes, macrophages, dendritic cells, and lymphocytes[8–10]. Besides the differences in target specificity, Ly-6G and Gr-1 antibodies differ in isotype and efficacy. While the Gr-1 antibody is a rat IgG2b, described to work via the fast-acting complement-dependent cytotoxicity (CDC) pathway[11,12], Ly-6G is a rat IgG2a antibody, shown to mediate neutrophil

killing through “slow” Fc-dependent antibody-dependent cellular cytotoxicity (ADCC) and antibody-dependent phagocytosis (ADCP) by monocytes and macrophages, making the neutrophil depletion less efficient[13]. Also, since both depletion antibodies are of rat origin, mouse anti-rat antibodies produced by the mice play a role in reduced efficacy, where increased clearance of the injected depletion antibodies is observed after one week of treatment[14].

In recent years, various suggestions have been made to overcome some of the problems observed with Ly-6G and Gr-1 depletion antibodies. Boivin et al. described a double antibody-based depletion strategy using Ly-6G and an additional anti-rat IgG2a antibody to facilitate an “isotype switch,” resulting in a 90% decrease in blood neutrophil numbers[14]. Others have tried to generate genetic neutrophil “knockout” models by targeting various key components of neutrophils (e.g., *CSF3R*, *CXCR2*, *GFI1*), resulting in only partial (60–90%) depletion of mature neutrophil subsets[15–18]. In addition to being partially effective, the majority of these genetic models are constitutive, and neutrophils can only be added to the equation by performing bone marrow transplantations.

Here we describe the use of a murinized version of the Ly-6G 1A8 antibody (hereafter referred to as mouse-Ly-6G), which has the same variable region of the fragment antigen-binding (Fab) domain as the original rat-Ly-6G 1A8 antibody but is of the mouse IgG2a isotype. Mouse IgG2a is the only isotype that can bind all murine Fcγ receptors, where it binds with high affinity to the activating FcγRI and FcγRIV receptors and has low affinity for FcγRIII and the inhibitory FcγRIIb receptor, making it the ideal isotype to induce ADCC and ADCP[19]. In addition, IgG2a can efficiently bind C1q, thereby activating the complement pathway and inducing CDC[20]. Due to the design of the mouse-Ly-6G antibody, it has the potential to show high specificity (since Ly-6G is only present on neutrophils), high efficacy (it should be able to activate ADCC, ADCP, and CDC), and be able to work more long-term (no mouse anti-rat antibodies will be produced, preventing clearance of the injected antibody). Here we describe an optimized and standardized neutrophil depletion strategy and show that the mouse-Ly-6G antibody shows efficient, long-term, and near-complete (>90%), neutrophil depletion in the peripheral blood of C57Bl6/J, Balb/c, NXG and SCID mice for up to four weeks. In addition, we show that neutrophils can be efficiently depleted in the blood and tumor tissue of IMR32 tumor bearing SCID mice, even six weeks after the start of the treatment.

METHODS

Mice

Mice were maintained in the animal facility of the University of Utrecht. Experiments were conducted using C57Bl/6J (C57Bl/6JRj), Balb/c (Balb/cByJRj), NXG (NOD.*Prkdc*^{scid} *Il2rg*^{tm1}/

Rj), SCID (NOD.CB17-*Prkdc*$^{scid/scid}$/Rj), and human FcαRI (CD89) transgenic SCID mice (all housed and bred at Janvier Labs, Paris, France)[21], or C57Bl/6J *FcRγ*$^{-/-}$ (C57Bl/6JRj FcRγ-chain knockout) mice (housed and bred at the University of Utrecht)[22]. Mice were housed in groups under a 12:12 light–dark cycle, with food and water available ad libitum. Mice were randomized based on age, and both treatment and analysis were performed blind. Upon transfer to Utrecht, mice were acclimatized for at least 1 week prior to the start of the experiment.

All experiments were performed in accordance with international guidelines and approved by the National Central Authority for Scientific Procedures on Animals (CCD) and the local experimental animal welfare body (AVD115002016410).

Neutrophil depletion

Mice were injected intra-peritoneally (i.p.) with 25, 50, or 100 µg mouse-Ly-6G, 50 or 100 µg rat- Ly-6G, or solvent control (PBS) 3 times a week. The rat-Ly-6G (1A8) hybridoma has been sequenced by Absolute Antibody and transformed into a commercially available recombinant mouse antibody (see **Table 1** for more information on the depletion antibodies used). To evaluate neutrophil depletion, blood was drawn via cheek puncture before antibody injection and collected in Lithium-Heparin tubes (Sarstedt, #20.1345, Etten-Leur, the Netherlands). Blood was stored on ice to prevent internalization of CD115, a marker used for flow cytometry detection of monocytes.

Antigen	Species	Isotype	Company	Catalog number
Ly-6G (clone 1A8)	Mouse	IgG2a Kappa	Absolute Antibody	Ab00295-2.0
Ly-6G (clone 1A8)	Rat	IgG2a Kappa	Bio X Cell	BP0075-1_5 mg

Table 1 | Antibodies used to deplete neutrophils.

Flow cytometry

Myeloid cell composition and neutrophil depletion were assessed using the antibodies used in **Table 2**. To detect other leukocytes present in the blood, we used the antibodies shown in **Table 3**. For blood and tumor samples from IMR32 tumor-bearing mice, the antibodies depicted in **Table 4** were used. Additionally, TO-PRO-3 (Thermo Fisher, #10710194, Bleiswijk, the Netherlands) was added to tumor samples in a 1:50000 dilution to exclude dead cells.

Antigen	Fluorophore	Company	Catalog number	Dilution
CD11b	Alexa488	BD	557672	100×
GR-1 (clone RB6-8C5)	PE-Cy7	eBioscience	25-5931-82	200×
CD115	APC	Sony Biotechnology	1277550	200×
Ly-6C	APC-Cy7	Biolegend	128025	200×
Siglec-F/CD170	BV421	BD	562681	100×
CD45	BV510	Biolegend	103137	200×

Table 2 | Antibodies used to assess myeloid cell composition.

Antigen	Fluorophore	Company	Catalog number	Dilution
CD3e	PE	Biolegend	100308	200×
NK1.1	PerCP-Cy5.5	Biolegend	108727	100×
B220/CD45R	PE-Cy7	BD	561881	100×
CD11b	APC	eBioscience	17-0112-80	100×
Ly-6C	APC-Cy7	Biolegend	128025	200×
CD45	Pacific Blue	Biolegend	103126	200×
GR-1 (clone RB6-8C5)	Pacific Orange	Invitrogen	RM3030	100×

Table 3 | Antibodies used to detect other leukocytes.

Antigen	Fluorophore	Company	Catalog number	Dilution
CD11b	FITC	Pharmingen	553310	50×
Ly-6C	PerCP-Cy5.5	Biolegend	128012	100×
Ly-6G	PE-Cy7	Biolegend	127618	300×
Siglec-F/CD170	BV421	BD	562681	100×
CD45	BV510	Biolegend	103137	200×

Table 4 | Antibodies used to analyze blood and tumor samples of IMR32 tumor-bearing mice.

Antibodies were diluted in FACS buffer (PBS + 0.1% BSA + 0.1% sodium azide) and added to mouse blood in a 1:1 ratio (15 µL each). After 30–45-min incubation at 4 °C, 1 mL 1× FACS lysis solution (BD, #349202, 10× diluted in mQ) was added to wash away unbound antibodies and lyse the erythrocytes. Cells were lysed for 5–8 min at room temperature, followed by a centrifugation step (1800 rpm, 5 min, 4 °C). Cells were washed in 1 mL FACS buffer, centrifuged (1800 rpm, 5 min, 4 °C), and resuspended in 150 µL FACS buffer containing microsphere latex beads (Thermo Fisher, #11550696, Bleiswijk, the Netherlands,

3000×). For tumor samples, 2.5×10^6 tumor cells were stained in a 50 µL antibody mix for 30–45-min at 4 °C. After washing, cells were fixed in 4% paraformaldehyde.
Flow cytometry on blood samples was performed using a BD Canto II flow cytometer, while a BD LSR Fortessa was used to measure tumor samples. Data analysis was done using FlowJo (TreeStar, Ashland, OR, USA).

Neutrophil attraction model in IMR32 tumor bearing mice

SCID mice were injected subcutaneously (s.c.) with 2.5×10^6 IMR32 cells in a 1:2 mix of IMR32 cells in PBS and Vitrogel Hydrogel Matrix (Tebu Bio, #306VHM01, Heerhugowaard, the Netherlands). Tumor outgrowth was measured using a caliper (length × width × height). Twenty-eight days after the start of the experiment, mice were randomized into treatment groups based on tumor size and age, after which mice were treated i.p. with solvent control (PBS) or IgA ch14.18 antibodies in combination with a IgG1 PGLALA SIRPα-D1 fusion protein (produced as described before) to attract intratumoral neutrophils[23–25]. PBS and 25 mg/kg IgA ch14.18 antibodies were administered 3 times a week, while the SIRPα-D1 fusion protein was given every 9 days at a dose of 30 mg/kg. To induce neutrophil depletion, mice were treated with 100 µg mouse-Ly-6G 3 times a week. Blood was sampled at days 35, 42, 49, 56, 63, and 70 after tumor cell injection (days 7, 14, 21, 28, 35, and 42 after the start of the treatments) as described above and analyzed by flow cytometry.
Neutrophil infiltration in the tumor microenvironment was evaluated on day 70. Mouse tumors were carefully excised and collected in ice-cold PBS. Tumors were cut smaller and digested using the mouse tumor dissociation kit from Miltenyi (#130-096-730, Leiden, the Netherlands). Up to 1 g of tumor tissue was transferred to C tubes (Miltenyi, #130-096-334, Leiden, the Netherlands) containing enzyme mix (RPMI culture medium, 100 µL Enzyme D, 50 µL Enzyme R, and 10µL Enzyme A) and the 37C_m_TDK_1 program was run on a gentleMACS Octo Dissociator. After dissociation, cells were put through a 70 µm cell strainer in medium containing 10% FCS (Sigma), washed with FACS buffer, and stained for flow cytometry.

Quantification and statistical analysis

Data are presented as mean ± SEM. Comparison of multiple groups was performed using one-way ANOVA with Bonferroni correction, repeated measures one-way ANOVA with Bonferroni correction, or two-way ANOVA with Bonferroni correction. Statistical analyses were performed using GraphPad Prism 9.3.0 (GraphPad Software Inc., San Diego, CA, USA). A p-value < 0.05 was considered significant.

RESULTS

Mouse-Ly-6G depletes neutrophils more efficiently than rat-Ly-6G in C57Bl6/J mice

To investigate whether the mouse-Ly-6G antibody was able to efficiently deplete neutrophils, we decided to use old (>20 weeks) C57Bl6/J mice since these mice show high neutrophil-turnover and are the most refractory to rat-Ly-6G mediated neutrophil depletion[14]. 22–25 week-old mice were injected three times a week with two different concentrations (25 or 100 µg) of the mouse-Ly-6G antibody, 50 µg rat-Ly-6G 1A8 antibody, or solvent control (PBS) (**Figure 1A**). The eight mice per group were randomly divided into two subgroups to be able to draw blood three times a week (four mice per time point) and subsequently perform flow cytometric analysis of the leukocyte composition. First, hematopoietic cells were selected using CD45, followed by the exclusion of Siglec-F positive eosinophils and CD115 positive monocytes. To detect remaining neutrophils, we used the Gr-1 RB6-8C5 antibody clone (to prevent possible epitope masking of Ly-6G) in combination with CD11b staining and the specific forward and sideward scatter properties of neutrophils (**Figure 1B**). Analysis of the number of neutrophils per 5000 microsphere latex beads indicated that the rat-Ly-6G antibody did not result in efficient neutrophil depletion at most of the time points analyzed (**Figure 1B** and **Supplemental Figure 1B**), as was described previously[5,7,14]. In contrast, the lowest concentration of mouse-Ly-6G (25 µg) significantly depleted neutrophils at days 2, 4, 7, 11, and 22 after the start of the experiment, indicating that 25 µg mouse-Ly-6G can efficiently deplete neutrophils for up to one week, after which it is insufficient to compete with neutrophil production (**Figure 1D** and **Supplemental Figure 1C**). Increasing the concentration of the mouse-Ly-6G antibody to 100 µg per mouse resulted in an almost complete absence of neutrophils in the peripheral blood at all time points tested, indicating efficient long-term depletion up to four weeks (**Figure 1E** and **Supplemental Figure 1D, E**).

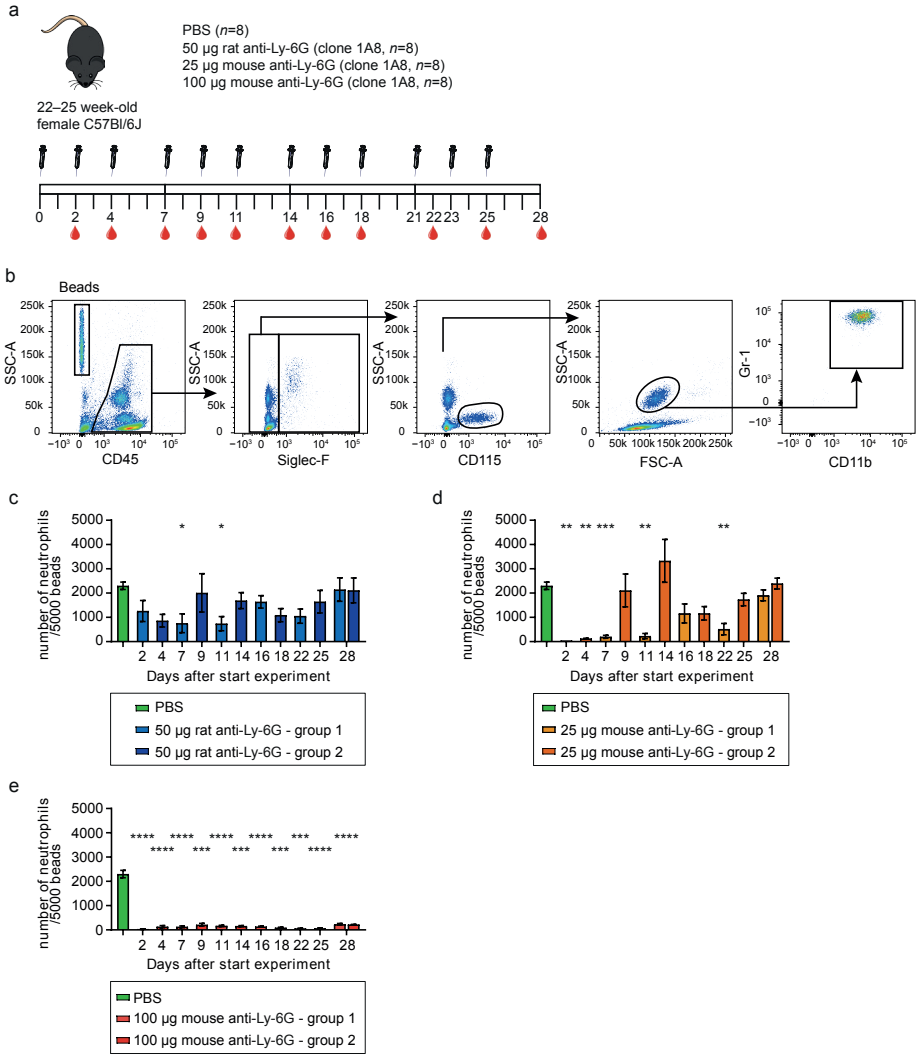

Figure 1 | Mouse-Ly-6G efficiently depletes neutrophils in old C57Bl6/J mice. (**A**) Experimental set-up; i.p. injections with the depletion-antibodies or vehicle control (PBS) were performed three times a week for four weeks. Blood was drawn via cheek puncture before injection with the antibodies; (**B**) FACS dot plots of a representative PBS-treated mouse, showing the gating strategy to retrieve the number of neutrophils per 5000 beads. First, the latex beads and $CD45^+$ cells were selected. From the $CD45^+$ population, Siglec-F and CD115 positive cells were excluded. Based on SSC/FSC profile, the neutrophils were selected and purity was confirmed using Gr-1 and CD11b positivity; (**C–E**) Longitudinal analysis of the number of $CD45^+$ Siglec-F^- $CD115^-$ SSC^{high} Gr-1^+ $CD11b^+$ neutrophils per 5000 beads in the peripheral blood (n = four mice per subgroup) showing (**C**) inefficient depletion with 50 µg rat-Ly-6G antibody; (**D**) efficient short-term depletion with 25 µg mouse-Ly-6G spanning the first week, and (**E**) efficient long-term depletion with 100 µg mouse-Ly-6G. Data is presented as mean with standard error of the mean (SEM). Statistics: one-way ANOVA with Bonferroni correction, * = $p < 0.05$, ** = $p < 0.01$, *** = $p < 0.001$, **** = $p < 0.0001$.

100 µg mouse-Ly-6G efficiently depletes neutrophils in C57Bl6/J, Balb/c, NXG and SCID mice

The promising results in C57Bl6/J mice tempted us to investigate whether neutrophils could also be depleted in other mouse strains, e.g., Balb/c, NXG, and SCID. Where C57Bl6/J and Balb/c mice are immunocompetent, SCID and NXG mice are immunodeficient. SCID mice depict a B- and T-cell deficiency, and NXG mice lack mature B-, T-, and NK-cells, show defective dendritic cells and macrophages due to impaired IL2R signaling, and lack hemolytic complement because of a 2-base pair deletion in the C5 structural gene[26,27].
Mice (*n* = 5 per strain) were injected three times a week with 100 µg mouse-Ly-6G antibody, and blood was analyzed once per week (**Figure 2A**). Flow cytometry analysis showed significant and almost complete depletion of neutrophils in all mouse strains, even the immunodeficient NXG mice that could not deplete antibodies via CDC (**Figure 2B** and **Supplemental Figure 2A–E**).

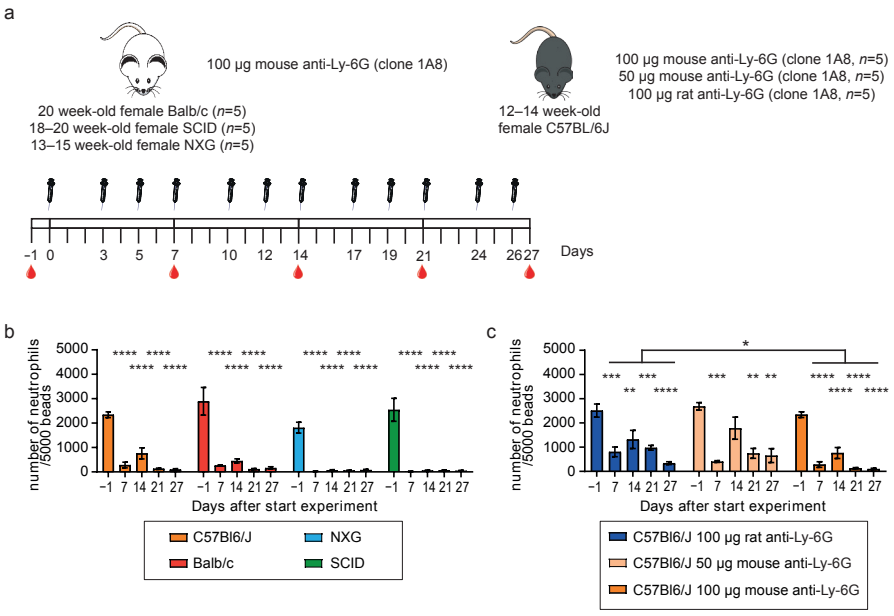

Figure 2 | Mouse-Ly-6G efficiently depleted neutrophils in C57Bl6/J, Balb/c, NXG, and SCID mice. (**A**) Experimental set-up; i.p. injections with the depletion antibodies were performed three times a week for four weeks. Blood was drawn via cheek puncture once a week before injection with the antibodies; (**B, C**) Longitudinal analysis of the number of CD45$^+$ Siglec-F$^-$ CD115$^-$ SSC^{high} Gr-1$^+$ CD11b$^+$ neutrophils in the peripheral blood (*n* = five mice per group) per 5000 latex beads, showing; (**B**) Significant, almost complete, neutrophil depletion in all mouse strains tested (C57Bl6/J, Balb/c, NXG, and SCID) upon treatment with 100 µg mouse-Ly-6G antibody, and (**C**) Significantly better neutrophil depletion in 100 µg mouse-Ly-6G treated C57Bl6/J mice than when treated with 100 µg rat-Ly-6G antibody. Data is presented as mean with SEM. Statistics: one-way ANOVA with Bonferroni correction. Repeated measures one-way ANOVA with Bonferroni correction was used to compare groups in **Figure 2C**, * = $p < 0.05$, ** = $p < 0.01$, *** = $p < 0.001$, **** = $p < 0.0001$.

To investigate whether the mouse-Ly-6G antibody was indeed outperforming the rat-Ly-6G antibody, we injected C57Bl6/J mice with 50 µg mouse-Ly-6G (compare to **Figure 1C**), 100 µg mouse-Ly-6G or 100 µg rat-Ly-6G. As shown in **Figure 2C**, 100 µg rat-Ly-6G injected mice showed significantly reduced numbers of neutrophils in the peripheral blood. However, the reduction was only partial and significantly less ($p = 0.04$) than when the same concentration of mouse-Ly-6G antibody was used. Of note, these mice were 12–14 weeks old, thereby ten weeks younger than the mice used in **Figure 1**, depicting lower neutrophil turnover, explaining why these mice were not completely refractory to rat-Ly-6G treatment[14]. Injecting mice with 50 µg mouse-Ly-6G did reduce the number of neutrophils in the peripheral blood, but the reduction was incomplete after one week, indicating that 100 µg mouse-Ly-6G is needed to efficiently deplete the excess neutrophils produced upon neutropenia.

Neutrophils can efficiently be depleted intratumorally in IMR32 tumor bearing mice

Multiple studies highlight the inefficiency of intratumoral neutrophil depletion using the rat-Ly-6G antibody[6,28]. To investigate whether the mouse-Ly-6G antibody is capable of efficient intratumoral neutrophil depletion, we injected SCID mice s.c. with 2.5×10^6 IMR32 cells in a 1:2 mix with Vitrogel Hydrogel Matrix. To attract neutrophils to the tumor site, mice were treated with a combination of IgA ch14.18 antibodies and an IgG1 PGLALA SIRPα-D1 fusion protein[29]. Other treatment groups consisted of vehicle control (PBS) and IgA/SIRPα-D1 in combination with 100 µg mouse-Ly-6G (**Figure 3A**). Flow cytometric analysis of the blood showed complete neutrophil depletion in the IgA/SIRPα-D1/mouse-Ly-6G treated mice until the end of the experiment, six weeks after the start of the treatment (**Figure 3B**). As expected, flow cytometric analysis of the tumor indicated a significant increase in the number of neutrophils when mice were treated with IgA/SIRPα-D1 (**Figure 3C**). Some neutrophils could be detected in the tumors of PBS-treated mice. However, in the IgA/SIRPα-D1/mouse-Ly-6G treated mice, neutrophils were completely absent, indicating that both the neutrophils attracted by the IgA/SIRPα-D1 treatment were ablated, as well as the neutrophils normally present in the tumors (**Figure 3C**).

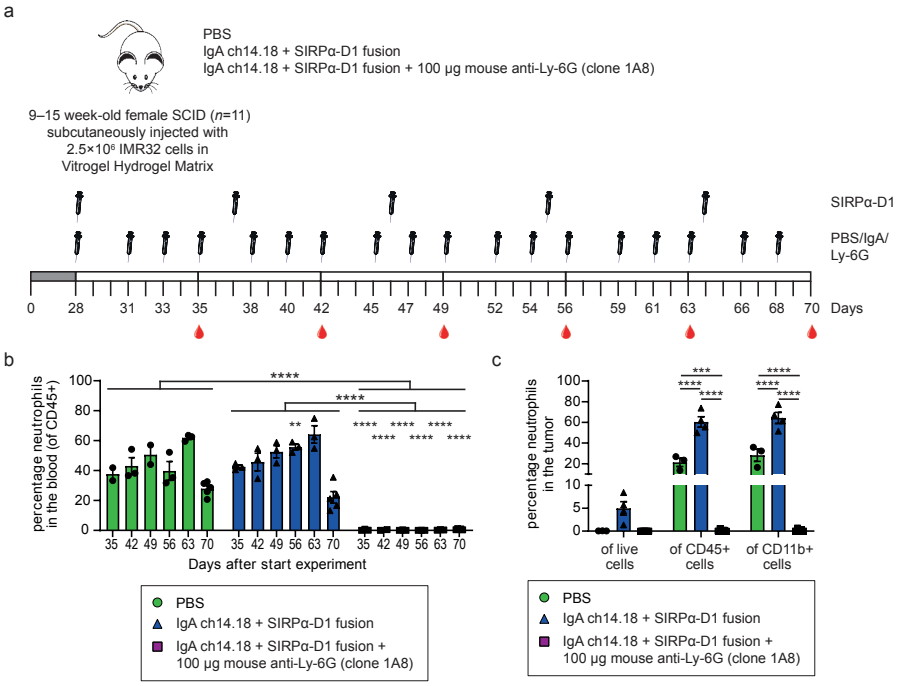

Figure 3 | Mouse-Ly-6G efficiently depletes neutrophils in the blood and tumor of IMR32 tumor-bearing SCID mice. (**A**) Experimental set-up; 2.5 × 10^6 IMR32 cells were s.c. injected in SCID mice in a 1:2 mix with Vitrogel Hydrogel Matrix. Tumors were established for 28 days, after which mice were randomized over the different treatment groups, and treatment was started. I.p. injections with PBS, IgA ch14.18, and mouse-Ly-6G were performed three times a week for six weeks. The SIRPα-D1 fusion protein was injected i.p. every nine days. Blood was drawn via cheek puncture once a week before injection with the antibodies; (**B**) Longitudinal analysis of the percentage of SSC^{high} Ly-$6C^{low}$ Ly-$6G^+$ $CD11b^+$ neutrophils in the peripheral blood (n = 2–5 mice per group) of the $CD45^+$ leukocyte population, showing complete neutrophil depletion upon treatment with 100 µg mouse-Ly-6G antibody. Of note; blood at day 70 was collected from the orbit and processed in a similar fashion as the tumor material, meaning cells were fixed at a later time point, possibly resulting in some neutrophil cell death; (**C**) Intratumoral analysis of the percentage of SSC^{high} Ly-$6C^{low}$ Ly-$6G^+$ $CD11b^+$ neutrophils of the live (TO-PRO-3 negative) cells, $CD45^+$ leukocytes, and $CD11b^+$ myeloid populations. Data showed increased tumor infiltration when the mice were treated with IgA ch14.18/SIRPα-D1 fusion, which was completely ablated when 100 µg mouse Ly-6G was added. Data is presented as mean with SEM. Statistics: one-way ANOVA with Bonferroni correction. Repeated measures one-way ANOVA with Bonferroni correction was used to compare groups in **Figure 3B**, ** = $p < 0.01$, *** = $p < 0.001$, **** = $p < 0.0001$.

Neutrophil depletion with mouse-Ly-6G is not solely complement- or Fc receptor-mediated

Neutrophil depletion with the rat-Ly-6G antibody is shown to be dependent on mononuclear phagocytosis but is facilitated by complement[30]. Since neutrophils were also efficiently depleted in NXG mice (**Figure 2B**), which - among other defects - did not show complement activity, the mouse-Ly-6G antibody should have been able to exert its function independent of complement[27]. Studies using allogeneic, species-matched antibodies concluded that

antibody-mediated cell depletion is complement-independent and mediated by monocytes and macrophages through the cooperation of multiple Fc receptors[31–33]. Hinting towards a role of these cells in neutrophil depletion was the observation that some of the 100 µg mouse-Ly-6G treated animals showed increased numbers of CD115^{+} monocytes (both Ly-6C positive and negative subsets) in the bloodstream, while this was not observed in rat-Ly-6G treated mice or with other leukocyte subsets (**Supplemental Figure 3A, B**). To investigate whether mouse-Ly-6G antibody-mediated cell depletion was mediated through the cooperation of multiple Fc receptors, we used gamma chain "knockout" mice (C57Bl/6J *FcRγ*$^{-/-}$; **Figure 4A**), which lack the Fc receptor gamma chain essential for, e.g., normal Fc receptor signaling, ADCC, and ADCP[22,34]. Treating *FcRγ*$^{-/-}$ mice with 100 µg mouse-Ly-6G resulted in a significant and almost complete depletion of neutrophils (**Figure 4B**), indicating that ADCC/ADCP was not the only mechanism of action. In line with this, the design of the mouse-Ly-6G, using an IgG2a isotype, suggests that this antibody could activate both ADCC/ADCP and CDC pathways, thereby possibly explaining why both NXG mice (no CDC) and *FcRγ*$^{-/-}$ mice (no ADCC and ADCP) showed efficient neutrophil depletion upon mouse-Ly-6G treatment, emphasizing the increased possibilities while using this antibody[19,20].

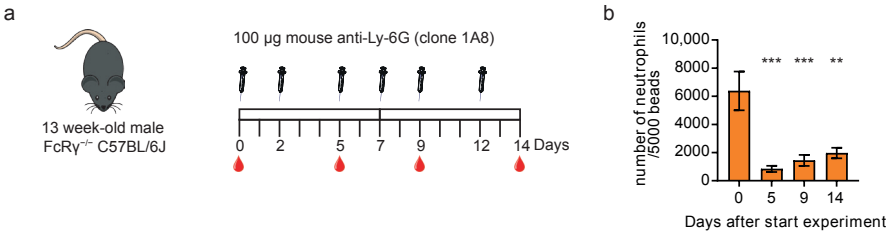

Figure 4 | Mouse-Ly-6G efficiently depletes neutrophils in FcRγ-deficient mice. (**A**) Experimental set-up; FcRγ$^{-/-}$ mice (n = 5) were i.p. injected three times a week with 100 µg mouse-Ly-6G antibody, and blood was drawn via cheek puncture before the start of the experiment, and at days 5, 9, and 14; (**B**): FcRγ$^{-/-}$ mice show depletion of the number of CD45^{+} Siglec-F^{-} CD115^{-} SSC^{high} Gr-1^{+} CD11b^{+} neutrophils in the peripheral blood (shown per 5000 latex beads) at all time points. Data is presented as mean with SEM. Statistics: one-way ANOVA with Bonferroni correction, ** = $p < 0.01$, *** = $p < 0.001$.

DISCUSSION

In this study, we evaluated the efficacy and specificity of the murinized Ly-6G 1A8 antibody as a tool to efficiently deplete neutrophils. By injecting C57Bl6/J, Balb/c, NXG, and SCID mice three times a week i.p., with 100 µg of the mouse-Ly-6G antibody, we showed efficient (>90%) neutrophil depletion for up to at least four weeks, while IMR32-tumor-bearing SCID mice showed neutrophil depletion for up to six weeks. The mouse-Ly-6G outperformed the

originally described rat-Ly-6G antibody and showed almost complete neutrophil depletion even in old C57Bl6/J mice, resistant to rat-Ly-6G antibody treatment[14].

Problems with the efficacy of the rat-Ly-6G antibody have clouded the results of many studies. Epitope masking by the injected depletion antibody has resulted in numerous false-negative results due to the usage of the same antibody clone for staining. In addition, the neutropenia achieved by using Ly-6G-depletion antibodies resulted in increased differentiation of myeloid progenitors present in the bone marrow, thereby producing more mature neutrophils and releasing them into the bloodstream[35]. The majority of cells that were present after Ly-6G treatment were shown to be newly made neutrophils, indicating that rat-Ly-6G depletion was not able to compensate for the increased neutrophil production[14]. In addition, the newly released neutrophils express lower levels of Ly-6G, making it more difficult to deplete and detect them[14]. Here, we describe a method to efficiently detect neutrophils by flow cytometry, not solely relying on Ly-6G expression. By excluding Siglec-F positive eosinophils and CD115 positive monocytes, neutrophils could be easily detected by their high sideward scatter (SSC) properties. Confirmation of the neutrophil phenotype with Gr-1 and CD11b expression shows >95% purity.

The Gr-1 antibody RB6-8C5 has shown fewer efficacy problems due to recognizing more antigens on the surface of neutrophils (Ly-6G and Ly-6C) while also being a rat IgG2a antibody functioning via the fast-acting CDC pathway, achieving ~90% reduction of peripheral blood neutrophils[14]. However, Gr-1 also targets Ly-6C positive subsets of monocytes, macrophages, dendritic cells, and lymphocytes, making it impossible, although often done, to draw conclusions about the role of neutrophils alone[8–10]. With the mouse-Ly-6G antibody, the best of both worlds was combined since depletion efficacy mimicked the Gr-1 RB6-8C5 antibody, while only Ly-6G-positive neutrophils were depleted, keeping the other leukocyte populations intact. In addition, by virtue of being a mouse IgG2a antibody, the mouse-Ly-6G can activate ADCC, ADCP, and CDC, therefore also being effective in models lacking one of these pathways. Furthermore, as a mouse antibody, the production of anti-rat antibodies was prevented, circumventing the problem of reduced efficacy due to increased clearance of the injected depletion antibodies. Due to this, it was possible to efficiently deplete neutrophils for at least four weeks using the same treatment regimen and emphasizing the importance of antibody species and isotypes.

A reliable, transient, long-term neutrophil depletion model is essential to study various functions of neutrophils, e.g., their role in tumor development and progression. In addition, neutrophils have been shown to play major roles in autoimmune diseases and IgA-mediated immunotherapy[36–39]. To really grasp the role neutrophils play in these diseases and therapies, it is important to be able to efficiently and reproducibly deplete neutrophils for the complete duration of the experiment. Using the treatment regimen described above, it is possible to efficiently deplete neutrophils in the peripheral blood for at least four weeks in C57Bl6/J, Balb/c, NXG, and SCID mice. IMR32 tumor-bearing

SCID mice showed efficient neutrophil depletion in blood and tumor tissue six weeks after the start of the treatment and ten weeks after the injection of the IMR32 tumor cells, making it possible to, e.g., study the role of neutrophils in tumor outgrowth, even after the tumor cells have engrafted. Therefore, the mouse-Ly-6G antibody is the perfect tool to conditionally, efficiently, and specifically deplete neutrophils in blood and tissue for a long period of time.

Acknowledgments

We thank the animal caretakers of the Utrecht University Animal Facility.

Author contributions

Conceptualization, P.A.O., M.C.S., J.H.M.J., C.C. and J.H.W.L.; methodology, P.A.O., M.C.S., J.H.M.J. and C.C.; formal analysis, P.A.O.; investigation, P.A.O., M.C.S., J.H.M.J., C.C., M.N., R.G.T. and M.T.; writing—original draft preparation, P.A.O.; writing—review and editing, M.C.S., J.H.M.J., C.C., M.N., M.T. and J.H.W.L.; visualization, P.A.O.; supervision, J.H.W.L.; funding acquisition, J.H.W.L. All authors have read and agreed to the published version of the manuscript.

Funding

This research was funded by Health~Holland, grant number LSHK19135, in collaboration with TigaTx B.V.

Competing interests

J.H.W.L. is co-founder of TigaTx B.V.

Ethical approval

The animal study protocols were approved by the National Central Authority for Scientific Procedures on Animals (CCD) and the local experimental animal welfare body of the Utrecht University (AVD115002016410, approval date 07-04-2016).

REFERENCES

1. Masucci, M. T., Minopoli, M. & Carriero, M. V. Tumor Associated Neutrophils. Their Role in Tumorigenesis, Metastasis, Prognosis and Therapy. *Front. Oncol.* **9**, 1146 (2019).

2. Musiani, P. *et al.* Role of neutrophils and lymphocytes in inhibition of a mouse mammary adenocarcinoma engineered to release IL-2, IL-4, IL-7, IL-10, IFN-alpha, IFN-gamma, and TNF-alpha. *Lab. Invest.* **74**, 146–157 (1996).

3. Schmielau, J. & Finn, O. J. Activated granulocytes and granulocyte-derived hydrogen peroxide are the underlying mechanism of suppression of t-cell function in advanced cancer patients. *Cancer Res.* **61**, 4756–4760 (2001).

4. Serafini, P., Borrello, I. & Bronte, V. Myeloid suppressor cells in cancer: recruitment, phenotype, properties, and mechanisms of immune suppression. *Semin. Cancer Biol.* **16**, 53–65 (2006).

5. Ma, C. & Greten, T. F. Editorial: 'Invisible' MDSC in tumor-bearing individuals after antibody depletion: fact or fiction? *Journal of leukocyte biology* vol. 99 794 (2016).

6. Moses, K. *et al.* Survival of residual neutrophils and accelerated myelopoiesis limit the efficacy of antibody-mediated depletion of Ly-6G+ cells in tumor-bearing mice. *J. Leukoc. Biol.* **99**, 811–823 (2016).

7. Pollenus, E. *et al.* Limitations of neutrophil depletion by anti-Ly6G antibodies in two heterogenic immunological models. *Immunology letters* vol. 212 30–36 (2019).

8. Hestdal, K. *et al.* Characterization and regulation of RB6-8C5 antigen expression on murine bone marrow cells. *J. Immunol.* **147**, 22–28 (1991).

9. Fleming, T. J., Fleming, M. L. & Malek, T. R. Selective expression of Ly-6G on myeloid lineage cells in mouse bone marrow. RB6-8C5 mAb to granulocyte-differentiation antigen (Gr-1) detects members of the Ly-6 family. *J. Immunol.* **151**, 2399–2408 (1993).

10. Daley, J. M., Thomay, A. A., Connolly, M. D., Reichner, J. S. & Albina, J. E. Use of Ly6G-specific monoclonal antibody to deplete neutrophils in mice. *J. Leukoc. Biol.* **83**, 64–70 (2008).

11. Morton, J. *et al.* Circulating neutrophils maintain physiological blood pressure by suppressing bacteria and IFNgamma-dependent iNOS expression in the vasculature of healthy mice. *Blood* **111**, 5187–5194 (2008).

12. Abbitt, K. B. *et al.* Antibody ligation of murine Ly-6G induces neutropenia, blood flow cessation, and death via complement-dependent and independent mechanisms. *J. Leukoc. Biol.* **85**, 55–63 (2009).

13. Bruhn, K. W., Dekitani, K., Nielsen, T. B., Pantapalangkoor, P. & Spellberg, B. Ly6G-mediated depletion of neutrophils is dependent on macrophages. *Results Immunol.* **6**, 5–7 (2016).

14. Boivin, G. *et al.* Durable and controlled depletion of neutrophils in mice. *Nat. Commun.* **11**, 2762 (2020).

15. Stackowicz, J., Jönsson, F. & Reber, L. L. Mouse Models and Tools for the in vivo Study of Neutrophils. *Front. Immunol.* **10**, 3130 (2019).

16. Liu, F., Wu, H. Y., Wesselschmidt, R., Kornaga, T. & Link, D. C. Impaired production and increased apoptosis of neutrophils in granulocyte colony-stimulating factor receptor-deficient mice. *Immunity* **5**, 491–501 (1996).

17. Eash, K. J., Greenbaum, A. M., Gopalan, P. K. & Link, D. C. CXCR2 and CXCR4 antagonistically regulate neutrophil trafficking from murine bone marrow. *J. Clin. Invest.* **120**, 2423–2431 (2010).

18. Karsunky, H. *et al.* Inflammatory reactions and severe neutropenia in mice lacking the transcriptional repressor Gfi1. *Nat. Genet.* **30**, 295–300 (2002).

19. Bruhns, P. Properties of mouse and human IgG receptors and their contribution to disease models. *Blood* **119**, 5640–5649 (2012).

20. Leatherbarrow, R. J. & Dwek, R. A. Binding of complement subcomponent C1q to mouse IgG1, IgG2a and IgG2b: a novel C1q binding assay. *Mol. Immunol.* **21**, 321–327 (1984).

21. Boross, P. *et al.* IgA EGFR antibodies mediate tumour killing in vivo. 1213–1226 (2013) doi:10.1002/emmm.201201929.

22. Takai, T., Li, M., Sylvestre, D., Clynes, R. & Ravetch, J. V. FcR gamma chain deletion results in pleiotrophic effector cell defects. *Cell* **76**, 519–529 (1994).

23. Meyer, S. *et al.* Improved in vivo anti-tumor effects of IgA-Her2 antibodies through half-life extension and serum exposure enhancement by FcRn targeting. *MAbs* **8**, 87–98 (2016).

24. Evers, M. *et al.* The selection of variable regions affects effector mechanisms of IgA antibodies against CD20. *Blood Adv.* **5**, 3807–3820 (2021).

25. Chernyavska, M. *et al.* Evaluation of immunotherapies improving macrophage anti-tumor response using a microfluidic model. *Organs-on-a-Chip* **4**, 100019 (2022).

26. Bosma, G. C., Custer, R. P. & Bosma, M. J. A severe combined immunodeficiency mutation in the mouse. *Nature* **301**, 527–530 (1983).

27. Shultz, L. D. *et al.* Multiple defects in innate and adaptive immunologic function in NOD/LtSz-scid mice. *J. Immunol.* **154**, 180–191 (1995).

28. Deyhle, M. R. *et al.* Depleting Ly6G Positive Myeloid Cells Reduces Pancreatic Cancer-Induced Skeletal Muscle Atrophy. *Cells* **11**, (2022).

29. Chan, C. *et al.* Targeting Myeloid Checkpoint Molecules in Combination With Antibody Therapy: A Novel Anti-Cancer Strategy With IgA Antibodies? *Front. Immunol.* **13**, 932155 (2022).

30. Sun, D., Sun, P., He, S. & Shi, M. Rat IgG mediated circulatory cell depletion in mice requires mononuclear phagocyte system and is facilitated by complement. *J. Leukoc. Biol.* **107**, 529–539 (2020).

31. Uchida, J. *et al.* The innate mononuclear phagocyte network depletes B lymphocytes through Fc receptor-dependent mechanisms during anti-CD20 antibody immunotherapy. *J. Exp. Med.* **199**, 1659–1669 (2004).

32. Otten, M. A. *et al.* Experimental antibody therapy of liver metastases reveals functional redundancy between Fc gammaRI and Fc gammaRIV. *J. Immunol.* **181**, 6829–6836 (2008).

33. Gül, N. *et al.* Macrophages eliminate circulating tumor cells after monoclonal antibody therapy. *J. Clin. Invest.* **124**, 812–823 (2014).

34. Daëron, M. Fc receptor biology. *Annu. Rev. Immunol.* **15**, 203–234 (1997).

35. Bugl, S. *et al.* Steady-state neutrophil homeostasis is dependent on TLR4/TRIF signaling. *Blood* **121**, 723–733 (2013).

36. Kaplan, M. J. Role of neutrophils in systemic autoimmune diseases. *Arthritis Res. Ther.* **15**, 219 (2013).

37. Leusen, J. H. W. IgA as therapeutic antibody. *Mol. Immunol.* **68**, 35–39 (2015).

38. Brandsma, A. M. *et al.* Potent Fc Receptor Signaling by IgA Leads to Superior Killing of Cancer Cells by Neutrophils Compared to IgG. *Front. Immunol.* **10**, 704 (2019).

39. Evers, M. *et al.* Novel chimerized IgA CD20 antibodies: Improving neutrophil activation against CD20-positive malignancies. *MAbs* **12**, 1795505 (2020).

SUPPLEMENTAL INFORMATION

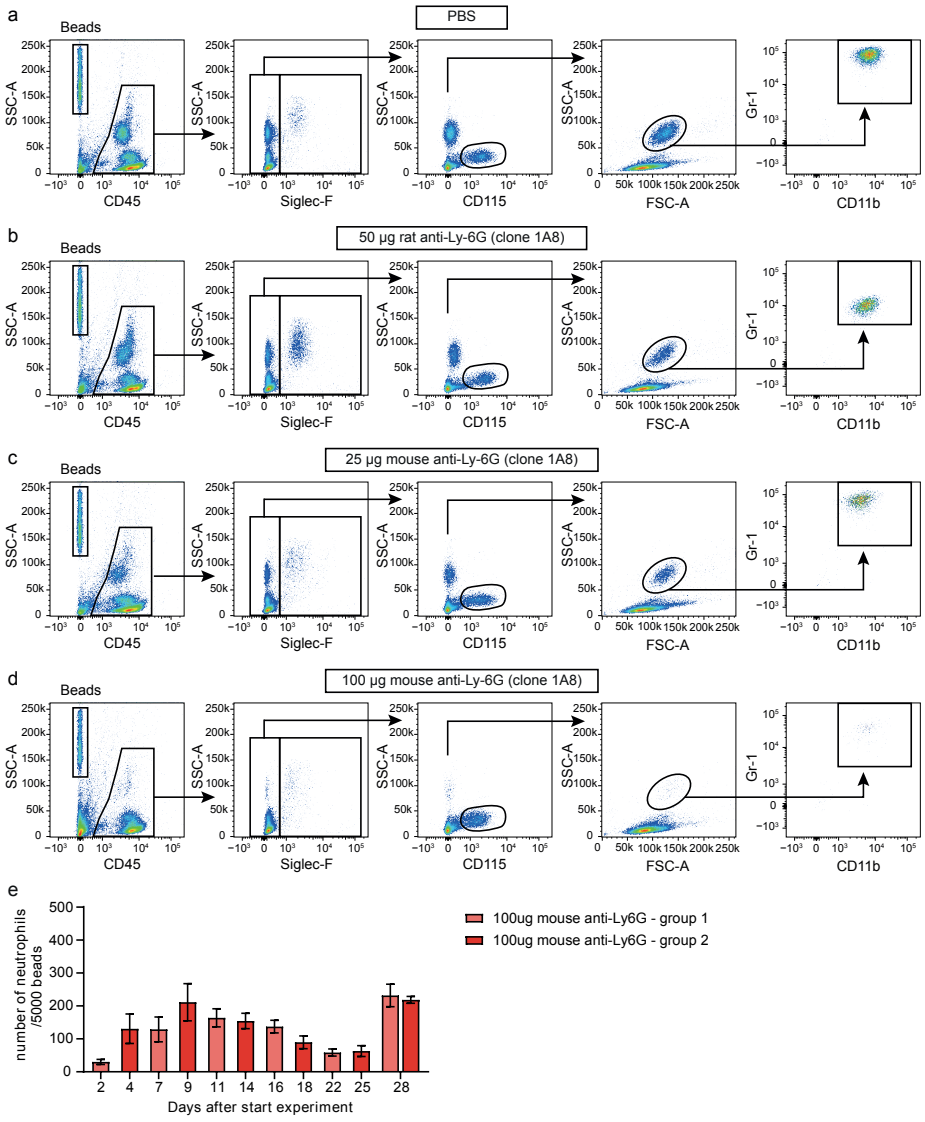

Figure S1 | Analysis of the number of neutrophils upon antibody treatment (related to Figure 1). (**A-D**) FACS dot plots showing representative blood samples at day 28 after the start of the experiment for (**a**) PBS injected control mice, (**B**) 50 µg rat-Ly-6G injected mice, (**C**) 25 µg mouse-Ly-6G injected mice, and (**D**) 100 µg mouse-Ly-6G injected mice. (**E**) Zoom in of the longitudinal analysis of the number of $CD45^+$ Siglec-F^- $CD115^-$ SSC^{high} $Gr\text{-}1^+$ $CD11b^+$ neutrophils per 5000 beads in the peripheral blood (n = 4 mice per subgroup) of 100 µg mouse-Ly-6G treated mice, as depicted in **Figure 1E**.

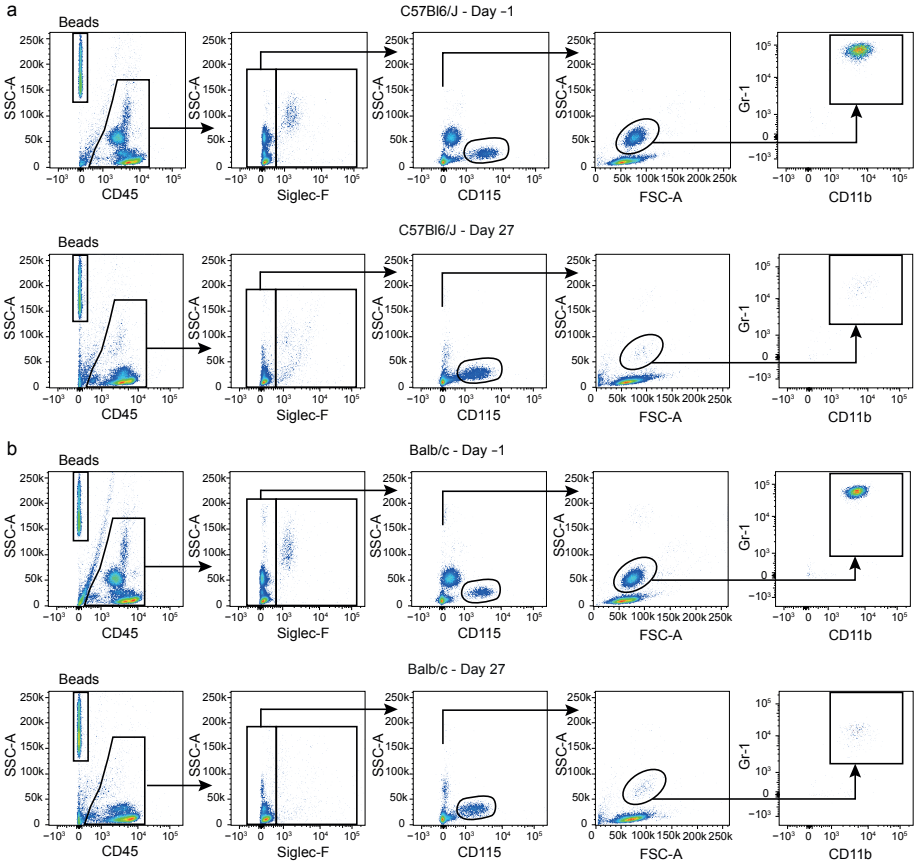
a
C57Bl6/J - Day -1
Beads
SSC-A
CD45
Siglec-F
CD115
FSC-A
Gr-1
CD11b
C57Bl6/J - Day 27
b
Balb/c - Day -1
Balb/c - Day 27

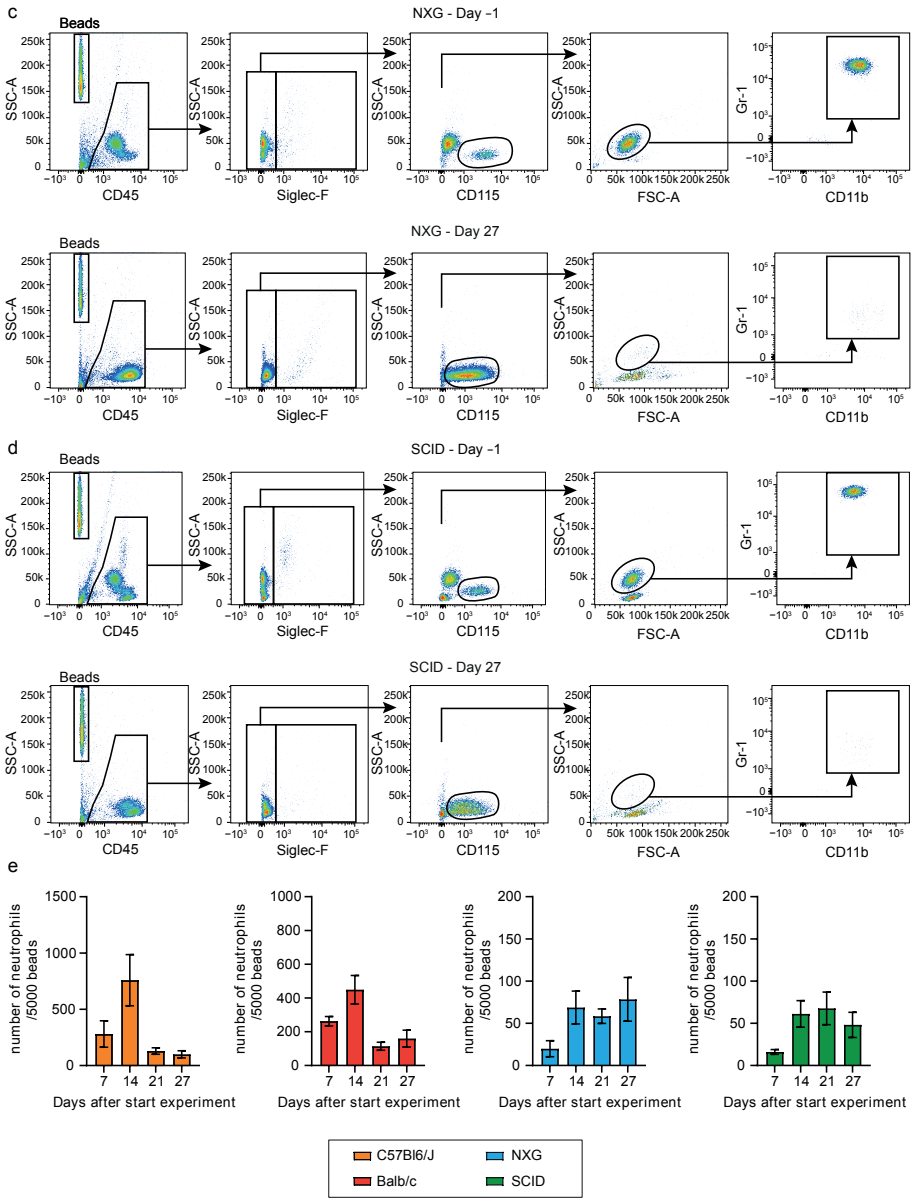

Figure S2 | Gating strategy to retrieve the number of neutrophils per 5000 beads (related to Figure 2). (**A-D**) FACS dot plots showing representative blood samples at the day before the start of the experiment (day –1) and at the end of the experiment (day 27) for (**A**) C57Bl6/J, (**B**) Balb/c, (**C**) NXG, and (**D**) SCID mice, injected with 100 µg mouse-Ly-6G. (**E**) Zoom in of the longitudinal analysis of the number of $CD45^+$ $Siglec\text{-}F^-$ $CD115^-$ SSC^{high} $Gr\text{-}1^+$ $CD11b^+$ neutrophils per 5000 beads in the peripheral blood (*n* = 5 mice per group) of 100 µg mouse-Ly-6G treated mice, as depicted in **Figure 2B**.

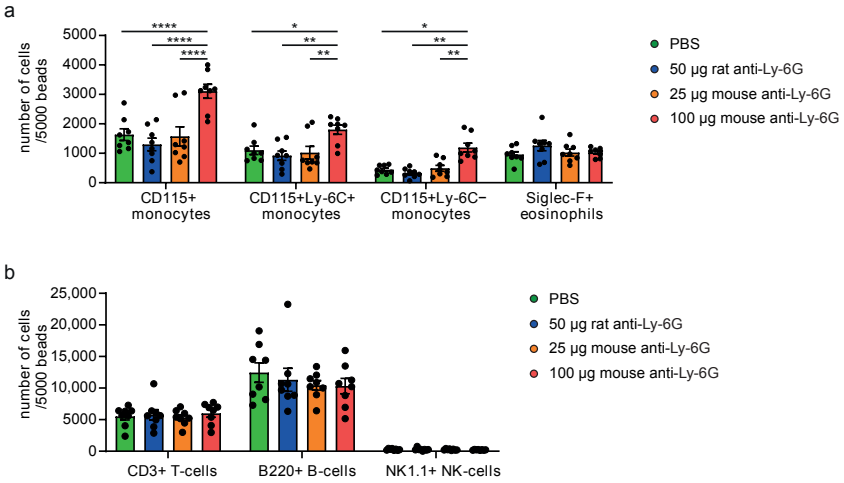

Figure S3 | Number of monocytes, eosinophils, T-, B-, and NK-cells upon Ly6G treatment (related to Figure 1). Flow cytometry analysis of the number of leukocytes in the peripheral blood at day 28 after the start of the experiment (n = 8 mice per group, as shown in **Figure 1**) per 5000 latex beads, showing (**A**) a significant increase in both Ly-6C$^+$ and Ly-6C$^-$ CD115$^+$ monocytes, but not eosinophils, upon neutrophil depletion with 100 µg mouse-Ly-6G antibody, and (**B**) no differences in CD3$^+$ T-cells, B220$^+$ B-cells and NK1.1$^+$ NK-cells. Statistics: two-way ANOVA with Bonferroni correction, * = $p < 0.05$, ** = $p < 0.01$, *** = $p < 0.001$, **** = $p < 0.0001$.


3

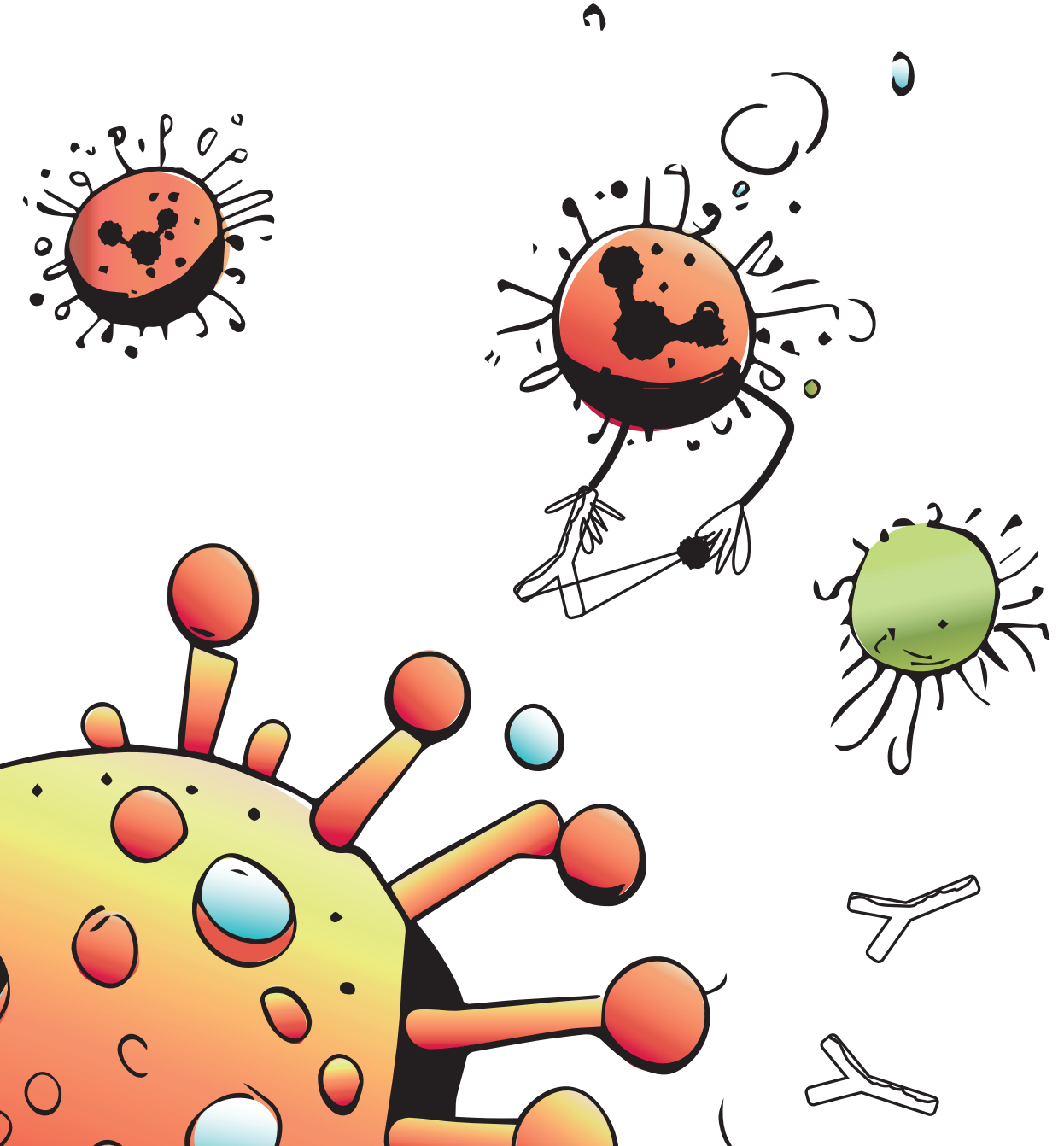

PART II

Applying IgA antibody therapy in neuroblastoma

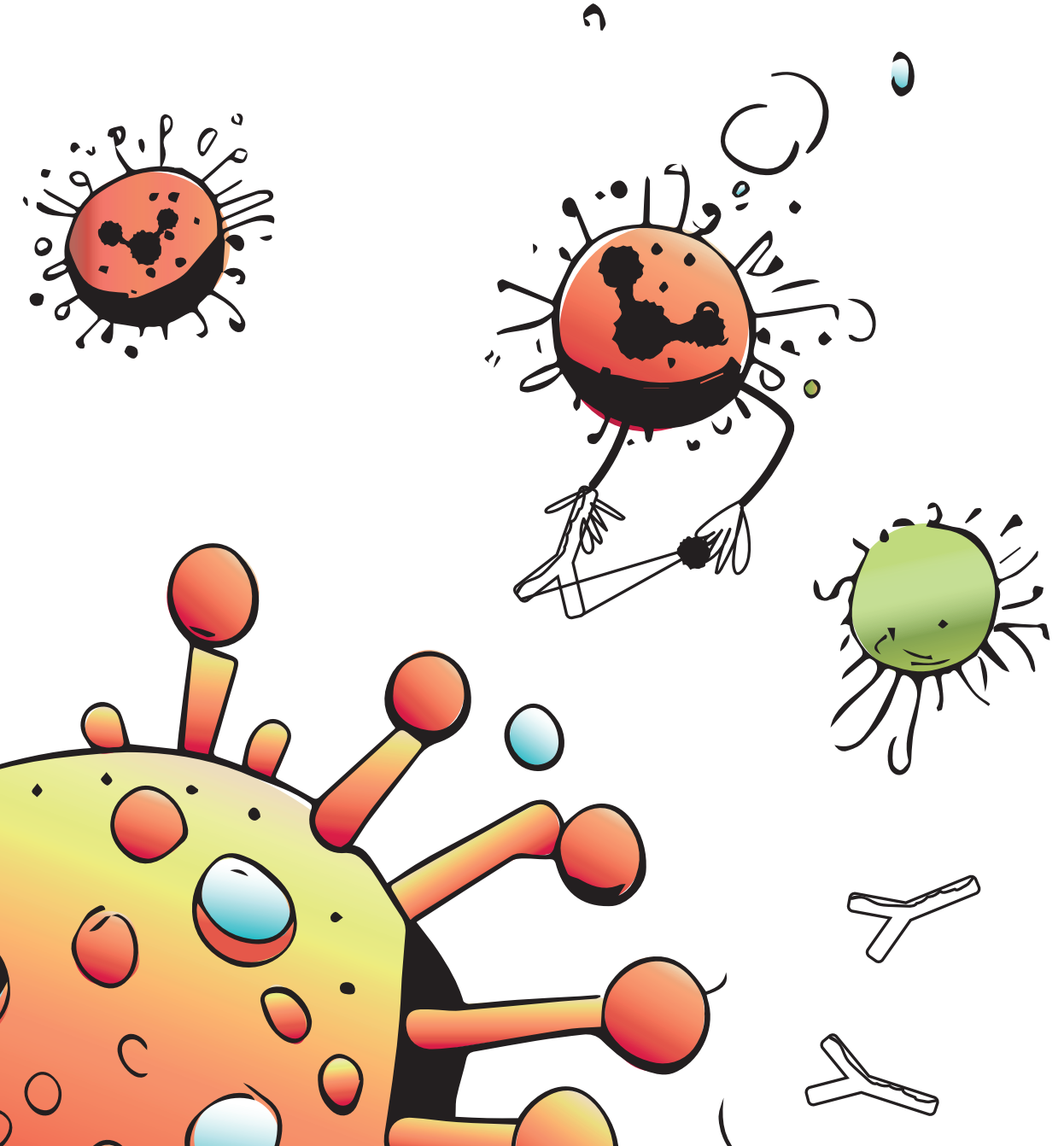

Chapter 4.

Targeting the myeloid microenvironment in neuroblastoma

Marjolein C. Stip[1], Loes Teeuwen[1], Miranda P. Dierselhuis[2], Jeanette H.W. Leusen[1], Daniëlle Krijgsman[1,3]

Affiliations

1. Center for Translational Immunology, University Medical Center Utrecht, 3584 CX Utrecht, The Netherlands.
2. Princess Máxima center for pediatric oncology, 3584 CS, Utrecht, The Netherlands.
3. Center for Molecular Medicine, University Medical Center Utrecht, 3584 CX Utrecht, the Netherlands.

Published in the Journal of Experimental & Clinical Cancer Research, 2023

ABSTRACT

Myeloid cells (granulocytes and monocytes/macrophages) play an important role in neuroblastoma. By inducing a complex immunosuppressive network, myeloid cells pose a challenge for the adaptive immune system to eliminate tumor cells, especially in high-risk neuroblastoma. This review first summarizes the pro- and anti-tumorigenic functions of myeloid cells, including granulocytes, monocytes, macrophages, and myeloid-derived suppressor cells (MDSC) during the development and progression of neuroblastoma. Secondly, we discuss how myeloid cells are engaged in the current treatment regimen and explore novel strategies to target these cells in neuroblastoma. These strategies include: (1) engaging myeloid cells as effector cells, (2) ablating myeloid cells or blocking the recruitment of myeloid cells to the tumor microenvironment and (3) reprogramming myeloid cells. Here we describe that despite their immunosuppressive traits, tumor-associated myeloid cells can still be engaged as effector cells, which is clear in anti-GD2 immunotherapy. However, their full potential is not yet reached, and myeloid cell engagement can be enhanced, for example by targeting the CD47/SIRPα axis. Though depletion of myeloid cells or blocking myeloid cell infiltration has been proven effective, this strategy also depletes possible effector cells for immunotherapy from the tumor microenvironment. Therefore, reprogramming of suppressive myeloid cells might be the optimal strategy, which reverses immunosuppressive traits, preserves myeloid cells as effectors of immunotherapy, and subsequently reactivates tumor-infiltrating T cells.

Keywords

Neuroblastoma, Myeloid cells, Macrophages, Monocytes, Neutrophils, Myeloid-derived suppressor cell, Immunotherapy, Immunosuppression

INTRODUCTION

Neuroblastoma is a pediatric tumor originating from sympathoadrenal lineage dysregulation [1] which exhibits high heterogeneity in disease severity. While low- and intermediate-risk neuroblastoma patients achieve a 80–95% 5-year overall survival rate, high-risk cases only reach 45%[2]. Approximately half of the diagnosed neuroblastoma cases are classified as high-risk, with 20–30% featuring MYCN amplification[3]. MYCN, a proto-oncogenic transcription factor, fosters tumor cell proliferation, angiogenesis, and metastasis, concurrently suppressing immune activation[4]. In low-risk cases, no treatment or solely surgery is often curative[5,6], while high-risk patients undergo induction chemotherapy, surgery, high-dose chemotherapy with autologous stem cell transplantation (ASCT), and radiation therapy[7]. Since 2015, anti-disialoganglioside (GD2) antibody immunotherapy

and 13-cis retinoic acid (isotretinoin) is applied as consolidation therapy. Initially anti-GD2 was combined with IL-2 and Granulocyte/Macrophage-Colony Stimulating Factor (GM-CSF) (USA) or IL-2 only (Europe). Since the administration of IL-2 has been proven to be of no additional benefit this has been omitted[8].

Neuroblastoma has a low mutational burden[9] as well as low human leukocyte antigen (HLA) type I expression[10], limiting tumor recognition by the T cells. Due to the scarcity of neo-antigens, the development of immunotherapeutics, including anti-tumor antibodies, T cell vaccines and chimeric antigen receptor (CAR) T cells hampered initially. However, success was achieved by targeting the highly expressed GD2[11] using antibody therapy, thereby activating NK cells and myeloid cells. Anti-GD2 antibody therapy significantly improved survival for high-risk neuroblastoma patients[12,13]. Although GD2-targeting CAR T cells have been developed, they failed to enhance survival initially, likely due to T cell exhaustion by the immunosuppressive tumor microenvironment (TME). However, recently, a phase I/II trial showed that the use of GD2-targeting CAR T cells (GD2-CART01) was feasible and safe in treating high-risk neuroblastoma, resulting in 3-year overall survival and event-free survival of 60% and 36%, respectively[14].

Neuroblastomas, like many solid tumors, harbor a complex immunosuppressive microenvironment hindering immune-mediated tumor clearance. Tumor-infiltrating lymphocytes are often inactivated or exhausted due to immunosuppressive factors, including cytokines (IL-6, IL-10, TGF-β, galectin-1) secreted by tumor, stromal, and myeloid immune cells[15–19]. Furthermore, MYCN overexpression in neuroblastoma cells diminishes NKG2D ligands, impeding NK cell activation[20]. Gangliosides like GD2 (cell-bound or soluble) suppress immunity by binding to myeloid checkpoint Siglec-7[21], and $CD8^+$ T cell cytotoxicity is curtailed via intracellular granule interference[22]. Lymphocyte activation is further hampered by recruitment and induction of immunosuppressive cells, such as regulatory T cells (Tregs), tumor-associated macrophages (TAMs) and myeloid-derived suppressor cells (MDSCs)[23].

While often implicated in immunosuppression, myeloid cell subsets also possess potent anti-tumorigenic properties. This review comprehensively outlines the dualistic roles of myeloid cells in neuroblastoma. The first part summarizes their pro- and anti-tumorigenic functions during the development and progression of neuroblastoma. The second part discusses the involvement of myeloid cells in current treatment regimen and explores novel strategies for their targeting, including: (1) engaging myeloid cells as effectors, (2) ablating myeloid cells, (3) blocking recruitment to the TME and (4) reprogramming of myeloid cells.

MYELOID SUBPOPULATIONS IN THE NEUROBLASTOMA MICROENVIRONMENT

While the field of tumor immunology initially focused on dissecting the role of lymphocytes, there is a growing awareness of the significance of myeloid cells. Myeloid cells comprise monocytes, macrophages, granulocytes (mainly neutrophils and eosinophils), MDSC and certain DC subsets. Though some DCs are of myeloid origin, they are beyond the scope of this review, as they have been extensively covered elsewhere (reviewed in [24]). MDSC can be categorized into three subsets: polymorphonuclear MDSC (PMN-MDSC, $CD33^{+}CD14^{-}CD15^{+}LOX1^{+}$), monocytic MDSC (M-MDSC, $CD33^{+}CD14^{+}CD15^{-}HLA\text{-}DR^{-/low}$) and early MDSCs (E-MDSC, $CD11b^{+}CD33^{+}CD14^{-}CD15^{-}$)[25–27]. Identifying specific MDSC subsets can be challenging due to overlapping lineage markers with other immune cells such as neutrophils and monocytes (reviewed in [28]). However, the main defining characteristic of MDSCs is their immunosuppressive function. Recent markers such as LOX-1 and CD84 expression on PMN-MDSCs[26,29] or gradient centrifugation[30] can aid in distinguishing PMN-MDSCs from neutrophils, as PMN-MDSCs reside in the low-density (peripheral blood mononuclear cells; PBMC) fraction, while neutrophils are high-density cells. Furthermore, M-MDSCs can be differentiated from monocytes by lower or absent HLA class II expression and increased C-X-C motif chemokine receptor 1 (CXCR1) expression[25,31]. The challenges in accurately identifying MDSCs often lead to inconsistencies in nomenclature across studies. In this review, we adhere to the nomenclature used in the referenced literature, considering the mentioned immune cell subsets as they are described. Now, we will first discuss the involvement of each of these myeloid immune subsets in neuroblastoma, starting with neutrophils (**Figure 1**).

Figure 1 | Overview of the interactions of myeloid cell subsets in the tumor microenvironment of neuroblastoma. A neuroblastoma is shown in the center, surrounded by various myeloid immune cells: neutrophils, MDSC, monocytes, TAM, and eosinophils. For each of these cell types, pertinent interactions within the TME are depicted. For neutrophils, a high NLR is associated with unfavorable clinical outcomes. Reported tumor-neutrophil interactions involve the induction of neutrophil adhesion to neuroblastoma cell lines through IFNγ and IL-1, resulting in increased ICAM-1 expression on neutrophils. MDSCs are linked to T cell activation inhibition, notably through P2X7 receptor activation leading to increased ATP levels within the TME. Additionally, neuroblastoma-conditioned medium induces MDSCs through M-CSF and Arg-1/2. While most mouse MDSCs exhibit an M-MDSC phenotype, human MDSCs present a PMN-MDSC signature. For monocytes, LMR was not correlated with clinical outcomes in neuroblastoma patients. In neuroblastoma, TAMs undergo polarization from M1 to M2 as the disease progresses. Additionally, TAMs contribute to the preparation of the metastatic niche by taking up tumor-secreted EVs, resulting in the upregulation of immunosuppressive cytokines and genes associated with tumor cell extravasation, and via the CXCL2/CXCR2 axis. In MYCN-amplified neuroblastoma, TAMs exhibit elevated expression of macrophage-related immune checkpoints CD47 and Siglec-7, in contrast to MYCN-nonamplified tumors. MYCN-nonamplified

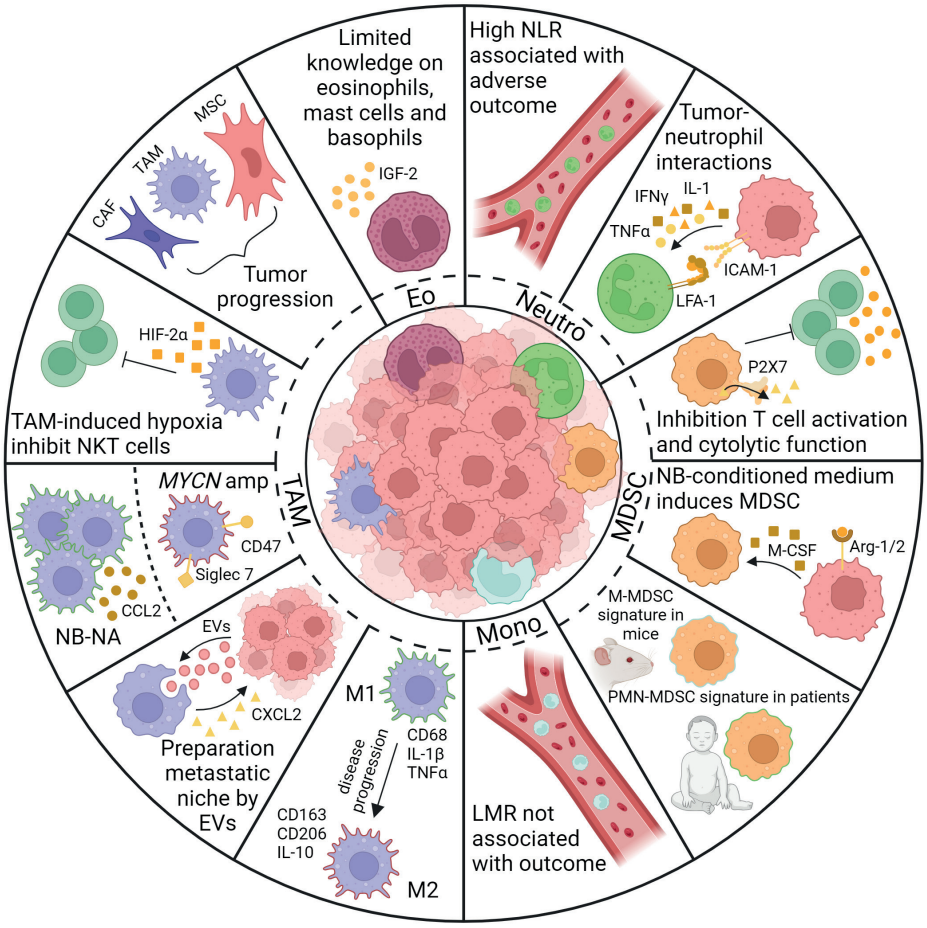

neuroblastoma is characterized by elevated CCL2 secretion by TAMs, resulting in the recruitment of TAMs, myeloid cells, and plasmacytoid DC. Furthermore, TAM-induced hypoxia leads to the inhibition of NK cells through HIF-2α production. TAMs also collaborate with CAFs and MSCs to promote tumor progression. Although our understanding of eosinophils, mast cells, and basophils is limited, IGF-2 secreted by eosinophils is suggested to play a role in neuroblastoma growth. Abbreviations: Arg-1/2 = arginase-1/2, ATP = adenosine triphosphate, CAF = cancer-associated fibroblasts, CCL2 = C–C motif chemokine ligand 2, CXCL2 = C-X-C motif chemokine ligand 2, CXCR2 = C-X-C motif chemokine receptor 2, DC = dendritic cell, Eo = eosinophil, EVs = extracellular vesicles, HIF-2a = hypoxia inducible factor 2α, ICAM-1 = intercellular adhesion molecule-1, IFNγ = interferon gamma, IGF-2 = insulin-like growth factor 2, LMR = lymphocyte-to-monocyte ratio, M-CSF = macrophage-colony stimulating factor, M-MDSC = monocytic myeloid-derived suppressor cells, MDSC = myeloid-derived suppressor cell, Mono = monocyte, MSC = mesenchymal stromal cells, NB = neuroblastoma, NB-NA = MYCN non-amplified neuroblastoma, Neutro = neutrophil, NK = natural killer, NLR = neutrophil-to-lymphocyte ratio, PMN-MDSC = polymorphonuclear myeloid-derived suppressor cells, TAM = tumor-associated macrophage, TME = tumor microenvironment.

Neutrophils

Neutrophils are short-lived phagocytes (though their exact lifespan is heavily under debate) and are the most abundant leukocyte population in the human body, primarily residing in the bone marrow[32,33]. Approximately 10^{11} neutrophils are released from the bone marrow and enter circulation daily, with an additional release during inflammatory conditions, upon which they migrate towards the sites of inflammation[34].

The prognostic significance of tumor-infiltrating neutrophils or the neutrophil-to-lymphocyte ratio (NLR) in various cancer types typically indicates unfavorable outcomes[35]. However, in the case of neuroblastoma, conflicting and inconclusive findings have been reported regarding the correlation between neutrophils and disease progression. Initial studies by Morandi et al. demonstrated increased neutrophil counts in peripheral blood samples from patients with localized neuroblastoma compared to patients with metastasized neuroblastoma, hence neutrophils were associated with improved overall survival (OS)[36]. Similarly, Zeng et al. found a positive correlation between higher numbers of tumor-infiltrating macrophages and neutrophils and increased OS[37]. Conversely, other studies did not observe significant associations between neutrophils and survival[38], or even found the opposite[39–41]. Zhang et al. reported that a higher NLR was associated with reduced OS[39]. Erbe et al. did not find a significant correlation between NLR and survival, but they did note that a higher neutrophils count was associated with shortened event-free survival (EFS)[41]. Lee et al. observed that elevated neutrophil counts were associated with a higher cumulative incidence of disease progression, although not significantly impacting EFS or OS[40]. However, in a subgroup analysis of high-risk neuroblastoma patients, the correlation was stronger, with a high neutrophil count significantly associated with reduced EFS. Although these results appear conflicting, there are indications that high neutrophil counts in blood may indicate a positive prognosis in localized neuroblastoma (low-risk), whereas high neutrophil counts in high-risk neuroblastoma are associated with a negative prognosis, as suggested by the studies of Morandi and Lee. Nevertheless, further investigations, specifically differentiating between low- and high-risk patients, are required to confirm these hypotheses in the future.

The interaction between neutrophils and neuroblastoma cells was studied already decades ago, albeit mostly *in vitro*. Two studies showed that cytokines like tumor necrosis factor alpha (TNFα), Interleukin (IL)-1 and interferon gamma (IFNγ) induce neutrophil adhesion to SK-N-SH and LAN-1 neuroblastoma cell lines by upregulating intercellular adhesion molecule-1 (ICAM-1) expression[42,43]. Blocking lymphocyte function-associated antigen 1 (LFA-1, formed by CD11a and CD18), the ligand of ICAM-1, prevented cytokine-induced neutrophil adhesion to neuroblastoma cells. However, neutrophil binding to SK-N-MC cells was very high and independent of stimulatory cytokines or LFA-1, indicating multiple adhesion mechanisms exist for different neuroblastoma cell lines. Interestingly, co-culture experiments demonstrated that endothelial cells down-regulated adhesion receptor

CD33 upon interaction with neuroblastoma cells, thus impairing neutrophil adhesion and extravasation[44]. Nevertheless, Fultang et al. indicated the presence of $CD15^+$ neutrophils in neuroblastoma, particularly in high-risk disease, suggesting their ability to extravasate and localize around the vasculature[45]. Direct co-culture of neuroblastoma cell lines with neutrophils exhibited both pro-tumorigenic (SMS-KCN and SMS-LHN) and anti-tumorigenic (LAN-1) effects, in a cell–cell contact independent manner[46]. These studies highlight both pro-tumorigenic and anti-tumorigenic effects of neutrophils and touch upon the intricate interplay between neutrophils and the neuroblastoma cells in the TME.

More recently, Martínez-Sanz and colleagues identified upregulated neutrophil-related mRNA transcripts (including *CGR3B*, *FPR1*, *S100A8/9*, and *SIGLEC9)* in both early and late-stage neuroblastoma, compared to healthy adrenal gland tissue[47]. However, the exact interactions between neutrophils and tumor cells in the TME remain largely unknown. After the initial interest in neutrophils, immunotherapy research focused more on harnessing the adaptive immune system and engaging NK cells through antibody therapy in the early 2000s, which may explain the scarcity of data on neutrophils. Furthermore, a nomenclature change has led to (immunosuppressive) neutrophils being described more frequently as PMN-MDSC in cancer. Consequently, we will now delve into the role of these cells in neuroblastoma.

Myeloid-derived suppressor cells

MDSCs represent an immature immunosuppressive subset of myeloid cells that undergo expansion during pathological conditions such as inflammation and cancer[48,49]. Their presence has been associated with poor clinical outcomes in various cancer types[50]. Under the influence of continuous cytokine production within the TME, undifferentiated myeloid cells from the bone marrow enter circulation and infiltrate the tumor, where they often fail to mature (reviewed in [50–52]). MDSCs exert immunosuppressive effects by suppressing T and NK cell activation and cytotoxicity, while promoting Treg and M2 macrophage polarization. They employ various mechanisms to induce immune suppression, including the production of reactive oxygen species (ROS), nitric oxide (NO), anti-inflammatory cytokines, and the depletion of L-arginine via arginase (Arg)-1[48,53,54]. In general, M-MDSCs exhibit higher immunosuppressive activity than PMN-MDSCs, suppressing both antigen-specific and non-specific T cell responses[48].

In neuroblastoma-bearing mice, both PMN-MDSC and M-MDSC induce T cell suppression[55–59]. Notably, TH-MYCN mice, which exhibit spontaneous neuroblastoma development due to MYCN overexpression, showed a higher PMN-MDSC abundance compared to M-MDSC[60]. Conversely, in a commonly used neuroblastoma mouse model involving A/J mice injected with NXS2 neuroblastoma cells intravenously, M-MDSC displayed higher levels of Arg-1 and iNOS, and produced higher levels of TGF-β1 and ROS compared to PMN-MDSC[56]. This hints at M-MDSCs' superior suppressive potency

compared to PMN-MDSC, a trend observed in other cancer types as well[61,62]. Co-injection of M-MDSCs with NXS2 neuroblastoma cells promoted tumor growth more than PMN-MDSC co-injection, underscoring their distinct roles. MDSCs' immunosuppressive actions involved P2X7 receptor activation, which elevates extracellular adenosine triphosphate (ATP) levels within the TME. P2X7R agonist BzATP induced M-MDSCs to secrete chemoattractant C–C motif chemokine ligand (CCL)-2, and upregulated Arg-1, ROS, and TGF-β1 in MDSC cell lines MSC-1 and MSC-2.

Furthermore, neuroblastoma-conditioned medium has been shown to induce MDSCs. Cultivating hematopoietic progenitors or monocytes in such media generated immunosuppressive myeloid cells[57,59,63]. Intriguingly, Arg-2-expressing neuroblastoma cells depleted local and circulating arginine levels, similar to the mechanism employed by MDSCs[63]. Arg-1 in neuroblastoma hindered myeloid activation and suppressed $CD34^+$ bone marrow progenitor cell proliferation, suggesting that arginine deprivation contributes to MDSC induction in neuroblastoma[64]. Additionally, the macrophage-colony stimulating factor (M-CSF)/colony stimulating factor 1 receptor (CSF-1R) axis was suggested to drive myeloid differentiation into M-MDSCs in neuroblastoma[57]. Elevated M-CSF, CSF-1R, CD68, and CD14 correlated with poor patient outcomes. Intriguingly, primary human monocytes polarized into suppressive $CD14^+CSF\text{-}1R^+$ M-MDSC upon co-culture with neuroblastoma cells, mediated by tumor-originating M-CSF and attenuated through CSF-1R blockade.

Limited neuroblastoma patient data exists on MDSC subsets in circulation. Santilli et al. found elevated PMN-MDSCs in the peripheral blood of patients with neuroblastoma vs. controls[65]. Furthermore, high-risk neuroblastoma exhibited higher levels of $CD33^+CD11b^+HLA\text{-}DR^-$ MDSCs (M-MDSC) than low-risk neuroblastoma[60]. Unexpectedly, responsive high-risk patients had more circulating $HLA\text{-}DR^-$ MDSCs compared to patients who were refractory to therapy[66]. Recent single-cell transcriptomics unveiled exclusive tumor-infiltrated immature myeloid/neutrophil cells in bone marrow metastasis of neuroblastoma patients, suggesting PMN-MDSC involvement[64]. PMN-MDSC signatures were observed in primary neuroblastomas based on single-cell transcriptomic analysis[58], with higher proportions of MDSCs detected in *MYCN*-amplified tumors compared to *MYCN*-nonamplified tumors. At relapse, tumors had increased MDSC proportions compared to diagnosis[60].

In summary, *in vivo* studies implicate a more important role for M-MDSC in neuroblastoma progression compared to PMN-MDSC due to their prominent suppressive function. However, it remains uncertain if this translates to the human context. Furthermore, it is important to note that MDSC spatial distribution, abundance, and interactions with other immune cell subsets within the TME remain undisclosed.

Monocytes & macrophages

Monocytes and macrophages play a significant role within the myeloid compartment of the TME and possess phagocytic abilities. Unlike neutrophils, circulating monocyte levels or leukocyte-to-monocyte ratio (LMR) are not linked to overall survival[38,41]. Tumor-derived chemokines and cytokines can recruit monocytes to the TME, where they can differentiate into monocyte-derived macrophages[67]. Additionally, tissue-resident macrophages can also be found in the TME, originating from yolk-sac precursors and exhibiting self-renewal capabilities[68]. Furthermore, recruited M-MDSCs can differentiate into macrophages at the tumor site[69]. Macrophages are traditionally categorized into M1 (pro-inflammatory) and M2 (anti-inflammatory) states[70], yet they exhibit notable plasticity and heterogeneity along this spectrum.

Macrophages in human neuroblastoma have a predominant M2-like phenotype, with some M1 presence[45,58,71–74]. In the TH-MYCN mouse model, TAMs transitioned from an M1 phenotype (MHCII^{high}/CD206^{low}) to an M2 phenotype (MHCII^{low}/CD206^{high}) during tumor progression[55]. Additionally, the number of infiltrating immune cells and the proportion of TAMs (F4/80^{+}/CD45^{+}) among total infiltrating cells increased in advanced TH-MYCN tumors. *In vitro*, neuroblastoma-exposed monocytes/macrophages upregulated M2 markers (CD163, CD204, IL-10)[73,75]. Conversely, Fultang et al. observed that neuroblastoma cells polarized macrophages toward an M1 phenotype (CD68^{+}CD163^{-})[45]. Consistent with these findings, low numbers of M2-polarized macrophages were observed to be correlated with unfavorable clinical outcome in neuroblastoma[37,76]. Importantly, TAMs emerge as the predominant PD-L1-expressing cells within the TMA, which was associated with improved clinical outcome in high-risk patients[77]. Finally, single-cell RNA sequencing revealed an augmented presence of an inflammatory monocyte cell state (*IL1B*^{high}*S100A*^{high}) in neuroblastoma compared to normal tissue[78].

Macrophages drive neuroblastoma dissemination by creating premetastatic niches, facilitating tumor cell colonization[79]. Studies utilizing SK-N-BE-derived primary tumors revealed the release of extracellular vesicles that are engulfed by macrophages at distant sites such as the liver and bone marrow. Consequently, this led to upregulation of immunosuppressive cytokines (IL-10), as well as genes involved in the recruitment of MDSC and tumor cell extravasation, rendering the premetastatic niche more attractive for tumor cell colonization. In accordance, high numbers of M2 macrophages in primary neuroblastoma correlated with the presence of bone marrow metastasis and poor clinical outcome[71,73,80]. Moreover, macrophage-derived CXCL2 promoted neuroblastoma invasiveness, but CXCL2/CXCR2 mechanism in this context remains unclear[73]. These are the only studies investigating the role of myeloid cells in neuroblastoma metastasis, though this has been described more extensively in other cancers, indicating there is a knowledge gap on this topic. However, recently it was described that macrophage migration inhibitory factor (MIF) and midkine (MDK) are expressed in neuroblastoma[81,82], factors that are known

to be involved in metastasis in other cancers[83,84]. Unraveling the involvement of MIF and MDK in neuroblastoma metastasis could provide important information in the future.

MYCN-amplified and non-amplified neuroblastomas exhibit varying macrophage infiltration, reflecting distinct immune profiles due to specific genetic alterations. Chromosome 11q deletion or *MYCN* amplification in neuroblastomas exhibit higher numbers of M2-polarized ($CD163^+$) macrophages and an activated Th2-lymphocytes/M2-macrophage axis compared to neuroblastoma lacking these mutations[72,73,85]. Interestingly, *MYCN* amplification is generally associated with lower immune infiltrate than non-amplified cases[86]. Theruvath et al. confirmed this by re-analyzing public databases, revealing higher Siglec-7 and CD47 expression on *MYCN*-amplified neuroblastoma macrophages[21]. In metastatic non-amplified neuroblastomas, TAM infiltration was higher compared to locoregional tumors, with a predominant M2 phenotype[71]. Furthermore, metastatic non-amplified tumors in patients ≥ 18 months showed elevated inflammation-related gene expression compared to those < 18 months. Consistent with these findings, a study involving 129 NA-NB patients reported upregulation expression of CD14, IL-6 and TGF-β in patients with poor clinical outcome[87].

The NB-tag mouse model[88], resembling human non-amplified neuroblastoma, recruits TAMs, myeloid cells, and plasmacytoid DCs through CCL2 signaling[88,89]. Macrophage-secreted CCL2 is prominent in non-amplified tumors, and inversely correlated with *MYCN* amplification[87,90]. The recruited DCs subsequently attracted $CD4^+$ and $CD8^+$ T cells via CCL22 and CCL19[89]. *In vitro* and *in vivo* studies have demonstrated that CCL2-attracted TAMs in neuroblastoma enhance IL-6 expression, promote tumor growth and inhibit apoptosis[87,88]. Furthermore, TAMs in non-amplified tumors activate STAT3 in neuroblastoma cells, upregulating c-Myc that reciprocally induces CCL2 secretion, forming a positive feedback loop[88]. Consistent with these findings, a recent *in vivo* study reported that depletion of macrophages expressing the CCL2 receptor (CCR2) prevented tumor formation in an ALK-mutated TH-MYCN mouse model[91].

Hypoxia, common in cancer due to insufficient oxygen supply (reviewed in [92]), upregulates membrane-bound TNFα on neuroblastoma cells, triggering TAMs to produce CCL20[93]. This TAM-derived CCL20 recruits natural killer T (NKT) which eliminate pro-tumorigenic $CD1d^+$ TAM at the tumor site[87]. Despite this anti-tumorigenic potential, hypoxia impairs NKT cell function against $CD1d^+$ TAMs[93]. Additionally, hypoxia inducible factor 2α (HIF-2α)-producing TAMs were detected alongside neuroblastoma neural crest-like cells in the perivascular niche, where high levels of vascular endothelial growth factor (VEGF) were observed[94]. This suggests a cooperative interaction between neuroblastoma crest-like cells and macrophages to promote angiogenesis via HIF-2α-mediated VEGF expression.

In neuroblastoma, TAMs collaborate with cancer-associated fibroblasts (CAFs) and mesenchymal stromal cells (MSCs) to support tumor progression, especially in relapse patients. TAMs induce CAF proliferation[73], and MSCs/CAFs shield monocytes from

apoptosis through in an IL-6-dependent manner[95]. The interactions of monocytes and MSCs resulted in the significant upregulation of several pro-tumorigenic cytokines and chemokines, including TGF-β1, MCP-1, IL-6, IL-8, and IL-4. Furthermore, the abundance of MSCs and CAFs was correlated with tumor progression, including high histological malignancy and low infiltration of T and NK cells[73,96].
In summary, despite some conflicting findings, most studies suggest a notable role for M2-polarized TAMs in neuroblastoma progression, driving c-Myc expression, CAF recruitment, and angiogenesis.

Eosinophils

Currently, limited knowledge exists regarding the roles of granulocytes other than neutrophils in neuroblastoma, including eosinophils, basophils, and mast cells. To our knowledge, no literature is available discussing the role of basophils and mast cells in neuroblastoma. Eosinophils, usually associated with allergic reactions and immune responses against parasites[97], may have a minor role in neuroblastoma. In cancer, eosinophils generally display anti-tumorigenic properties, although some pro-tumorigenic effects have also been described (reviewed in [98]).
Eosinophils were first identified in neuroblastoma in the 1990s when a study of 21 tumors revealed their presence, along with insulin-like growth factor 2 (IGF-2) expression in these cells[99]. The authors proposed a mechanism whereby IGF-2, expressed both autocrinally and paracrinally (including by eosinophils), promotes tumor growth, but this mechanism was never confirmed. A subsequent study reported a positive link between low eosinophil count and patient survival[100]. Though not yet reported in neuroblastoma, tumor-infiltrating eosinophils are common in various cancer types[98], suggesting they are possibly present in the neuroblastoma TME as well.

THE ROLE OF EPIGENETICS IN MYELOID CELLS AND THERAPY RESISTANCE

Myeloid cells exhibit a high degree of plasticity, characterized by their ability to deviate from typical differentiation pathways and generate diverse tolerogenic myeloid cell states within the TME. A substantial component of this plasticity can be attributed to epigenetic mechanisms, with myeloid cells displaying marked responsiveness to histone modifications, alterations in DNA methylation patterns, chromatin remodeling, and the regulatory impact of non-coding RNA molecules[101–103]. Importantly, abnormal epigenetic modifications have been reported in the development and progression of cancer and therapy resistance[104,105], and are closely related to altered glucose, lipid, and amino acid metabolism in the TME as thoroughly reviewed elsewhere[103,105,106]. For instance, histone

citrullination, catalyzed by peptide arginine deiminase (PAD), is associated with the creation of neutrophil extracellular traps (NETs) in cancer, contributing to both innate immunity and tumor progression[107]. In addition, hypoxia and M1 macrophages drive histone lactylation through lactate accumulation in the TME. This can upregulate methyltransferase-like 3 (METTL3) in infiltrating myeloid cells in colon cancer via H3K18 lactylation, crucial for the transcription of immunosuppressive genes[108]. Furthermore, reduction of methylation at the *Arg1* and *STAT3* promoter regions has been reported in *ex vivo* induced MDSCs, resulting in the release of STAT3-associated cytokines IL-6 and IL-10, which subsequently activated STAT3 phosphorylation. The phosphorylated STAT3, in turn, bound to the *Arg1* and *S100A8* promoter regions, leading to upregulation of *Arg1* and *S100A8*, thereby augmenting the immunosuppressive capacity of MDSCs[109,110]. Fetahu et al. identified key transcription factors in myeloid cells of neuroblastoma bone marrow metastases linked to open chromatin regions in genes associated with M2 polarization, tumor growth, and metastases, including *IL10*, *TIMP1* and *EREG*[111]. Finally, several studies suggest that PD-1 and PD-L1 expression in tumors is decreased due to epigenetic changes, resulting in resistance to immune checkpoint therapy. Interestingly, the DNA-demethylating agent azacytidine increased PD-L1 expression in non-small cell lung cancer patients[112,113].

In neuroblastoma, two different epigenetic states have been defined: mesenchymal or neuro crest cell-like cells (MES) with a less-differentiated state, and adrenergic or sympathetic noradrenergic cells (ADRN) with a more differentiated state[114–116]. In primary neuroblastomas, the initial tumor mainly consists of the ADRN state[114,115], but the MES state becomes more prominent during relapse and metastasis[117]. Studies showed that human neuroblastoma cells with stronger MES signature have a higher basal inflammatory state, promote T cell infiltration by secreting inflammatory cytokines, and respond to immune checkpoint therapy in an immunocompetent mouse model[118,119]. Specifically, *PRRX1* a component of the mesenchymal core regulatory circuitry, activates the transcription of MHC class I and antigen processing and presentation genes, which subsequently enhance the immunogenic state of neuroblastoma cells[119]. Furthermore, sensing of double-stranded RNA in MES state neuroblastoma cell lines resulted in secretion of proinflammatory cytokines, enrichment of inflammatory transcriptomic signatures and increased tumor killing by T cells *in vitro*[118]. Interestingly, genetic switching of unresponsive ADRN state neuroblastoma cell lines towards the MES state fully restored responsiveness. These studies did, however, not investigate the role of myeloid cells in relation to the epigenetic states of neuroblastoma cells.

In summary, epigenetic alterations are important for immunotherapy resistance, governing not just the expression of immune checkpoint inhibitors, but also influencing immune cell infiltration, antigen presentation, and the expression and release of cytokine profiles within the tumor. Furthermore, they drive myeloid cell reprogramming toward immunosuppressive subsets within the TME, amplifying their suppressive potential.

THE ROLE OF MYELOID CELLS IN IMMUNOTHERAPY

As previously discussed, myeloid cells have been shown to predominantly exhibit a pro-tumorigenic role in neuroblastoma, making them attractive targets for immunotherapeutic interventions. In this section, we provide a summary of established and emerging therapeutic strategies that specifically target myeloid cells in neuroblastoma (**Figure 2**).

Myeloid cells as effector cells of immunotherapy

Myeloid effector cells in anti-GD2 immunotherapy

It is widely recognized that in addition to NK cells, macrophages possess the potential to serve as effector cells in current anti-GD2 antibody therapy. As early as 1990, it was demonstrated that M-CSF-differentiated macrophages could phagocytose neuroblastoma cells upon stimulation with the 3F8 anti-GD2 antibody[120]. Recent studies have further emphasized the efficacy of macrophages as effector cells in antibody immunotherapy [21,77,121]. However, within the TME, macrophages (or TAMs) often exhibit inactivation, refractoriness, or highly immunosuppressive traits, thereby contributing to antibody therapy resistance. Interestingly, in two neuroblastoma patient cohorts, the presence of TAMs expressing PD-L1, as well as the expression of the SLAMF7 pathway and CD163 in TAMs, was found to be beneficial for high-risk patients and correlated with improved survival following immunotherapy[77]. While this may appear counterintuitive, it suggests that despite their immunosuppressive characteristics, TAMs can still be engaged as effector cells in immunotherapy.

Similarly, despite their association with tumor progression in high-risk neuroblastoma, neutrophils and monocytes (or MDSCs) can still be effectively engaged in anti-GD2 antibody therapy (**Table 1**)[46]. In the late 1980s and early 1990s, it was demonstrated that neutrophils could perform antigen-dependent cellular cytotoxicity (ADCC) against human neuroblastoma cells *in vitro* with anti-GD2 antibodies (ch14.18 or 3F8 IgG)[122–125]. Remarkably, Barker and colleagues discovered that granulocytes, displayed superior killing capacity against NMB-7 neuroblastoma cells compared to PBMC[124], which is generally the opposite in IgG antibody therapy. Furthermore, neutrophils derived from neuroblastoma patients (stage IV) retained potent *ex vivo* killing ability against neuroblastoma cells, matching that of neutrophils from healthy donors. This neutrophil-mediated killing is marked by the release of lytic granules[125] and dependent on CD11b/CD18 (collectively known as membrane-activated complex 1 (Mac-1) or complement receptor 3 (CR3)), as well as FcγRII and FcγRIII[126].

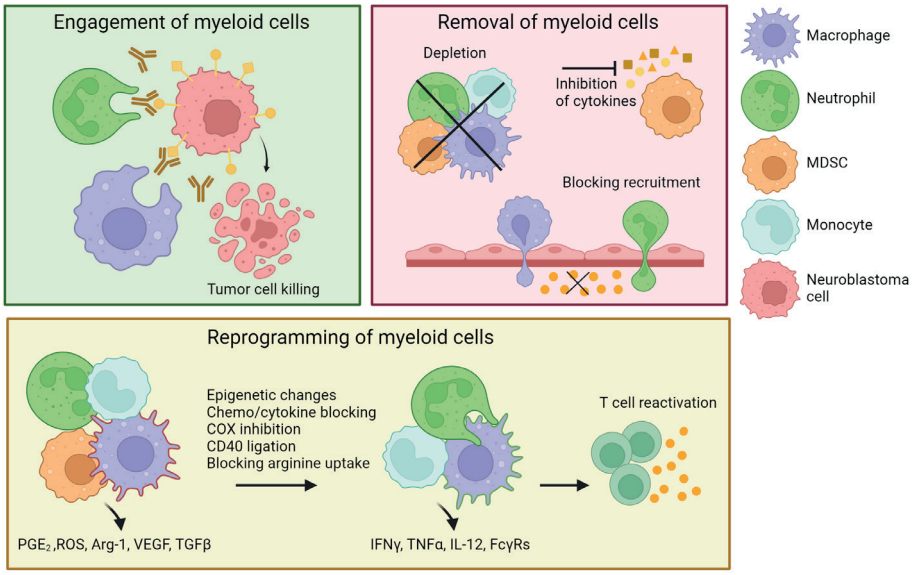

Figure 2 | Three main strategies of targeting myeloid cells in neuroblastoma. Myeloid cells can be 1.) engaged as effector cells of immunotherapy via ADCC. 2.) removed from the TME by depletion with antibodies (anti-CD11b, anti-CD105, anti-CD33, or anti-CSF-1R) or myoablative chemotherapy. Additionally, myeloid cells can be depleted via inhibition of cytokines via IL-6R blockade, or inhibition of TGFβ or STAT3. Finally, their recruitment can be blocked with CCR2 inhibitors, or anti-CCL2 or anti- TGFβ. 3.) reprogrammed to an anti-tumor, immunostimulatory phenotype, leading to reactivation of T cells. Myeloid cell reprogramming can be achieved by inducing epigenetic modifications, inhibiting cytokines and chemokines, suppressing COX activity, stimulating CD40 ligation, and preventing arginine uptake. Abbreviations: ADCC = antigen-dependent cellular cytotoxicity, Arg-1 = arginase-1, CCL2 = C–C motif chemokine ligand 2, CCR2 = CCL2 receptor, COX = cyclooxygenase, CSF-1R = colony stimulating factor 1 receptor, FcγRs = Fc gamma receptors, IFNγ = interferon gamma, ROS = reactive oxygen species, TGFβ = transforming growth factor beta, TME = tumor microenvironment, TNFα = tumor necrosis factor alpha, VEGF = vascular endothelial growth factor.

Subsequently, in two clinical trials investigating 3F8 anti-GD2 antibody therapy, it was demonstrated that neutrophil-mediated ADCC was indeed responsible for therapeutic efficacy in neuroblastoma patients[128,129]. Activated neutrophils, characterized by the CD11b activation epitope CBRM1/5, were associated with prolonged progression-free survival[130]. Moreover, an *FCGR2A* polymorphism in patients showed a correlation with clinical outcome following anti-GD2 antibody and GM-CSF therapy[130,144]. The FcγRIIa-R131 variant exhibited higher affinity for the murine IgG3 3F8 antibody than FcγRIIa-H131, resulting in enhanced ADCC. Consequently, patients homozygous for the *FCGR2A-R131* allele demonstrated extended progression-free survival after treatment with murine 3F8 antibody and GM-CSF compared to patients who were heterozygous or homozygous for *FCGR2A-H131*[130]. It is noteworthy that the affinity of these polymorphisms is reversed for *human* IgG1 antibodies, thus leading to an opposite correlation with dinutuximab (anti-GD2, ch14.18 antibody), which is of the human IgG1 isotype[144]. Given the high expression of FcγRIIa on

neutrophils, macrophages, and monocytes and its absence on NK cells, the prognostic value of this FcγRIIa polymorphism indicates that myeloid cells constitute a major effector cell population in antibody therapy for neuroblastoma.

Therapeutic target	Treatment	Studied population	(Pre-) clinical model	Outcome	Ref
GD2	Anti-GD2	PMN	*In vitro*, *ex vivo*	Induces ADCC of NB cell lines by healthy and patient-derived PMN, via FcγRII, FcγRIII and Mac-1	122–127
GD2	Anti-GD2	PMN, other myeloid cells	Clinical trials	PMN-mediated ADCC via FcγRII and FcγRIII, improvement EFS and OS	12,13,77,128–130
GD2	Anti-GD2 + GM-CSF	PMN, other myeloid cells	*In vitro*, clinical trials	GM-CSF increases and activates myeloid cells, increases CD11b expression, enhances PMN-mediated ADCC by anti-GD2	12,123,125,126, 128,131,132
GD2	Anti-GD2 + G-CSF	PMN	*In vitro*	Similar to GM-CSF, enhances PMN-mediated ADCC by anti-GD2	133
GD2	Anti-GD2 + retinoic acid	PMN	*In vitro*	Retinoic acid attracts PMN via IL-8 production	134
IL-2R	IL-2 or IL-2-expressing NB cells	Eosinophils	In patients, clinical trials	Increase of eosinophil numbers, elevated IL-5 serum levels	131,135–137
GD2	IgA anti-GD2	PMN, TAM	*In vitro*, 9464D syngeneic and IMR32 xenograft models	Superior neutrophil activation compared to IgG anti-GD2 especially with patient-derived PMN, prolonged survival *in vivo*	138,139
GD2 + CD47	Anti-GD2 IgG + anti-CD47	PMN, TAM	*In vitro*, multiple mouse models	Enhanced phagocytosis and PMN-mediated killing of NB cells by disrupting CD47/SIRPα axis, prolonged survival *in vivo*, influx of intratumoral macrophages	21,47,121
B7-H3	B7-H3/GD2 bispecific or anti-B7-H3 ADC	Myeloid cells	PDX models	Efficacy possibly mediated by myeloid cells	140,141
GPC2	anti-GPC2 ADC	Monocytes, TAM, MDSC	NXS2 xenograft and 9464D syngeneic models	Recruitment monocytes, TAM and MDSC, phagocytosis of NB cells, prolonged survival	142,143

Table 1 | Comprehensive overview of treatments in neuroblastoma engaging myeloid cells as effector cells.

Although the introduction of anti-GD2 antibody therapy significantly improved survival rates, resistance still develops in many patients. *In vitro* studies have revealed that GD2 expression levels do not correlate with neutrophil-mediated ADCC, suggesting abundant GD2 levels on all neuroblastoma cells[127]. However, the effectiveness of neutrophil-mediated tumor cell killing was diminished in tumor cells displaying high rates of antibody internalization, thus proposing a potential mechanism for treatment resistance.

Previously, anti-GD2 immunotherapy was combined with IL-2. However, this was discontinued, since a recent randomized phase III trial of patients with high-risk neuroblastoma showed that the addition of IL-2 to anti-GD2 antibody therapy did not improve outcome and increased treatment toxicity[8]. Besides its stimulatory effects on NK-cell mediated ADCC[145], IL-2 was shown to upregulate expression of the adhesion molecule CD18 on neutrophils, but to decrease total neutrophil numbers[131,146]. Additionally, two immune monitoring studies in neuroblastoma observed that IL-2 cycles increased eosinophil counts[131,135]. It is generally known that eosinophils can be pre-activated by IL-2 and subsequently exert ADCC[147]. However, eosinophils are likely not involved in tumor killing, since similar levels of ADCC were found in patients with high compared to low eosinophil count and eosinophil counts were not significantly correlated with survival. Furthermore, long-term infusion of anti-GD2 in combination with IL-2 resulted in induction of Tregs, which inversely correlated with IFN-γ levels and progression-free survival[135].

In the United States, anti-GD2 antibody therapy is enhanced with GM-CSF, but its accessibility and availability outside the country are restricted due to regulatory constraints. GM-CSF increases numbers of circulating neutrophils, monocytes, and eosinophils and promotes the release of myeloid cell-associated factors such as CXCL11, CCL17, CCL23, and MCP4[131]. However, the primary mechanism of GM-CSF is augmenting neutrophil-mediated ADCC and to a lesser extent activating macrophages and monocytes. Both *in vitro* and in patients, the combination of GM-CSF with anti-GD2 antibodies activates neutrophils and upregulates CD11b expression[12,123,125,126,128]. Particularly in patients with refractory or minimal residual disease, the addition of GM-CSF to the treatment regimen has shown favorable responses[12,132]. Interestingly, the route of GM-CSF administration influences the degree of neutrophil activation, with subcutaneous injection resulting in a higher percentage of activated neutrophils compared to intravenous injection[129]. However, in other cancer types, such as liver carcinoma and glioblastoma, GM-CSF is involved in the induction of MDSCs[148,149], but during immunotherapy in neuroblastoma, GM-CSF appears to activate neutrophils instead. This may be attributed to the concurrent antibody therapy skewing neutrophils toward an anti-tumor phenotype and/or the intermittent cycles of GM-CSF administration rather than a continuous treatment. It is plausible that low-concentration, chronic GM-CSF stimulation induces MDSCs through negative feedback loops, whereas high-concentration, acute GM-CSF stimulation as applied in neuroblastoma therapy, activates neutrophils. Since GM-CSF is not available in Europe, several research

groups in the Netherlands have explored the potential use of G-CSF as an alternative to GM-CSF[133]. They concluded that G-CSF exhibited comparable potency to GM-CSF in enhancing ADCC by neutrophils from both healthy donors and neuroblastoma patients. Similar to GM-CSF-enhanced ADCC, the killing mechanism was dependent on FcγRIIa and CD11b/CD18. Given the similarity in performance between G-CSF and GM-CSF, the authors proposed that the addition of G-CSF to anti-GD2 immunotherapy should be evaluated in patients.

Next to GM-CSF, the current treatment regimen for high-risk neuroblastoma includes 13-*cis* retinoic acid, also known as isotretinoin. *In vitro* studies have demonstrated that retinoic acid inhibits neuroblastoma cell growth and promotes cellular differentiation[150]. While retinoic acid alone does not improve overall survival[151], pretreatment with retinoic acid enhances the susceptibility of neuroblastoma cells to antibody therapy. Furthermore, differentiated neuroblastoma cells treated with retinoic acid produce IL-8, a crucial cytokine involved in the attraction of neutrophils[134]. IL-8-mediated neutrophil attraction may augment neutrophil-mediated killing induced by anti-GD2 antibody therapy. However, studies conducted in other advanced cancers have reported that IL-8 production and subsequent recruitment of neutrophils/PMN-MDSC can be detrimental, particularly in the context of checkpoint inhibitor treatment[152,153]. Additionally, retinoic acid can exhibit both immunosuppressive effects, such as differentiation of immunosuppressive TAM[154,155], and immunostimulatory effects, such as induction of inflammatory anti-tumor macrophages in other cancer types[156,157]. It is important to note though that most of these studies involved an isomer of 13-*cis* retinoic acid—all-trans retinoic acid—which may have a slightly different mechanism of action. These studies combined underscore the potential effects of 13-*cis* retinoic acid treatment on the TME, although its specific impact on the neuroblastoma TME remains largely unknown.

Improving myeloid engagement in anti-GD2 immunotherapy

Several strategies have been developed to improve efficacy of anti-GD2 antibody therapy by targeting myeloid cells. For example, neutrophils exhibit stronger activation in response to IgA antibodies, via their Fc alpha receptor (FcαRI or CD89), compared to IgG antibodies. Our laboratory demonstrated the superior ability of IgA1 anti-GD2 antibodies, which share the same variable region as dinutuximab (ch14.18), in mediating neutrophil-mediated tumor cell killing compared to IgG1 ch14.18[138]. Importantly, IgA anti-GD2 antibodies did not induce neuropathic pain in mice, unlike IgG anti-GD2 antibodies, primarily due to the absence of the complement factor C1q-binding site. Consequently, IgA antibodies do not activate complement on GD2 expressing nerves, a factor implicated in IgG-induced neuropathic pain[158]. Moreover, we developed a novel form of IgA anti-GD2 antibody (IgA3.0 ch14.18) that is suitable for clinical application, lacking *O*-glycosylation and featuring mutations that enhance antibody stability and prolong half-life[139]. In long-term mouse

models, including xenograft and immunocompetent models with IMR32 and 9464D cells, IgA3.0 ch14.18 demonstrated remarkable anti-tumor efficacy. Furthermore, IgA3.0 ch14.18 effectively induced tumor cell killing by patient neutrophils, while IgG1 ch14.18-mediated tumor cell killing was significantly diminished with patient PBMC compared to healthy donor PBMC. In summary, harnessing and enhancing the anti-tumorigenic activity of neutrophils holds significant promise as a novel approach in the treatment of neuroblastoma.

Another novel strategy to enhance anti-GD2 antibody therapy is to block the CD47/SIRPα axis, analogous to immune checkpoints in T cell biology such as CTLA-4 and PD1/PD-L1. CD47, known as the 'don't eat me' signal, is frequently upregulated in various cancers, including neuroblastoma[47]. Through its interaction with the SIRPα (signal regulatory protein alpha or CD172a) receptor, CD47 inhibits myeloid cell-mediated killing. In the context of neuroblastoma, Theruvath et al. demonstrated that the combination of IgG anti-GD2 and anti-CD47 therapy enhanced macrophage-mediated phagocytosis of neuroblastoma cells *in vitro* synergistically and led to tumor eradication in mouse xenograft and syngeneic models[21]. The efficacy of this combination therapy primarily relied on phagocytosis of tumor cells by macrophages. Furthermore, the study revealed that ligation of anti-GD2 antibodies upregulated surface calreticulin, which primes macrophages for phagocytosis and disrupts the interaction between GD2 and Siglec-7, another myeloid checkpoint. Consequently, the authors found that the synergy was specific to the combination of anti-GD2 antibodies, as anti-CD47 therapy showed less synergy with antibodies targeting other antigens, such as B7-H3. Encouraged by these findings, a clinical trial investigating the combination of anti-GD2 (dinutuximab) and anti-CD47 (magrolimab) antibodies in neuroblastoma relapse patients was initiated (NCT04751383).

Similarly, anti-CD47 synergizes with antibodies solely recognizing the *O*-acetyl variant of GD2, developed by the lab of Stephane Birklé[121]. Interestingly, anti-*O*-acetyl-GD2 antibody therapy enhanced CD47 expression on tumor cells and induced influx of F4/80^{+} macrophages in a NXS2 liver metastasis model, which further explains the synergy of anti-GD2 and anti-CD47 therapy. Though the previous studies did not find a significant role for neutrophils in mouse models upon anti-GD2 and anti-CD47 combination treatment, Martínez-Sanz and colleagues showed that human neutrophils can be unleashed by this combination strategy *in vitro*[47]. Dinutuximab induced neutrophil-mediated killing of unmodified neuroblastoma cell lines up to 5–20%, whereas up to 80% killing was achieved in CD47 knockout cell lines. It will be interesting to evaluate in patients whether only macrophages or also other myeloid cells, such as neutrophils are involved in tumor clearance upon combination therapy.

Recently, in other cancers it was described that neutrophils can be activated to their full killing potential by supplementing IgG antibody therapy with TNF and CD40 agonists[159]. Since Voeller and colleagues already described synergy between CD40 agonists and anti-

GD2 therapy in neuroblastoma[160], the addition of TNF and CD40 agonists to the treatment regimen could prove a promising new strategy.

Novel strategies for antibody immunotherapy engaging myeloid cells

Currently, alternative targets for antibody therapy in neuroblastoma are being explored, to circumvent the problem of GD2 downregulation, which is particularly prominent in a mesenchymal subset of neuroblastoma cells. Studies have identified B7-H3 as a viable alternative target, given its sustained expression in mesenchymal neuroblastoma cells[161,162]. The laboratory of Paul Sondel is currently investigating a bispecific SNIPER antibody that targets both GD2 and B7-H3, demonstrating superior efficacy compared to monospecific anti-B7-H3 antibodies and lacking the induction of neuropathic pain[140]. Furthermore, Kendsersky et al. have demonstrated *in vivo* efficacy of the B7-H3-targeting antibody–drug conjugate (ADC) m276-SL-PBD in patient-derived xenograft (PDX) models of neuroblastoma[141]. However, the involvement of myeloid cells in the effector mechanisms of these novel therapies remains unknown.

Another promising target against which ADCs have been developed is the oncoprotein GPC2, which is overexpressed in neuroblastoma and drives tumor cell proliferation[142,143]. Anti-GPC2 ADCs have been shown to induce immunogenic cell death in mouse models (NXS2 and 9464D) with GPC2 overexpression, leading to the recruitment of monocytes, macrophages, and MDSCs to the TME. Alongside T cells, macrophages have emerged as major mediators of the anti-GPC2 ADC treatment, and the combination of anti-GPC2 ADCs with anti-CD47 blockade has demonstrated a modest reduction in tumor burden[143].

Though myeloid cells have a negative image in the context of cancer due to their immunosuppressive traits, their potential as effector cells should not be underestimated. Though neutrophils and macrophages are already important mediators in antibody therapy their full potential is not yet reached and myeloid cell engagement can be enhanced, for example by targeting the CD47/SIRPα myeloid checkpoint.

Removal of suppressive myeloid cells from the TME

Direct depletion of myeloid cells

A potential strategy to counteract the suppressive function of myeloid cells in the TME is the depletion of these cell populations as summarized in **Table 2**. One approach involves using anti-CD11b antibodies to target and deplete all cells of the myeloid lineage. In a study conducted on NXS2 tumor-bearing mice treated with dinutuximab, anti-CD11b antibodies resulted in a modest delay in tumor growth and prolonged survival[163]. Another approach employs anti-CD105 antibodies, which specifically target a transmembrane co-receptor for both TGF-β and bone morphogenic protein-9 (BMP-9). By administering anti-CD105 antibodies, not only monocytes but also MDS and endothelial cells could be depleted[164].

This approach resulted in improved efficacy of anti-GD2 antibodies when combined with adoptively transferred activated human NK cells in neuroblastoma patient-derived xenograft (PDX) models.

Park et al. studied myeloid depletion methods in a neuroblastoma PDX model with bispecific GD2 antibodies (GD2-EATs)[165]. They employed various approaches including anti-Ly6G antibodies (targeting neutrophils and PMN-MDSC), anti-Ly6C antibodies (targeting M-MDSC and TAM), anti-CSF-1R antibodies or clodronate liposome (targeting macrophages) and dexamethasone (targeting monocytes). All improved T cell infiltration and survival when combined with GD2-EATs, with macrophage depletion being most effective. Similarly, depletion of human monocytes and macrophages through CSF-1R inhibition using BLZ945, in combination with anti-CSF-1R treatment, enhanced chemotherapeutic efficacy in immunodeficient NOD/SCID mice with neuroblastoma xenografts, independently of T cell contribution[166]. Additionally, Abraham et al. demonstrated that intratumoral injections of small interfering RNAs targeting mouse CSF-1 resulted in significant suppression of tumor growth in SK-N-AS and SK-N-DZ neuroblastoma xenografts, accompanied by decreased TAM infiltration[167]. Finally, treatment of human MDSC with the anti-CD33 ADC gemtuzumab ozogamicin led to cell death *in vitro*[168]. In co-culture experiments, gemtuzumab ozogamicin restored T cell proliferation and enhanced the activity of anti-GD2 CAR-T cells.

Importantly, depletion of myeloid cells is considered a 'sledgehammer approach' as myeloid effector cells that are required for immunotherapy are depleted as well. Targeting specific suppressive myeloid subsets might be more effective. NKT cells offer promise, as they can selectively eliminate immunosuppressive TAMs and MDSCs via CD1d interaction[87,169]. NKT cells also produce GM-CSF, inducing M1-like TAMs[87,170] and decreased IL-10 expression in PMN-MDSCs[169], thereby reverting their suppressive function. Although NKT cells are typically present in low numbers within the TME, GD2-CAR NKT cells have shown promise by maintaining their cytotoxic activity against suppressive TAMs[171]. Therefore, harnessing GD2-CAR NKT cells could serve as an indirect approach to deplete immunosuppressive TAMs and MDSCs in the TME.

Myeloablative chemotherapy

The chemotherapeutic doxorubicin (DOX) is currently the most specific drug for the selective removal of MDSC through ROS-mediated apoptosis induction[182], enhancing T cell activity and reducing Tregs in a BALB/c NB mouse model[172,173]. Residual myeloid cells exhibited reduced expression of Arg-1, indoleamine-pyrrole 2,3-dioxygenase (IDO), as well as STAT3, STAT5, and STAT6, which are key signaling pathways involved in MDSC activation. Notably, in contrast to findings in a murine study on breast cancer[182], DOX affected macrophages in neuroblastoma by inhibiting their polarization from M1 to M2 phenotype[173]. Dopamine yielded similar outcomes, albeit less potent than DOX. Furthermore, DOX enhanced antigen-specific $CD8^+$ T cell cytotoxicity against neuroblastoma cells by upregulating CD3ζ

and L-selectin[174]. Importantly, DOX improved efficacy of anti-GD2 therapy and adoptive T cell transfer, resulting in enhanced survival rates in BALB/c mice[172].

Platinum-based chemotherapeutics, such as cisplatin, have been demonstrated to inhibit STAT signaling, as evidenced by their ability to suppress cyclooxygenase (COX)-2-expressing M-MDSCs induced by melanoma tumor cells *in vitro*[183]. This inhibitory effect of cisplatin on M-MDSCs was further observed in patients with head and neck squamous cell carcinoma who underwent intravenous cisplatin treatment, leading to a drastic reduction in M-MDSC frequency. Furthermore, the surviving M-MDSCs exhibited decreased expression of COX2 and Arg-1, a result of attenuated STAT3 signaling, consequently impairing their *ex vivo* T cell inhibitory capacity. In a mouse model of SK-N-DX neuroblastoma, cisplatin was effective in reducing tumor burden. However, the specific mechanism underlying its action in this model was not investigated[175]. 5-FU, a chemotherapeutic agent, exerts its effects by targeting thymidylate synthase and depleting myeloid suppressive cells. In a syngeneic neuroblastoma mouse model, treatment with 5-FU resulted in a reduction of $CD11b^+$ cells within the tumor and enhanced the efficacy of anti-GD2 antibodies[163]. Furthermore, depletion of MDSCs following 5-FU treatment improved the inhibitory effect of recipient leukocyte infusion on local tumor growth in murine neuroblastoma (Neuro2A)-bearing chimeras[176]. Importantly, it should be noted that one of the current chemotherapy regimens COJEC, has been associated with the induction of M2 macrophages in *MYCN*-amplified neuroblastoma[184]. Similarly, a neuroblastoma PDX model demonstrated that macrophage infiltration promoted the outgrowth of tumor cells that had survived COJEC-like chemotherapy. Consequently, the COJEC regimen could contribute to the development of resistance to anti-GD2 therapy in neuroblastoma and T cell-based therapeutics. Currently, the COJEC regimen, consisting of cisplatin, vincristine, carboplatin, etoposide, and cyclophosphamide, is frequently applied[185]. From a clinical point of view there is a strong wish to add anti-GD2 therapy during induction chemotherapy. Therefore, it could be important to explore alternative chemotherapeutic regimens that can synergize with immunotherapy.

Therapeutic target	Treatment	Treatment strategy	Studied population	Pre-clinical model	Outcome	Ref
CD11b	Anti-CD11b	Depletion	Myeloid lineage	NXS2 xenograft model	Tumor growth delay, prolonged survival	163
CD105	Anti-CD105	Depletion	Monocytes, MSC, endothelial cells	PDX models	Improved efficacy of anti-GD2 antibodies when combined with adoptively transferred activated human NK cells	164
Ly6G	Anti-Ly6G (+ GD2-EATs)	Depletion	PMN, PMN-MDSC	PDX models	Higher T cell and M-MDSC infiltration in the tumor, prolonged survival	165
Ly6C	Anti-Ly6C (+ GD2-EATs)	Depletion	Monocytes, M-MDSC	PDX models	Decrease in TAM and increase in intratumoral PMN-MDSC and T cells, prolonged survival	165
Macrophages/ CSF1R	Clodronate liposomes or anti-CSF-1R (+ GD2-EATs)	Depletion	TAM	PDX models	Decrease in M-MDSC and increase in PMN-MDSC and T cells, prolonged survival	165
CSF1R	Inhibitor BLZ945 + anti-CSF-1R	Depletion	Monocytes, TAM	CHLA-136 and CHLA-255 xenograft and PDX models	Improvement of chemotherapeutic efficacy, which was independent of T cell contribution	166
CSF-1	Small interfering RNAs	Depletion	TAM	SK-N-AS and SK-N-DZ xenograft models	Decreased intratumoral TAM, matrix metalloprotease 12 levels and angiogenesis, suppression of tumor outgrowth	167
Glucocorticoid receptor	Dexamethason (+ GD2-EATs)	Depletion and reprogramming	Monocytes, TAM, M-MDSC	PDX models	Decrease in IL-2, IL-6, and TNFα release, increase in PMN-MDSC and T cells, and enhanced survival	165
CD33	Gemtuzumab ozogamicin	Depletion	MDSC	*In vitro*	Restored T cell proliferation, MDSC cell death, enhanced anti-GD2 CAR-T cell activity	168
CD1d/GM-CSF	NKT cells	Depletion and reprogramming	MDSC, TAM	*In vitro*, CHLA-255 xenograft model	Killing of suppressive TAM and MDSC via CD1d, NKT cells-derived GM-CSF differentiates TAM to M1, decrease of IL-10 expression in PMN-MDSC	87,169–171
Apoptosis (via ROS)	Doxorubicin	Depletion and reprogramming	MDSC	*In vitro,* Neuro2a syngeneic model	Increased T cell proliferation and function, reduction in Tregs, less suppressive myeloid cells, inhibition of TAM polarization to M2, improved efficacy of anti-GD2 and adoptive T cell transfer, improved survival	172,173
Apoptosis (via ROS)	Doxorubicin	Depletion	MDSC	*In vitro*	Improved antigen-specific CTL-killing, via upregulating CD3ζ and L-selectin	174

Forming DNA adducts	Cisplatin	Depletion	M-MDSC	SK-N-DX xenograft model	Reducing tumor burden	175
Thymidylate synthase	5-FU	Depletion	MDSC	Syngeneic mouse model	Reduction of $CD11b^+$ cells in the tumor, improved efficacy of anti-GD2	163
Thymidylate synthase	5-FU	Depletion	MDSC	Neuro2A-bearing chimeras	Improved local tumor growth-inhibitory effect of recipient leukocyte infusion	176
STAT3	AZD1480, ruxolitinib	Inhibition of cytokines	TAM	NBT2 model in NB-TAG and NSG mice	Reduction of TAM-mediated upregulation of MYCN tumor growth inhibition	88
STAT3	STAT3 inhibition, or knockdown	Inhibition of cytokines	TAM	*In vitro*	Abrogates drug-resistance to etoposide and melphalan due to monocyte-derived IL-6 inducing STAT3 signaling	177
IL-6R	Tocilizumab	Inhibition of cytokines	TAM	CHLA-255 and CHLA-136 xenograft models	Apoptosis of TAM	95
TGF-βR1	Galunisertib	Inhibition of cytokines	TAM, MSC	CHLA-255 and CHLA-136 xenograft models	Decrease of IL-6 production by NB cells, apoptosis of TAM, restored NK cell activity	95
TGF-β	Anti-TGF-β	Blocking recruitment	TAM	TH-MYCN mice	Decreased recruitment of M2 TAM	178
COX enzymes	Aspirin	Blocking recruitment	MDSC, immature DC, TAM	TH-MYCN mice	Decreased recruitment of MDSCs, immature DCs and TAMs, reduced tumor burden	55,179
CXCR2	Anti-CXCR2	Blocking recruitment	TAM, CAF	*In vitro*	Abrogation of the invasive ability of NB cells induced by TAM-derived CXCL2	73
CCL2	S1P2 agonist AB1 and JTE-013	Blocking recruitment	TAM	SK-N-AS xenograft model	Inhibition of TAM infiltration, reduced VEGF expression and reduced tumor outgrowth	180,181
DNA synthesis	Oxaliplatin	Blocking recruitment	PMN	TH-MYCN mice	Low-dose decreases recruitment PMN	178

Table 2 | Comprehensive overview of treatments in neuroblastoma removing myeloid cells from the tumor microenvironment.

Inhibition of cytokines

As described above, IL-6 stimulation and STAT signaling in myeloid cells are associated with immunosuppressive characteristics, including Arg-1 expression. STAT3 inhibition with AZD1480 or ruxolitinib reduced TAM-mediated MYC upregulation, restraining NBT2 tumor growth in NB-tag and NSG mice[88]. Moreover, Ara et al. demonstrated that IL-6 from monocytes activated STAT3 in neuroblastoma cells, causing drug resistance against etoposide and melphalan *in vitro*, which was counteracted by STAT3 inhibition or knockdown[177]. Studies in other cancer types suggest that STAT3 inhibition impedes the local proliferation of TAMs, thereby reducing their abundance within the tumor[186]. Furthermore, Louault et al. showed that IL-6 produced by MSC and neuroblastoma cells promoted the survival of TAMs *ex vivo*[95]. Apoptosis of TAMs was observed upon blocking the IL-6 receptor using the monoclonal antibody Tocilizumab. Upstream, TGF-β stimulated IL-6 production in neuroblastoma cells and MSC, contributing to the suppression of NK cell cytotoxic activity. Treatment with Galunisertib, a TGF-βR1 inhibitor, decreased IL-6 production in co-cultures and restored the activity of NK cells. Therefore, targeting the IL-6/TGF-β axis holds promise as a strategy to selectively deplete TAMs from the neuroblastoma TME.

Blocking recruitment of myeloid cells

Rather than eradicating the myeloid compartment entirely, an alternative strategy involves impeding myeloid cell recruitment to the tumor site. Overexpressed COX enzymes in neuroblastoma drive myeloid cell attraction by synthesizing prostaglandins, including PGE_2[55,187,188]. Blocking COX with aspirin in TH-MYCN mice led to diminished tumor burden and reduced tumor-associated myeloid cells like MDSCs, immature DCs, and TAMs[55,179]. The CCL2/CCR2 axis is pivotal for recruiting monocytes, myeloid cells, and plasmacytoid DCs in *MYCN*-nonamplified neuroblastoma[89]. In other cancer types, inhibiting the CCL2/CCR2 axis with CCR2 inhibitors or anti-CCL2 antibodies has demonstrated reduced myeloid cell recruitment and improved clinical outcomes[189–191]. Sphingosine-1 (S1P), a bioactive lipid, induced CCL2 expression in neuroblastoma via S1P2[180]. Inhibiting S1P2 with the stable derivative AB1, but not its precursor JTE-013, decreased macrophage infiltration in neuroblastoma xenografts, underscoring AB1's potential to inhibit TAM infiltration[181]. Furthermore, certain chemotherapeutic and immunotherapeutic drugs impact immune cell recruitment to tumors. For example, anti-TGF-β reduced M2 TAM recruitment in a neuroblastoma model, and low-dose oxaliplatin hindered neutrophil migration to tumors[178]. While depleting or blocking myeloid cells has been proven effective in neuroblastoma, it also depletes potential immunotherapy effectors. Additionally, targeting specific cytokines or immunosuppressive mediators produced by MDSC can be useful, but this only targets a small part of the problem. Reprogramming suppressive myeloid cells may be the optimal strategy, interrupting immunosuppressive traits while preserving myeloid cells as effectors of immunotherapy.

Reprogramming suppressive myeloid cells into an active phenotype

Finally, a highly elegant approach to target immunosuppressive myeloid cells involves reprogramming their suppressive phenotype into an antitumor, immunostimulatory state (**Table 3**). Various published therapeutic approaches have demonstrated successful myeloid cell reprogramming with consequent T cell activation. For instance, ibrutinib, an irreversible molecular inhibitor of Bruton's tyrosine kinase (BTK), was shown to reverse T cell suppression mediated by murine MDSC in a neuroblastoma mouse model[192]. This was evidenced by altered NO production and decreased mRNA expression of immunosuppressive factors *Ido*, *Arg*, and *Tgfb*. Moreover, ibrutinib-mediated BTK inhibition increased $CD8^+$ T cell infiltration and enhanced response to anti-PD-L1 checkpoint inhibitor therapy. As previously discussed, neuroblastoma-derived factors hinder early myeloid cell differentiation to monocytes and macrophages, promoting monocyte suppressive function via M-CSF/CSF-1R interaction[57]. CSF-1R inhibitor BLZ945 effectively blocked CSF-1R-expressing suppressive myeloid cell generation and reversed tumor-educated monocyte suppression. Combining CSF-1R inhibition with anti-PD-1/PD-L1 immune checkpoint blockade in TH-MYCN mice enhanced activation of tumor-reactive T cells. Interestingly, PD-1 blockade induced enhanced T cell M-CSF secretion, enhancing monocyte suppressive capacity[193]. Thus, BLZ945-CSF-1R inhibition combined with PD-1 blockade synergistically controlled tumor growth. Additionally, catechins such as Polyphenon E exhibit neuroblastoma anticancer effects by inhibiting MDSC activity. Administered via drinking water in multiple neuroblastoma mouse models, Polyphenon E hindered MDSC development and mobility, and facilitated their differentiation into neutrophils through 67 kDa laminin receptor signaling and G-CSF induction[65]. Moreover, it lowered Arg-1 expression on MDSCs, promoting T cell proliferation in patient metastases. Another treatment strategy that potentiates T cells by reprogramming myeloid cells is addition of neutrophil-activating protein (NAP) in therapies like CAR T cell or oncolytic virus treatments. Tumino et al. reported an increase in circulating PMN-MDSC numbers upon GD2.CAR T-cell therapy[194]. Circulating PMN-MDSCs inversely correlated with GD2.CAR T-cell levels, potentially predicting treatment response. Moreover, Stroncek et al. demonstrated that monocytes inhibit the expansion of GD2.CAR T cells in neuroblastoma patients[195]. In accordance with this, GD2.CAR T cells were ineffective in a syngeneic NXS2 neuroblastoma model. However, GD2.CAR T cells designed to express NAP delayed tumor outgrowth by generating a 'hot' TME with high infiltration of neutrophils, M1 macrophages, NK cells, $CD8^+$ T cells, DCs, and a reduced number of Tregs[196], which potentiated GD2.CAR T cell therapy. Likewise, oncolytic virus therapy can be enhanced by incorporating NAP into the virus load. Oncolytic Vaccinia viruses carrying a GD2 mimotope were ineffective against NXS2 tumors, but the inclusion of NAP led to tumor growth inhibition[197].

Therapeutic target	Treatment	Studied population	Pre-clinical model	Outcome	Ref
BTK	Ibrutinib	MDSC	9464D syngeneic model	Decrease of NO expression and of *Ido*, *Arg*, and *Tgfb* mRNA expression in MDSC, reversion of T cell suppression, increased $CD8^+$ T cell infiltration, improved response to anti-PD-L1	192
CSF1R (and PD1)	BLZ945 (+ anti-PD-1)	MDSC, monocytes	TH-MYCN mice	Reverted suppressive functions of tumor-educated monocytes, abolished induction of MDSC, activation of tumor-reactive T cells, improved anti-PD-1/PD-L1 blockade	57,193
TLR2	NAP (+ CAR T cells or oncolytic virus)	PMN	NXS2 syngeneic model	infiltration of neutrophils, M1 macrophages, NK cells, $CD8^+$ T cells and DCs, reduced number of Tregs, reduced tumor growth	196,197
mPGES-1	Small molecule inhibitor	CAFs, TAM	SK-N-AS xenograft model and TH-MYCN mice	PGE_2 production was inhibited by CAFs, resulting in reduced tumor growth, impaired angiogenesis, and polarization of TAM to pro-inflammatory M1	198
Histone deacetylation	Vorinostat (+ retinoic acid or MIBG)	TAM, M-MDSC	TH-MYCN mice, phase I clinical trial	Upregulation of GD2 in NB cells, increase of TAM with mixed M1 and M2 phenotype, depletion of M-MDSC, downregulation of suppressive markers on myeloid cells, beneficial response rates in NB patients	199–201
IFNγ	IFNγ-expressing MSC	TAM	CHLA-255 orthotopic xenograft model	TAM polarization to M1 phenotype, reduced tumor growth, prolonged survival	202
FABP4	Anti-IL-1a	TAM	*In vitro*	Suppression of FABP4-mediated migration and invasion of NB cells	203
CD40	CD40 agonist	TAM	NXS2 syngeneic model	M1 polarization of TAMs	204
CD40	CD40 agonist + CpG	TAM	NXS2 syngeneic model	Anti-CD40 primes TAM to respond to CpG, resulting in M1 polarization and tumor growth inhibition	205
CD40	CD40 agonist + CpG + chemo, or radiation, anti-GD2 and anti-CTLA-4	TAM	9464D syngeneic model	Synergistic anti-tumor effects of combination treatments via repolarization of TAMs to M1 phenotype	160,206
Rac2	Rac2 knockout	TAM	$Rac2^{-/-}$ mice with 9464D model	Rac2 knockout promotes M1 TAM differentiation, reduced tumor growth	207
67 kDa laminin receptor	Polyphenon E	MDSC, PMN	TH-MYCN mice	Impairment of development and motility of MDSC, MDSC differentiation towards PMN, induction of G-CSF, decreased Arg-1 expression on remaining MDSC, increased T cell proliferation	65
BRD3/4	BET bromodomain inhibitors	Myeloid cells	*In vitro*, multiple *in vivo* models	Tumor growth inhibition, *MYCN* downregulation, possibly reprogramming of myeloid cells	208–210

Table 3 | Comprehensive overview of treatments in neuroblastoma reprogramming myeloid cells into an immunostimulatory phenotype.

Other studies did report strategies to reprogram myeloid cells, but did not observe or investigate the indirect effects on T cells. COX inhibitors have shown promise in limiting myeloid infiltration by inhibiting PGE_2, but their use is constrained by potential side effects. An alternative approach by Kock et al. selectively targeted microsomal prostaglandin E synthase-1 (mPGES-1) using a small molecule inhibitor in an immunocompetent transgenic neuroblastoma mouse model with *MYCN* oncogene expression[198]. This targeted inhibition of mPGES-1 suppressed PGE_2 production specifically in CAFs, resulting in reduced tumor growth, impaired angiogenesis, and macrophage polarization towards a pro-inflammatory M1 phenotype. In addition, human FABP4-expressing macrophages were discovered to promote migration, invasion, and tumor growth of neuroblastoma cell lines[203]. This was facilitated through FABP4 binding to ATPB, which triggered ATPB ubiquitination, reduced ATP levels, and deactivated the NF-kB/RelA-IL-1a pathways, driving macrophages into an M2 phenotype. Blocking antibodies against IL-1a effectively countered FABP4-induced increased migration and invasion. Ligating CD40 offers another approach to target myeloid cells, as it activates antigen-presenting cells including macrophages. In murine NXS2 models, anti-CD40 treatment led to delayed tumor progression by inducing a proinflammatory M1 phenotype in macrophages and stimulating Th1 cytokine production[204]. This treatment also synergized with CpG-containing oligodeoxynucleotides (CpG), promoting upregulation of intracellular Toll-like receptor (TLR)-9 and generating NO, IFNγ, TNFα, and IL-12 in A/J mice bearing NXS2 tumors[205]. When combined with multidrug chemotherapy, radiation, anti-GD2, and anti-CTLA-4, this anti-CD40 and CpG therapy exhibited potent anti-tumor effects in mice with 9464D neuroblastoma, repolarizing TAMs towards an M1 phenotype[160]. Furthermore, histone deacetylase (HDAC) inhibitors have been explored in cancer therapy due to their ability to prevent histone deacetylation, resulting in altered gene and protein expression[211]. In neuroblastoma, the HDAC inhibitor vorinostat has shown enhanced efficacy in combination with anti-GD2 antibody treatment in a TH-MYCN mouse model[199]. Vorinostat treatment increased GD2 expression in neuroblastoma, improving responsiveness to anti-GD2 therapy. It also modified the myeloid composition of the TME, enhancing TAMs with mixed M1 and M2 phenotypes while reducing M-MDSC. Vorinostat-treated TAMs exhibited heightened ADCC capability, downregulated immunosuppressive genes, and upregulated FcyRI and FcyRII/III. Although clinical trials are lacking, the combination of anti-GD2 therapy and vorinostat holds promise for neuroblastoma treatment. Vorinostat was well-tolerated in a phase I trial with isotretinoin[200] and showed favorable response rates in a phase II trial with 131I-metaiodobenzylguanidine (MIBG)[201]. Furthermore, several therapeutic strategies have been reported that suggest alteration of gene expression of tumor cells or macrophages as a promising strategy to reprogram myeloid cells. BET bromodomain inhibitors like JQ1 and I-BET726 displace BRD4 from the *MYCN* promoter, leading to improved survival in various *in vivo* neuroblastoma models by inhibiting tumor growth and *MYCN* downregulation[208,209]. Combined PI3K and BRD4

inhibition also shows promise, suppressing *MYCN* expression and inhibiting neuroblastoma cell growth and metastasis both *in vitro* and *in vivo*[210]. While not investigated in neuroblastoma, PI3K/BRD4 blockade has demonstrated immunomodulatory effects. In tumor-bearing mice, it reduces MDSC recruitment, enhances MHCII$^+$ TAMs with a pro-inflammatory M1 phenotype, and promotes CD8$^+$ T cell infiltration and activation within the tumor[212]. These findings suggest that aside from *MYCN*, PI3K/BRD4 blockade may influence myeloid cell migration and polarization, potentially contributing to its anti-tumor effects in neuroblastoma. Further research is needed to fully understand this mechanism. In addition, Rac2, a small GTPase, has been linked to the polarization of macrophages from M1 to M2 phenotype *in vivo*[207]. Rac2-deficient mice studies indicated that although macrophage infiltration into the TME remained unchanged, the absence of Rac2 led to a prevalent M1 phenotype in macrophages. In a syngeneic neuroblastoma (9464D) model, Rac2-deficient mice exhibited significantly reduced tumor growth, suggesting the contribution of M2 macrophages to tumor progression. Notably, Rac2 is also implicated in tumor-induced angiogenesis, implying that the impact of Rac2 knockdown on tumor inhibition might involve both M1 macrophage polarization and the suppression of tumor angiogenesis. Potential therapeutic strategies involving Rac2 inhibition, using inhibitors like NSC23766, wortmannin, and LY294002, warrant further exploration in neuroblastoma development[213,214].

Finally, some studies have been published that demonstrate the possibility to target cytokines to reprogram myeloid cells. Relation et al. introduced a novel strategy involving MSCs engineered to express IFNγ, injected directly into neuroblastomas[202]. This led to decreased tumor proliferation and improved survival in a CHL-255 orthotopic neuroblastoma model, without increasing macrophage infiltration, but instead polarizing TAMs to an M1 phenotype. Additionally, incubating neuroblastoma cell lines with human monocytes increased IL-1β and TNFα-expressing macrophages, signifying an M1 phenotype via AKT phosphorylation[45]. IL-1β and TNFα from these macrophages stimulated arginine metabolism in neuroblastoma cells, promoting tumor cell proliferation. AKT inhibition using MK-2206 halted this effect by blocking IL-1β and TNFα secretion by macrophages. Blocking arginine uptake in tumor cells with L-NAME or depleting arginine with BCT-100 hindered neuroblastoma cell differentiation. BCT-100 treatment delayed neuroblastoma development in a TH-MYCN mouse model, prolonging survival. A phase I/II study with BCT-100 treatment is currently conducted in patients with neuroblastoma (NCT03455140). To our knowledge, results of this study have not been published yet.

Reprogramming the myeloid compartment in neuroblastoma offers an elegant strategy, preserving potential effector cells. This approach can also indirectly reactivate tumor-infiltrating T cells, and enhance T cell therapies, such as CAR T cells and checkpoint inhibitors. In addition to all myeloid-targeting treatments discussed in this review, many other treatment strategies are promising, but have not yet been studied in neuroblastoma.

Some examples are the inhibition of myeloperoxidase, preventing lipid peroxidation in PMN-MDSC, inhibition of fatty acid transport protein 2 (FATP2), preventing uptake of arachidonic acid and synthesis of PGE_2, DR5 agonists inducing MDSC apoptosis via TNF-related apoptosis-inducing ligand (TRAIL) and inhibition of Arg-1[215–218]. Strategies involving IDO, NO, or TOLLIP inhibition, ATRA treatment or other HDAC inhibitors than vorinostat, such as entinostat and ricolinostat were proven effective as well and are thoroughly reviewed elsewhere[28,219–221]. These approaches hold opportunities for new neuroblastoma treatments, and should be further investigated in the future.

DISCUSSION

As in other solid tumors, the presence of neutrophils, MDSCs and macrophages in neuroblastoma is generally associated with worse survival and immunosuppression. Neutrophils appear to be associated with a worse prognosis in high-risk neuroblastoma, though exact mechanisms remain unknown and are obscured by changing nomenclature, with (suppressive) neutrophils now often referred to as PMN-MDSC. It is clear that MDSC are immunosuppressive in both patients and in mouse models. Interestingly, we observed that M-MDSC were more immunosuppressive than PMN-MDSC in mouse models, but due to limited patient studies it is uncertain whether this is the case in neuroblastoma patients as well. Regarding macrophages, research findings diverge. While some noted M2 macrophage induction by neuroblastoma, others primarily observed M1 macrophages, with both types potentially linked to poor clinical outcome. These discrepancies likely stem from distinct genetic profiles within neuroblastoma; tumors with chromosome 11q deletion or *MYCN* amplification tend to favor M2 phenotypes, whereas *MYCN*-nonamplified tumors have a higher prevalence of M1 macrophages[21,72,73,85].

Because of their immunosuppressive nature and association with disease progression, myeloid cells are an excellent target for immunotherapy. Interestingly, immunosuppressive myeloid cells can still be engaged as effector cells, as is illustrated by the fact that neutrophils are important effector cells in anti-GD2 antibody therapy. This major role for neutrophils appears to be specific for anti-GD2 immunotherapy and/or neuroblastoma since neutrophils are much less involved as effectors of IgG antibody therapy in other cancers. One potential explanation for this phenomenon could be the timing of immunotherapy, often administered shortly after ASCT (90–120 days). Neutrophils, being highly abundant and among the first immune cells to recover post-ASCT, may possess a relative advantage compared to immune cells such as NK cells[222]. Additionally, post-ASCT NK cell recovery revealed a sustained enhanced metabolic immune cell profile relative to pre-ASCT levels in multiple myeloma patients[223,224]. This is accompanied by a shift in NK

cell subset distribution, correlating with reduced progression-free survival. These findings imply long-lasting ASCT-induced impacts on NK cell function.

In summary, substantial effort is put in developing T cell- and NKT cell-based therapeutics for neuroblastoma, among which CAR T cells and PD1/PD-L checkpoint inhibitors are the most prominent. However, results have been disappointing, apart from a breakthrough regarding GD2.CAR T cells for neuroblastoma patients with low tumor burden[14]. For adaptive immunity to be restored in neuroblastoma, first the immunosuppressive myeloid cells must be tackled. In this review, we highlighted several myeloid-targeting strategies that restored the ability of T cells to kill tumor cells, including depletion of myeloid cells using anti-Ly6G, anti-CD33 or the BTK inhibitor ibrutinib and myeloid reprogramming by DOX chemotherapy, anti-CSF1R, administration of Polyphenon E, or the addition of NAP to therapies. The combination of myeloid-targeting drugs and T cell-based therapeutics for neuroblastoma holds great promise for the future.

Author contributions

MS initiated this project and wrote the manuscript. LT conducted literature research and wrote the first draft of the manuscript. MD provided clinical feedback and was involved in reviewing and editing the manuscript. JL provided immunological and biological feedback and was involved in reviewing and editing the manuscript. DK wrote the manuscript and was responsible for its execution. All authors read and approved the final manuscript.

Funding

This study was funded by TKI-Health Holland (TumMyTOF) (to Jeanette Leusen) and by Villa Joep (project 17 IgA and anti-GD2).

Competing interests

Jeanette Leusen is scientific founder and shareholder of TigaTx.

REFERENCES

1. Preter, K. De *et al.* Human fetal neuroblast and neuroblastoma transcriptome analysis confirms neuroblast origin and highlights neuroblastoma candidate genes. *Genome Biol.* **7**, R84-r84. (2006).

2. Neuroblastoma - Childhood: Statistics. vol. 2020 (2019).

3. Brodeur, G. M., Seeger, R. C., Schwab, M., Varmus, H. E. & Bishop, J. M. Amplification of N-myc in untreated human neuroblastomas correlates with advanced disease stage. *Science (80-.).* **224**, 1121–1124 (1984).

4. Huang, M. & Weiss, W. A. Neuroblastoma and MYCN. *Cold Spring Harb Perspect.Med.* **3**, a014415 (2013).

5. De Bernardi, B. *et al.* Treatment of localised resectable neuroblastoma. Results of the LNESG1 study by the SIOP Europe Neuroblastoma Group. *Br. J. Cancer* **99**, 1027–1033 (2008).

6. Strother, D. R. *et al.* Outcome after surgery alone or with restricted use of chemotherapy for patients with low-risk neuroblastoma: results of Children's Oncology Group study P9641. *J. Clin. Oncol. Off. J. Am. Soc. Clin. Oncol.* **30**, 1842–1848 (2012).

7. Maris, J. M. Recent advances in neuroblastoma. *N. Engl. J. Med.* **362**, 2202–2211 (2010).

8. Ladenstein, R. *et al.* Interleukin 2 with anti-GD2 antibody ch14.18/CHO (dinutuximab beta) in patients with high-risk neuroblastoma (HR-NBL1/SIOPEN): a multicentre, randomised, phase 3 trial. *Lancet Oncol.* **19**, 1617–1629 (2018).

9. Pugh, T. J. *et al.* The genetic landscape of high-risk neuroblastoma. *Nat. Genet.* **45**, 279–284 (2013).

10. Lampson, L. A., Fisher, C. A. & Whelan, J. P. Striking paucity of HLA-A, B, C and beta 2-microglobulin on human neuroblastoma cell lines. *J. Immunol.* **130**, 2471–2478 (1983).

11. Kramer, K. *et al.* Disialoganglioside G(D2) loss following monoclonal antibody therapy is rare in neuroblastoma. *Clin. Cancer Res.* **4**, 2135–2139 (1998).

12. Yu, A. L. *et al.* Anti-GD2 antibody with GM-CSF, interleukin-2, and isotretinoin for neuroblastoma. *N. Engl. J. Med.* **363**, 1324–1334 (2010).

13. Cheung, N. K. *et al.* Murine anti-GD2 monoclonal antibody 3F8 combined with granulocyte-macrophage colony-stimulating factor and 13-cis-retinoic acid in high-risk patients with stage 4 neuroblastoma in first remission. *J. Clin. Oncol.* **30**, 3264–3270 (2012).

14. Del Bufalo, F. *et al.* GD2-CART01 for Relapsed or Refractory High-Risk Neuroblastoma. *N. Engl. J. Med.* **388**, 1284–1295 (2023).

15. Egler, R. A., Burlingame, S. M., Nuchtern, J. G. & Russell, H. V. Interleukin-6 and soluble interleukin-6 receptor levels as markers of disease extent and prognosis in neuroblastoma. *Clin. Cancer Res.* **14**, 7028–7034 (2008).

16. Silverman, A. M., Nakata, R., Shimada, H., Sposto, R. & DeClerck, Y. A. A galectin-3-dependent pathway upregulates interleukin-6 in the microenvironment of human neuroblastoma. *Cancer Res.* **72**, 2228–2238 (2012).

17. Zhen, Z. *et al.* Involvement of IL-10 and TGF-beta in HLA-E-mediated neuroblastoma migration and invasion. *Oncotarget* **7**, 44340–44349 (2016).

18. Soldati, R. *et al.* Neuroblastoma triggers an immunoevasive program involving galectin-1-dependent modulation of T cell and dendritic cell compartments. *Int. J. Cancer* **131**, 1131–1141 (2012).

19. Buchel, G. *et al.* Immune response modulation by Galectin-1 in a transgenic model of neuroblastoma. *Oncoimmunology* **5**, e1131378 (2016).

20. Brandetti, E. *et al.* MYCN is an immunosuppressive oncogene dampening the expression of ligands for NK-cell-activating receptors in human high-risk neuroblastoma. *Oncoimmunology* **6**, e1316439 (2017).

21. Theruvath, J. *et al.* Anti-GD2 synergizes with CD47 blockade to mediate tumor eradication. *Nat. Med.* **28**, 333–344 (2022).

22. Lee, H. C. *et al.* Ganglioside inhibition of CD8+ T cell cytotoxicity: interference with lytic granule trafficking and exocytosis. *J. Immunol. (Baltimore, Md. 1950)* **189**, 3521–3527 (2012).

23. Binnewies, M. *et al.* Understanding the tumor immune microenvironment (TIME) for effective therapy. *Nat. Med.* **24**, 541–550 (2018).

24. Zafari, R., Razi, S. & Rezaei, N. The role of dendritic cells in neuroblastoma: Implications for immunotherapy. *Immunobiology* **227**, 152293 (2022).

25. Bronte, V. *et al.* Recommendations for myeloid-derived suppressor cell nomenclature and characterization standards. *Nature Communications* vol. 7 1–10 (2016).

26. Condamine, T. *et al.* Lectin-type oxidized LDL receptor-1 distinguishes population of human polymorphonuclear myeloid-derived suppressor cells in cancer patients. *Sci. Immunol.* **1**, (2016).

27. Cassetta, L. *et al.* Deciphering myeloid-derived suppressor cells: isolation and markers in humans, mice and non-human primates. *Cancer Immunol. Immunother.* **68**, 687–697 (2019).

28. Veglia, F., Sanseviero, E. & Gabrilovich, D. I. Myeloid-derived suppressor cells in the era of increasing myeloid cell diversity. *Nat. Rev. Immunol.* **21**, 485–498 (2021).

29. Alshetaiwi, H. *et al.* Defining the emergence of myeloid-derived suppressor cells in breast cancer using single-cell transcriptomics. *Sci. Immunol.* **5**, (2020).

30. Sagiv, J. Y. *et al.* Phenotypic diversity and plasticity in circulating neutrophil subpopulations in cancer. *Cell Rep.* **10**, 562–573 (2015).

31. Mastio, J. *et al.* Identification of monocyte-like precursors of granulocytes in cancer as a mechanism for accumulation of PMN-MDSCs. *J. Exp. Med.* **216**, 2150–2169 (2019).

32. Furze, R. C. & Rankin, S. M. Neutrophil mobilization and clearance in the bone marrow. *Immunology* **125**, 281–288 (2008).

33. Tak, T., Tesselaar, K., Pillay, J., Borghans, J. A. M. & Koenderman, L. What's your age again? Determination of human neutrophil half-lives revisited. *J. Leukoc. Biol.* **94**, 595–601 (2013).

34. Rankin, S. M. The bone marrow: a site of neutrophil clearance. *J. Leukoc. Biol.* **88**, 241–251 (2010).

35. Gentles, A. J. *et al.* The prognostic landscape of genes and infiltrating immune cells across human cancers. *Nat. Med.* **21**, 938–945 (2015).

36. Morandi, F. *et al.* Altered erythropoiesis and decreased number of erythrocytes in children with neuroblastoma. *Oncotarget* **8**, 53194–53209 (2017).

37. Zeng, L. *et al.* Phosphoserine phosphatase as an indicator for survival through potentially influencing the infiltration levels of immune cells in neuroblastoma. *Front. cell Dev. Biol.* **10**, 873710 (2022).

38. Zheng, C., Liu, S., Feng, J. & Zhao, X. Prognostic Value of Inflammation Biomarkers for Survival of Patients with Neuroblastoma. *Cancer Manag. Res.* **12**, 2415–2425 (2020).

39. Zhang, Y. *et al.* Prediction to the prognosis of children with neuroblastoma by nomogram based on the first-diagnosed inflammatory markers. *Pediatr. Surg. Int.* **39**, 17 (2022).

40. Lee, J. W. *et al.* Absolute Neutrophil Count after the First Chemotherapy Cycle as a Surrogate Marker for Treatment Outcomes in Patients with Neuroblastoma. *Cancer Res. Treat.* **54**, 259–268 (2022).

41. Erbe, A. K. *et al.* KIR/KIR-ligand genotypes and clinical outcomes following chemoimmunotherapy in patients with relapsed or refractory neuroblastoma: a report from the Children's Oncology Group. *J. Immunother. cancer* **11**, (2023).

42. Birdsall, H. H. Induction of ICAM-1 on human neural cells and mechanisms of neutrophil-mediated injury. *Am. J. Pathol.* **139**, 1341–1350 (1991).

43. Chuluyan, H. E., Lang, B. J. & Issekutz, A. C. Differential mechanisms of neutrophil and monocyte adhesion on neuroblastoma cells: CD18 and VLA-4 integrins mediate adhesion to SK-N-SH, but not to SK-N-MC cell line. *J. Neurosci. Res.* **60**, 649–655 (2000).

44. Blaheta, R. A. *et al.* Tumor-endothelium cross talk blocks recruitment of neutrophils to endothelial cells: a novel mechanism of endothelial cell anergy. *Neoplasia* **11**, 1054–1063 (2009).

45. Fultang, L. *et al.* Macrophage-Derived IL1β and TNFα Regulate Arginine Metabolism in Neuroblastoma. *Cancer Res.* **79**, 611–624 (2019).

46. Chen, R. L., Reynolds, C. P. & Seeger, R. C. Neutrophils are cytotoxic and growth-inhibiting for neuroblastoma cells with an anti-GD2 antibody but, without cytotoxicity, can be growth-stimulating. *Cancer Immunol. Immunother.* **48**, 603–612 (2000).

47. Martínez-Sanz, P. *et al.* CD47-SIRPα Checkpoint Inhibition Enhances Neutrophil-Mediated Killing of Dinutuximab-Opsonized Neuroblastoma Cells. *Cancers (Basel).* **13**, (2021).

48. Gabrilovich, D. I., Ostrand-Rosenberg, S. & Bronte, V. Coordinated regulation of myeloid cells by tumours. *Nat.Rev.Immunol.* **12**, 253–268 (2012).

49. Veglia, F., Perego, M. & Gabrilovich, D. Myeloid-derived suppressor cells coming of age review-article. *Nature Immunology* vol. 19 108–119 (2018).

50. Ostrand-Rosenberg, S. Myeloid derived-suppressor cells: their role in cancer and obesity. *Curr. Opin. Immunol.* **51:68-75.**, 68–75 (2018).

51. Marvel, D. & Gabrilovich, D. I. Myeloid-derived suppressor cells in the tumor microenvironment: expect the unexpected. *J. Clin. Invest.* **125**, 3356–3364 (2015).

52. Gabrilovich, D. I. Myeloid-Derived Suppressor Cells. *Cancer.Immunol.Res.* **5**, 3–8 (2017).

53. Mazzoni, A. *et al.* Myeloid suppressor lines inhibit T cell responses by an NO-dependent mechanism. *J. Immunol.* **168**, 689–695 (2002).

54. Kusmartsev, S., Nefedova, Y., Yoder, D. & Gabrilovich, D. I. Antigen-specific inhibition of CD8+ T cell response by immature myeloid cells in cancer is mediated by reactive oxygen species. *J. Immunol.* **172**, 989–999 (2004).

55. Carlson, L. M. *et al.* Low-dose aspirin delays an inflammatory tumor progression in vivo in a transgenic mouse model of neuroblastoma. *Carcinogenesis* **34**, 1081–1088 (2013).

56. Bianchi, G. *et al.* ATP/P2X7 axis modulates myeloid-derived suppressor cell functions in neuroblastoma microenvironment. *Cell.Death Dis.* **5:e1135. d**, e1135 (2014).

57. Mao, Y. *et al.* Targeting Suppressive Myeloid Cells Potentiates Checkpoint Inhibitors to Control Spontaneous Neuroblastoma. *Clin. Cancer Res.* **22**, 3849–3859 (2016).

58. Costa, A. *et al.* Single-cell transcriptomics reveals shared immunosuppressive landscapes of mouse and human neuroblastoma. *J. Immunother. cancer* **10**, (2022).

59. Eissler, N., Sveinbjörnsson, B., Kock, A., Johnsen, J. I. & Kogner, P. Immune suppression by myeloid-derived suppressor cells, MDSCs, in MYCN-driven neuroblastoma provides a potential target for cancer immunotherapy. *J. Immunother. Cancer* **2**, P203 (2014).

60. Gowda, M. *et al.* Distinct signatures of the immune responses in low risk versus high risk neuroblastoma. *J. Transl. Med.* **9**, 170 (2011).

61. Dolcetti, L. *et al.* Hierarchy of immunosuppressive strength among myeloid-derived suppressor cell subsets is determined by GM-CSF. *Eur. J. Immunol.* **40**, 22–35 (2010).

62. Haverkamp, J. M. *et al.* Myeloid-derived suppressor activity is mediated by monocytic lineages maintained by continuous inhibition of extrinsic and intrinsic death pathways. *Immunity* **41**, 947–959 (2014).

63. Mussai, F. *et al.* Neuroblastoma Arginase Activity Creates an Immunosuppressive Microenvironment That Impairs Autologous and Engineered Immunity. *Cancer Res.* **75**, 3043–3053 (2015).

64. Lazic, D. *et al.* Landscape of Bone Marrow Metastasis in Human Neuroblastoma Unraveled by Transcriptomics and Deep Multiplex Imaging. *Cancers (Basel).* **13**, (2021).

65. Santilli, G. *et al.* Polyphenon [corrected] E enhances the antitumor immune response in neuroblastoma by inactivating myeloid suppressor cells. *Clin. Cancer Res.* **19**, 1116–1125 (2013).

66. Gowda, M., Payne, K. K., Godder, K. & Manjili, M. H. HLA-DR expression on myeloid cells is a potential prognostic factor in patients with high-risk neuroblastoma. *Oncoimmunology* **2**, e26616 (2013).

67. Richards, D. M., Hettinger, J. & Feuerer, M. Monocytes and macrophages in cancer: development and functions. *Cancer Microenviron. Off. J. Int. Cancer Microenviron. Soc.* **6**, 179–191 (2013).

68. Wu, Y. & Hirschi, K. K. Tissue-Resident Macrophage Development and Function. *Front. cell Dev. Biol.* **8**, 617879 (2020).

69. Kumar, V., Patel, S., Tcyganov, E. & Gabrilovich, D. I. The Nature of Myeloid-Derived Suppressor Cells in the Tumor Microenvironment. *Trends Immunol.* **37**, 208–220 (2016).

70. Mosser, D. M. & Edwards, J. P. Exploring the full spectrum of macrophage activation. *Nature Reviews Immunology* vol. 8 958–969 (2008).

71. Asgharzadeh, S. *et al.* Clinical significance of tumor-associated inflammatory cells in metastatic neuroblastoma. *J. Clin. Oncol.* **30**, 3525–3532 (2012).

72. Larsson, K. *et al.* COX/mPGES-1/PGE2 pathway depicts an inflammatory-dependent high-risk neuroblastoma subset. *Proc. Natl. Acad. Sci. U. S. A.* **112**, 8070–8075 (2015).

73. Hashimoto, O. *et al.* Collaboration of cancer-associated fibroblasts and tumour-associated macrophages for neuroblastoma development. *J. Pathol.* **240**, 211–223 (2016).

74. Batchu, S. Immunological landscape of Neuroblastoma and its clinical significance. *Cancer Treat. Res. Commun.* **26**, 100274 (2021).

75. Challagundla, K. B. *et al.* Exosome-mediated transfer of microRNAs within the tumor microenvironment and neuroblastoma resistance to chemotherapy. *J. Natl. Cancer Inst.* **107(7). pi**, 10.1093/jnci/djv135. Print 2015 Jul. (2015).

76. Liu, Q. *et al.* Single-cell landscape analysis reveals distinct regression trajectories and novel prognostic biomarkers in primary neuroblastoma. *Genes Dis.* **9**, 1624–1638 (2022).

77. Tang, X. X., Shimada, H. & Ikegaki, N. Macrophage-mediated anti-tumor immunity against high-risk neuroblastoma. *Genes Immun.* **23**, 129–140 (2022).

78. Verhoeven, B. M. *et al.* The immune cell atlas of human neuroblastoma. *Cell reports. Med.* **3**, 100657 (2022).

79. Blavier, L. *et al.* The capture of extracellular vesicles endogenously released by xenotransplanted tumours induces an inflammatory reaction in the premetastatic niche. *J. Extracell. vesicles* **12**, e12326 (2023).

80. Yu, Y., Zeng, Y., Xia, X., Zhou, J.-G. & Cao, F. Establishment and Validation of a Prognostic Immune Signature in Neuroblastoma. *Cancer Control* **28**, 10732748211033752 (2021).

81. Fiegel, H. C. *et al.* Midkine is highly expressed in neuroblastoma tissues. *Pediatr. Surg. Int.* **24**, 1355–1359 (2008).

82. Garcia-Gerique, L. *et al.* MIF/CXCR4 signaling axis contributes to survival, invasion, and drug resistance of metastatic neuroblastoma cells in the bone marrow microenvironment. *BMC Cancer* **22**, 669 (2022).

83. Zhang, Y. *et al.* Single-cell RNA-sequencing atlas reveals an MDK-dependent immunosuppressive environment in ErbB pathway-mutated gallbladder cancer. *J. Hepatol.* **75**, 1128–1141 (2021).

84. Klemke, L. *et al.* Hsp90-stabilized MIF supports tumor progression via macrophage recruitment and angiogenesis in colorectal cancer. *Cell Death Dis.* **12**, 155 (2021).

85. Raieli, S. *et al.* MYCN Drives a Tumor Immunosuppressive Environment Which Impacts Survival in Neuroblastoma. *Front. Oncol.* **11**, 625207 (2021).

86. Zhang, P. *et al.* MYCN Amplification Is Associated with Repressed Cellular Immunity in Neuroblastoma: An In Silico Immunological Analysis of TARGET Database. *Front. Immunol.* **8**, 1473 (2017).

87. Song, L. *et al.* Valpha24-invariant NKT cells mediate antitumor activity via killing of tumor-associated macrophages. *J. Clin. Invest.* **119**, 1524–1536 (2009).

88. Hadjidaniel, M. D. *et al.* Tumor-associated macrophages promote neuroblastoma via STAT3 phosphorylation and up-regulation of c-MYC. *Oncotarget* **8**, 91516–91529 (2017).

89. Kacher, J., Manches, O., Aspord, C., Sartelet, H. & Chaperot, L. Impaired Antitumor Immune Response in MYCN-amplified Neuroblastoma Is Associated with Lack of CCL2 Secretion and Poor Dendritic Cell Recruitment. *Cancer Res. Commun.* **2**, 577–589 (2022).

90. Metelitsa, L. S. *et al.* Natural killer T cells infiltrate neuroblastomas expressing the chemokine CCL2. *J. Exp. Med.* **199**, 1213–1221 (2004).

91. Van de Velde, L.-A. *et al.* Neuroblastoma Formation Requires Unconventional CD4 T Cells and Arginase-1-Dependent Myeloid Cells. *Cancer Res.* **81**, 5047–5059 (2021).

92. Pahlman, S. & Mohlin, S. Hypoxia and hypoxia-inducible factors in neuroblastoma. *Cell Tissue Res.* **372**, 269–275 (2018).

93. Liu, D. *et al.* IL-15 protects NKT cells from inhibition by tumor-associated macrophages and enhances antimetastatic activity. *J. Clin. Invest.* **122**, 2221–2233 (2012).

94. Pietras, A. *et al.* High levels of HIF-2alpha highlight an immature neural crest-like neuroblastoma cell cohort located in a perivascular niche. *J. Pathol.* **214**, 482–488 (2008).

95. Louault, K. *et al.* Fibroblasts and macrophages cooperate to create a pro-tumorigenic and immune resistant environment via activation of TGF-β/IL-6 pathway in neuroblastoma. *Oncoimmunology* **11**, 2146860 (2022).

96. Borriello, L. *et al.* Cancer-Associated Fibroblasts Share Characteristics and Protumorigenic Activity with Mesenchymal Stromal Cells. *Cancer Res.* **77**, 5142–5157 (2017).

97. Uhm, T. G., Kim, B. S. & Chung, I. Y. Eosinophil development, regulation of eosinophil-specific genes, and role of eosinophils in the pathogenesis of asthma. *Allergy Asthma Immunol.Res.* **4**, 68–79 (2012).

98. Grisaru-Tal, S., Itan, M., Klion, A. D. & Munitz, A. A new dawn for eosinophils in the tumour microenvironment. *Nat. Rev. Cancer* **20**, 594–607 (2020).

99. El-Badry, O. *et al.* Insulin-Like growth-Factor-II-Mediated proliferation of human neuroblastoma. *J. Clin. Invest.* **87**, 648–657 (1991).

100. El-Badry, O. M. Growth regulation of human neuroblastoma. in (eds. Benz, C. & Liu, E. T.) 105–128 (Springer US, 1993).

101. Alvarez-Rueda, N. *et al.* A monoclonal antibody to O-acetyl-GD2 ganglioside and not to GD2 shows potent anti-tumor activity without peripheral nervous system cross-reactivity. *PLoS One* **6**, e25220 (2011).

102. Ivashkiv, L. B. & Park, S. H. Epigenetic Regulation of Myeloid Cells. *Microbiol. Spectr.* **4**, (2016).

103. Porta, C., Riboldi, E., Ippolito, A. & Sica, A. Molecular and epigenetic basis of macrophage polarized activation. *Semin. Immunol.* **27**, 237–248 (2015).

104. Quagliano, A., Gopalakrishnapillai, A. & Barwe, S. P. Understanding the Mechanisms by Which Epigenetic Modifiers Avert Therapy Resistance in Cancer. *Front. Oncol.* **10**, 992 (2020).

105. Xu, X. *et al.* Metabolic reprogramming and epigenetic modifications in cancer: from the impacts and mechanisms to the treatment potential. *Exp. Mol. Med.* **55**, 1357–1370 (2023).

106. Xu, L. *et al.* Epigenetic modifications in the accumulation and function of myeloid-derived suppressor cells. *Front. Immunol.* **13**, 1016870 (2022).

107. Zhu, D., Zhang, Y. & Wang, S. Histone citrullination: a new target for tumors. *Mol. Cancer* **20**, 90 (2021).

108. Xiong, J. *et al.* Lactylation-driven METTL3-mediated RNA m(6)A modification promotes immunosuppression of tumor-infiltrating myeloid cells. *Mol. Cell* **82**, 1660-1677.e10 (2022).

109. Sido, J. M., Yang, X., Nagarkatti, P. S. & Nagarkatti, M. Δ9-Tetrahydrocannabinol-mediated epigenetic modifications elicit myeloid-derived suppressor cell activation via STAT3/S100A8. *J. Leukoc. Biol.* **97**, 677–688 (2015).

110. Hegde, V. L., Singh, U. P., Nagarkatti, P. S. & Nagarkatti, M. Critical Role of Mast Cells and Peroxisome Proliferator-Activated Receptor γ in the Induction of Myeloid-Derived Suppressor Cells by Marijuana Cannabidiol In Vivo. *J. Immunol.* **194**, 5211–5222 (2015).

111. Fetahu, I. S. *et al.* Single-cell transcriptomics and epigenomics unravel the role of monocytes in neuroblastoma bone marrow metastasis. *Nat. Commun.* **14**, 3620 (2023).

112. Wrangle, J. *et al.* Alterations of immune response of Non-Small Cell Lung Cancer with Azacytidine. *Oncotarget* **4**, 2067–2079 (2013).

113. Juergens, R. A. *et al.* Combination epigenetic therapy has efficacy in patients with refractory advanced non-small cell lung cancer. *Cancer Discov.* **1**, 598–607 (2011).

114. van Groningen, T. *et al.* Neuroblastoma is composed of two super-enhancer-associated differentiation states. *Nat. Genet.* **49**, 1261–1266 (2017).

115. Boeva, V. *et al.* Heterogeneity of neuroblastoma cell identity defined by transcriptional circuitries. *Nat. Genet.* **49**, 1408–1413 (2017).

116. van Groningen, T. *et al.* A NOTCH feed-forward loop drives reprogramming from adrenergic to mesenchymal state in neuroblastoma. *Nat. Commun.* **10**, 1530 (2019).

117. van Nes, J. *et al.* A NOTCH3 transcriptional module induces cell motility in neuroblastoma. *Clin. cancer Res. an Off. J. Am. Assoc. Cancer Res.* **19**, 3485–3494 (2013).

118. Wolpaw, A. J. *et al.* Epigenetic state determines inflammatory sensing in neuroblastoma. *Proc. Natl. Acad. Sci. U. S. A.* **119**, (2022).

119. Sengupta, S. *et al.* Mesenchymal and adrenergic cell lineage states in neuroblastoma possess distinct immunogenic phenotypes. *Nat. cancer* **3**, 1228–1246 (2022).

120. Munn, D. H. & Cheung, N. K. Antibody-dependent antitumor cytotoxicity by human monocytes cultured with recombinant macrophage colony-stimulating factor. Induction of efficient antibody-mediated antitumor cytotoxicity not detected by isotope release assays. *J. Exp. Med.* **170**, 511–526 (1989).

121. Bahri, M. *et al.* SIRPα-specific monoclonal antibody enables antibody-dependent phagocytosis of neuroblastoma cells. *Cancer Immunol. Immunother.* **71**, 71–83 (2022).

122. Bruchelt, G. *et al.* Effects of granulocytes on human neuroblastoma cells measured by chemiluminescence and chromium-51 release assay. *J. Biolumin. Chemilumin.* **3**, 93–96 (1989).

123. Kushner, B. H. & Cheung, N. K. GM-CSF enhances 3F8 monoclonal antibody-dependent cellular cytotoxicity against human melanoma and neuroblastoma. *Blood* **73**, 1936–1941 (1989).

124. Barker, E. *et al.* Effect of a chimeric anti-ganglioside GD2 antibody on cell-mediated lysis of human neuroblastoma cells. *Cancer Res.* **51**, 144–149 (1991).

125. Barker, E. & Reisfeld, R. A. A mechanism for neutrophil-mediated lysis of human neuroblastoma cells. *Cancer Res.* **53**, 362–367 (1993).

126. Kushner, B. H. & Cheung, N. K. Absolute requirement of CD11/CD18 adhesion molecules, FcRII and the phosphatidylinositol-linked FcRIII for monoclonal antibody-mediated neutrophil antihuman tumor cytotoxicity. *Blood* **79**, 1484–1490 (1992).

127. Tibbetts, R. *et al.* Anti-disialoganglioside antibody internalization by neuroblastoma cells as a mechanism of immunotherapy resistance. *Cancer Immunol. Immunother.* **71**, 153–164 (2022).

128. Cheung, N. K. *et al.* Key role for myeloid cells: phase II results of anti-G(D2) antibody 3F8 plus granulocyte-macrophage colony-stimulating factor for chemoresistant osteomedullary neuroblastoma. *Int. J. cancer* **135**, 2199–2205 (2014).

129. Cheung, I. Y., Hsu, K. & Cheung, N. K. Activation of peripheral-blood granulocytes is strongly correlated with patient outcome after immunotherapy with anti-GD2 monoclonal antibody and granulocyte-macrophage colony-stimulating factor. *J. Clin. Oncol.* **30**, 426–432 (2012).

130. Cheung, N. K. *et al.* FCGR2A polymorphism is correlated with clinical outcome after immunotherapy of neuroblastoma with anti-GD2 antibody and granulocyte macrophage colony-stimulating factor. *J. Clin. Oncol.* **24**, 2885–2890 (2006).

131. Szanto, C. L. *et al.* Immune Monitoring during Therapy Reveals Activitory and Regulatory Immune Responses in High-Risk Neuroblastoma. *Cancers (Basel).* **13**, (2021).

132. Yu, A. L. *et al.* Phase I trial of a human-mouse chimeric anti-disialoganglioside monoclonal antibody ch14.18 in patients with refractory neuroblastoma and osteosarcoma. *J. Clin. Oncol.* **16**, 2169–2180 (1998).

133. Martinez Sanz, P. *et al.* G-CSF as a suitable alternative to GM-CSF to boost dinutuximab-mediated neutrophil cytotoxicity in neuroblastoma treatment. *J. Immunother. cancer* **9**, (2021).

134. Yang, K. D., Cheng, S. N., Wu, N. C. & Shaio, M. F. Induction of interleukin-8 expression in neuroblastoma cells by retinoic acid: implication of leukocyte chemotaxis and activation. *Pediatr. Res.* **34**, 720–724 (1993).

135. Troschke-Meurer, S. *et al.* Low CD4(+)/CD25(+)/CD127(-) regulatory T cell- and high INF-gamma levels are associated with improved survival of neuroblastoma patients treated with long-term infusion of ch14.18/CHO combined with interleukin-2. *Oncoimmunology* **8**, 1661194 (2019).

136. Rousseau, R. F. *et al.* Local and systemic effects of an allogeneic tumor cell vaccine combining transgenic human lymphotactin with interleukin-2 in patients with advanced or refractory neuroblastoma. *Blood* **101**, 1718–1726 (2003).

137. Russell, H. V *et al.* A phase 1/2 study of autologous neuroblastoma tumor cells genetically modified to secrete IL-2 in patients with high-risk neuroblastoma. *J. Immunother.* **31**, 812–819 (2008).

138. Evers, M. *et al.* Anti-GD2 IgA kills tumors by neutrophils without antibody-associated pain in the preclinical treatment of high-risk neuroblastoma. *J. Immunother. cancer* **9**, (2021).

139. Stip, M. C. *et al.* IgA antibody immunotherapy targeting GD2 is effective in preclinical neuroblastoma models. *Jitc* **11**, (2023).

140. Erbe, A. *et al.* 461 Improving specific targeting of tumors through bispecific SNIPER antibodies. *J. Immunother. Cancer* **8**, A280 LP-A280 (2020).

141. Kendsersky, N. M. *et al.* The B7-H3-Targeting Antibody-Drug Conjugate m276-SL-PBD Is Potently Effective Against Pediatric Cancer Preclinical Solid Tumor Models. *Clin. cancer Res. an Off. J. Am. Assoc. Cancer Res.* **27**, 2938–2946 (2021).

142. Bosse, K. R. *et al.* Identification of GPC2 as an Oncoprotein and Candidate Immunotherapeutic Target in High-Risk Neuroblastoma. *Cancer Cell* **32**, 295-309.e12 (2017).

143. Pascual-Pasto, G. *et al.* GPC2 antibody-drug conjugate reprograms the neuroblastoma immune milieu to enhance macrophage-driven therapies. *J. Immunother. cancer* **10**, (2022).

144. Siebert, N. *et al.* Neuroblastoma patients with high-affinity FCGR2A, -3A and stimulatory KIR 2DS2 treated by long-term infusion of anti-GD(2) antibody ch14.18/CHO show higher ADCC levels and improved event-free survival. *Oncoimmunology* **5**, e1235108 (2016).

145. Hank, J. A. *et al.* Augmentation of antibody dependent cell mediated cytotoxicity following in vivo therapy with recombinant interleukin 2. *Cancer Res.* **50**, 5234–5239 (1990).

146. Li, J., Gyorffy, S., Lee, S. & Kwok, C. S. Effect of recombinant human interleukin 2 on neutrophil adherence to endothelial cells in vitro. *Inflammation* **20**, 361–372 (1996).

147. Rivoltini, L. *et al.* In vitro anti-tumor activity of eosinophils from cancer patients treated with subcutaneous administration of interleukin 2. Role of interleukin 5. *Int. J. Cancer* **54**, 8–15 (1993).

148. Kohanbash, G. *et al.* GM-CSF promotes the immunosuppressive activity of glioma-infiltrating myeloid cells through interleukin-4 receptor-alpha. *Cancer Res.* **73**, 6413–6423 (2013).

149. Thorn, M. *et al.* Tumor-associated GM-CSF overexpression induces immunoinhibitory molecules via STAT3 in myeloid-suppressor cells infiltrating liver metastases. *Cancer Gene Ther.* **23**, 188–198 (2016).

150. Sidell, N. Retinoic acid-induced growth inhibition and morphologic differentiation of human neuroblastoma cells in vitro. *J. Natl. Cancer Inst.* **68**, 589–596 (1982).

151. Matthay, K. K. *et al.* Long-term results for children with high-risk neuroblastoma treated on a randomized trial of myeloablative therapy followed by 13-cis-retinoic acid: a children's oncology group study. *J. Clin. Oncol.* **27**, 1007–1013 (2009).

152. Yuen, K. C. *et al.* High systemic and tumor-associated IL-8 correlates with reduced clinical benefit of PD-L1 blockade. *Nat. Med.* **26**, 693–698 (2020).

153. Schalper, K. A. *et al.* Elevated serum interleukin-8 is associated with enhanced intratumor neutrophils and reduced clinical benefit of immune-checkpoint inhibitors. *Nat. Med.* **26**, 688–692 (2020).

154. Devalaraja, S. *et al.* Tumor-Derived Retinoic Acid Regulates Intratumoral Monocyte Differentiation to Promote Immune Suppression. *Cell* **180**, 1098-1114.e16 (2020).

155. Cancer Discovery editorial staff. Retinoic Acid Mediates Monocyte Differentiation and Immune Response. *Cancer Discov.* **10**, OF7 (2020).

156. Rao, E. *et al.* All-trans retinoic acid overcomes solid tumor radioresistance by inducing inflammatory macrophages. *Sci. Immunol.* **6**, (2021).

157. Tilsed, C. M. *et al.* Retinoic Acid Induces an IFN-Driven Inflammatory Tumour Microenvironment, Sensitizing to Immune Checkpoint Therapy. *Front. Oncol.* **12**, 849793 (2022).

158. Sorkin, L. S. *et al.* Anti-GD(2) with an FC point mutation reduces complement fixation and decreases antibody-induced allodynia. *Cancer Res.* **149**, 362–367 (2010).

159. Linde, I. L. *et al.* Neutrophil-activating therapy for the treatment of cancer. *Cancer Cell* **41**, 356-372. e10 (2023).

160. Voeller, J. *et al.* Combined innate and adaptive immunotherapy overcomes resistance of immunologically cold syngeneic murine neuroblastoma to checkpoint inhibition. *J. Immunother. cancer* **7**, 344 (2019).

161. Castriconi, R. *et al.* Identification of 4Ig-B7-H3 as a neuroblastoma-associated molecule that exerts a protective role from an NK cell-mediated lysis. *Proc. Natl. Acad. Sci. U. S. A.* **101**, 12640–12645 (2004).

162. Dondero, A. *et al.* Multiparametric flow cytometry highlights B7-H3 as a novel diagnostic/therapeutic target in GD2neg/low neuroblastoma variants. *J. Immunother. cancer* **9**, (2021).

163. Siebert, N. *et al.* Reduction of CD11b(+) myeloid suppressive cells augments anti-neuroblastoma immune response induced by the anti-GD(2) antibody ch14.18/CHO. *Oncoimmunology* **9**, 1836768 (2020).

164. Wu, H. W. *et al.* Anti-CD105 antibody eliminates tumor microenvironment cells and enhances Anti-GD2 antibody immunotherapy of neuroblastoma with activated natural killer cells. *Clin. Cancer Res.* **25**, 4761–4774 (2019).

165. Park, J. A., Wang, L. & Cheung, N.-K. V. Modulating tumor infiltrating myeloid cells to enhance bispecific antibody-driven T cell infiltration and anti-tumor response. *J. Hematol. Oncol.* **14**, 142 (2021).

166. Webb, M. W. *et al.* Colony stimulating factor 1 receptor blockade improves the efficacy of chemotherapy against human neuroblastoma in the absence of T lymphocytes. *Int. J. Cancer* **143**, 1483–1493 (2018).

167. Abraham, D. *et al.* Stromal cell-derived CSF-1 blockade prolongs xenograft survival of CSF-1-negative neuroblastoma. *Int. J. cancer* **126**, 1339–1352 (2010).

168. Fultang, L. *et al.* MDSC targeting with Gemtuzumab ozogamicin restores T cell immunity and immunotherapy against cancers. *EBioMedicine* **47**, 235–246 (2019).

169. Mussai, F., De Santo, C. & Cerundolo, V. Interaction between invariant NKT cells and myeloid-derived suppressor cells in cancer patients: evidence and therapeutic opportunities. *J. Immunother.* **35**, 449–459 (2012).

170. Courtney, A. N. *et al.* NKT cells control tumor associated macrophages and metastatic growth in neuroblastoma. *J. Immunol.* **198**, 204.24-204.24 (2017).

171. Heczey, A. *et al.* Invariant NKT cells with chimeric antigen receptor provide a novel platform for safe and effective cancer immunotherapy. *Blood* **124**, 2824–2833 (2014).

172. Xu, W.-L. *et al.* Targeted inhibition of myeloid-derived suppressor cells in the tumor microenvironment by low-dose doxorubicin to improve immune efficacy in murine neuroblastoma. *Chin. Med. J. (Engl).* **134**, 334–343 (2020).

173. Xu, W. *et al.* Targeted elimination of myeloid-derived suppressor cells via regulation of the STAT pathway alleviates tumor immunosuppression in neuroblastoma. *Immunol. Lett.* **240**, 31–40 (2021).

174. Xu, W., Li, S., Li, M., Zhou, H. & Yang, X. Upregulation of CD3ζ and L-selectin in antigen-specific cytotoxic T lymphocytes by eliminating myeloid-derived suppressor cells with doxorubicin to improve killing efficacy of neuroblastoma cells in vitro. *J. Clin. Lab. Anal.* **36**, e24158 (2022).

175. D'Incalci, M. *et al.* The combination of yondelis and cisplatin is synergistic against human tumor xenografts. *Eur. J. Cancer* **39**, 1920–1926 (2003).

176. Dierckx de Casterlé, I. *et al.* Reduction of myeloid-derived suppressor cells reinforces the anti-solid tumor effect of recipient leukocyte infusion in murine neuroblastoma-bearing allogeneic bone marrow chimeras. *Cancer Immunol. Immunother.* **67**, 589–603 (2018).

177. Ara, T. *et al.* Critical role of STAT3 in IL-6-mediated drug resistance in human neuroblastoma. *Cancer Res.* **73**, 3852–3864 (2013).

178. Lucarini, V. *et al.* Combined mitoxantrone and anti-TGFβ treatment with PD-1 blockade enhances antitumor immunity by remodelling the tumor immune landscape in neuroblastoma. *J. Exp. Clin. Cancer Res.* **41**, 326 (2022).

179. Carlson, L. M. & Kogner, P. Neuroblastoma-related inflammation: May small doses of aspirin be suitable for small cancer patients? *Oncoimmunology* **2**, e24658 (2013).

180. Li, M.-H., Harel, M., Hla, T. & Ferrer, F. Induction of chemokine (C-C motif) ligand 2 by sphingosine-1-phosphate signaling in neuroblastoma. *J. Pediatr. Surg.* **49**, 1286–1291 (2014).

181. Li, M.-H. *et al.* Antitumor Activity of a Novel Sphingosine-1-Phosphate 2 Antagonist, AB1, in Neuroblastoma. *J. Pharmacol. Exp. Ther.* **354**, 261–268 (2015).

182. Alizadeh, D. *et al.* Doxorubicin eliminates myeloid-derived suppressor cells and enhances the efficacy of adoptive T-cell transfer in breast cancer. *Cancer Res.* **74**, 104–118 (2014).

183. Van Wigcheren, G. F. *et al.* Cisplatin inhibits frequency and suppressive activity of monocytic myeloid-derived suppressor cells in cancer patients. *Oncoimmunology* **10**, 1935557 (2021).

184. Valind, A. *et al.* Macrophage infiltration promotes regrowth in MYCN-amplified neuroblastoma after chemotherapy. *Oncoimmunology* **12**, 2184130 (2023).

185. Peinemann, F., Tushabe, D. A., van Dalen, E. C. & Berthold, F. Rapid COJEC versus standard induction therapies for high-risk neuroblastoma. *Cochrane database Syst. Rev.* CD010774 (2015) doi:10.1002/14651858.CD010774.pub2.

186. Fletcher, J. S. *et al.* STAT3 inhibition reduces macrophage number and tumor growth in neurofibroma. *Oncogene* **38**, 2876–2884 (2019).

187. Johnsen, J. I. *et al.* Cyclooxygenase-2 is expressed in neuroblastoma, and nonsteroidal anti-inflammatory drugs induce apoptosis and inhibit tumor growth in vivo. *Cancer Res.* **64**, 7210–7215 (2004).

188. Rasmuson, A. *et al.* Autocrine prostaglandin E2 signaling promotes tumor cell survival and proliferation in childhood neuroblastoma. *PLoS One* **7**, e29331 (2012).

189. Pienta, K. J. *et al.* Phase 2 study of carlumab (CNTO 888), a human monoclonal antibody against CC-chemokine ligand 2 (CCL2), in metastatic castration-resistant prostate cancer. *Invest. New Drugs* **31**, 760–768 (2013).

190. Sandhu, S. K. *et al.* A first-in-human, first-in-class, phase I study of carlumab (CNTO 888), a human monoclonal antibody against CC-chemokine ligand 2 in patients with solid tumors. *Cancer Chemother. Pharmacol.* **71**, 1041–1050 (2013).

191. Nywening, T. M. *et al.* Targeting tumour-associated macrophages with CCR2 inhibition in combination with FOLFIRINOX in patients with borderline resectable and locally advanced pancreatic cancer: a single-centre, open-label, dose-finding, non-randomised, phase 1b trial. *Lancet. Oncol.* **17**, 651–662 (2016).

192. Ishfaq, M. *et al.* BTK Inhibition Reverses MDSC-Mediated Immunosuppression and Enhances Response to Anti-PDL1 Therapy in Neuroblastoma. *Cancers (Basel).* **13**, (2021).

193. Eissler, N. *et al.* Regulation of myeloid cells by activated T cells determines the efficacy of PD-1 blockade. *Oncoimmunology* **5**, e1232222 (2016).

194. Tumino, N. *et al.* Polymorphonuclear myeloid-derived suppressor cells impair the anti-tumor efficacy of GD2.CAR T-cells in patients with neuroblastoma. *Journal of hematology & oncology* vol. 14 191 (2021).

195. Stroncek, D. F. *et al.* Myeloid cells in peripheral blood mononuclear cell concentrates inhibit the expansion of chimeric antigen receptor T cells. *Cytotherapy* **18**, 893–901 (2016).

196. Jin, C., Ma, J., Ramachandran, M., Yu, D. & Essand, M. CAR T cells expressing a bacterial virulence factor trigger potent bystander antitumour responses in solid cancers. *Nat. Biomed. Eng.* **6**, 830–841 (2022).

197. Ma, J. *et al.* Concurrent expression of HP-NAP enhances antitumor efficacy of oncolytic vaccinia virus but not for Semliki Forest virus. *Mol. Ther. oncolytics* **21**, 356–366 (2021).

198. Kock, A. *et al.* Inhibition of Microsomal Prostaglandin E Synthase-1 in Cancer-Associated Fibroblasts Suppresses Neuroblastoma Tumor Growth. *EBioMedicine* **32**, 84–92 (2018).

199. Kroesen, M. *et al.* Anti-GD2 mAb and Vorinostat synergize in the treatment of neuroblastoma. *Oncoimmunology* **5**, e1164919 (2016).

200. Pinto, N. *et al.* Phase I study of vorinostat in combination with isotretinoin in patients with refractory/recurrent neuroblastoma: A new approaches to Neuroblastoma Therapy (NANT) trial. *Pediatr. Blood Cancer* **65**, e27023 (2018).

201. DuBois, S. G. *et al.* Randomized Phase II Trial of MIBG Versus MIBG, Vincristine, and Irinotecan Versus MIBG and Vorinostat for Patients With Relapsed or Refractory Neuroblastoma: A Report From NANT Consortium. *J. Clin. Oncol. Off. J. Am. Soc. Clin. Oncol.* **39**, 3506–3514 (2021).

202. Relation, T. *et al.* Intratumoral Delivery of Interferongamma-Secreting Mesenchymal Stromal Cells Repolarizes Tumor-Associated Macrophages and Suppresses Neuroblastoma Proliferation In Vivo. *Stem Cells* **36**, 915–924 (2018).

203. Miao, L. *et al.* FABP4 deactivates NF-κB-IL1α pathway by ubiquitinating ATPB in tumor-associated macrophages and promotes neuroblastoma progression. *Clin. Transl. Med.* **11**, e395 (2021).

204. Lum, H. D. *et al.* In vivo CD40 ligation can induce T-cell-independent antitumor effects that involve macrophages. *J. Leukoc. Biol.* **79**, 1181–1192 (2006).

205. Buhtoiarov, I. N., Lum, H. D., Berke, G., Sondel, P. M. & Rakhmilevich, A. L. Synergistic activation of macrophages via CD40 and TLR9 results in T cell independent antitumor effects. *J. Immunol.* **176**, 309–318 (2006).

206. Buhtoiarov, I. N. *et al.* Anti-tumour synergy of cytotoxic chemotherapy and anti-CD40 plus CpG-ODN immunotherapy through repolarization of tumour-associated macrophages. *Immunology* **132**, 226–239 (2011).

207. Joshi, S. *et al.* Rac2 controls tumor growth, metastasis and M1-M2 macrophage differentiation in vivo. *PLoS One* **9**, e95893 (2014).

208. Wyce, A. *et al.* BET inhibition silences expression of MYCN and BCL2 and induces cytotoxicity in neuroblastoma tumor models. *PLoS One* **8**, e72967 (2013).

209. Puissant, A. *et al.* Targeting MYCN in neuroblastoma by BET bromodomain inhibition. *Cancer Discov.* **3**, 308–323 (2013).

210. Andrews, F. H. *et al.* Dual-activity PI3K-BRD4 inhibitor for the orthogonal inhibition of MYC to block tumor growth and metastasis. *Proc. Natl. Acad. Sci. U. S. A.* **114**, E1072–E1080 (2017).

211. Shankar, S. & Srivastava, R. K. Histone deacetylase inhibitors: mechanisms and clinical significance in cancer: HDAC inhibitor-induced apoptosis. *Adv. Exp. Med. Biol.* **615:261–98**, 261–298 (2008).

212. Joshi, S. *et al.* SF2523: Dual PI3K/BRD4 Inhibitor Blocks Tumor Immunosuppression and Promotes Adaptive Immune Responses in Cancer. *Mol. Cancer Ther.* **18**, 1036–1044 (2019).

213. Mizukawa, B. *et al.* Inhibition of Rac GTPase signaling and downstream prosurvival Bcl-2 proteins as combination targeted therapy in MLL-AF9 leukemia. *Blood* **118**, 5235–5245 (2011).

214. Akasaki, T., Koga, H. & Sumimoto, H. Phosphoinositide 3-kinase-dependent and -independent activation of the small GTPase Rac2 in human neutrophils. *J. Biol. Chem.* **274**, 18055–18059 (1999).

215. Ugolini, A. *et al.* Polymorphonuclear myeloid-derived suppressor cells limit antigen cross-presentation by dendritic cells in cancer. *JCI insight* **5**, (2020).

216. Veglia, F. *et al.* Fatty acid transport protein 2 reprograms neutrophils in cancer. *Nature* **569**, 73–78 (2019).

217. Tang, Y. *et al.* Targeting depletion of myeloid-derived suppressor cells potentiates PD-L1 blockade efficacy in gastric and colon cancers. *Oncoimmunology* **11**, 2131084 (2022).

218. Steggerda, S. M. *et al.* Inhibition of arginase by CB-1158 blocks myeloid cell-mediated immune suppression in the tumor microenvironment. *J. Immunother. cancer* **5**, 101 (2017).

219. Barry, S. T., Gabrilovich, D. I., Sansom, O. J., Campbell, A. D. & Morton, J. P. Therapeutic targeting of tumour myeloid cells. *Nat. Rev. Cancer* **23**, 216–237 (2023).

220. Chaib, M., Chauhan, S. C. & Makowski, L. Friend or Foe? Recent Strategies to Target Myeloid Cells in Cancer. *Front. cell Dev. Biol.* **8**, 351 (2020).

221. Wang, Y., Johnson, K. C. C., Gatti-Mays, M. E. & Li, Z. Emerging strategies in targeting tumor-resident myeloid cells for cancer immunotherapy. *J. Hematol. Oncol.* **15**, 118 (2022).

222. Ozkaynak, M. F. *et al.* Phase I study of chimeric human/murine anti-ganglioside G(D2) monoclonal antibody (ch14.18) with granulocyte-macrophage colony-stimulating factor in children with neuroblastoma immediately after hematopoietic stem-cell transplantation: a Children's Cancer. *J. Clin. Oncol.* **18**, 4077–4085 (2000).

223. Orrantia, A., Terrén, I., Astarloa-Pando, G., Zenarruzabeitia, O. & Borrego, F. Human NK Cells in Autologous Hematopoietic Stem Cell Transplantation for Cancer Treatment. *Cancers (Basel).* **13**, (2021).

224. Orrantia, A. *et al.* NK Cell Reconstitution After Autologous Hematopoietic Stem Cell Transplantation: Association Between NK Cell Maturation Stage and Outcome in Multiple Myeloma. *Front. Immunol.* **12**, 748207 (2021).

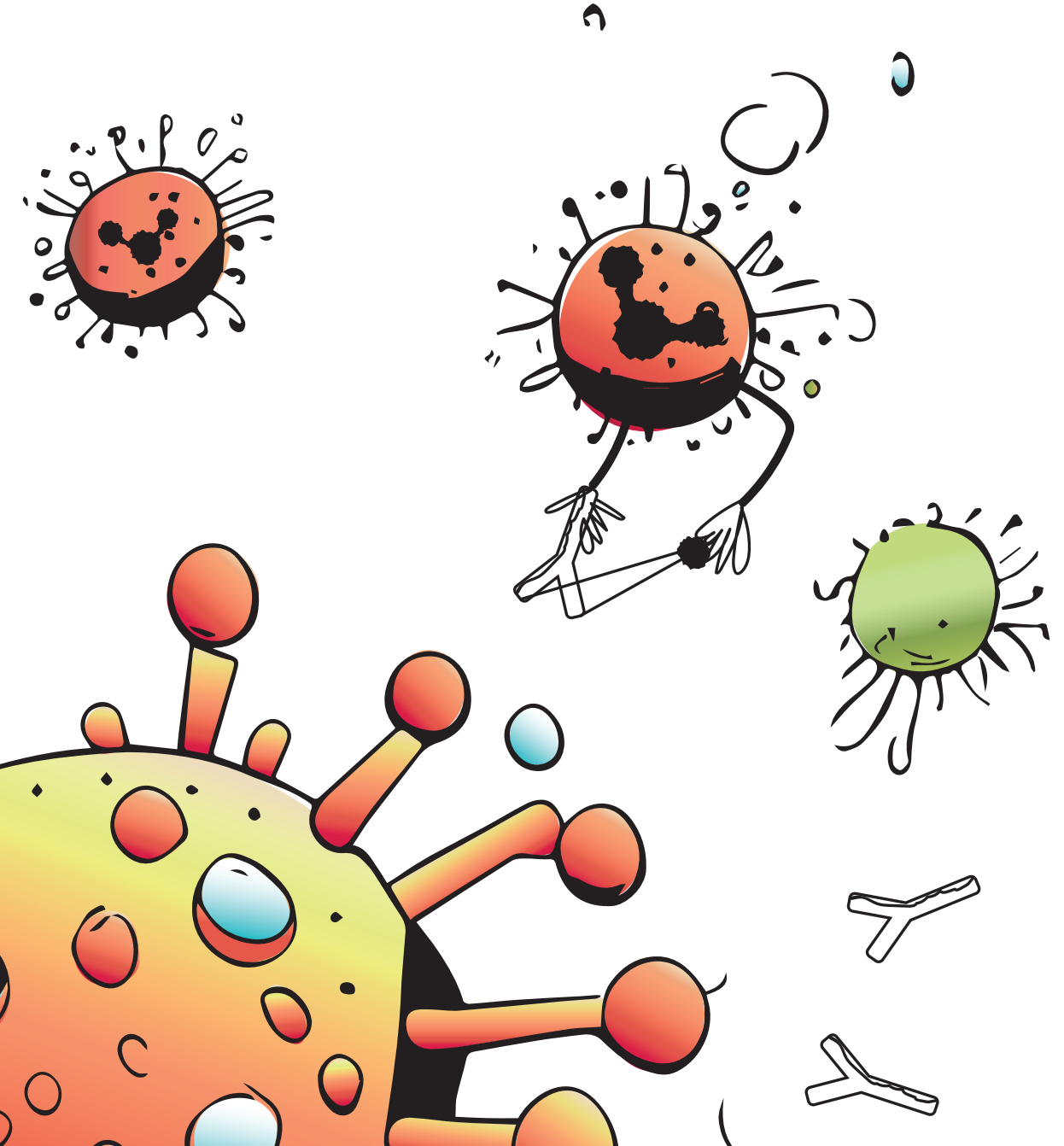

Chapter 5.

Anti-GD2 IgA kills tumors by neutrophils without antibody-associated pain in the preclinical treatment of high-risk neuroblastoma

Mitchell Evers[1] Marjolein Stip[1] Kaylee Keller[2] Hanneke Willemen[1] Maaike Nederend[1] Marco Jansen[1] Chilam Chan[1] Kevin Budding[1] Stefan Nierkens[1,2] Thomas Valerius[3] Friederike Meyer-Wentrup[2] Niels Eijkelkamp[1] and Jeanette Leusen[1]

Affiliations

1. Center for Translational Immunology, UMC Utrecht, Utrecht, The Netherlands
2. Department of Pediatric Hemato-oncology, Princess Maxima Center for Pediatric Oncology, Utrecht, The Netherlands
3. Section for Stem Cell Transplantation and Immunotherapy, Department of Medicine II, Christian-Albrechts-University Kiel and University Medical Center Schleswig-Holstein Campus Kiel, Germany

Published in Journal for Immunotherapy of Cancer, 2021

ABSTRACT

Background

The addition of monoclonal antibody therapy against GD2 to the treatment of high-risk neuroblastoma led to improved responses in patients. Nevertheless, administration of GD2 antibodies against neuroblastoma is associated with therapy-limiting neuropathic pain. This severe pain is evoked at least partially through complement activation on GD2-expressing sensory neurons.

Methods

To reduce pain while maintaining antitumor activity, we have reformatted the approved GD2 antibody ch14.18 into the IgA1 isotype. This novel reformatted IgA is unable to activate the complement system but efficiently activates leukocytes through the FcαRI (CD89).

Results

IgA GD2 did not activate the complement system *in vitro* nor induced pain in mice. Importantly, neutrophil-mediated killing of neuroblastoma cells is enhanced with IgA in comparison to IgG, resulting in efficient tumoricidal capacity of the antibody *in vitro* and *in vivo*.

Conclusions

Our results indicate that employing IgA GD2 as a novel isotype has two major benefits: it halts antibody-induced excruciating pain and improves neutrophil-mediated lysis of neuroblastoma. Thus, we postulate that patients with high-risk neuroblastoma would strongly benefit from IgA GD2 therapy.

Keywords

Neuroblastoma, Pain, Immunotherapy, Pediatrics

INTRODUCTION

Neuroblastoma is a pediatric tumor derived from the neural crest, and accounts for 15% of pediatric cancer mortality. Approximately half of the diagnosed cases of neuroblastoma are classified as high-risk, with a 5-year survival rate of less than 40% when treated with surgery, chemotherapy and radiotherapy[1]. A major improvement in patient survival came in 2015, with the Food and Drug Administration approval of ch14.18, a chimeric antibody of the IgG1 isotype directed against the ganglioside GD2, expressed on neuroblastoma cells, but also on peripheral and central nervous tissue. Ch14.18 is applied as second-

line treatment in combination with interleukin (IL)-2, Granulocyte-macrophage colony-stimulating factor (GM-CSF) and 11-*cis* retinoic acid for the treatment of high-risk neuroblastoma after hematopoietic stem cell transplantation. In a large phase III clinical trial, ch14.18 combination therapy resulted in 20% more event-free survival (EFS) than standard therapy, 2 years after treatment[2]. Although the inclusion of immunotherapy improved the survival of patients with neuroblastoma, excruciating pain is a major dose-limiting side effect caused by the administration of ch14.18 affecting therapy success[2]. This severe pain is difficult to manage, and all children who undergo treatment with dinutuximab require the use of significant dosing of morphine (10 µg/kg/hour at minimum), and sometimes pretreatment with gabapentin and treatment with lidocaine or ketamine[3,4]. Patients would therefore strongly benefit from GD2 treatment that does not induce severe pain.

Ch14.18 has two modes of action. First, antibody-opsonized tumor cells are killed by leukocytes through antibody-dependent cell-mediated cytotoxicity (ADCC) that depends on antibody binding to Fc receptors on leukocytes. For IgG1-mediated antibody therapy, natural killer (NK) cells are regarded as the most important effector cell type. However, for IgG-mediated ADCC against neuroblastoma, there is evidence that granulocytes play an important role, because granulocyte activation positively correlates with therapeutic outcome when treated with an antibody directed against GD2[5–7]. Second, ch14.18 directly activates the complement system on the tumor cell surface, leading to cell lysis by complement-dependent cytotoxicity (CDC)[8]. Since GD2 is expressed on sensory nerve fibers as well, ch14.18 binds to GD2 on sensory nerve fibers and activates the complement system locally, which generates anaphylatoxins such as C5a that can activate sensory neurons, thereby promoting pain[9]. As complement activation is one of the mechanisms contributing to pain after ch14.18, attempts have been made to circumvent complement activation on peripheral nerves with GD2 antibodies. For example, the introduction of the K322A mutation in the IgG1 Fc region, resulted in reduced CDC. However, this K322A variant still induces neuropathic pain in patients[10,11].

We hypothesized that enhancing ch14.18-mediated activation of granulocytes is beneficial, while avoiding antibody-induced complement activation relieves pain observed in patients treated with ch14.18. This urged us to investigate IgA as an alternative isotype for ch14.18, since IgA is superior to IgG in activating granulocytes, while having no binding site for C1q, the first component of the classical complement pathway[12,13].

METHODS

Antibody production, isolation and quality control

The variable heavy and light chain sequences of ch14.18 were derived from Biologic License Application 125516. The variable chain sequences were cloned into expression vectors (pEE14.4), coding for the IgA1 or IgG1 heavy chain or kappa light chain. Monomeric antibodies were produced by transient transfection of HEK293F cells with vectors coding for the heavy chain, light chain and pAdvantage (accession number U47294; Promega), using 293Fectin transfection reagent according to the manufacturer's instructions. IgG1 antibodies were purified using protein A columns (Hi-trap protein A) coupled to an ÄKTA prime plus chromatography system (GE Lifesciences). Bound antibody was eluted with 0.1 M sodium acetate pH 2.5 and neutralized with 1M TRIS-HCl pH 8.8. The eluate was dialyzed against phosphate-buffered saline (PBS). IgA1 antibodies were purified using kappa light chain affinity chromatography columns (HiTrap KappaSelect, GE Healthcare) and eluted with 0.1 M glycine buffer pH 2.5. The eluate was applied on a size-exclusion chromatography (SEC) column ran with PBS as mobile phase. The fractions containing monomeric IgA were collected and concentrated with a 100 KDa spin column (Vivaspin 20, GE Healthcare). All antibodies were filtered over 0.22 µm filters. Purity and stability of the antibodies was analyzed by HP-SEC (Yarra 3u SEC-2000 column) with 100 mM sodium phosphate, 150 mM NaCl pH 6.8 as mobile phase with detection at 280 nm.

Fluorescent labeling of antibodies

Purified antibodies were labeled with fluorescein by incubation at room temperature for 2 hours with *N*-hydroxy-succimidyl-FITC (Thermo Fisher) while stirring. Unbound NHS-fluorescein was removed by using sephadex columns (NAP-5, GE Healthcare), according to the manufacturer's instructions. Antibodies were labeled with Alexa fluor-488 antibody labeling kit (Thermo Fisher) according to the manufacturer's instructions.

Cell culture

All neuroblastoma cell lines were acquired from the ATCC and cultured in Dulbecco''s modified Eagle's medium (DMEM) culture medium supplemented with HEPES, GlutaMAX, 10% heat-inactivated fetal calf serum, 100 U/mL penicillin–streptomycin (Gibco Life Technologies) and 2% non-essential amino acids (Thermo Fisher) at 37°C in a humidified incubator containing 5% carbon dioxide (CO_2). HEK293F cells were cultured in FreeStyle 293 expression medium at 37°C in a humidified incubator with orbital shaker platform containing 8% CO_2. Cells were not cultured past passage number 20 and comparisons between IgA and IgG were conducted paired to prevent bias between cell line batches. Cells were regularly tested for mycoplasma contamination by MycoAlert Mycoplasma Detection Kit (Lonza).

Binding assays

1×10^5 neuroblastoma cells were plated out in 96 well plates and centrifuged for 2 min at 1500 RPM. Cells were washed and incubated with fluorescein-labeled antibody at several concentrations for 45 min on ice. Next, cells were centrifuged for 2 min at 1500 RPM, washed and resuspended in PBS. The amount of bound antibody to the cells was quantified by flow cytometry (BD FACSCanto II).

Cell-based affinity measurements

IMR32 neuroblastoma cells were plated out on the side of a culture dish in an elliptical shape and incubated overnight for attachment to the plate. Subsequently, plates were washed with culture medium and transferred to the LigandTracer apparatus (Ridgeview Instruments). First, background signal of cells with medium was measured for 15 min. Afterwards, association was measured for 1 hour at 10 nM of antibody and subsequently at 20 nM for 1 hour. Finally, dissociation was measured by replacing the antibody containing solution for antibody-free medium for 2 hours. The affinity of the antibodies was calculated via TraceDrawer software.

ADCC assays

ADCC was quantified as described previously[14]. In short, target cells were labeled with ^{51}Cr (PerkinElmer). Afterwards, cells were washed. Blood for ADCC's was obtained from healthy donors at the UMC Utrecht (approval number 07–125/O). For leukocyte isolation, blood was incubated in water for 30 s to lyse erythrocytes. Afterwards, 10× PBS was added to reach physiological osmolality. Cells were washed and resuspended. For polymorphonuclear cells (PMN) and peripheral blood mononuclear cell (PBMC) isolation, blood was added on top of a Ficoll (GE Healthcare)/Histopaque 1119 (Sigma) layer and centrifuged for 20 min at 1500 RPM. Afterwards, PBMCs and PMNs were collected from the interphase between serum and ficoll or in the histopaque layer, respectively. The used effector-to-target (E:T) ratios were 100:1 for PBMCs, 40:1 for PMNs. Effector cells with or without pretreatment of 10 μM of 11-*cis* retinoic acid (Sigma), antibodies at various concentration, 10 ng/mL IL-2 (650 IU/mL) (eBioscience) and 10 ng/mL GM-CSF (ImmunoTools), 15% pooled human serum and tumor cells were added to round-bottom microtiter plates (Corning Incorporated) and incubated for 37 °C in a humidified incubator containing 5% CO_2. Plates were centrifuged for 2 min at 1500 RPM and the supernatant was transferred to lumaplates (PerkinElmer). Radioactive scintillation (in cpm) was quantified in a beta–gamma counter (PerkinElmer). Specific lysis was calculated using the formula: ((experimental cpm – basal cpm)/(maximal cpm – basal cpm))×100, with maximal lysis determined by incubating labeled cells with 1.25% triton and minimal lysis in the absence of antibodies and effector cells.

Live cell imaging

IMR32 cells were seeded in an 8 well µ-slide (Ibidi) 1 day prior to live cell imaging. Target cells were labeled with 20 µM Calcein-AM according to the manufacturers protocol (Thermo Fisher). Subsequently, either 10 µg/mL IgG1 ch14.18 or IgA2.0 ch14.18 and 1 µM TO-PRO-3 (Thermo Fisher) were added to the target cells. Primary PMNs were labeled with eFluor 450 (Thermo Fisher) according to the manufacturers protocol and were added 15 min after antibodies treatment. Live-cell imaging recordings were performed with a Deltavision RT widefield microscope (GE Healthcare) housed in a conditioned, temperature-controlled (37 °C), humidified chamber containing 5% CO_2. Images were recorded using an Olympus 40×/1.35 NA oil immersion objective on a Cascade II 1K EMCCD/E2V CCD-201 camera. Imaging data was analyzed using Imaris (Bitplane).

CDC assays

10^5 neuroblastoma cells were added per well to 96 wells microtiter plates and incubated for 30 min with antibodies at various concentrations at room temperature. Afterwards, pooled human serum (from eight different healthy donors) was added to a concentration of 15% and incubated for 1 hour or 4 hours. Afterwards, cells were washed and stained with 7-AAD (BD Pharmingen) for 15 min. 7-AAD uptake, representing cell lysis was quantified by flow cytometry (FACSCanto II, BD Biosciences).

C5a quantification

MaxiSorp 96 well ELISA plates (NUNC) were coated with 10 ug/ul anti-GD2 antibody overnight at 4 °C. Afterwards, plates were washed and pooled human serum was added for 15 min or 60 min at 37 °C. Subsequently C5a was quantified by performing a C5a ELISA (R&D systems) according to the manufacturers protocol.

Antibody concentration determination in mouse serum

MaxiSorp 96 well ELISA plates (NUNC, Thermo Fisher) were coated overnight with 0.5 µg/mL polyclonal goat IgG anti-human kappa (Southern Biotech) diluted in PBS. Next, plates were washed three times with 0.05% TWEEN 20 in PBS (PBST) and blocked for 1 hour by incubating with 1% BSA (Roche) in PBST. Serum samples were diluted 1:2000 in 1% BSA in PBST and incubated for 1.5 hours at room temperature. Next, plates were washed three times with PBST. HRP-labeled-anti-human IgA or HRP-labeled-anti-human-IgG (SouthernBiotech) were used to bind human IgA or human IgG, respectively. Plates were developed for 10 min with ABTS (Roche) and read out on a spectrophotometer (Bio-Rad) at 415 nm.

Animals and animal experiments

Mice were maintained in the animal facility of the University of Utrecht. Experiments were conducted using both male and female C57BL/6JRj mice (Janvier)

For evaluating the *in vivo* efficacy of antibodies, mice were intraperitoneally (i.p.) injected with 5×10^6 GD2 expressing EL4 cells expressing Luc2. After 1 day, mice were i.p. injected with 100 µg of IgG1 ch14.18, or 100 µg of IgA1 ch14.18. After 2 days, blood was taken and mice were injected with 100 µl of 0.025 g/mL luciferin (Promega) i.p. and subjected to bioluminescence analysis 1 min after injection with 5 min exposure time to quantify tumor cells (PhotonImager, Biospace Lab). Image analysis was performed using M3Vision software (Biospace Lab). Afterwards mice were euthanized by cervical dislocation. In a second model, mice were intravenously (i.v.) injected with 1×10^6 cells and treated i.p. with 100 µg IgG1 ch14.18 or 100 µg IgA1 ch14.18. After 2 days, mice were retreated with antibodies. After 24 hours, blood was taken and mice were injected with luciferin and subjected to bioluminescence analysis to quantify tumor cells.

Mechanical thresholds were determined using the von Frey test (Stoelting) with the up-and-down method as was described before[15,16]. In brief, mechanical allodynia was assessed with calibrated von Frey hair monofilaments (Stoelting). First, mice were acclimated for 15–20 min in a transparent box with a metal mesh floor. Mice were i.v. treated with 100 µg of IgG1 isotype control, 4 µg or 20 µg of IgG1 ch14.18, or 20 and 100 µg of IgA1 ch14.18. The von Frey hair monofilaments were applied through the mesh floor to the plantar skin of the hind paw. The hair force was increased or decreased according to the response. Clear paw withdrawal, shaking or licking were considered as nociceptive-like responses. In each experiment, the average of the left and right paw was considered as an independent measure. To minimize bias, animals were randomly assigned to the different groups prior to the start of experiment, and all experiments were performed by experimenters blinded to treatment. Von Frey data was obtained from separate experiments. Equivalent dosing in pain experiments was based on data from previous studies[17].

Antibody binding to neurons was visualized by i.v. injection of 20 or 100 µg alexa-488 labeled IgG1 ch14.18 or 100 µg of IgA1 ch14.18. Sciatic nerves were isolated and 10 µm thick slices were prepared with a cryostat cryotome and placed on slides. Slides were fixed for 10 min in 4% paraformaldehyde (PFA) and washed. Finally, slides were counterstained with 4',6-diamidino-2-phenylindole (DAPI), washed and treated with FluorSave (Calbiochem). Slides were dried overnight at 4 °C and images were taken by fluorescence microscopy (Zeiss).

C4 deposition was determined by immunofluorescence on mouse sciatic nerves. Slides were fixed in 4% PFA, washed and incubated with 10 mM ammonium chloride in PBS. After washing, slides were incubated with 10 µg/mL of IgG1 ch14.18 or IgA1 ch14.18 for 1 hour. Slides were washed and incubated with 15% pooled human serum or heat-inactivated serum for 1 hour at room temperature. Afterwards, slides were washed and incubated

with biotin conjugated polyclonal anti-human C4 antibody (MyBioSource). For detection, slides were incubated with alexa-594 conjugated to streptavidin (Thermo Fisher Scientific). Finally, slides were counterstained with DAPI by incubation with ProLong diamond antifade mountant (Thermo Fisher Scientific). Fluorescence quantification was performed with ImageJ.

Data processing and statistical analysis

Statistical analyses were performed in GraphPad Prism V.7.0 software (GraphPad). Data are represented as mean±SD. For comparing mean values of two groups, an unpaired two-tailed Student's t-test was performed. For multiple comparisons, two-tailed one-way analysis of variance (ANOVA) was performed with Tukey's range test. For multiple comparisons with multiple concentrations, two-tailed two-way ANOVA was performed with Sidak's multiple comparisons test. Dose-response curves for ADCC experiments were calculated via non-linear regression using GraphPad V.7.0 software. Asterisks were used to indicate statistical significance: * = $p < 0.05$, ** = $p < 0.01$, *** = $p < 0.001$ or n.s. if no statistical significance was obtained.

RESULTS

IgA1 and IgG1 ch14.18 specifically bind GD2 with similar affinity

First, we determined the binding of IgA1 and IgG1 ch14.18 to neuroblastoma cell lines. IgA1 and IgG1 antibodies with the ch14.18 variable region were produced and purified in-house. All antibodies were monomeric, with a purity above 95% (**Supplemental Figure 1**). Both antibodies bound similarly to the GD2 expressing neuroblastoma cell line IMR32, while the GIMEN cell line without GD2 expression was not recognized (**Figure 1A**). To investigate whether the affinity of the antibodies is independent of the isotype, real time cell-based affinity measurements on IMR32 cells were performed with LigandTracer. The IgG1 and IgA1 antibodies closely follow the same association pattern at two different concentrations and overlapped in the dissociation phase, showing that the affinity of both isotypes do not differ significantly (3.8±0.3 nM vs 4.8±0.5 nM) (**Figure 1B, C**).

Mechanism of action of IgA1 and IgG1 ch14.18 antibodies

Subsequently, we compared the *in vitro* mechanisms of action of IgA1 and IgG1 ch14.18. To compare killing of neuroblastoma with a mix of effector cells, ADCC assays were performed on IMR32, SKNFI and LAN-5 neuroblastoma cell lines, with leukocytes from peripheral blood as effector cells. LAN-5 cells showed the highest binding of ch14.18 IgA, followed by IMR32, SKNFI and GIMEN (**Supplemental Figure 1C**). Both IgA1 and IgG1 antibodies lysed IMR32 cells to a similar extent, while SKNFI and LAN-5 cells were killed

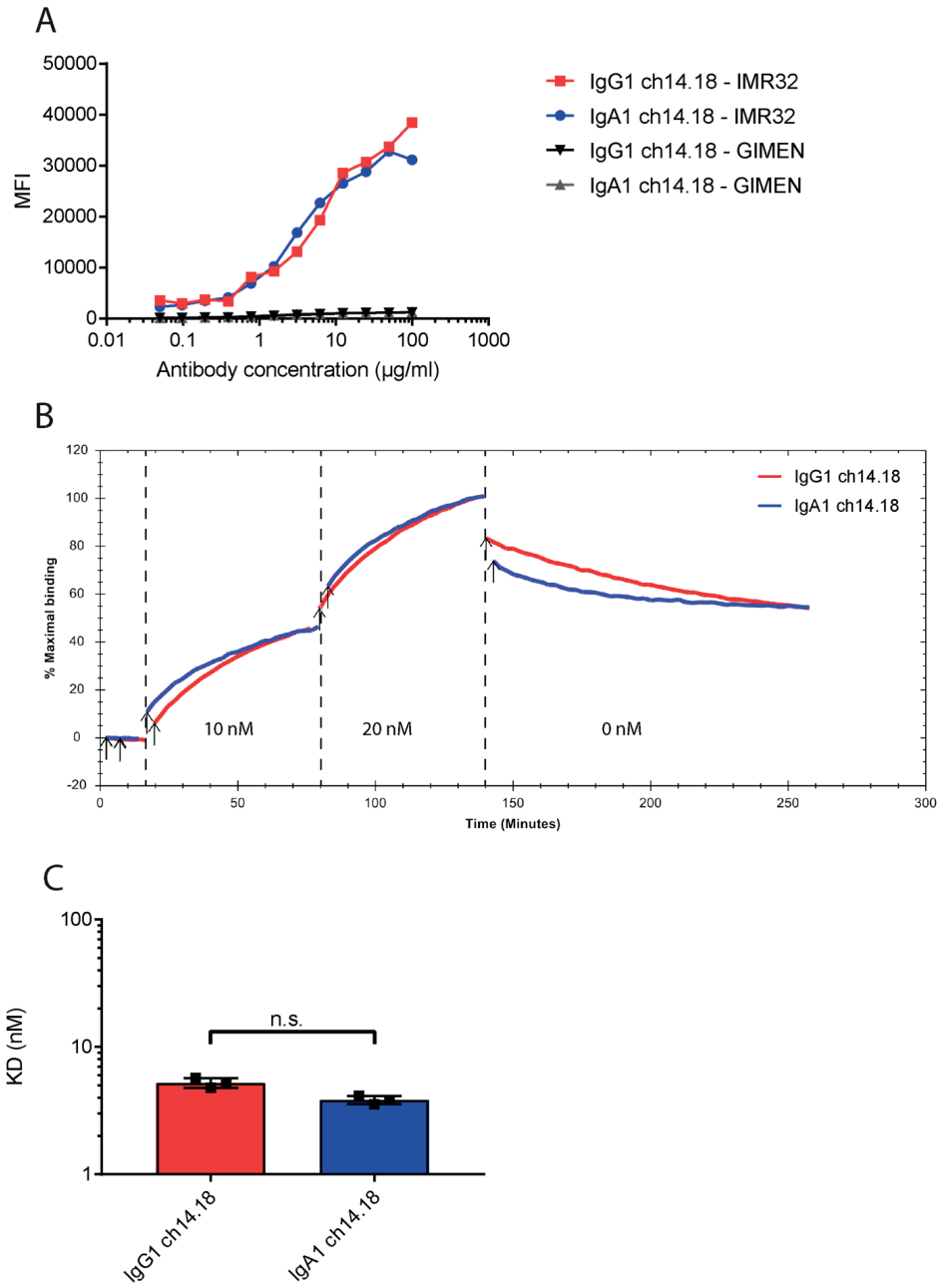

Figure 1 | Binding of IgG1 and IgA1 ch14.18 antibodies to neuroblastoma cell lines. (**A**) Flow cytometric assessment of antibody binding of IgA1-FITC and IgG1-FITC ch14.18 to GD2-expressing neuroblastoma cell line IMR32 and GD2-negative cell line GIMEN. (**B**) Real-time cell-based affinity measurement of FITC-labeled IgA1 and IgG1 ch14.18 on IMR32 cells. IMR32 cell lines were treated with 10 nM of antibody. Subsequently, antibody concentration was increased to 20 nM of antibody. Dissociation was followed for 2 hours. The traces show the fluorescent signal of three individual measurements per antibody (IgG1 in red, IgA1 in blue,). (**C**) Calculated affinities from cell-based affinity measurements shown in B using one-to-one fitting. Data show mean affinity ±SD (*n* = 3, technical triplicate). MFI, mean fluorescent intensity; FITC, fluorescein isothiocyanate; n.s., no statistical significance.

better with IgA1 ch14.18 compared with IgG1 (**Figure 2A**). The GIMEN cell line which has no detectable GD2 expression, was not lysed by either antibody, showing that GD2 expression is a prerequisite for ch14.18-mediated ADCC (**Supplemental Figure 2A**).To evaluate the relative contribution of leukocyte subsets in mediating ADCC against neuroblastoma cell lines, isolated neutrophils or PBMC from healthy donors were separately used as effector cells. IgG1 ch14.18 effectively induced lysis in neuroblastoma cell lines with PBMCs as effector cells, while the IgA antibody did not lyse these cells (**Figure 2B, Supplemental Figure 2B**). Conversely, when neutrophils were used as effector cells, IgA ch14.18 mediated ADCC was superior for all tested cell lines in comparison to IgG1 (**Figure 2C, Supplemental Figure 2C**). These observations were also confirmed by *in vitro* imaging experiments, showing rapid engulfment and killing of IMR32 cells by neutrophils when treated with IgA anti-GD2, while this process was slower and inefficient with IgG1 anti-GD2 (**Figure 2D**). In patients, ch14.18 is administered as combination therapy with GM-CSF, IL-2 and retinoic acid. Therefore, the impact of these compounds on ADCC was assessed. Addition of GM-CSF did not increase ADCC by IgG1, when PBMCs were used as effector cells. Addition of the combination of GM-CSF and IL-2 led to a small increase of cell death without the presence of antibody, showing increases in PBMC-mediated killing of neuroblastoma regardless of antibody. GM-CSF and IL-2 did not affect maximal killing by PBMC-mediated ADCC by IgG1, but improved killing at lower concentrations. Pre-exposure of target cells to 11-*cis* retinoic acid for 24 hours to the previous combination further increased the IgG1-independent and IgG1-dependent killing of neuroblastoma cell lines (**Figure 2E, Supplemental Figure 2D**). IgA1 did not induce killing by PBMCs, but neuroblastoma cells were lysed in the presence of IL-2 alone or in combination with 11-*cis*-retinoic acid, indicating antibody-independent recognition of neuroblastoma cells by PBMCs (**Supplemental Figure 2E**).

With neutrophils as effector cells, GM-CSF in combination with IgA1 or IgG1 ch14.18 boosted ADCC (**Figure 2F, Supplemental Figure 2F**), while combination with GM-CSF and IL-2 did not further improve GM-CSF enhanced neutrophil mediated killing. Pre-exposure of target cells with 11-*cis*-retinoic acid increased maximal lysis. In contrast to IgA1, IgG1-mediated ADCC with neutrophils was only improved slightly by GM-CSF. Furthermore, addition of IL-2 or retinoic acid did not further enhance killing (**Supplemental Figure 2G**).

Figure 2 | Induction of ADCC by IgA1 and IgG1 ch14.18 against neuroblastoma cell lines. (**A**) ADCC assays with IgA1 and IgG1 ch14.18 on three different neuroblastoma cell lines with leukocytes from blood as effector cells. (**B**) ADCC assays with IgG1 and IgA1 ch14.18 on neuroblastoma cell line IMR32 with isolated PBMCs (E:T ratio of 100:1) as effector cells. (**C**) ADCC assays with IgG1 and IgA1 ch14.18 on IMR32 neuroblastoma cell line with isolated neutrophils (E:T ratio of 40:1) as effector cells. (**D**) Live-cell imaging of PMN-mediated ADCC. Calcein-AM labeled IMR32 cells (Green) were treated with 10 µg/mL IgG1 ch14.18 or IgA ch14.18. eFluor450-labeled PMNs were added at an 83:1 E:T ratio to tumor cells. Cell death was visualized with TO-PRO-3 (Red). (**E**) ADCC assays with IgG1 ch14.18 on IMR32 neuroblastoma cell line with isolated PBMCs (E:T ratio of 100:1) as effector cells with or without co-treatment of GM-CSF, IL-2 and 11-cis retinoic acid. (**F**) ADCC assays as in E with IgA1 ch14.18 with isolated neutrophils (E:T ratio of 40:1) as effector cells. All ADCC assays were incubated for 4 hours at 37 °C. Data represent mean lysis of a representative donor ±SD (technical triplicate at least *n* = 3 donors per assay). Statistical significance was

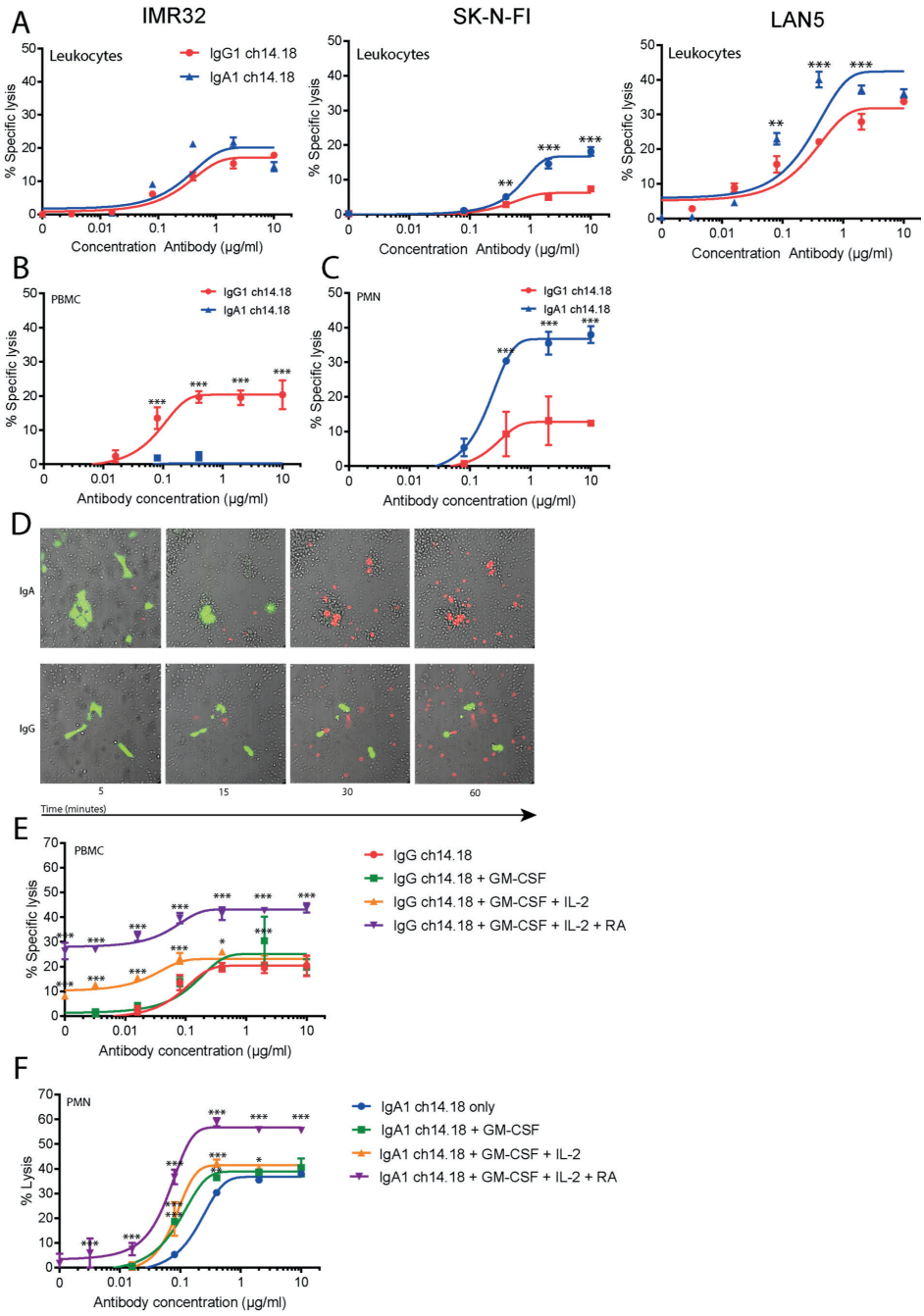

determined by two-way analysis of variance. ADCC, antibody-dependent cell-mediated cytotoxicity; E:T, effector-to-target; IL, interleukin; RA, 11-cis retinoic acid; GM-CSF, granulocyte-macrophage colony-stimulating factor; PMN, polymorphonuclear cells; PBMC, peripheral blood mononuclear cells.

IgA1 ch14.18 does not trigger complement activation

Ch14.18 lyses neuroblastoma target cells via CDC *in vitro*, however, the same complement activation is at least partially responsible *in vivo* for inducing treatment-associated pain on sensory neurons expressing GD2. Therefore, we assessed *in vitro* complement activation by these antibodies on a panel of neuroblastoma cell lines. As expected, IgG1 ch14.18 induced CDC on GD2-expressing neuroblastoma cell lines within 15 min. In contrast, no complement-mediated lysis was observed for IgA1 ch14.18 (**Figure 3A**). With longer incubation for 4 hours, the amount of lysis further increased for IgG1, but remained similarly low for IgA1 (**Figure 3B**). The neuroblastoma cell line SKNFI expressed more complement regulatory proteins than the other tested neuroblastoma cell lines, potentially explaining its resistance against complement mediated lysis (**Supplemental Figure 3A, B**). Additionally, we investigated whether IgG-mediated CDC increased neuroblastoma cell lysis when combined with ADCC by mixed leukocytes. No significant increases in lysis were observed on IMR32 cells after addition of serum (**Figure 3C**). Recently, an engineered IgG1 antibody (K322A) with reduced complement activation has entered clinical trials[10]. As a different measure of complement activation, we quantified C5a generation in serum by plate bound IgG1, IgG1 K322A and IgA ch14.18. Interestingly, IgG1 ch14.18 K322A generated less C5a compared with the wild type IgG1 antibody, but IgA ch14.18 showed even less C5a formation (**Figure 3D**). While C5a generation increased for both IgG ch14.18 antibodies over time, this was absent with IgA ch14.18.

IgA1 ch14.18 performs tumor cell killing *in vivo*

Next, we analyzed the capacity of the IgG1 and IgA1 antibodies to kill GD2 expressing cells *in vivo* in two syngeneic immune-competent mouse models. As a model for a localized tumor, human CD89 transgenic C57Bl/6 mice were i.p. injected with EL4 cells, which naturally express GD2. CD89 transgenic mice express CD89 under the endogenous promotor, thereby limiting expression to granulocytes and activated monocytes and macrophages[18]. After 24 hours of outgrowth, animals were treated with IgA1 or IgG1. Outgrowth of tumor cells was evaluated 24 hours after injection of the antibody by bioluminescent analysis (**Figure 4A**). Both IgA and IgG treatment resulted in killing of tumor cells, although not significant (**Figure 4B, C**).

Figure 3 | Complement assays on a panel of neuroblastoma cell lines by IgG1 and IgA1 ch14.18 antibodies. (**A**) Lysis by IgG1 or IgA1 ch14.18 antibodies on four different neuroblastoma cell lines. Cells were incubated with three different concentrations of antibody for 30 min and subsequently with 15% pooled human serum for 15 min. Data represents mean percentage of 7-AAD$^+$ cells ± SD (n = 3). (**B**) Lysis by IgG1 or IgA1 ch14.18 antibodies on four different neuroblastoma cell lines. Cells were incubated with three different concentrations of antibody for 30 min and subsequently with 15% pooled human serum for 4 hours. Data represents mean percentage of 7-AAD$^+$ cells±SD (n = 3). Statistical significance was determined by two-way analysis of variance. (**C**) ADCC assays with IgA1 ch14.18 or IgG1 ch14.18 with or without 15% serum on IMR32 neuroblastoma cell line and with leukocytes from peripheral blood as effector cells. Data represent mean±SD. (**D**) C5a quantification in pooled human serum after incubation with plate-bound antibody for 15 min, or 60 min. Data show a representative example (n = 3).

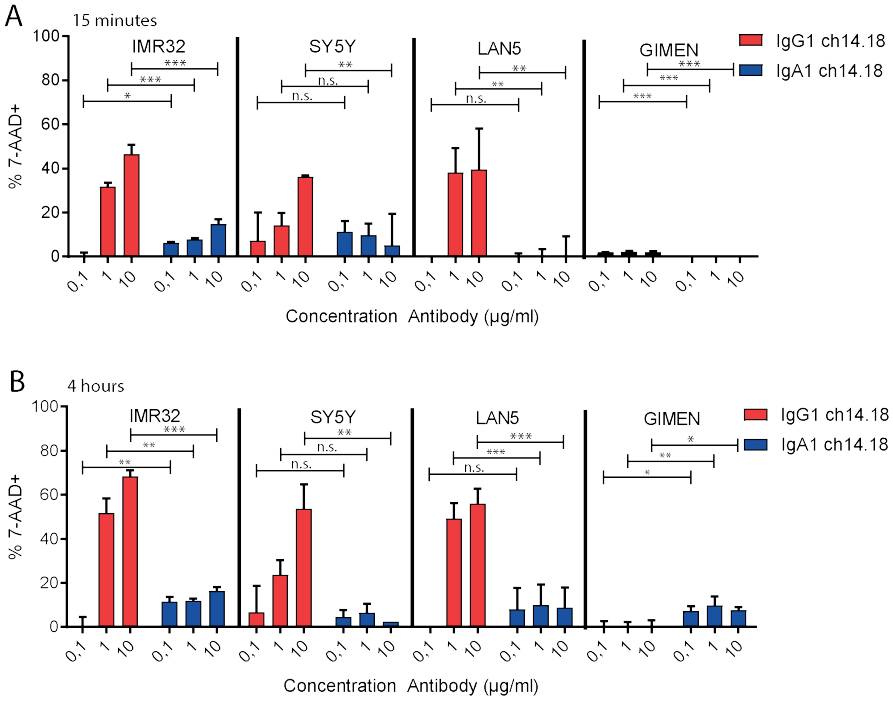
A
15 minutes
IMR32
SY5Y
LAN5
GIMEN
IgG1 ch14.18
IgA1 ch14.18
% 7-AAD+
Concentration Antibody (µg/ml)
B
4 hours
IMR32
SY5Y
LAN5
GIMEN
IgG1 ch14.18
IgA1 ch14.18
% 7-AAD+
Concentration Antibody (µg/ml)
C
Leukocytes
ch14.18 IgG1
ch14.18 IgG1 + Serum
ch14.18 IgA1
% Specific lysis
Antibody concentration (µg/ml)
D
IgG1 ch14.18
IgG1 K322A ch14.18
IgA ch14.18
C5a concentration (ng/mL)
15min
1h

In a second systemic tumor mouse model, EL4 cells were i.v. injected, and treatment was injected i.p. (**Figure 4D**). After 3 days of treatment, both IgA1 and IgG1 cleared the tumor cells, while tumor cells were still present in mice treated with PBS (**Figure 4E, F**).

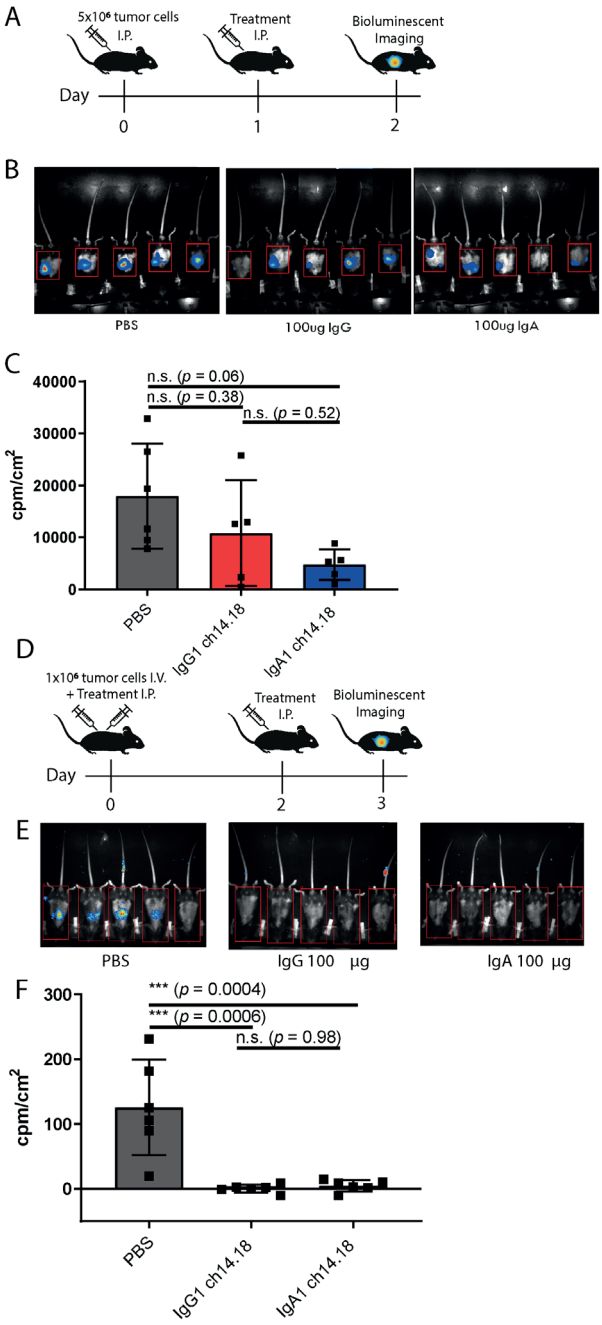

IgA1 does not activate complement on neurons *in vivo* and does not induce pain

A major limitation of IgG1 antibodies directed against GD2 is the induction of pain and allodynia after treatment. Similarly, systemic administration of GD2 antibodies increases mechanical sensitivity (allodynia) in rats[11]. To test whether the lack of complement activation by IgA would halt the development of pain by administration of an GD2 antibody, we tested allodynia development after antibody administration *in vivo* in mice.

To control for differences between the half-life of IgA1 and IgG1, mice were i.v. injected with either a subtherapeutic dose of IgG1 (4 μg), corresponding to the serum levels of a dose of 20 μg of IgA1 at 3 hours or a therapeutic dose of IgG1 (20 μg) or IgA1 (100 μg) (**Figure 5A**). In line with the clinical phenotype after ch14.18 treatment and rat studies, treatment with 20 μg of IgG1 ch14.18 elicited mechanical hypersensitivity in mice, that peaked 6 hours after administration and slowly returned to baseline (**Figure 5B**). Four μg of IgG1 did not elicit mechanical hypersensitivity. Conversely, most doses of IgA1 did not affect paw withdrawal threshold, except for 100 μg at 6 and 24 hours that slightly reduced thresholds but the reduction was threefold less than with 20 μg IgG. Thus, IgA1 does not induce allodynia at levels that would be therapeutic for IgG1. IgA also did not reduce mechanical threshold in mice that express FcαRI, indicating that mice able to perform tumor killing with IgA still do not develop pain after IgA administration (**Figure 5C**). Subsequently, mice were injected with fluorescently-labeled GD2 antibodies. Fluorescently-labeled IgG1 ch14.18 reduced the withdrawal threshold while IgA1 did not (**Figure 5D**). We visualized the *in vivo* binding of the GD2 antibodies to sensory neurons in the sciatic nerve *ex vivo*. Antibody exposure was observed with 20 μg of IgG1 and 100 μg of IgA1 ch14.18 to a similar extent and corresponded to the amount of antibody present in the serum (**Figure 5E**). *Ex vivo* staining of GD2 on sciatic nerves overlapped with the signal from directly labeled antibodies. The isotype control (rituximab) did not bind sciatic nerves. Finally, we assessed *ex vivo* complement activation on sciatic nerves from naïve mice. IgG1 ch14.18 elicited C4 deposition, while no C4 deposition was observed when heat-inactivated serum was used. With IgA1 ch14.18 no C4 deposition was observed (**Figure 5F**). Our results summarized in **Figure 6**, provide a novel approach to halt GD2 antibody-induced neuropathic pain and improve neutrophil-mediated killing of neuroblastoma.

Figure 4 | *In vivo* efficacy of IgG1 and IgA1 ch14.18 antibodies. (**A**) Graphical representation of treatment schedule of mice used in short IP model. (**B**) Bioluminescent imaging of EL4-Luc2 tumor cells after 24 hours of treatment with PBS, IgA1 or IgG1 ch14.18. (**C**) Quantification of bioluminescent signal in B. Data represents mean counts/cm^2—background ±SD of at least five mice. Statistical significance was determined by one-way analysis of variance (ANOVA) with Tukey's post-hoc correction. (**D**) Graphical representation of treatment schedule of mice used in i.v. model. (**E**) Bioluminescent imaging of EL4-Luc2 tumor cells on day 3 of treatment after i.v. injection of tumor cells. (**F**) Quantification of bioluminescent signal after 3 days of treatment. Data represents mean counts/cm^2—background ±SD of six mice per group. Statistical significance was determined by one-way ANOVA. i.p., intraperitoneally; i.v., PBS, phosphate-buffered saline; n.s., no statistical significance.

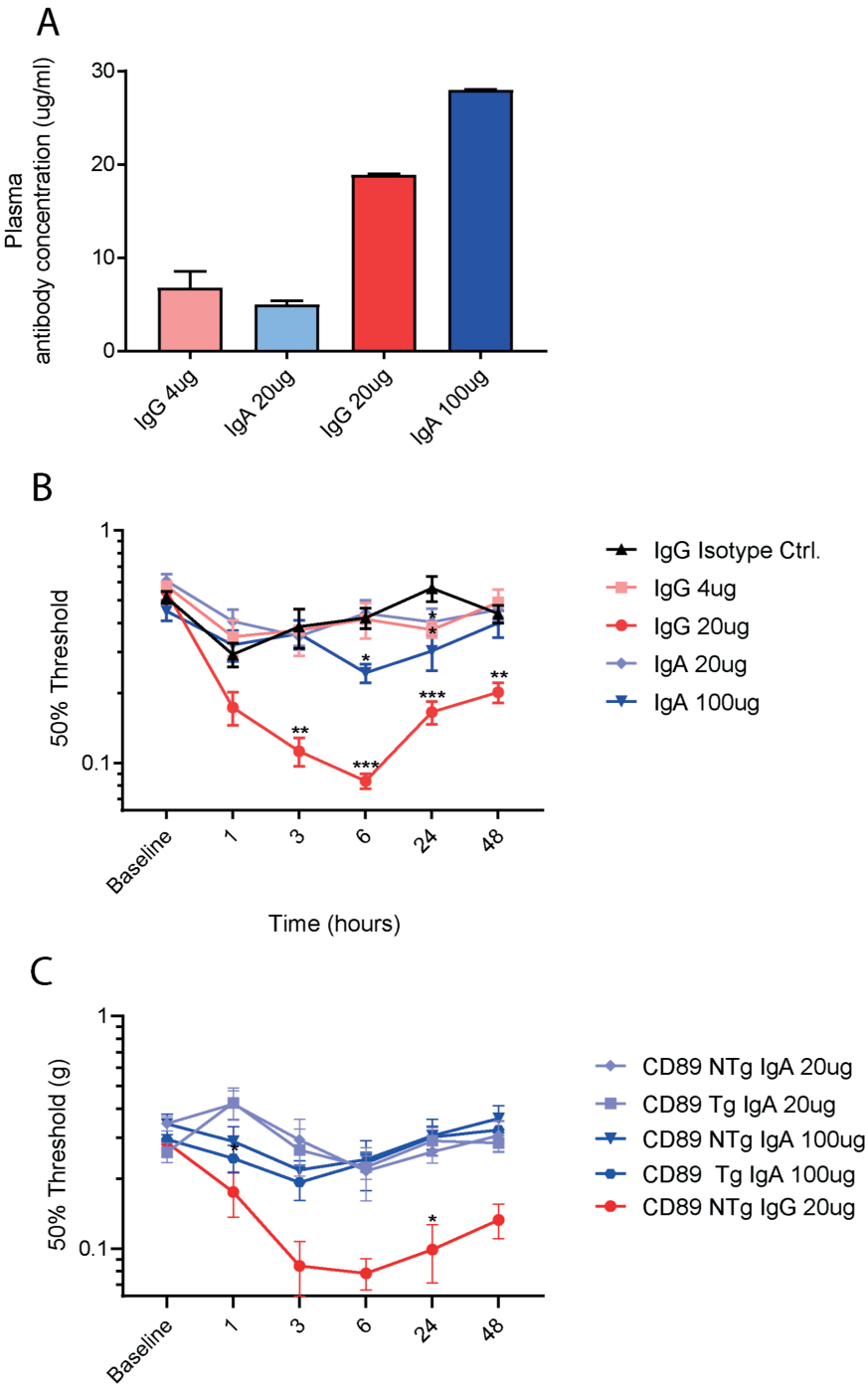

Figure 5 | Neuronal exposure of to IgA1 does not lead to decreases in mechanical withdrawal thresholds nor C4 deposition. (**A**) Plasma concentrations of IgA1 and IgG1 ch14.18 3 hours after i.v. injection determined by ELISA. Data represents mean antibody concentration in µg/ml±SD of at least two mice per

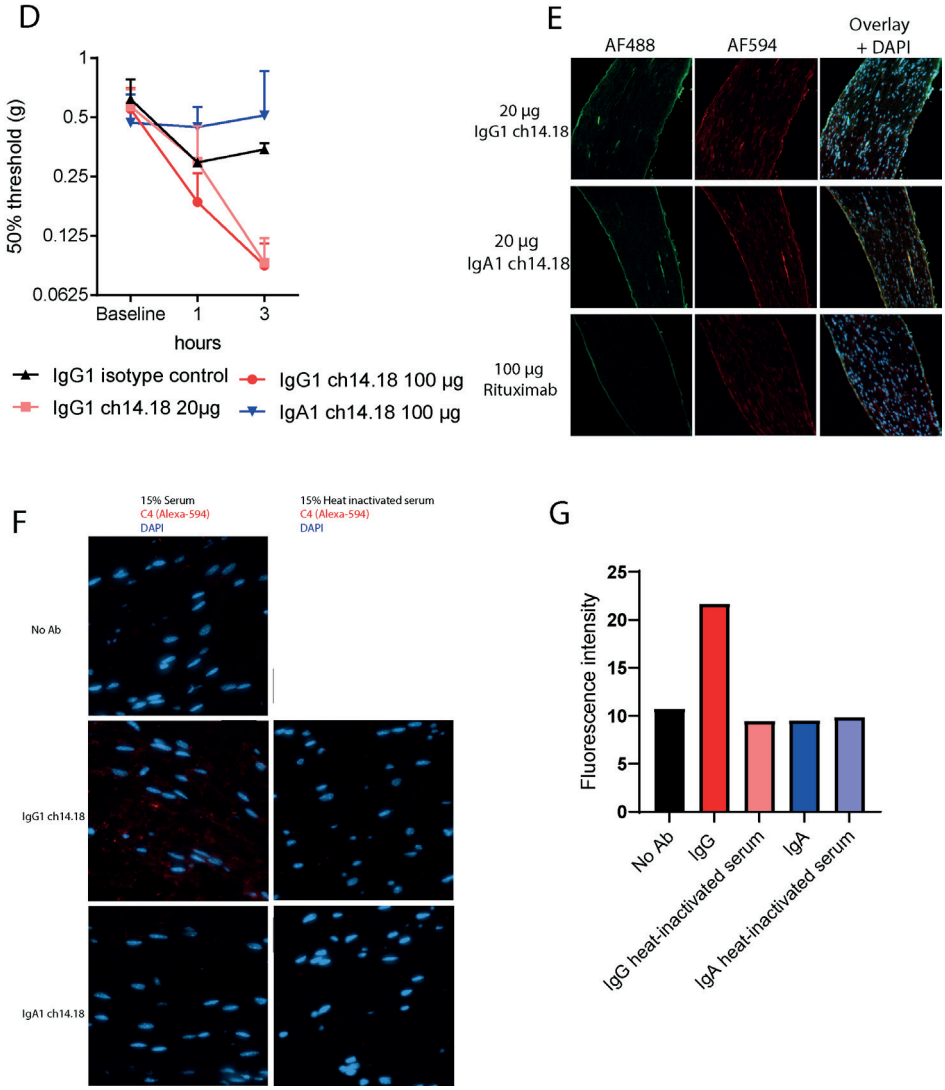

group. (**B**) Course of mechanical sensitivity as determined with von Frey test over time after i.v. injection of IgA1 or IgG1 ch14.18. Data represents mean 50% withdrawal thresholds±SEM of at least eight mice per group. Statistical significance was determined by repeated measures analysis of variance (ANOVA) followed by Sidak's post-hoc analyses. (**C**) Von-Frey withdrawal thresholds over time after i.v. injection of IgA1 or IgG1 ch14.18 in mice expressing FcαRI (CD89 Tg) or control littermate (NTg) mice. Data represents mean withdrawal thresholds±SEM of at least five mice per group pooled from separate experiments. Statistical significance was determined by repeated repeated-measures ANOVA followed by Sidak's post-hoc analyses. (**D**) Mechanical sensitivity as determined with von Frey test over time after i.v. injection of IgA1-AF488 or IgG1-AF488 ch14.18. Data represents mean withdrawal thresholds±SEM of at least two mice per group. (**E**) Left column: Visualization of intravenously injected Alexa-488 labeled GD2 antibodies on sciatic nerves. Middle column: Visualization of *ex vivo* staining of GD2 by incubation of sciatic nerve slides with Alexa-549 labeled IgG1 ch14.18. Right column: Overlay (**F**) Visualization of *ex vivo* C4 fixation on sciatic nerves by IgG1 and IgA1 ch14.18 with complement active or heat-inactivated mouse serum. (**G**) Quantification of C4 deposition from F. i.v., intravenously.

DISCUSSION

The approval of ch14.18 for high-risk neuroblastoma led to improvements in the survival of patients with neuroblastoma. Nevertheless, IgG1 antibody therapy for neuroblastoma comes with a major limitation: severe pain caused in part through complement activation by the antibody on GD2-expressing neurons. We hypothesized that changing the isotype of ch14.18 from IgG1 to IgA1 leads to increased activation of neutrophils against neuroblastoma while abrogating antibody-induced pain. Our results show that IgA1 ch14.18 offers strong antitumoral effects through neutrophil-mediated ADCC without inducing allodynia *in vivo*.

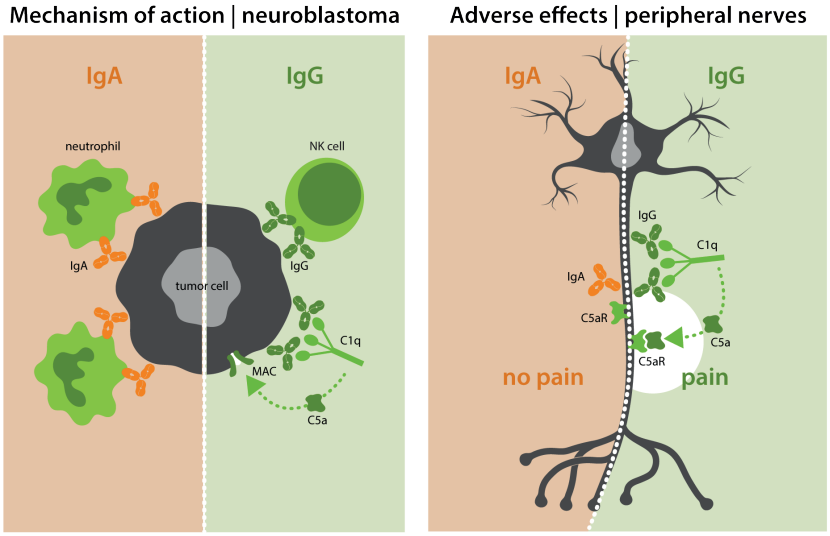

Figure 6 | Summarizing Figure. The left side of the figure shows the mechanism of action of IgA and IgG antibodies against GD2. IgA antibodies mediate killing of neuroblastoma cells with neutrophils as effector cells, while IgG antibodies do so via NK cells and CDC. On the right side of the figure, effects on GD2-expressing peripheral neurons are shown. Here, IgG activates the complement system, leading to pain. In contrast, IgA does not. CDC, complement-dependent cytotoxicity; NK, natural killer.

Thus far two approaches were undertaken to amend the side effects of ch14.18, which focused on means to reduce complement activation or binding to GD2-expressing neurons. A first approach to mitigate pain was to mutate the C1q-binding site of a humanized variant of ch14.18 (K322A) to abrogate antibody-mediated complement activation[11,19]. Lysine on position 322 in the IgG1 Fc-region is essential for interaction with C1q. Although reducing the affinity to C1q with a single amino acid mutation is possible, the C1q-binding site in the IgG1 Fc compromises multiple amino acids[20]. Therefore, this approach only partially reduced complement activation, and as such systemic administration of hu14.18K322A in rats did not completely abrogate antibody-induced pain[11]. Similarly, in a phase I clinical

trial with this antibody, grade 3–4 pain still occurred in 68% of patients, which was dose limiting in 11% of patients[10,21]. We show here that IgA ch14.18 does not initiate complement activation, since no CDC and C5a activation by IgA ch14.18 was observed in our assays. More importantly, systemic administration of IgA that effectively killed neuroblastoma cells in mice, did not elicit any signs of allodynia indicating that switching to IgA is an effective means to prevent severe side effects of IgG1 ch14.18. The second approach to circumvent ch14.18 induced allodynia was performed by targeting a different variant of GD2 (*O*-acetyl-GD2) with the antibody c.8B6. *O*-acetyl-GD2 is solely present on neuroblastoma cells and not on peripheral nervous tissue[22]. Although c.8B6 does not bind pain fibers, the expression of *O*-acetyl-GD2 is twice as low on neuroblastoma cell lines and tissue and is therefore expected to be less efficacious in patients.

Regarding the effector mechanism, the IgG1 isotype suboptimally activates neutrophils against neuroblastoma, which might limit its effectiveness. Our data and data of others show that IgA is superior to IgG1 in activating neutrophils, which could be explained by the differential expression of Fc receptors on neutrophils[23,24]. Human neutrophils express only one FcαRI, but 2 FcγRs: FcγRIIIb and FcγRIIa. FcγRIIIb is exclusively expressed on neutrophils and is the most abundant FcR on these cells. FcγRIIIb is an GPI-linked molecule and binding of IgG will not lead to ADCC by PMN through this receptor. Therefore, FcγRIIIb might act as a decoy receptor for IgG, reducing the ability of IgG to engage neutrophils in ADCC[25]. In addition, IgA binds with a 1:2 stoichiometry to FcαRI[26], leading to greater activation of neutrophils[13]. In our studies, we have used ch14.18 of the IgA1 isotype. In a clinical setting, use of IgA2 might be preferred due to the association of aberrantly glycosylated IgA1 antibodies with autoimmune disease[27].

Besides neutrophils, monocytes and macrophages are potential effector cells in the treatment of neuroblastoma with IgA. Both monocytes and certain subsets of tissue resident macrophages express CD89[28–30]. Due to the natural occurrence of tumor-associated macrophages within the neuroblastoma tumor microenvironment, they may represent a population of interest to activate against neuroblastoma[31]. Indeed, IgA antibodies can induce similar ADCC with monocytes and antibody-dependent cell-mediated phagocytosis with macrophages against tumor cells as IgG, which warrants further investigation for use of these cells against neuroblastoma[14,32,33].

Next to an inherent vulnerability of neuroblastoma cells to neutrophil-mediated killing, the timing of the current treatment protocol also favors an approach where neutrophils are used as effector cells. Currently, patients with high-risk neuroblastoma are treated with a myeloablative regimen followed by autologous stem cell transplantation[2]. Shortly thereafter, the immunotherapeutic protocol with IgG1 ch14.18 is started. Less than 25% of patients reached proper immune reconstitution for NK cells at the moment of immunotherapy, which might reduce NK cell-mediated killing against neuroblastoma[34]. In contrast, neutrophils are among the first leukocyte subsets to be

restored to physiological levels and are therefore a clinically important population to engage for tumor killing in this partially immune-compromised state[34,35]. Alternatively, the Children's oncology group is also conducting a trial (ANBL17P1) to assess dinutuximab upfront with chemotherapy which is based on a previous single-institution phase II trial that showed promising responses (NCT01576692).

At present, the preferred treatment schedule with ch14.18 treatment contains GM-CSF and IL-2. GM-CSF improves granulocyte and macrophage-mediated ADCC against neuroblastoma[36]. In our studies, IgA mediated killing, was improved by the addition of GM-CSF. On the contrary, IL-2 did not improve IgA-mediated or IgG-mediated killing by neutrophils, as expected. IL-2 was added to the clinical regimen after positive results were seen in adult patients with GD2-expressing melanoma and sarcoma after treatment with ch14.18 in combination with IL-2[37]. A clinical trial which compared immunotherapy with and without IL-2 for treatment of neuroblastoma indicated that the addition of IL-2 did not have significant effects on EFS or overall survival and that early termination because of toxicity was significantly higher in the IL-2 arm[38]. Recently, a phase-III clinical study indicated that addition of subcutaneous administration of IL-2 in combination with ch14.18 cells did not improve outcome in comparison to ch14.18 alone[39]. Although IL-2 is of importance for the immune reconstitution of NK cells and lymphocytes, the necessity of IL-2 treatment for further studies with IgA should be reevaluated.

Improving the predictability of *in vivo models* is much desired, and patient-derived xenografts (PDXs) can offer models which mimic the molecular and phenotypical features of patients more closely. Although these PDXs offer tumors that are more similar to the clinical situation, the mice used for these studies are not[40]. NOD-SCID-gamma mice are often used for these studies and lack a functional, T, B and NK cell compartment and the occurring macrophages and dendritic cells are defective. In addition, the complement system of these mice is also compromised, while neutrophils are still present and functional. Therefore, a comparison of IgA and IgG in these mice is not appropriate. This is the reason why we used syngeneic immune-competent mouse models, because the aforementioned effector cells and mechanisms are present.

Although EL4 cells do naturally express GD2 and are often used for anti-GD2 *in vivo* antibody models, they are not neuroblastoma cells[41–44]. Alternatively, to the EL4 *in vivo* models, NXS2 murine neuroblastoma cells are another model to study therapeutic antibodies against neuroblastoma *in vivo*[45]. Unfortunately, these cells are derived from the A/J mouse strain and an FcαRI-transgenic mouse on that background does not exist, so this model could not be used for our experiments.

Neuropathic pain is a complex side effect caused after ch14.18 administration. To assess induction of pain *in vivo* we used the von Frey method as was described previously for ch14.18 induced pain[11]. Other methods have been described to determine pain behavior in mice[46]. Ideally, antibody-induced pain should be assessed by more than a single type

of nociception assay. However, it remains unknown which methodology would be most relevant to quantify the pain mediated by ch14.18. This is an important question which requires further investigation.

In our pain studies, we dosed mice with five times the amount of IgA compared with IgG1 to adjust for the innate difference in half-life between these isotypes in mice. Although this complicates head-to-head *in vivo* comparisons, a similar neuronal exposure and serum concentration could be achieved. In humans, the *in vivo* half-life of IgA is approximately 1 week, which strikingly approximates that of ch14.18 in children with high-risk neuroblastoma[47]. Therefore, we do not envision the half-life of IgA to limit its clinical efficacy. In contrast, the difference in half-life between IgG and IgA in mice is much bigger, due to strong hepatic clearance and an artificially high binding of human IgG to mouse FcRn[17,48]. Several approaches have been undertaken to improve the half-life of IgA[49,50].

In summary, our studies stimulate further investigations on the use of IgA against neuroblastoma. IgA offers both improved neutrophil activation and the benefit of overcoming pain in one single molecule. Our preclinical data suggests that IgA could be dosed higher than IgG without side effects. Therefore, IgA should be further explored as a next-generation therapeutic for neuroblastoma

Acknowledgments

We would like to thank Eline van Diest for help with HPLC of antibodies.

Author contributions

MS, KK and HW contributed equally. NE and JL contributed equally.

ME conceptualized and designed the study, performed data acquisition, data interpretation and analysis and drafted/revised the manuscript. MS performed data acquisition, data interpretation and analysis and revised the manuscript. KK designed the study, performed data acquisition, data interpretation and analysis and drafted/revised the manuscript. HW performed data acquisition, data interpretation and analysis and revised the manuscript. MN performed data acquisition, data interpretation and analysis and drafted/revised the manuscript. MJ performed data acquisition, data interpretation and analysis and revised the manuscript. CC performed data acquisition, data interpretation and analysis and drafted/revised the manuscript. KB performed data interpretation and analysis and revised the manuscript. SN revised the manuscript. TV drafted/revised the manuscript. NE conceptualized and designed the study and drafted/revised the manuscript. JL conceptualized and designed the study, performed data interpretation and analysis, drafted/ revised the manuscript and is the guarantor of this manuscript.

Funding

ME and MJ are both funded by The Dutch cancer association: Grant number 7650. TV is supported by the German Research Organization (DFG Va124/9-1) and by intramural funding from the CAU. MS, KK, MN are funded by Villa Joep (project 17 IgA and anti-GD2). SN is funded by Villa Joep and de vrienden van het UMC Utrecht.

Competing interests

JL is co-founder of TigaTx and ME is employed by TigaTx.

Ethical approval

All animal experiments were performed in accordance with international guidelines and approved by the Dutch Central Authority for Scientific Procedures on Animals (CCD) and the local experimental animal welfare body (AVD115002016410 and AVD115002015323).

REFERENCES

1. Maris, J. M. Recent advances in neuroblastoma. *N. Engl. J. Med.* **362**, 2202–2211 (2010).

2. Yu, A. L. *et al.* Anti-GD2 antibody with GM-CSF, interleukin-2, and isotretinoin for neuroblastoma. *N. Engl. J. Med.* **363**, 1324–1334 (2010).

3. Armideo, E., Callahan, C. & Madonia, L. Immunotherapy for High-Risk Neuroblastoma: Management of Side Effects and Complications. *J. Adv. Pract. Oncol.* **8**, 44–55 (2017).

4. Bertolizio, G. *et al.* Multimodal Analgesic Plan for Children Undergoing Chimeric 14.18 Immunotherapy. *J. Pediatr. Hematol. Oncol.* **43**, e169–e172 (2021).

5. Gilman, A. L. *et al.* Phase I study of ch14.18 with granulocyte-macrophage colony-stimulating factor and interleukin-2 in children with neuroblastoma after autologous bone marrow transplantation or stem-cell rescue: a report from the Children's Oncology Group. *J. Clin. Oncol. Off. J. Am. Soc. Clin. Oncol.* **27**, 85–91 (2009).

6. Bruchelt, G. *et al.* Lysis of neuroblastoma cells by the ADCC-reaction: granulocytes of patients with chronic granulomatous disease are more effective than those of healthy donors. *Immunol. Lett.* **22**, 217–220 (1989).

7. Cheung, I. Y., Hsu, K. & Cheung, N. K. Activation of peripheral-blood granulocytes is strongly correlated with patient outcome after immunotherapy with anti-GD2 monoclonal antibody and granulocyte-macrophage colony-stimulating factor. *J. Clin. Oncol.* **30**, 426–432 (2012).

8. Mueller, B. M., Romerdahl, C. A., Gillies, S. D. & Reisfeld, R. A. Enhancement of antibody-dependent cytotoxicity with a chimeric anti-GD2 antibody. *J. Immunol.* **144**, 1382–1386 (1990).

9. Xiao, W. H., Yu, A. L. & Sorkin, L. S. Electrophysiological characteristics of primary afferent fibers after systemic administration of anti-GD2 ganglioside antibody. *Pain* **69**, 145–151 (1997).

10. Navid, F. *et al.* Phase I trial of a novel anti-GD2 monoclonal antibody, hu14.18K322A, designed to decrease toxicity in children with refractory or recurrent neuroblastoma. *J. Clin. Oncol.* **32**, 1445–1452 (2014).

11. Sorkin, L. S. *et al.* Anti-GD(2) with an FC point mutation reduces complement fixation and decreases antibody-induced allodynia. *Cancer Res.* **149**, 362–367 (2010).

12. de Sousa-Pereira, P. & Woof, J. M. IgA: Structure, Function, and Developability. *Antibodies (Basel, Switzerland)* **8**, (2019).

13. Brandsma, A. M. *et al.* Potent Fc Receptor Signaling by IgA Leads to Superior Killing of Cancer Cells by Neutrophils Compared to IgG. *Front. Immunol.* **10**, 704 (2019).

14. Brandsma, A. M. *et al.* Simultaneous Targeting of FcγRs and FcαRI Enhances Tumor Cell Killing. *Cancer Immunol. Res.* **3**, 1316–1324 (2015).

15. Willemen, H. L. D. M. *et al.* Identification of FAM173B as a protein methyltransferase promoting chronic pain. *PLoS Biol.* **16**, e2003452 (2018).

16. Chaplan, S. R., Bach, F. W., Pogrel, J. W., Chung, J. M. & Yaksh, T. L. Quantitative assessment of tactile allodynia in the rat paw. *J. Neurosci. Methods* **53**, 55–63 (1994).

17. Boross, P. *et al.* IgA EGFR antibodies mediate tumour killing in vivo. 1213–1226 (2013) doi:10.1002/emmm.201201929.

18. van Egmond, M. *et al.* Human immunoglobulin A receptor (FcalphaRI, CD89) function in transgenic mice requires both FcR gamma chain and CR3 (CD11b/CD18). *Blood* **93**, 4387–4394 (1999).

19. Furman, W. L. *et al.* A Phase II Trial of Hu14.18K322A in Combination with Induction Chemotherapy in Children with Newly Diagnosed High-Risk Neuroblastoma. *Clin. cancer Res. an Off. J. Am. Assoc. Cancer Res.* **25**, 6320–6328 (2019).

20. Li, J. *et al.* Membrane-Proximal Epitope Facilitates Efficient T Cell Synapse Formation by Anti-FcRH5/CD3 and Is a Requirement for Myeloma Cell Killing. *Cancer Cell* **31**, 383–395 (2017).

21. Anghelescu, D. L. *et al.* Comparison of pain outcomes between two anti-GD2 antibodies in patients with neuroblastoma. *Pediatr. Blood Cancer* **62**, 224–228 (2015).

22. Terme, M. *et al.* Chimeric antibody c.8B6 to O-acetyl-GD2 mediates the same efficient anti-neuroblastoma effects as therapeutic ch14.18 antibody to GD2 without antibody induced allodynia. *PLoS One* **9**, e87210 (2014).

23. Leusen, J. H. W. IgA as therapeutic antibody. *Mol. Immunol.* **68**, 35–39 (2015).

24. Unkeless, J. C., Shen, Z., Lin, C. W. & DeBeus, E. Function of human Fc gamma RIIA and Fc gamma RIIIB. *Semin. Immunol.* **7**, 37–44 (1995).

25. Derer, S. *et al.* Increasing FcγRIIa affinity of an FcγRIII-optimized anti-EGFR antibody restores neutrophil-mediated cytotoxicity. *MAbs* **6**, 409–421 (2014).

26. Herr, A. B., Ballister, E. R. & Bjorkman, P. J. Insights into IgA-mediated immune responses from the crystal structures of human FcalphaRI and its complex with IgA1-Fc. *Nature* **423**, 614–620 (2003).

27. Suzuki, H. *et al.* IgA nephropathy and IgA vasculitis with nephritis have a shared feature involving galactose-deficient IgA1-oriented pathogenesis. *Kidney Int.* **93**, 700–705 (2018).

28. Monteiro, R. C., Kubagawa, H. & Cooper, M. D. Cellular distribution, regulation, and biochemical nature of an Fc alpha receptor in humans. *J. Exp. Med.* **171**, 597–613 (1990).

29. van Egmond, M. *et al.* FcalphaRI-positive liver Kupffer cells: reappraisal of the function of immunoglobulin A in immunity. *Nat. Med.* **6**, 680–685 (2000).

30. Sibille, Y., Chatelain, B., Staquet, P., Delacroix, D. L. & Vaerman, J. P. IgA receptors on human alveolar macrophages. *Monogr. Allergy* **24**, 282–286 (1988).

31. Asgharzadeh, S. *et al.* Clinical significance of tumor-associated inflammatory cells in metastatic neuroblastoma. *J. Clin. Oncol.* **30**, 3525–3532 (2012).

32. Borrok, M. J. *et al.* Enhancement of antibody-dependent cell-mediated cytotoxicity by endowing IgG with FcαRI (CD89) binding. *MAbs* **7**, 743–751 (2015).

33. Lohse, S. *et al.* Characterization of a mutated IgA2 antibody of the m(1) allotype against the epidermal growth factor receptor for the recruitment of monocytes and macrophages. *J. Biol. Chem.* **287**, 25139–25150 (2012).

34. Nassin, M. L. *et al.* Immune Reconstitution Following Autologous Stem Cell Transplantation in Patients with High-Risk Neuroblastoma at the Time of Immunotherapy. *Biol. blood marrow Transplant. J. Am. Soc. Blood Marrow Transplant.* **24**, 452–459 (2018).

35. Szanto, C. L. *et al.* Immune Monitoring during Therapy Reveals Activitory and Regulatory Immune Responses in High-Risk Neuroblastoma. *Cancers (Basel).* **13**, (2021).

36. Batova, A., Kamps, A., Gillies, S. D., Reisfeld, R. A. & Yu, A. L. The Ch14.18-GM-CSF fusion protein is effective at mediating antibody-dependent cellular cytotoxicity and complement-dependent cytotoxicity in vitro. *Clin. Cancer Res.* **5**, 4259–63 (1999).

37. Choi, B. S. *et al.* Phase I trial of combined treatment with ch14.18 and R24 monoclonal antibodies and interleukin-2 for patients with melanoma or sarcoma. *Cancer Immunol. Immunother.* **55**, 761–774 (2006).

38. Ladenstein, R. *et al.* Ch14.18 antibody produced in CHO cells in relapsed or refractory Stage 4 neuroblastoma patients: a SIOPEN Phase 1 study. *MAbs* **5**, 801–809 (2013).

39. Ladenstein, R. *et al.* Interleukin 2 with anti-GD2 antibody ch14.18/CHO (dinutuximab beta) in patients with high-risk neuroblastoma (HR-NBL1/SIOPEN): a multicentre, randomised, phase 3 trial. *Lancet Oncol.* **19**, 1617–1629 (2018).

40. Braekeveldt, N. & Bexell, D. Patient-derived xenografts as preclinical neuroblastoma models. *Cell Tissue Res.* **372**, 233–243 (2018).

41. Vincent, M. *et al.* Tumor targeting of the IL-15 superagonist RLI by an anti-GD2 antibody strongly enhances its antitumor potency. *Int. J. cancer* **133**, 757–765 (2013).

42. Imai, M., Landen, C., Ohta, R., Cheung, N.-K. V & Tomlinson, S. Complement-mediated mechanisms in anti-GD2 monoclonal antibody therapy of murine metastatic cancer. *Cancer Res.* **65**, 10562–10568 (2005).

43. Kim, S.-K. *et al.* Impact of minimal tumor burden on antibody response to vaccination. *Cancer Immunol. Immunother.* **60**, 621–627 (2011).

44. Alvarez-Rueda, N. *et al.* A monoclonal antibody to O-acetyl-GD2 ganglioside and not to GD2 shows potent anti-tumor activity without peripheral nervous system cross-reactivity. *PLoS One* **6**, e25220 (2011).

45. Neal, Z. C. *et al.* NXS2 murine neuroblastomas express increased levels of MHC class I antigens upon recurrence following NK-dependent immunotherapy. *Cancer Immunol. Immunother.* **53**, 41–52 (2004).

46. Turner, P. V, Pang, D. S. & Lofgren, J. L. A Review of Pain Assessment Methods in Laboratory Rodents. *Comp. Med.* **69**, 451–467 (2019).

47. Desai, A. V *et al.* Pharmacokinetics of the chimeric anti-GD2 antibody, ch14.18, in children with high-risk neuroblastoma. *Cancer Chemother. Pharmacol.* **74**, 1047–1055 (2014).

48. Nilsen, J. *et al.* Human and mouse albumin bind their respective neonatal Fc receptors differently. *Sci. Rep.* **8**, 14648 (2018).

49. Mester, S. *et al.* Extended plasma half-life of albumin-binding domain fused human IgA upon pH-dependent albumin engagement of human FcRn in vitro and in vivo. *MAbs* **13**, 1893888 (2021).

50. van Tetering, G., Evers, M., Chan, C., Stip, M. & Leusen, J. Fc Engineering Strategies to Advance IgA Antibodies as Therapeutic Agents. *Antibodies (Basel, Switzerland)* **9**, (2020).

SUPPLEMENTAL INFORMATION

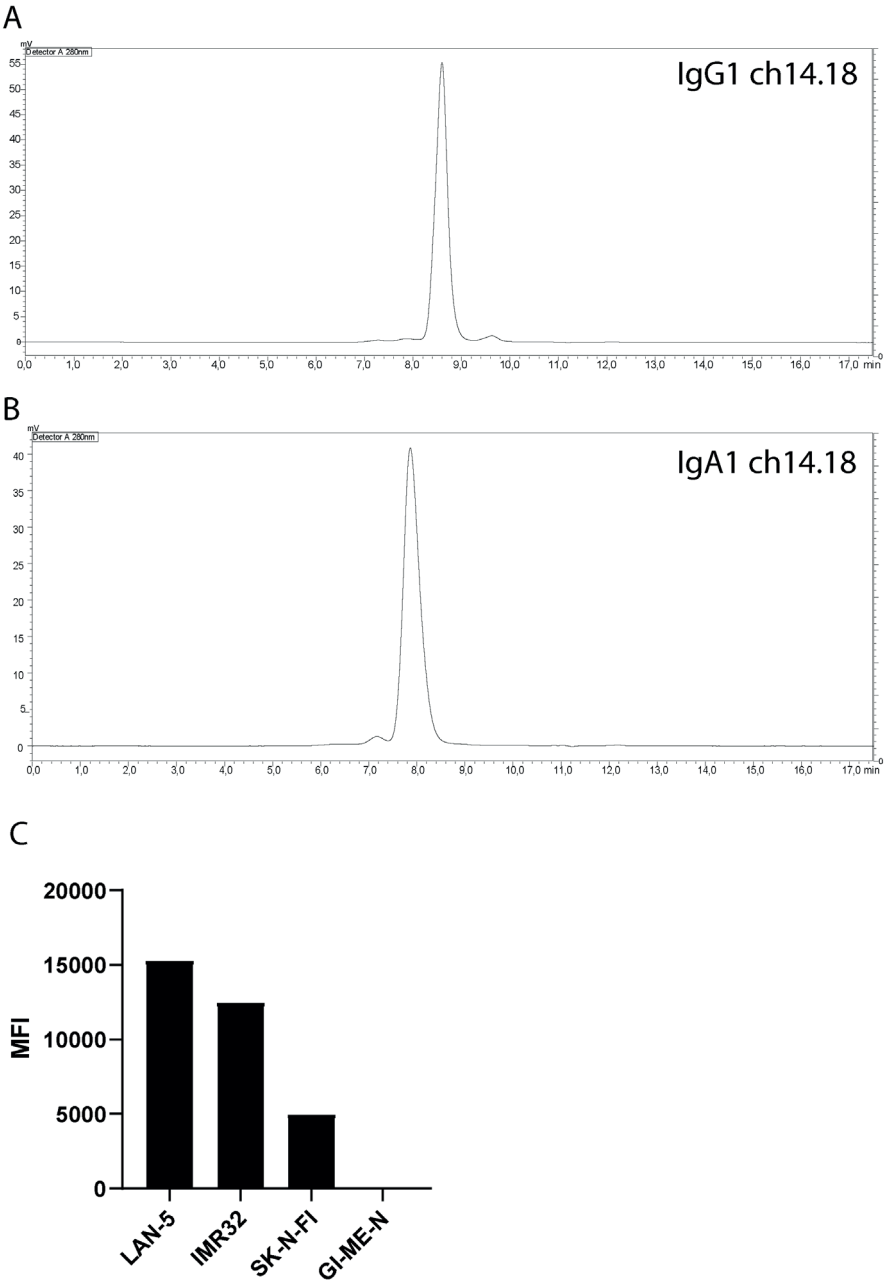

Figure S1 | HP-SEC analysis of IgA1 and IgG1 ch14.18. Purified antibodies were subjected to HP-SEC analysis. Both IgG1 ch14.18 (**A**) and IgA1 ch14.18 (**B**) were highly monomeric. Traces show absorbance at 280 nm. (**C**) IgA binding at 10 µg/ml to neuroblastoma cell lines measured by flow cytometry. MFI = median fluorescence intensity.

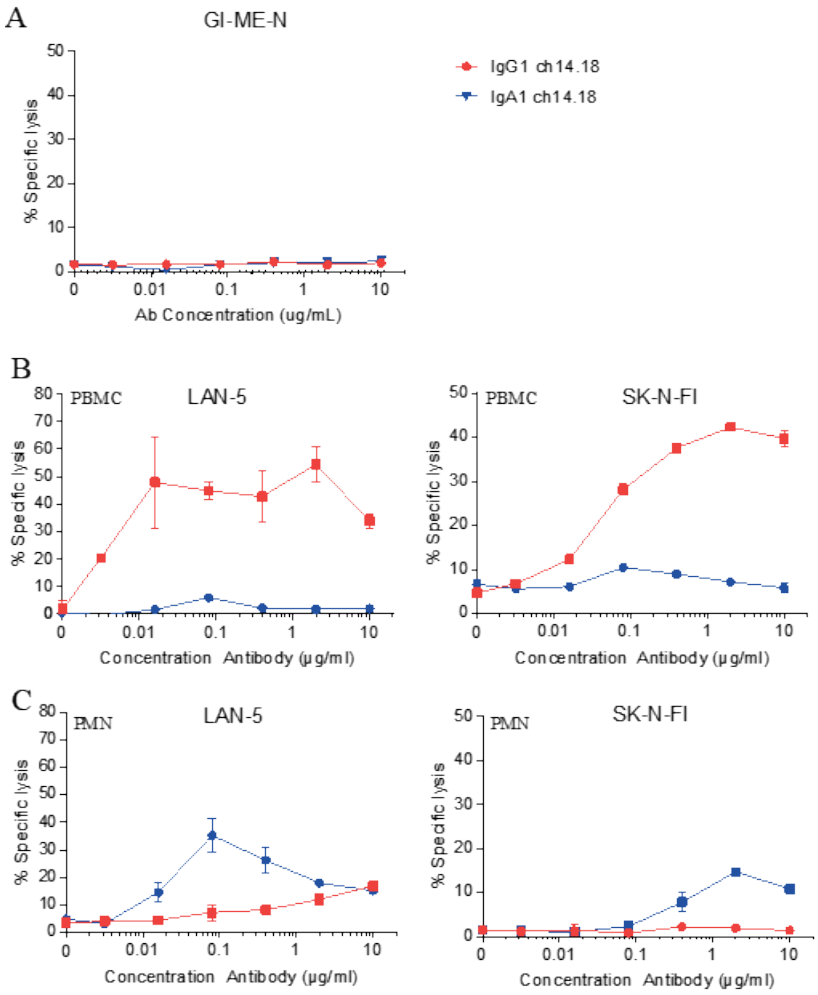
A
GI-ME-N
IgG1 ch14.18
IgA1 ch14.18
% Specific lysis
Ab Concentration (ug/mL)
B
PBMC
LAN-5
PBMC
SK-N-FI
% Specific lysis
Concentration Antibody (µg/ml)
C
PMN
LAN-5
PMN
SK-N-FI
% Specific lysis
Concentration Antibody (µg/ml)

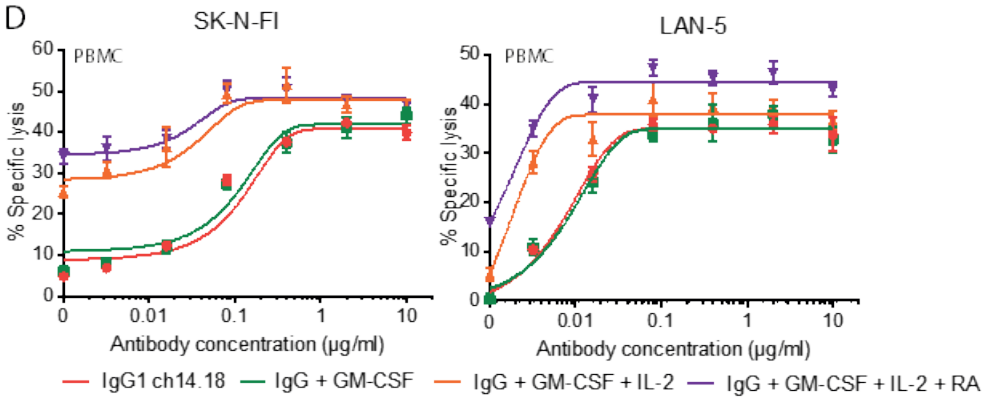
D
SK-N-FI
LAN-5
PBMC
% Specific lysis
Antibody concentration (µg/ml)
IgG1 ch14.18
IgG + GM-CSF
IgG + GM-CSF + IL-2
IgG + GM-CSF + IL-2 + RA

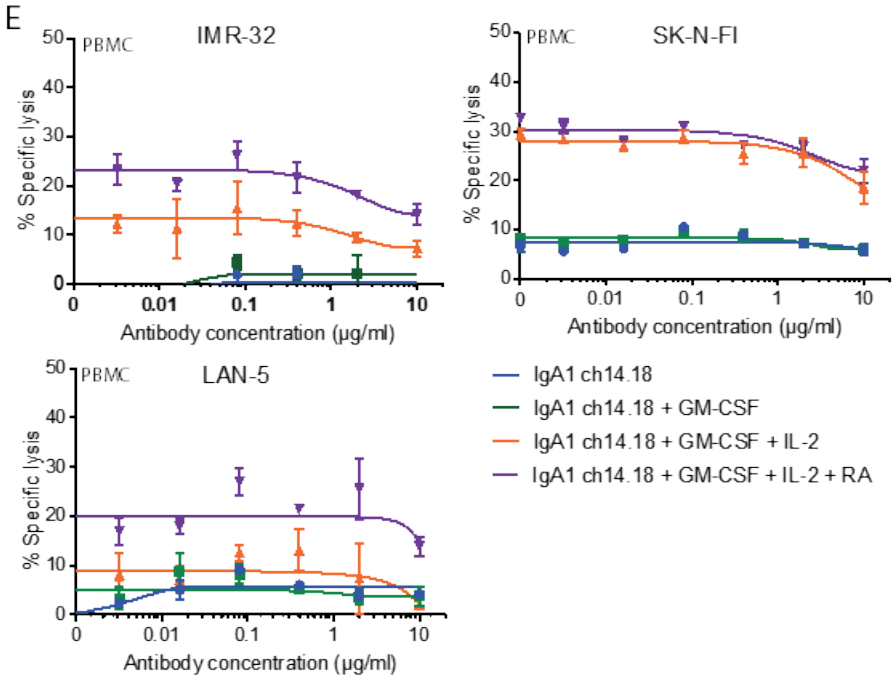
E
IMR-32
SK-N-FI
LAN-5
PBMC
% Specific lysis
Antibody concentration (µg/ml)
IgA1 ch14.18
IgA1 ch14.18 + GM-CSF
IgA1 ch14.18 + GM-CSF + IL-2
IgA1 ch14.18 + GM-CSF + IL-2 + RA

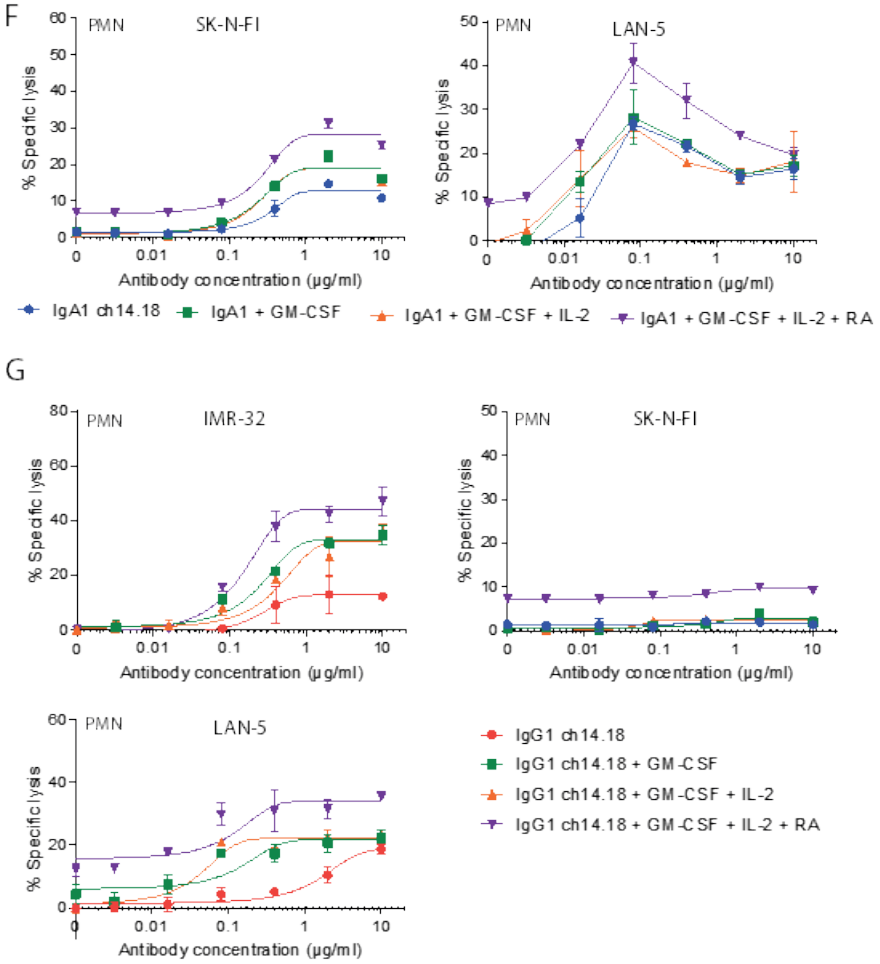

Figure S2 (**A**) ADCC assays with IgA1 and IgG1 ch14.18 on GIMEN cell line with leukocytes from peripheral blood as effector cells. (**B**) ADCC assays with IgG1 ch14.18 on neuroblastoma cell line SKNFI and LAN-5 cell line with isolated PBMCs (E:T ratio of 100:1) as effector cells. (**C**) ADCC assays with IgA1 ch14.18 on SKNFI and LAN-5 cell line with isolated neutrophils (E:T ratio of 40:1) as effector cells. (**D**) ADCC assays with IgG1 ch14.18 on SKNFI and LAN-5 cell lines with isolated PBMCs (E:T ratio of 100:1) as effector cells with or without co-treatment of GM-CSF, IL-2 and 11-*cis* retinoic acid. (**E**) ADCC assays with IgA1 ch14.18 on SKNFI and LAN-5 cell lines with isolated PBMCs (E:T ratio of 100:1) as effector cells with or without co-treatment of GM-CSF, IL-2 and 11-*cis* retinoic acid. (**F**) ADCC assays with IgA1 ch14.18 on SKNFI and LAN-5 cell line with isolated neutrophils (E:T ratio of 40:1) as effector cells with or without co-treatment of GM-CSF, IL-2 and 11-*cis* retinoic acid. (**G**) ADCC assays with IgG1 ch14.18 on neuroblastoma cell lines with isolated neutrophils (E:T ratio of 40:1) as effector cells with or without co-treatment of GM-CSF, IL-2 and 11-*cis* retinoic acid.

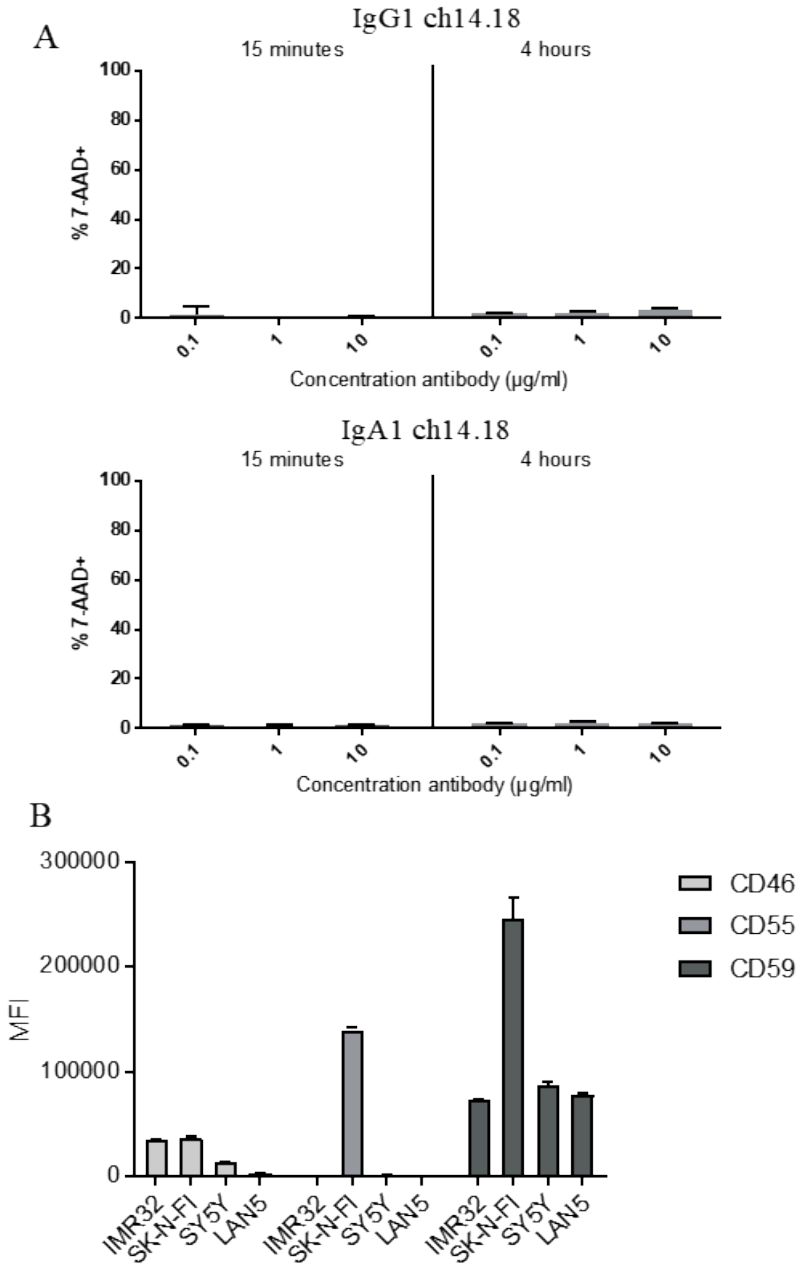

Figure S3 (**A**) CDC assays with SKNFI as target cells treated with IgG1 ch14.18 (Top graph) or IgA1 ch14.18 (Lower graph) for 15 minutes or 4 hours. (**B**) Complement regulatory protein expression on a panel of neuroblastoma cell lines.

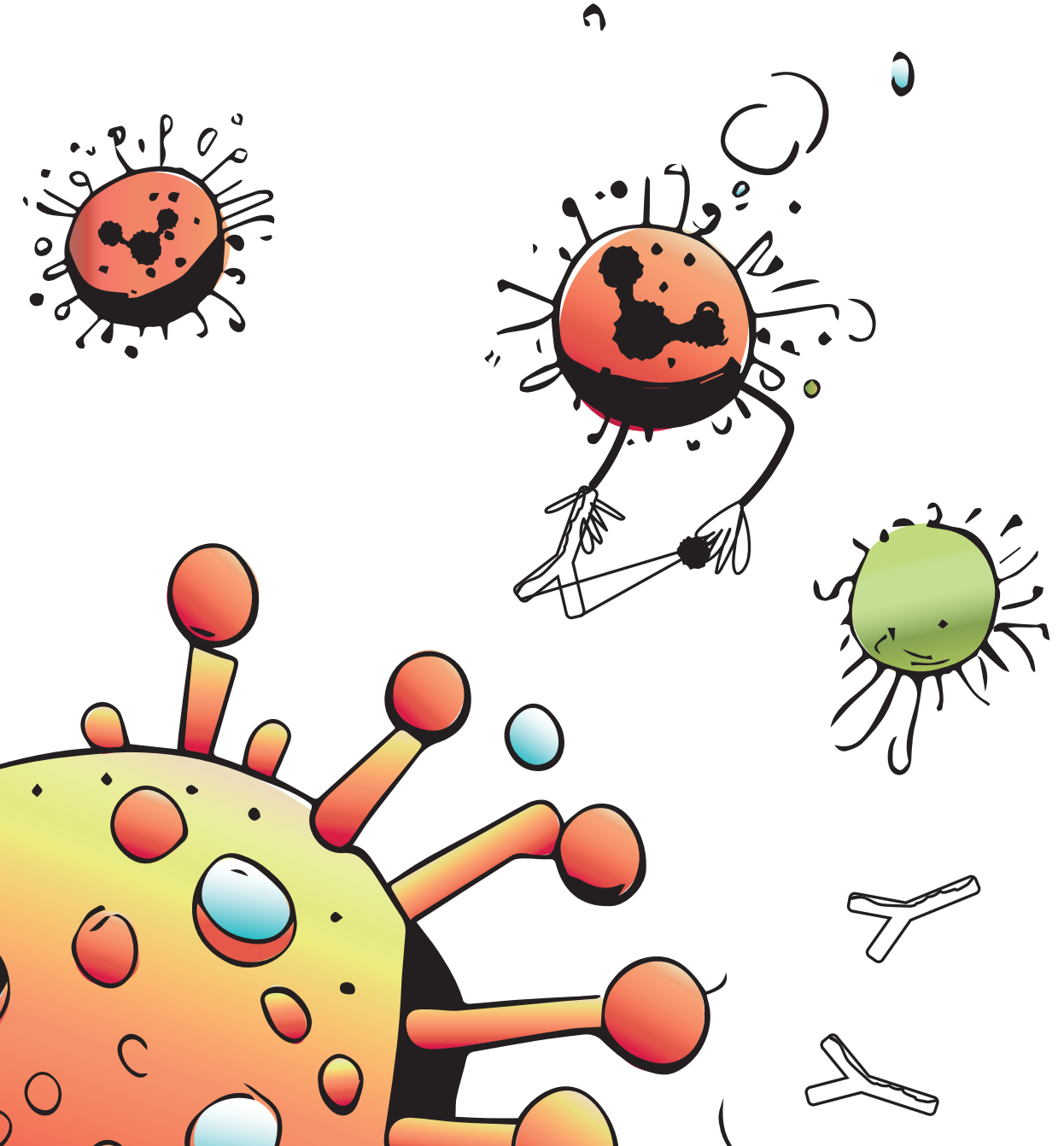

Chapter 6.

IgA antibody immunotherapy targeting GD2 is effective in preclinical neuroblastoma models

Marjolein C Stip[1], Mitchell Evers[1], Maaike Nederend[1], Chilam Chan[1], Karli R Reiding[2,3], Mirjam J Damen[2], Albert JR Heck[2,3], Sofia Koustoulidou[4], Ruud Ramakers[4], Gerard C Krijger[5], Remmert de Roos[5], Edouard Souteyrand[1], Annelisa M Cornel[1,6], Miranda P Dierselhuis[6], Marco Jansen[1], Mark de Boer[7], Thomas Valerius[8], Geert van Tetering[1], Jeanette HW Leusen[1], Friederike Meyer-Wentrup[6]

Affiliations

1. Center for Translational Immunology, UMC Utrecht, Utrecht, The Netherlands.
2. Biomolecular Mass Spectrometry and Proteomics, Bijvoet Center for Biomolecular Research and Utrecht Institute for Biopharmaceutical Sciences, University of Utrecht, Utrecht, The Netherlands.
3. Netherlands Proteomics Center, Utrecht, The Netherlands.
4. MIlabs, Utrecht, The Netherlands.
5. Radionuclide Pharmacy, UMC Utrecht, Utrecht, The Netherlands.
6. Princess Máxima Center for Pediatric Oncology, Utrecht, The Netherlands.
7. De Boer Biotech Consultancy B.V, Blaricum, The Netherlands.
8. Section for Stem Cell Transplantation and Immunotherapy, Department of Medicine II, University Hospital Schleswig Holstein, Kiel, Germany.

Published in Journal for Immunotherapy of Cancer, 2023

ABSTRACT

Background

Immunotherapy targeting GD2 is very effective against high-risk neuroblastoma, though administration of anti-GD2 antibodies induces severe and dose-limiting neuropathic pain by binding GD2-expressing sensory neurons. Previously, the IgG1 ch14.18 (dinutuximab) antibody was reformatted into the IgA1 isotype, which abolishes neuropathic pain and induces efficient neutrophil-mediated antibody-dependent cellular cytotoxicity (ADCC) via activation of the Fc alpha receptor (FcαRI/CD89).

Methods

To generate an antibody suitable for clinical application, we engineered an IgA molecule (named IgA3.0 ch14.18) with increased stability, mutated glycosylation sites and substituted free (reactive) cysteines. The following mutations were introduced: N45.2G and P124R (CH1 domain), C92S, N120T, I121L and T122S (CH2 domain) and a deletion of the tail piece P131-Y148 (CH3 domain). IgA3.0 ch14.18 was evaluated in binding assays and in ADCC and antibody-dependent cellular phagocytosis (ADCP) assays with human, neuroblastoma patient and non-human primate effector cells. We performed mass spectrometry analysis of *N*-glycans and evaluated the impact of altered glycosylation in IgA3.0 ch14.18 on antibody half-life by performing pharmacokinetic (PK) studies in mice injected intravenously with 5 mg/kg antibody solution. A dose escalation study was performed to determine *in vivo* efficacy of IgA3.0 ch14.18 in an intraperitoneal mouse model using 9464D-GD2 neuroblastoma cells as well as in a subcutaneous human xenograft model using IMR32 neuroblastoma cells. Binding assays and PK studies were compared with one-way analysis of variance (ANOVA), ADCC and ADCP assays and *in vivo* tumor outgrowth with two-way ANOVA followed by Tukey's post-hoc test.

Results

ADCC and ADCP assays showed that particularly neutrophils and macrophages from healthy donors, non-human primates and patients with neuroblastoma are able to kill neuroblastoma cells efficiently with IgA3.0 ch14.18. IgA3.0 ch14.18 contains a more favorable glycosylation pattern, corresponding to an increased antibody half-life in mice compared with IgA1 and IgA2. Furthermore, IgA3.0 ch14.18 penetrates neuroblastomas *in vivo* and halts tumor outgrowth in both 9464D-GD2 and IMR32 long-term tumor models.

Conclusions

IgA3.0 ch14.18 is a promising new therapy for neuroblastoma, showing (1) increased half-life compared to natural IgA antibodies, (2) increased protein stability enabling effortless production and purification, (3) potent CD89-mediated tumor killing *in vitro* by healthy

subjects and patients with neuroblastoma and (4) antitumor efficacy in long-term mouse neuroblastoma models.

Keywords

IgA, Neuroblastoma, Antibody immunotherapy, Tumor immunology, Neutrophils, Antibody glycosylation, GD-2

INTRODUCTION

Neuroblastoma is a pediatric tumor originating from dysregulation of the development of neural crest cells from the sympathoadrenal lineage[1]. A distinctive characteristic of neuroblastoma is the high heterogeneity in disease severity. Whereas the 5-year survival rate of low-risk and intermediate-risk neuroblastoma can be up to 95%, only 45% of patients with high-risk neuroblastoma live longer than 5 years. Currently, after an extensive treatment regimen containing chemotherapy, surgery, radiation therapy and hematopoietic stem cell transplantation[2,3], high-risk patients can receive immunotherapy. This immunotherapy encompasses anti-GD2 IgG antibodies, of which dinutuximab (IgG1 ch14.18), a chimeric antibody directed against the ganglioside GD2, was the first clinically

WHAT IS ALREADY KNOWN ON THIS TOPIC

- Previously, the IgG1 ch14.18 (dinutuximab) antibody was reformatted into the IgA1 isotype, which abolishes neuropathic pain and induces efficient neutrophil-mediated tumor killing. However, this IgA1 format was not ready for clinical application yet, since (1) the O-glycosylation in IgA1 antibodies is associated with the development of Berger's disease, (2) IgA1 has a short half-life and (3) IgA1 is not stable, which complicates production and purification of a clinical batch.

WHAT THIS STUDY ADDS

- In this study we developed a novel format of IgA anti-GD2 immunotherapy (IgA3.0 ch14.18), which is suitable for clinical application since it lacks O-glycosylation, has an increased half-life and enhanced stability.

HOW THIS STUDY MIGHT AFFECT RESEARCH, PRACTICE OR POLICY

- IgA3.0 ch14.18 could replace the current immunotherapy for neuroblastoma (IgG1 ch14.18, dinutuximab), since IgA3.0 ch14.18 is at least as efficacious and does not induce severe neuropathic pain.

approved antibody. Anti-GD2 immunotherapy is currently combined with granulocyte-macrophage colony-stimulating factor (GM-CSF, when available) and 13-cis retinoic acid[4]. The addition of immunotherapy to the treatment regimen improved event-free survival by 20%, but unfortunately induces severe neuropathic pain, probably evoked through complement activation on GD2-expressing sensory neurons[4]. Though long-term infusion strategies were introduced to reduce pain, still 37.7% of the patients experiences grade ≥3 neuropathic pain[5]. Anti-GD2 antibodies inhibit tumor growth mainly by inducing antibody-dependent cell-mediated cytotoxicity (ADCC). Natural killer (NK) cells are often considered to be the most important effector cells performing ADCC, but in neuroblastoma immunotherapy neutrophil-mediated ADCC plays a major role as well[6–10]. Additionally, anti-GD2 antibodies activate the complement system on GD2-expressing tumor cells via its C1q binding domain. This effector mechanism appears less important than ADCC though, since an Fc point mutation in the C1q domain (K322A) abolishing complement-dependant cytotoxicity does not reduce therapeutic efficacy in patients[11,12].

Previously, IgG1 ch14.18 (dinutuximab) was reformatted to the IgA1 isotype and it was observed that this abolishes neuropathic pain in a mouse model and induces efficient neutrophil-mediated ADCC through activation of the Fc alpha receptor (FcαRI, CD89)[13]. Human IgA antibodies are naturally occurring in two isotypes—IgA1 and IgA2—with three possible allotypes for IgA2 (IgA2m(1), IgA2m(2), and IgA2n)[14,15]. IgA1 and IgA2 molecules contain 2 and 4–5 *N*-glycosylation sites respectively, whereas IgG1 only has one[16]. This extensive glycosylation contributes to the short half-life of endogenous IgA (4–7 days)[17,18] compared with endogenous IgG (ranging from 11 to 30 days)[19] and monoclonal IgG1 antibodies (21 days)[20,21]. In mice, IgA half-life is even shorter (15 hours)[22]. First, this short half-life is caused by fast clearance of IgA in the distribution phase by the asialoglycoprotein receptor (ASGPR)[22–24], recognizing asialylated galactoses on proteins. Second, clearance can occur via the mannose receptor (CD206), which binds terminal mannose glycan structures[25,26]. Third, IgA antibodies lack a binding site for the neonatal Fc receptor (FcRn) and are thereby not recycled by FcRn, while IgG antibodies are[27–29].

To bring IgA ch14.18 to the clinic, we have taken several steps in this study to improve the format, which we named IgA3.0 (**Figure 1A**). The IgA3.0 format is a next generation engineered IgA molecule based on the IgA2.0 molecule as described and studied previously by Lohse and colleagues[30–32]. First of all, the IgA3.0 antibody is a derivative of the IgA2 isotype, since IgA1 antibodies can be critically involved in the development of IgA nephropathy (Berger's disease) mediated by aberrant *O*-glycosylation sites in the hinge region[33]. Second, we aimed to reduce antibody clearance by the ASGPR and mannose receptor, by reducing the absolute amount of glycosylation. To achieve this, N45.2G (CH1) and N120T (CH2) mutations were introduced at these *N*-glycosylation sites[32]. The penultimate glycosylation site (N135) was removed by a complete deletion of

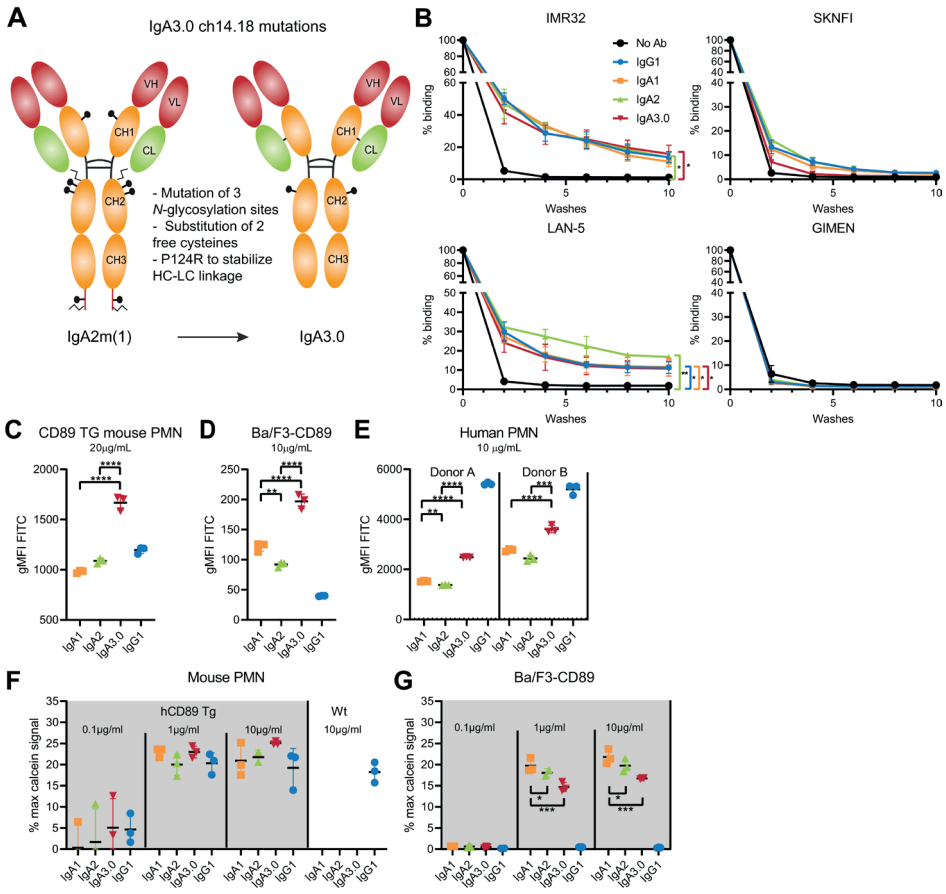

Figure 1 | Characterization of IgA3.0 ch14.18 target (Fab) and Fc binding. (**A**) Description of mutations in the IgA3.0 molecule compared to the original IgA2m(1) antibody[32]. (**B**) Target-specific binding was measured by incubating calcein-labeled neuroblastoma cells on antibody-coated plates and measuring residual fluorescence after several washes. Binding was compared using a Repeated Measurements one-way ANOVA. Monomeric Fc-binding to CD89 was assessed by incubating ch14.18 antibodies with (**C**) CD89 transgenic mouse neutrophils, (**D**) Ba/F3-CD89 cells or (**E**) human PMN followed by detection with FITC anti-human kappa antibody. Binding of complexed IgA to CD89 was assessed by incubating calcein-labeled (**F**) CD89 transgenic mouse neutrophils or (**G**) Ba/F3-CD89 cells on antibody-coated plates and measuring remaining fluorescence after 10 washes. Monomeric binding was compared using a one-way and complexed binding using a two-way ANOVA. Data as shown are mean±SD, $n = 3$ for all experiments. GD2 binding experiments were repeated five times, CD89 binding experiments were repeated twice. * = $p < 0.05$, **= $p < 0.01$, *** = $p < 0.001$ and **** = $p < 0.0001$. ANOVA, analysis of variance; FITC, fluorescein isothiocyanate; hCD89 Tg, human CD89 transgenic mice; PMN, polymorphonuclear leukocytes; Wt, wild type mice.

the tail piece, leaving only the glycosylation site at N20 in the CH2 domain. Since the tail piece is critically involved in dimerization of IgA[34], it was deleted to prevent aggregation. Third, the P124R mutation in the CH1 domain was introduced to stabilize the pairing of heavy chain (HC) and kappa light chain (κLC)[30] and free cysteines were substituted or removed by tail piece deletion. In this study, we first characterized the novel IgA3.0 ch14.18 antibody and compared it to the original IgG1 and unmodified IgA1 and IgA2

formats. We performed functional assays (ADCC and antibody-dependent cell-mediated phagocytosis (ADCP)) with effector cells from healthy donors, non-human primates and patients with neuroblastoma and compared the formats in pharmacokinetic (PK) studies, mass spectrometry and thermal stability tests. Next, we evaluated the efficacy of IgA3.0 ch14.18 in long-term preclinical neuroblastoma mouse models.

METHODS

Antibody design and production

Variable sequences of the ch14.18 HC and κLC were derived from Biologic License Application 125516 and cloned into expression vectors (pEE14.4) containing the κLC or HC of IgA1, IgA2m(1), IgA3.0 or IgG1. The IgA3.0 amino acid sequence is based on the IgA2m(1) sequence and contains the following mutations (according to ImMunoGeneTics (IMGT) unique numbering for C domain): in the CH1 domain N45.2G and P124R, in the CH2 domain C92S, N120T, I121L and T122S and in the CH3 domain a deletion of the tail piece P131-Y148. Subsequently, all antibody variants were produced by transient transfection of HEK293 Freestyle (HEK293F) cells with HC, κLC and pAdvantage (U47294; Promega) encoding vectors using 293fectin (Thermo Fisher). Additionally, IgG1 and IgA3.0 antibodies were produced in Expi-CHO-S (Chinese Hamster Ovarian) cells (using the Expi-CHO-S transfection kit) and in CHO-K1 cells (produced and purified by WuXi Biologics). In-house produced antibodies were isolated from filtered culture supernatants and purified by affinity and size-exclusion chromatography as described before[13].

Generation of fluorescently labeled antibodies

Antibodies were labeled with *N*-hydroxy-succimidyl-fluorescein isothiocyanate (NHS-FITC, Thermo Fisher) at room temperature (RT) for 2 hours while stirring. Unbound NHS-FITC and unlabeled antibody was removed by size-exclusion using Sephadex columns (NAP-5, GE Healthcare). AF594-labeled antibodies were generated using the Alexa Fluor 594 protein labeling kit (Thermo Fisher).

Cell culture

Human neuroblastoma cell lines were acquired from the American Type Culture Collection (ATCC) and cultured in Dulbecco's modified eagle medium (DMEM). Mouse 9464D neuroblastoma cells (derived from the National Institutes of Health) were a kind gift from Dr. Juliet Gray (University of Southampton) and were cultured in Roswell Park Memorial Institute (RPMI) medium. All neuroblastoma culture media were supplemented with HEPES, Glutamax, 10% heat-inactivated fetal calf serum (FCS, Bodinco), 100 U/mL penicillin-streptomycin (p/s, Gibco) and 2% non-essential amino acids (Thermo Fisher).

Ba/F3 and HEK293T cells were cultured in RPMI supplemented with 10% FCS and 1% p/s. Additionally, 0.1 ng/mL murine interleukin (IL)-3 (Immunotools) was added to Ba/F3 cultures. All cells were cultured at 37°C in a humidified incubator containing 5% CO_2. HEK293F and Expi-CHO-S cells were cultured in respectively FreeStyle-293 and ExpiCHO expression medium (Gibco) at 37°C in a humidified incubator with orbital shaker platform containing 8% CO_2. Cells were not cultured past 20 passages and they were tested every 6 weeks using a Mycoalert mycoplasma detection kit (Lonza). Authenticity of 9464D cells was confirmed by STR (short-tandem repeat) profiling.

Virus production and transductions

A bacterial stab containing the MP9956:SFG.GD3synthase-2A-GD2synthase (Addgene Plasmid #75013) DNA construct was expanded at 37°C in LB medium (MP Biomedicals) and DNA was purified using the NucleoBond Xtra Maxi kit (Macherey-Nagel). Next, 0.9 µg MP9956:SFG.GD3synthase-2A-GD2synthase construct, 0.1 µg of pCL-Ampho Retrovirus Packaging construct and 2.5 µL Fugene was added to 100 µL RPMI medium and complexed for 30 min at RT. For Luc2 transductions, 3 µg DNA constructs (pS-Luc2-T2A-GFP-P2A-BSD (transfer vector), pMDIg/p-pRRE, pRSV-REV pMD2-VSVg) and 1 mg/mL PEI (in 25 mM Hepes, pH 7.5, 150 mM NaCL) were added to 100 µL OptiMEM and complexed for 30 min at RT. For virus production, 3×10^5 adherent HEK293T cells in a 6-well plate were transfected with one of the DNA mixes. Virus supernatant was harvested after 48 hours and 72 hours. Forty per cent confluent 9464D or GIMEN cells were transduced with 3 mL virus supernatant containing 6 µg/mL polybrene (Sigma) and centrifuged for 2 hours at 1000 × g at 33 °C. GD2-expressing clones were selected after limiting dilutions by staining with AF594-labeled ch14.18 and subsequent flow cytometric analysis. Luc2-positive cells were positively selected by culturing in 10 µg/mL blasticidin (InvivoGen).

Target and CD89 binding assays

For assessment of target-specific binding, ch14.18 antibodies were coated overnight in carbonate-bicarbonate buffer (Sigma) at 4 °C on NUNC MaxiSorp 96-well plates (Thermo Fisher). After blocking with 1% bovine serum albumin (BSA, Roche) in phosphate-buffered saline (PBS), 1.5×10^5 cells/100 µL/well calcein-labeled neuroblastoma cells were added, centrifuged for 5 min at 300 rpm and incubated for 30–45 min at 37 °C and 5% CO_2. Thereafter, cells were washed 10 times and after every two washes fluorescence was measured on a Spectramax (excitation: 485 nm, emission: 527 nm).

For assessment of monomeric Fc binding, 1×10^5 Ba/F3-CD89 cells, murine bone marrow-derived neutrophils (C57BL/6, transgenic for human CD89) or human polymorphonuclear leukocytes (PMN) were incubated with a range of concentrations of ch14.18 variants for 45–60 min at 4 °C. After washing, samples were incubated with anti-human kappa FITC antibody for 30–45 min at RT, washed and analyzed using a FACSCanto II. For assessment

of complexed Fc binding, the target binding assay as described above was performed, but now Ba/F3-CD89 cells and murine neutrophils were used instead of neuroblastoma cells.

ADCC assays

^{51}Cr-release assays were performed as described previously[35]. In short, target cells were labeled with radioactive chromium-51 ($Na_2{}^{51}CrO_4$, PerkinElmer) and washed three times. Whole blood leukocytes (WBL) were isolated by incubating blood samples in water for 30 s to lyse erythrocytes, after which 10× PBS was added. PMN and peripheral blood mononuclear cells (PBMC) were isolated using Ficoll (GE Healthcare)/Histopaque 1119 (Sigma) density gradient centrifugation and subsequent erythrocyte lysis using red blood cell (RBC) Lysis Buffer (BioLegend). PMN and PBMC composition was determined using the antibody panel in **Supplemental Table 1 and 2** followed by analysis on the LSRFortessa (BD). Cynomolgus PMN were isolated similarly from cynomolgus blood samples collected at Covance, Germany. Mouse neutrophils were isolated from blood collected 4 days after subcutaneous (s.c.) injection of PEGylated granulocyte colony-stimulating factor (G-CSF, 20 µg/mouse). Murine neutrophils were isolated by performing erythrocyte lysis (BioLegend), followed by magnetic separation using anti-Ly-6G Microbeads (Miltenyi) according to manufacturer's instructions.

PBMC were added in a 100:1 effector-target (E:T) ratio and PMN or mouse neutrophils in a 40:1 ratio (ratios determined in previous studies[35]). Antibodies were added in concentrations as indicated per experiment. Assays were incubated for 4 hours at 37 °C in a humidified incubator containing 5% CO_2. Plates were centrifuged and supernatant was transferred to lumaplates (PerkinElmer) to assess radioactivity induced scintillation (in cpm) on a beta-gamma counter (PerkinElmer). Specific lysis was calculated using the formula: ((experimental cpm – basal cpm)/(maximal cpm – basal cpm))×100, with maximal lysis determined by incubating target cells with 1.25% triton and minimal lysis determined by chromium release of target cells in the absence of antibodies and effector cells.

Phagocytosis assays and confocal imaging

Human monocytes were isolated from PBMC using CD14 microbeads (Miltenyi) and cultured for 7–14 days in the presence of 20 ng/mL rhM-CSF (Gibco) or rhGM-CSF (Miltenyi). When indicated, macrophages were further polarized for 24 hours with 20 ng/mL IL-4 (Immunotools), 50 ng/mL interferon (IFN)-γ (Thermo Fisher) or 5 µM NECA (Santa Cruz).

Target cells were labeled with pHrodo-AM (Thermo Fisher) and macrophages with CellTrace Violet (CTV, Thermo Fisher), both according to manufacturer's instructions. Macrophages were added in a 1:2 E:T ratio and antibodies were added in indicated concentrations. After 3 hours, cells were detached using accutase (Sigma) and analyzed by flow cytometry (LSRFortessa).

Target cells (IMR32) were labeled with pHrodo-AM and seeded in an 8 well µ-slide (Ibidi) 4 days prior to cell imaging. Subsequently, 10 µg/mL FITC-labeled anti-GD2 antibodies and macrophage colony-stimulating factor (M-SCF) differentiated, CTV-labeled macrophages were added in a 1:2 E:T ratio. Images were taken using a Stellaris 5 confocal microscope (Leica), housed in a conditioned, temperature-controlled (37°C), humidified chamber containing 5% CO_2. Images were recorded using an HC PL APO 63x/1.40 OIL C immersion objective and analyzed using LAS X software (Leica).

Thermal shift assays

Volumes of 5 µL of 2.5 mg/mL antibody, 12.5 µL PBS and 7.5 µL 300× SYPRO orange (Invitrogen) were added in a 96-well PCR plate (BIOplastics). PCR plates were sealed with MicroAmp optical adhesive film (Thermo Fisher) and centrifuged to remove air. Plates were measured on a viiA7 Real-Time PCR system (Thermo Fisher) from 37 °C up to 99 °C with a ramp rate of 1 °C/min. Samples were excited at 490 nm and fluorescence was measured at 575 nm. Melting temperatures (Tm values) are calculated by transforming temperature values to log(10) followed by non-linear regression (agonist vs response – find EC50) on the transformed data.

Glycoprofiling by mass spectrometry

N-Glycosylation profiles on ch14.18 antibody variants were analyzed using mass spectrometry as specified in detail in the **Supplemental Methods**.

Animal experiments

Mice were housed and bred at Janvier Labs (France) and transported to the animal facility of the Utrecht University (GDL) at least 1 week prior to the experiment. Food and water were provided ad libitum and mice were housed in groups under a 12:12 light–dark cycle. Mice were sacrificed by cervical dislocation. Both male and female mice from C57BL/6JRj, BALB/cByJ (both Janvier) and NXG (NOD.*Cg-Prkdc*^{scid} *Il2rg*^{tm1Wjl}/SzJ, Charles River) strains were used with age ranging from 8 to 30 weeks. Human CD89 transgenic mice were generated as described before[36], subsequently backcrossed (15–40 generations) into C57BL/6JRj, BALB/cByJ and NXG strains and maintained hemizygously. Mice in experimental groups were randomized based on weight, age and cage, researchers were single-blinded and group size was calculated a priori with a power of 0.8.

PK studies and antibody concentration measurement in mouse serum by ELISA

Female Balb/c and male NSG mice were injected intravenously (i.v.) with 5 mg/kg antibody solution in PBS and blood was sampled from the submandibular vein at indicated time points. Samples were left to coagulate overnight in Eppendorf tubes at 4 °C. After centrifuging twice at 3000 × g, serum was collected and stored at −20 °C. MaxiSorp 96-

well plates were coated with 0.5 µg/mL polyclonal goat-IgG anti-human kappa (1:2000, SouthernBiotech) in PBS overnight at 4 °C. Next, plates were washed thrice with wash buffer (0.05% Tween20 in PBS) and blocked for 1 hour with 1% BSA in wash buffer. Serum samples and standards were diluted in PBS and incubated for 1.5 hours at RT. After washing thrice, polyclonal goat anti-human IgA/IgG-HRP (1:2000, SouthernBiotech) was added for 1 hour. After washing thrice again, plates were developed for 10 min with ABTS (Roche) and measured on a spectrophotometer (Bio-Rad) at 415 nm.

Mouse neuroblastoma models

IMR32 cells were diluted in a 1:1 mix of PBS and high concentration matrigel (Corning). CD89 transgenic female NSG mice were injected s.c. with 2.5×10^6 cells in 150 µL and tumor outgrowth was measured using a caliper (length × width × height) until tumor size reached 1500 mm^3. In indicated experiments, mice were treated intraperitoneally (i.p.) thrice a week (starting from day 5) with indicated doses of IgG1 ch14.18, IgA3.0 ch14.18 or PBS as a control.

For the immunocompetent model, CD89 transgenic male C57BL/6 mice were injected i.p. with 5×10^5 luc2-transduced 9464D-GD2 cells. From day 6 onward, mice were injected i.p. twice per week with PBS or indicated doses of IgA3.0 ch14.18. To quantify tumor outgrowth, mice were injected i.p. with 100 µl of 25 mg/mL luciferin (Promega). 10 min after injection, mice were subjected to bioluminescence imaging at autoexposure settings (PhotonImager, MIlabs).

Indium-111 labeling and SPECT/CT scans

IgG1 and IgA3.0 ch14.18 (500 µg, 1 mg/mL) were attached to a Bn-DTPA metal linker (Macrocyclics) and Bn-DTPA-antibodies were labeled with Indium-111 ($^{111}InCl_3$, activity of 370 MBq/mL, Mallinckrodt). Fractions containing ^{111}In-labeled antibody were collected. Purity was assessed by running samples with 0.1 M citrate buffer on an iTLC (instant Thin-Layer Chromatography) strip (Agilent) followed by radio-TLC scanning. Purity for both IgA3.0 and IgG1 was over 97% (**Supplemental Figure 4D**). CD89 transgenic NSG mice with s.c. IMR32 tumors (±1200 mm^3) were injected i.v. with either 1.6 MBq ^{111}In-labeled IgG1 or 3.2 MBq ^{111}In-labeled IgA3.0 ch14.18. After 24 hours and 48 hours single-photon emission computed tomography (SPECT)/CT scans were acquired as specified in the **Supplemental Methods**.

Mouse tissue collection and flow cytometric analysis

Peritoneal lavage was performed using 6 mL PBS containing 5 mM EDTA. Mouse tumors and spleens were carefully excised and collected in ice cold PBS. Mouse blood was collected in lithium-heparin tubes (Sarstedt) and erythrocyte lysis was performed twice at room temperature for 5 min. Tumors were cut and digested using the mouse tumor dissociation

kit from Miltenyi. Up to 1 g of tumor tissue was transferred to C tubes (Miltenyi) containing enzyme mix (DMEM culture medium, 100 µL Enzyme D, 50 µL Enzyme R, and 10 µL Enzyme A) and the 37C_m_TDK_1 program was run on a gentleMACS Octo Dissociator. Dissociated tumor cells and spleens were put through a 100 µm cell strainer and together with mouse blood stained (see **Supplemental Table 3**) for analysis on the LSRFortessa. Tumor and spleen opsonization and IgA3.0 Fc-binding on neutrophils was determined by staining with goat F(ab')2 anti-human IgA-PE (1:200, SouthernBiotech).

Statistics and software

Statistical analysis was conducted using GraphPad Prism software (V.9.3.0). Means are represented with SD values, unless specified otherwise. Specific statistical analyses are indicated per experiment. All analyses were two-tailed and when post-hoc testing was required, we applied Tukey's post-hoc test. Significance is indicated by * = $p < 0.05$, **= $p < 0.01$, *** = $p < 0.001$ and **** = $p < 0.0001$. Flow cytometry analysis was done in FlowJo (Tree Star).

RESULTS

Characterization of IgA3.0 ch14.18 target (Fab) and Fc binding

After production and purification of the antibody variants, we assessed their binding to endogenous GD2 by immobilizing the antibodies to a plate and allowing neuroblastoma cells with high (IMR32, Lan-5), low (SKNFI) and no (GIMEN) GD2 expression to bind (**Supplemental Figure 1A**). We chose this set-up instead of more conventional FACS-based assays, since it is less susceptible to variation induced by antibody internalization and GD2/antibody shedding. All antibody isotypes displayed similar binding to GD2, since neuroblastoma cells detached at similar rates on washing (**Figure 1B**). Neuroblastoma cells with higher GD2 expression (IMR32, Lan-5) detached slower than cells with low expression (SKNFI) and GD2-negative GIMEN cells did not bind to the antibody variants at all, indicating antibody binding is dependent on GD2 expression.

Next to target binding, we investigated Fc-mediated, monomeric (cytophilic) binding to CD89 by incubating CD89-expressing Ba/F3 cells, CD89 transgenic murine neutrophils and human PMN with the ch14.18 variants. Interestingly, at various concentrations IgA3.0 ch14.18 showed increased binding to CD89 on these three cell types compared with IgA1 and IgA2 (**Figure 1C–E**, **Supplemental Figure 1B–E**). IgG1 ch14.18 was taken along as a reference, but was not analyzed since binding is mediated by Fc gamma receptors (FcγRs). IgA variants did not bind to murine neutrophils from non-transgenic mice (**Supplemental Figure 1B**), indicating that binding is CD89-specific. We studied complexed IgA binding by incubating calcein-labeled murine neutrophils and Ba/F3-CD89 cells on plates coated

with antibody complexes. Though complexed IgA3.0 binding to Ba/F3-CD89 cells was slightly decreased compared with IgA1 and IgA2, no major differences in binding to CD89 transgenic neutrophils was observed (**Figure 1F, G**, **Supplemental Figure 1F–H**).

IgA3.0-mediated ADCC is similar to IgA1 and superior to IgA2

To study the influence of IgA3.0 mutations on ADCC induction, we performed ^{51}Cr release assays using multiple neuroblastoma cell lines with both low (SKNAS, SKNFI) and high (IMR32) GD2 expression (**Supplemental Figure 1A**). As expected, IgG1 ch14.18 induced more ADCC of SKNAS and IMR32 cells than IgA with PBMC as effector cells (**Figure 2A**), but all IgA variants induced better ADCC with PMN as effector cells (**Figure 2B**). Though no differences were observed between IgA variants when PBMC were used as effector cells, IgA1 and IgA3.0 outperform IgA2 in ADCC assays with PMN (**Figure 2B**), suggesting that the optimized IgA3.0 format improved ADCC. However, in WBL ADCC assays all ch14.18 antibodies performed similarly, only at lower antibody concentrations IgA1 and IgA3.0 performed slightly better than IgA2 (**Figure 2C**). ADCC induction was dependent on GD2-expression, since GD2-negative cell lines (9464D, GIMEN) were not lysed (**Supplemental Figure 2A**). In order to explore a non-human primate model for preclinical testing in the future, we measured CD89 expression and ADCC in cynomolgus monkeys (*Macaca fascicularis*). We found that cynomolgus monkeys express high levels of CD89 on granulocytes and lower levels on monocytes, corresponding to the human expression profile (**Figure 2D**). IgA3.0 ch14.18 induced killing of IMR32 cells by PMN from all cynomolgus donors tested and the percentage of tumor cell lysis was comparable to human PMN (**Figure 2E**, **Supplemental Figure 2B**).

Furthermore, we tested whether neuroblastoma patient-derived effector cells can kill IMR32 tumor cells with IgA3.0 ch14.18, since immune cells in cancer patients can be exhausted and/or dysfunctional. Interestingly, neuroblastoma patient-derived PMN killed IMR32 cells efficiently when stimulated with IgA3.0 ch14.18 (**Figure 2F**, **Supplemental Figure 2C**).

Figure 2 | IgA3.0-mediated ADCC is similar to IgA1 and superior to IgA2. Efficiency of antibodies in inducing ADCC against neuroblastoma target cells in ^{51}Cr-release assays with either (**A**) PBMC, (**B**) PMN or (**C**) WBL as effector cells. ADCCs were compared using two-way ANOVA. (**D**) Flow cytometry analysis of CD89 expression on cynomolgus leukocytes. (**E**) ^{51}Cr-release assays with cynomolgus PMN as effector cells against IMR32 cells. (**F**) ^{51}Cr-release assays with neuroblastoma patient PMN against IMR32 cells. Dotted line is the no antibody background. Means were compared using two-way ANOVA. (**G**) ^{51}Cr-release assays with neuroblastoma patient PBMC and healthy donor PBMC from three different donors/patients against IMR32 cells. Means were compared using a paired t-test. (**H**) PBMC and (**I**) PMN composition in healthy

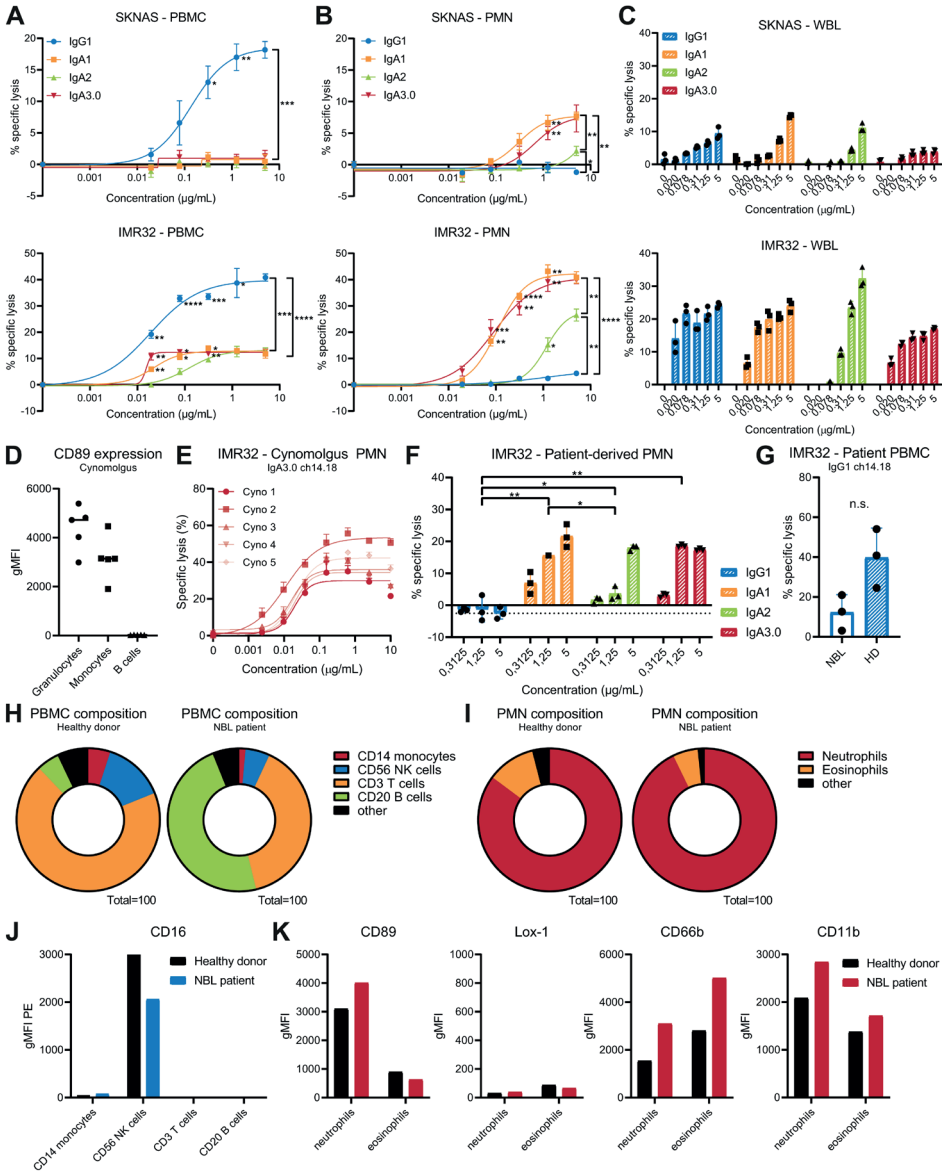

donor and neuroblastoma patient blood. (**J**) CD16 expression in healthy donor and neuroblastoma patient blood. (**K**) Expression of neutrophil activation markers in healthy donor and neuroblastoma patient blood. Data as shown are mean±SD, *n* = 3 for all ADCC assays. Healthy donor and patient ADCCs were performed three times and cynomolgus ADCC once. * = $p < 0.05$, **= $p < 0.01$, *** = $p < 0.001$ and **** = $p < 0.0001$. ADCC, antibody-dependent cell-mediated cytotoxicity; ANOVA, analysis of variance; gMFI, geometric mean fluorescence intensity; NBL, neuroblastoma; NK, natural killer; PBMC, peripheral blood mononuclear cells; PE, phycoerythrin; PMN, polymorphonuclear leukocytes; WBL, whole blood leukocytes.

However, IgG-mediated killing with patient PBMC was severely reduced compared with healthy donor PBMC, with both anti-GD2 and anti-EGFR IgG antibodies (**Figure 2G**, **Supplemental Figure 2C, D**). Relative quantification showed that NK cells and monocytes were reduced, though total number of PBMC and PMN was similar between patients with neuroblastoma and healthy donors (**Figure 2H, I**). Additionally, CD16 (FcγRIIIa) expression on NK cells was reduced in patients with neuroblastoma (**Figure 2J**). On the other hand, PMN from patients with neuroblastoma expressed higher levels of CD89, CD66b and CD11b (**Figure 2K**), reflecting a more activated phenotype. Therefore, considering the immune cell composition of patients with neuroblastoma, IgA3.0 ch14.18 immunotherapy might be favorable compared with IgG1 ch14.18.

IgA3.0 ch14.18 induces ADCP with both M0, M1 and immunosuppressive M2 mϕ

ADCP is considered a major mode of action for IgG antibodies, but since monocytes and macrophages also express CD89 to some extent[37], IgA-mediated phagocytosis could contribute to the antitumor effect of IgA3.0 ch14.18. Therefore we established ADCP assays in which macrophages (mϕ) become fluorescent after engulfing pHrodo-labeled target cells that are opsonized with anti-GD2 antibody (**Figure 3A**). As in ADCC, IgA1 and IgA3.0 antibodies slightly outperformed IgA2 in inducing phagocytosis of IMR32, Lan-5 and SKNAS cells by M-CSF differentiated M0 mϕ (**Figure 3B**). Again, IMR32 and Lan-5 cells are phagocytosed more efficiently compared with SKNAS cells. SKNFI cells were poorly phagocytosed on both IgG1 or IgA3.0 ch14.18 stimulation (**Supplemental Figure 2E**). Generally, cells that are susceptible to IgG-induced phagocytosis are susceptible to IgA-mediated phagocytosis as well.

In the tumor microenvironment however, often more activated and/or polarized macrophages are present. Therefore, we investigated whether M1 mϕ (induced by IFN-γ), M2a mϕ (induced by IL-4) and M2d mϕ (induced by an adenosine receptor agonist, NECA)[38] are able to kill neuroblastoma cells with IgA antibodies as well. Surprisingly, IgA3.0 ch14.18 induced relatively more tumor cell lysis with M2a mϕ and M2d mϕ compared with M1 mϕ (**Figure 3C**), though it must be noted that M2d mϕ were already killing more tumor cells spontaneously without antibody stimulation (0 µg/mL condition). Additionally, GM-CSF differentiated macrophages phagocytosed tumor cells less well compared with macrophages differentiated by M-CSF.

Protein stability is improved by IgA3.0 mutations

To evaluate whether IgA3.0 mutations have improved antibody stability, we performed Sypro Orange thermal shift assays. In general, the IgA3.0 isotype displays a higher melting temperature relative to all other isotypes as observed for antibodies targeting CD47, CD20, Her2/neu and EGFR (**Supplemental Figure 2F**). Similar to these antibodies against

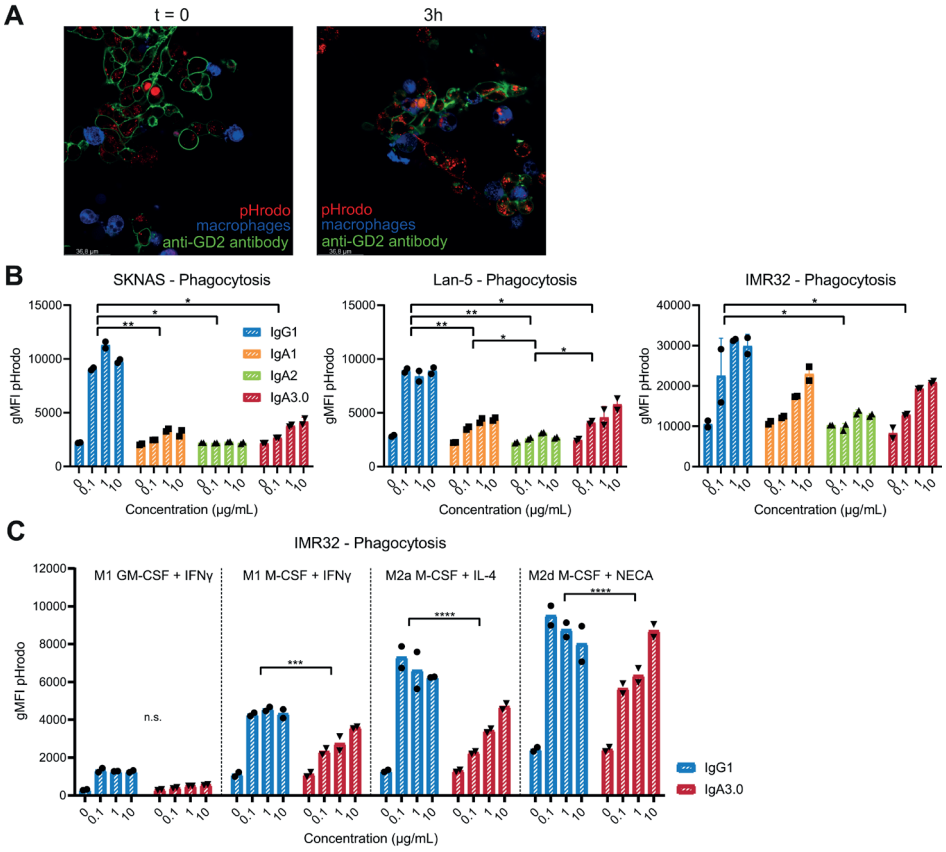

Figure 3 | IgA3.0 ch14.18 induces ADCP in both M0, M1 and M2 macrophages. (**A**) Confocal images before and after 3 hours incubation of pHrodo-labeled target cells with FITC-labeled anti-GD2 antibody and CTV-labeled macrophages. (**B**) The efficiency of antibodies in inducing phagocytosis against pHrodo-labeled human neuroblastoma target cells by M-CSF-differentiated, monocyte-derived macrophages as effector cells. (**C**) The efficiency of antibodies in inducing phagocytosis by macrophages polarized with IFN-γ, IL-4, or 5 µM NECA. Antibodies were compared using two-way ANOVA. Data as shown are means, $n = 2$. Phagocytosis assays were performed twice. * = $p < 0.05$, **= $p < 0.01$, *** = $p < 0.001$ and **** = $p < 0.0001$. ADCP, antibody-dependent cell-mediated phagocytosis; ANOVA, analysis of variance; CTV, CellTrace Violet; FITC, fluorescein isothiocyanate; GM-CSF, granulocyte-macrophage colony-stimulating factor, gMFI, geometric mean fluorescence intensity; IFN, interferon; IL, interleukin; M-CSF, macrophage colony-stimulating factor.

other targets, IgG1 ch14.18 started dissociating at lower temperatures compared with all ch14.18 IgA variants (**Figure 4A**). From all ch14.18 IgA variants, IgA2 has the lowest melting temperature (**Figure 4B**), although the difference is rather small. These results combined suggest that IgA3.0 mutations increase antibody stability, although of less significance in the ch14.18 format. Additionally, we investigated whether different production cell lines (HEK293F, ExpiCHO-S and CHO K1) influence protein stability. As no differences in Tm values were observed, the type of production cell did not impact antibody stability (**Figure 4B, C**).

N-glycosylation pattern on IgA3.0 ch14.18 is favorable for its half-life

We further characterized the IgA3.0 ch14.18 molecule by performing mass spectrometry to study the *N*-linked glycosylation profile. Mass spectrometry confirmed that *N*-linked glycosylation on IgA3.0 antibodies was silenced at all sites except for the N20 site in the CH2 domain and therefore IgA3.0 has less glycosylation in general compared with IgA1 and IgA2. As in IgG antibodies, most *N*-linked glycan structures present on the IgA variants were complex, diantennary glycans (**Figure 4D**, **Supplemental Figure 3**) except for the N135 site in the CH3 domain of IgA2, where some tri-antennary or tetra-antennary glycans were found as well. Core fucosylation is present on IgG1, IgA1 and IgA2 antibodies, but since core fucosylation is almost absent at the N20 site, IgA3.0 antibodies are practically devoid of core fucosylation (**Figure 4E**).

Interestingly, when comparing glycosylation at the N20 site between IgA2 and IgA3.0 produced in HEK293F cells, sialic acids are relatively increased in IgA3.0 (**Figure 4F, G**). However, the presence of terminal sialylation appears to be dependent on the production host cell line, since sialylation of IgA3.0 ch14.18 produced in CHO-K1 or Expi-CHO-S is not increased (**Figure 4H, I**). Since high levels of sialylation on IgA antibodies limit degradation via the ASGPR, this glycosylation pattern could be beneficial for the half-life of IgA3.0. Similarly, IgA3.0 ch14.18 produced in HEK293F contains less terminal mannose structures on N20 when compared with IgA2, but IgA3.0 ch14.18 produced in CHO-K1 or Expi-CHO-S systems have similar amounts of terminal mannoses (**Figure 4F and H**, **Supplemental Figure 3**). IgA antibodies with reduced uncapped mannoses could have a longer half-life as well, since proteins containing glycans with terminal mannoses are susceptible for scavenging via the mannose receptor. Overall, IgA3.0 mutations decrease the absolute amount of glycosylation and production of IgA3.0 ch14.18 in HEK293F cells results in a more mature glycosylation pattern containing less terminal mannose and galactose residues, rendering IgA3.0 ch14.18 less susceptible to degradation via glycan receptors.

IgA3.0 ch14.18 serum half-life is prolonged compared with IgA1 and IgA2

To assess whether this favorable glycosylation pattern indeed correlates with increased half-life *in vivo*, we performed PK studies in CD89 transgenic Balb/c and NSG mice. As described previously[39], we found that IgG ch14.18 has a shorter half-life in NSG mice compared with Balb/c mice (**Figure 5A, B**). However, half-lives of IgA antibody variants are similar between these two mouse strains (**Figure 5A, B**). Next, we focused on the distribution phase of IgA antibodies and observed that whereas IgA1 and IgA2 serum concentrations decline considerably in the first hour, IgA3.0 antibody concentrations remain high, similar to IgG1 (**Figure 5C**). The significantly higher cumulative antibody exposure of IgA3.0 (**Figure 5D**) can be attributed to this improved distribution phase, since no major changes in half-life values between IgA variants were observed in the elimination phase (**Figure 5A, B**). These PK data strongly support the hypothesis that the

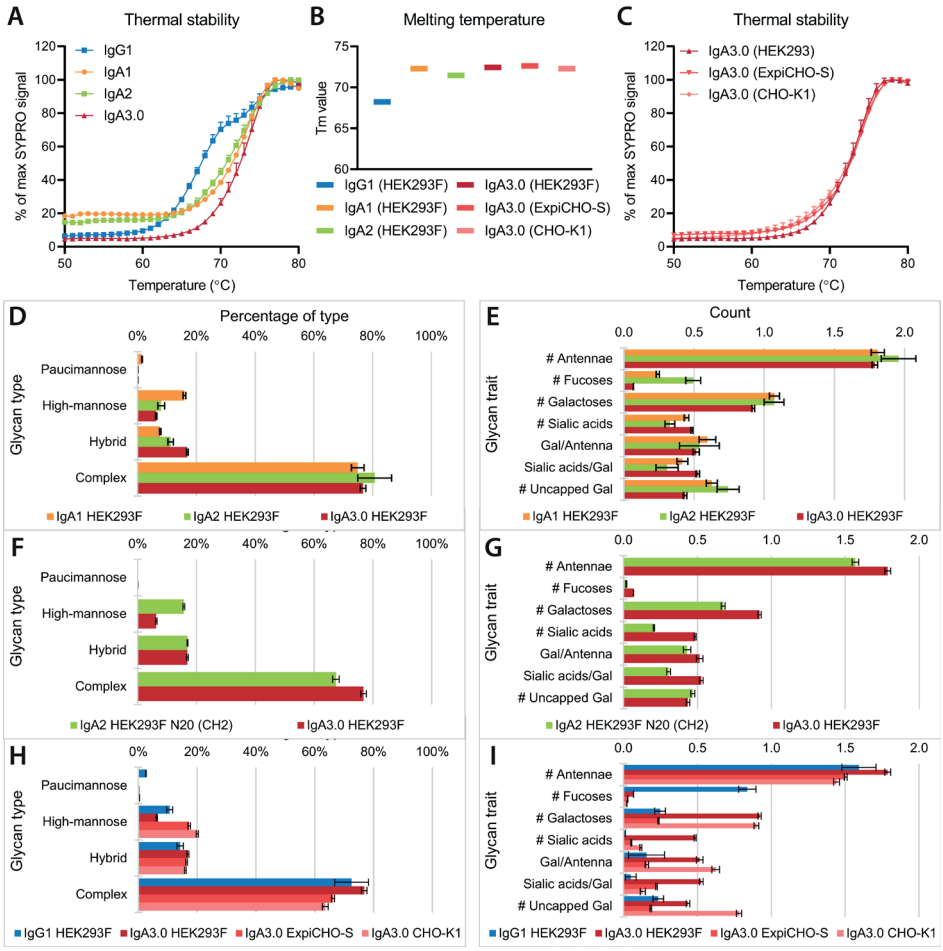

Figure 4 | IgA3.0 mutations result in improved stability and in a favorable glycosylation pattern. (**A**) Sypro orange thermal shift assays for ch14.18 antibody variants. (**B**) Tm values as calculated by transforming temperature values to log(10) followed by non-linear regression on the transformed data from thermal shift assays. (**C**) Sypro orange thermal shift assays for ch14.18 IgA3.0 produced in different production cell lines. Mass spectrometry analysis (**D**, **E**) of overall glycosylation in IgA ch14.18 variants, (**F**, **G**) of glycosylation at the N20 site in the CH2 domain and (**H**, **I**) of glycosylation of IgA3.0 ch14.18 produced in HEK293F, Expi-CHO-S or CHO-K1. Data as shown are mean±SD, *n* = 3.

decreased and improved glycosylation of IgA3.0 ch14.18 rescues the molecule from rapid glycan-mediated uptake via the ASGPR and mannose receptor.

Additionally, serum concentrations of IgA3.0 ch14.18 produced in Expi-CHO-S declined faster compared with HEK293F-produced IgA3.0, though not significantly. (**Figure 5E**) This corresponds with the favorable glycosylation pattern of HEK293F-produced IgA3.0 ch14.18 as described earlier. We have observed similar findings for IgA3.0 antibodies targeting for example CD20 (**Supplemental Figure 4A**), but it is possible that HEK293F cells are not the

best production cell line for IgA antibodies against all targets. These data underscore the importance of choosing the best cell line for clinical batch production.

IgA3.0 ch14.18 penetrates and opsonizes IMR32 neuroblastomas *in vivo*

Next, we studied the biodistribution of IgA3.0 ch14.18 *in vivo* to confirm that it is able to reach and opsonize neuroblastomas. First, we injected 25 mg/kg IgA3.0 ch14.18 to evaluate whether the small increase in monomeric binding observed *in vitro* would result in binding to CD89 *in vivo*. Neutrophils from CD89 transgenic mice did not have bound IgA3.0 ch14.18 after 24 hours (**Figure 5F**). However, when we incubated these neutrophils with IgA3.0 ch14.18 *ex vivo*, it was able to bind to CD89 on neutrophils.

Second, we injected CD89 transgenic IMR32 tumor-bearing mice with either IgA3.0 or IgG1 ch14.18 or an isotype control (palivizumab) and measured tumor opsonization after 24 hours. Both IgA3.0 and IgG1 ch14.18 opsonized neuroblastomas to a large extent, since tumor single cell suspensions spiked with antibodies *ex vivo* (at saturating concentrations) showed comparable levels of opsonization (**Supplemental Figure 4B**). Some background staining for the isotype control was observed, which is probably binding to non-tumor cells expressing FcγRs, since IgG antibodies bound splenocytes as well (**Supplemental Figure 4C**). To confirm our findings, we performed biodistribution SPECT/CT scans of mice injected with ^{111}-In-labeled IgG1 or IgA3.0 ch14.18. Both IgG1 and IgA3.0 specifically concentrated in the tumor and reached the tumor center (**Figure 5F, G, Supplemental Figure 4E**). Especially IgA3.0 was retained in the tumor after 48 hours. Additionally, high signal was observed in the liver (catabolism) and to a lower extent in the bladder (excretion). In conclusion, IgA3.0 ch14.18 reaches and opsonizes IMR32 neuroblastoma *in vivo* at least as well as IgG1 ch14.18.

Subcutaneous IMR32 tumor outgrowth in NSG mice is halted by IgA3.0 ch14.18

Assessing the *in vivo* efficacy of IgA antibodies can be rather challenging, since mice do not naturally express CD89 and mice have a much lower number of neutrophils (~10% of circulating leukocytes) compared with humans (~50–70%). On top of that, murine neutrophils are less effective in killing tumor cells upon IgA3.0 treatment compared to human neutrophils (**Figure 6A**). Nevertheless, we developed a human xenograft and an immunocompetent model in mice transgenically expressing human CD89 to evaluate the *in vivo* efficacy of IgA3.0 ch14.18.

To establish a human xenograft model, we injected CD89 transgenic NSG mice s.c. with IMR32 neuroblastoma cells and subsequently treated with different doses of IgA3.0 ch14.18 starting from day 5. Doses were based on literature describing dinutuximab treatment in mouse tumor models[40–42] and corrected for the difference in half-life. All doses showed

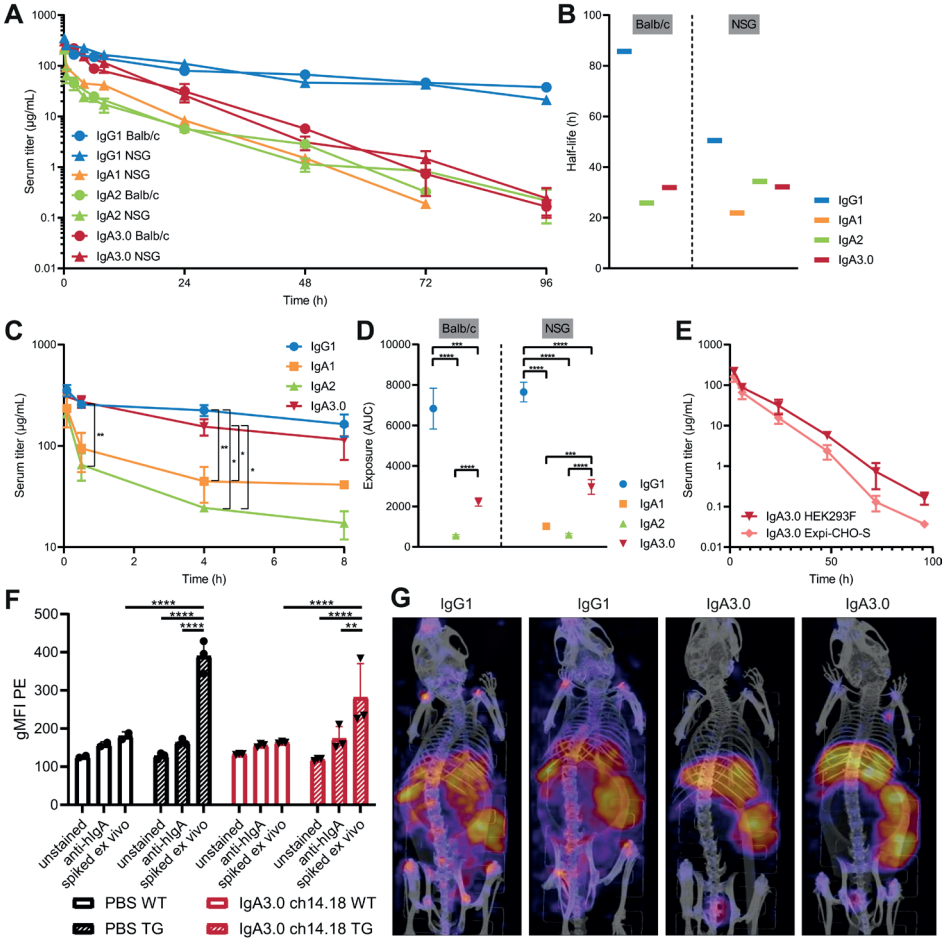

Figure 5 | PK and biodistribution studies for ch14.18 antibody isotypes in Balb/c and NSG mice. (**A**) CD89 transgenic Balb/c and NSG mice were injected i.v. with 5 mg/kg antibody solution (HEK293F produced) and serum concentrations over time were determined using ELISA on blood samples collected from the submandibular vein. (**B**) Half-life values calculated for the elimination phase (24–96 hour). (**C**) Distribution phase of the ch14.18 antibody variants. A mixed models analysis was performed on 30 min, 4-hour and 8-hour time points. (**D**) Cumulative antibody exposure in NSG mice as calculated by AUC analysis. AUC was compared with one-way ANOVA analysis. (**E**) Serum concentrations in Balb/c mice over time after i.v. injection of 5 mg/kg HEK293F produced and Expi-CHO-S produced IgA3.0 ch14.18. Means were compared using a mixed models analysis. (**F**) Circulating neutrophils of mice treated with PBS or 25 mg/kg IgA3.0 ch14.18 were isolated, incubated *ex vivo* with IgA3.0 ch14.18 and/or stained with PE-labeled anti-hIgA antibodies to determine monomeric CD89 binding. (**G**) Overlay of SPECT/CT scans displaying the biodistribution after 24 hours of ^{111}In-labeled ch14.18 antibodies in CD89 transgenic mice bearing an IMR32 neuroblastoma. Data as shown are mean±SD, $n = 3$ for PK studies and monomeric binding, $n = 2$ for biodistribution scans. * = $p < 0.05$, **= $p < 0.01$, *** = $p < 0.001$ and **** = $p < 0.0001$. AUC, area under the curve; CHO, Chinese hamster ovarian cells; gMFI, geometric mean fluorescence intensity; HEK293F cells, human293 cells; NSG, NOD SCID gamma mice; PBS, phosphate-buffered saline, PE, phycoerythrin; TG, transgenic mice; WT, wild type mice.

small treatment effects, but only the highest dose (60 mg/kg) of IgA3.0 ch14.18 impeded tumor growth (**Figure 6B**) and prolonged tumor-specific survival of IMR32 tumor-bearing mice significantly (**Figure 6C**). All doses resulted in tumor opsonization with IgA3.0 ch14.18 (**Figure 6D**) and additionally, IgA3.0 was binding to intratumoral neutrophils, which increased along with higher doses administered (**Figure 6E**). Detection of CD89 on tumor-infiltrating neutrophils and monocytes was reduced (**Supplemental Figure 5 and 6A**), suggesting Fc-mediated binding of IgA3.0 ch14.18 to CD89 hindering binding of detection antibodies.
Flow cytometric analysis of immune cells in the tumor microenvironment showed no attraction of myeloid cells, such as neutrophils, monocytes and macrophages after IgA3.0 therapy (**Figure 6F**). Blood and spleen immune cell composition remained unaffected as well (**Supplemental Figure 6B**). Considering the relative absence of myeloid cells and the small therapeutic effect it appears that murine myeloid cells are only minimally activated to kill tumor cells as was observed in *ex vivo* ADCC assays.
For comparing efficacy between IgA3.0 and IgG ch14.18, similar serum levels were used as comparators rather than equal dosages, because of the substantial difference in half-life. When we compared IgA3.0 ch14.18 efficacy with an historical experiment with similar IgG1 ch14.18 serum concentrations (**Supplemental Figure 6C**), we observed that IgA3.0 ch14.18 has a similar or slightly better therapeutic effect compared with IgG1 (**Supplemental Figure 6D–E**).

IgA3.0 ch14.18 is reducing outgrowth of intraperitoneal 9464D-GD2 tumors

Next, we assessed the efficacy of IgA3.0 ch14.18 in an immunocompetent mouse model by injecting luciferase-expressing 9464D-GD2 cells i.p. in CD89 expressing C57BL/6 mice. Treatment started on day 7 and mice received IgA3.0 ch14.18 or PBS treatment i.p. twice a week. Doses were decreased compared with the s.c. IMR32 model, since therapy is injected close to the tumor site. Both the 10 mg/kg and the 25 mg/kg dose induced a significant delay of tumor outgrowth and prolonged survival and even the lowest dose (2.5 mg/kg) exhibits a minor effect (**Figure 7A, B**, **Supplemental Figure 8A**). As in the IMR32 tumor model, there is no influx of myeloid cells in the peritoneum or tumor microenvironment after treatment (**Figure 7C, D**, **Supplemental Figure 7**). If there is any effect, we observed a minor reduction of neutrophils and monocytes compared with the PBS control tumors, but most differences are not significant. No changes of myeloid cells in the blood (**Supplemental Figure 8B**) or T cell numbers (**Supplemental Figure 8C**) were noticed either. However, similar to the IMR32 tumors, lower levels of CD89 were detected on intratumoral and intraperitoneal myeloid cells, especially in the highest dosed group (**Supplemental Figure 8D**). Combining these results, it is likely that the therapeutic efficacy of IgA3.0 ch14.18 is executed mostly by tumor-resident immune cells. This hypothesis would explain that IgA3.0 ch14.18 is more effective in the 9464D-GD2 model as well, since these tumors have roughly 10 times more myeloid cells infiltrating the tumor (**Figures 6F and 7C**).

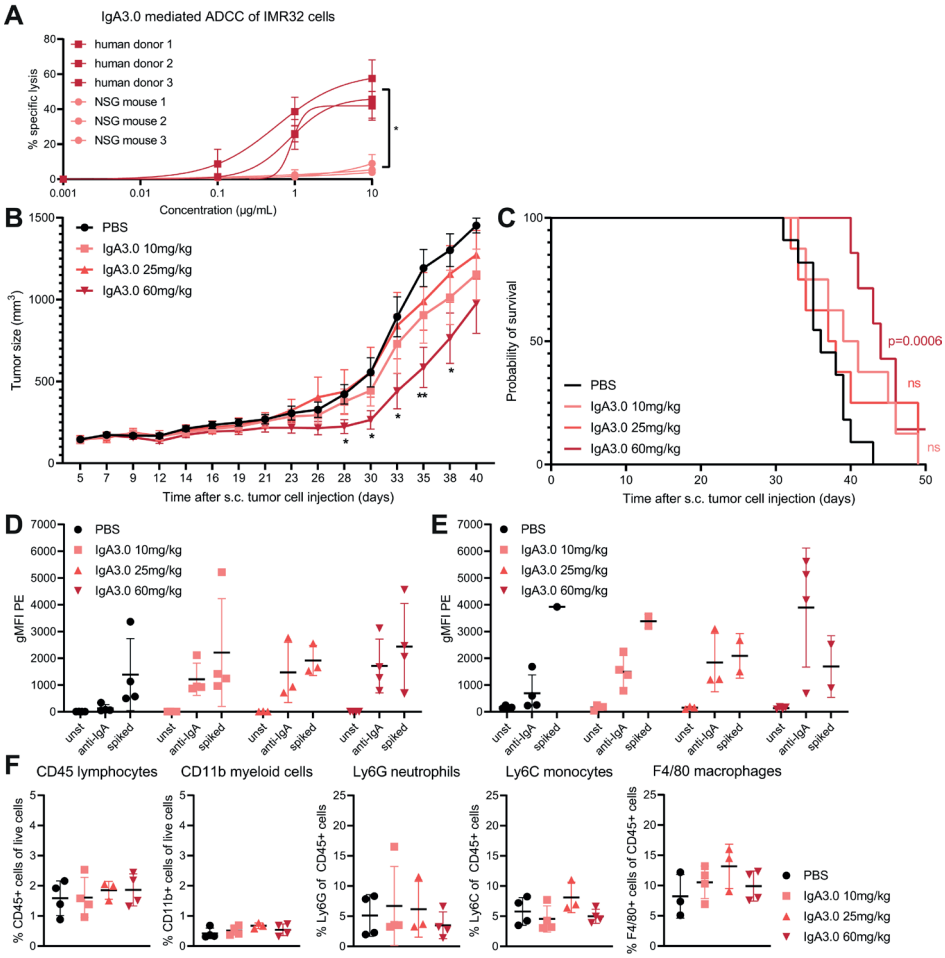

Figure 6 | Subcutaneous IMR32 tumor outgrowth in NSG mice is halted by IgA3.0 ch14.18. (**A**) Comparison of human PMN and NSG mouse neutrophil ADCC against neuroblastoma target cells with IgA3.0 ch14.18 in ^{51}Cr-release assays. (**B**) NSG mice were injected s.c. with 2.5×10^6 IMR32 tumor cells and treated thrice a week with PBS or increasing dosages of IgA3.0 ch14.18 from day 5 onwards. Tumor outgrowth was measured thrice a week until the end point (tumor size of 1500 mm^3) was reached. Tumor sizes were compared using a two-way ANOVA. Asterisks indicate significance compared with PBS control group. (**C**) Kaplan-Meier curve of tumor-specific survival. Log-rank test for trend p = 0.0092. PBS/ IgA3.0 10 mg/kg ns, PBS/IgA3.0 25 mg/kg ns, PBS 60 mg/kg p = 0.0006 (log-rank test). Single-cell suspensions derived from IMR32 tumors were stained with anti-hIgA antibodies to determine (**D**) tumor cell opsonization and (**E**) Fc-mediated, cytophilic binding to intratumoral neutrophils by flow cytometry. (**F**) Immune cell composition of IMR32 tumors at the end point was determined by flow cytometry on tumor single cell suspension. PBS and treatment groups were compared with one-way ANOVA. Data as shown are mean±SEM for tumor measurements and mean±SD for flow cytometry data. N = 10 for PBS, *n* = 8 for 10 mg/kg and 25 mg/kg and *n* = 7 for 60 mg/kg. * = $p < 0.05$, **= $p < 0.01$, *** = $p < 0.001$ and **** = $p < 0.0001$. ADCC, antibody-dependent cell-mediated cytotoxicity; ANOVA, analysis of variance; gMFI, geometric mean fluorescence intensity; NSG, NOD SCID gamma mice; PBS, phosphate-buffered saline; PE, phycoerythrin; PMN, polymorphonuclear leukocytes; s.c., subcutaneous; Unst, unstained.

Finally, as described for the IMR32 model, we compared efficacy of IgA3.0 ch14.18 with IgG1 ch14.18 in the 9464D-GD2 model historically, based on similar serum levels (**Supplemental Figure 8E**). Again, we observed that IgA3.0 ch14.18 has a similar or slightly better therapeutic effect compared with IgG1 (**Supplemental Figure 8F and G**).

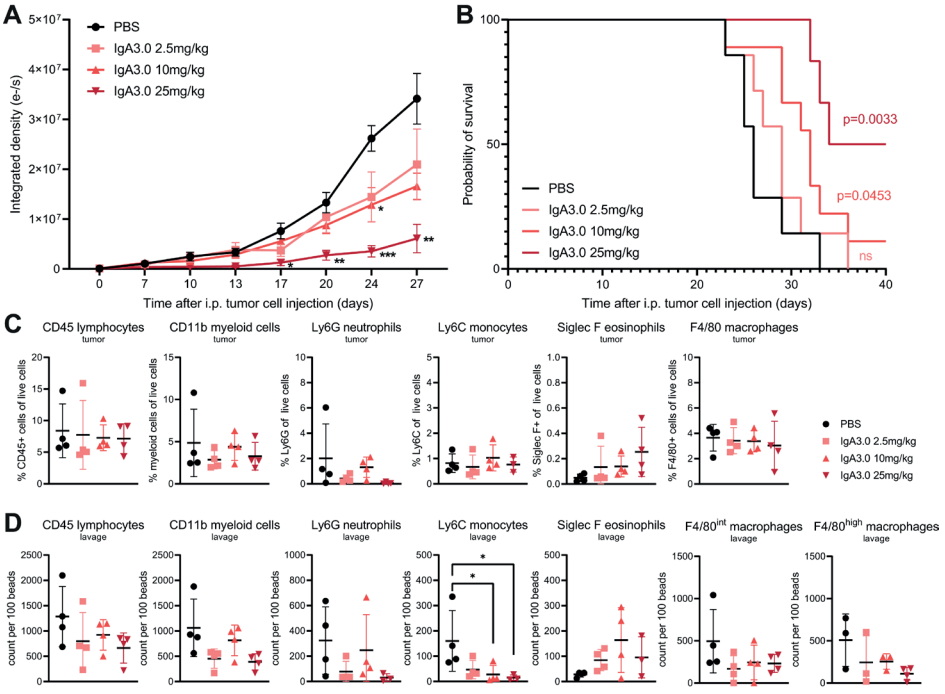

Figure 7 | IgA3.0 ch14.18 is reducing outgrowth of intraperitoneal 9464D-GD2 tumors. Tumor outgrowth was measured twice a week until the end point (BLI signal of 30×10^6) was reached. (**A**) Tumor sizes were compared using a mixed-effects model analysis. Asterisks indicate significance compared with PBS control group. (**B**) Kaplan-Meier curve of tumor-specific survival. Log-rank test for trend p = 0.0002. PBS/IgA3.0 2.5 mg/kg ns, PBS/IgA3.0 10 mg/kg 0.0453, PBS 25 mg/kg p = 0.0033 (log-rank test). Immune cell composition of (**C**) 9464D-GD2 tumors (**D**) and peritoneal lavage at the end point was determined by flow cytometry analysis on single cell suspension. PBS and treatment groups were compared with one-way ANOVA. Data as shown are mean±SEM for tumor measurements and mean±SD for flow cytometry data. N = 7 for PBS, *n* = 8 for 2.5 mg/kg, *n* = 9 for 10 mg/kg and *n* = 6 for 60 mg/kg. * = $p < 0.05$, **= $p < 0.01$, *** = $p < 0.001$ and **** = $p < 0.0001$. ANOVA, analysis of variance; BLI, bioluminescence imaging; i.p., intraperitoneal; PBS, phosphate-buffered saline.

DISCUSSION

Previously, it was demonstrated that IgA1 ch14.18 antibodies are effective against neuroblastoma models *in vitro* and *in vivo* and that they do not induce neuropathic pain, whereas IgG1 ch14.18 does[13]. In the present study, we engineered IgA2m(1) into a novel

IgA3.0 molecule, which resulted in similar binding and tumor killing, but increased stability, improved glycosylation and elongated half-life compared with non-engineered IgA1 and IgA2. Additionally, we have shown that IgA3.0 ch14.18 penetrates neuroblastomas *in vivo* and reduces tumor outgrowth in both immunocompetent and human xenograft mouse tumor models.

Though target binding is similar for all ch14.18 isotypes, we observed a small increase in monomeric binding of the IgA3.0 ch14.18 Fc tail to CD89. In the past, no increased Fc tail affinity was found for antibodies in the IgA2.0 format[32]. Since the only difference between the IgA2.0 and the IgA3.0 molecule is the removal of the tail piece, the tail piece (including the *N*-glycan N135) may be critically involved in binding to CD89. However, we did not compare Fc tail affinity of IgA2.0 and IgA3.0 head-to-head in the ch14.18 format. Hence these results should be validated in the future, for example, with surface plasmon resonance or ligand tracer experiments. Furthermore, it would be of interest to know whether only the glycan structure at N135 is responsible for differences in affinity for CD89, or whether the whole tail piece is involved. Göritzer and colleagues studied *N*-glycosylation by producing IgA antibodies in *Nicotiana benthamiana* plants lacking the enzymes synthesizing *N*-glycans[43,44]. They did not observe an increase in Fc tail affinity in IgA molecules lacking *N*-glycans, suggesting that deletion of the entire tail piece is responsible for the small increase in Fc affinity that we found. Increased Fc tail affinity could theoretically be problematic for tumor penetration of antibodies, by spontaneously binding to CD89-expressing leukocytes in the circulation. However, we observed clear opsonization and penetration of neuroblastomas in CD89 transgenic mice by IgA3.0 ch14.18 (**Figure 5F**). Since affinity for complexed IgA was not increased and monomeric antibody binding does not crosslink the FcαRI, we do not expect neutrophil activation in the circulation. No adverse effects were observed in mice exposed to high doses of IgA (60 mg/kg), suggesting that neutrophils are not randomly activated *in vivo*.
In the present study, we did observe that IgA3.0 ch14.18 increased PMN ADCC and macrophage ADCP (but not WBL ADCC) compared with IgA2, which could be caused by the changes in the glycosylation pattern and/or tail piece deletion. Additionally, we detected a modest increase in protein stability, which is known to be affected by glycosylation as well[45,46]. Currently, there is limited insight in the impact of glycosylation patterns on the Fc-mediated effector function of IgA antibodies, although it has been described that removal of sialic acids in IgA1 results in more pro-inflammatory function[47]. Therefore, it would be interesting to study the impact of each of the IgA3.0 mutations and accompanying changes in glycosylation on effector functions such as ADCC, neutrophil extracellular trap formation and cytokine secretion by neutrophils and other myeloid cells.
Next, we observed a more mature, terminally sialylated glycosylation pattern on IgA3.0 ch14.18 at the N20 site corresponding to an increased half-life in mice, but only when

antibodies were produced in HEK293F cells. However, currently CHO cells are the most opted choice for production of clinical-grade antibodies. If CHO cells will be used for clinical batch production, it should be considered to complement cells with, for example, glycan precursors[45] and/or enzymes responsible for the addition of terminal sialic acids[46]. It is important to note that mouse half-life experiments are informative, but not directly translational to humans, since the IgA system is different in among others antibody repertoire development, pIgR-mediated transport, colostral IgA content, hepatobiliary transport and function[48]. Next to that, human IgG1 has an artificially long half-life in mice, because of its higher affinity for mouse FcRn compared with mouse IgG[49]. Finally, the half-life of IgG antibodies can differ between mouse models[39,50] which we observed as well in this study, as IgG1 ch14.18 had a shorter half-life in NSG compared with Balb/c mice. It has been described that the relatively fast clearance of IgG antibodies in NSG mice is dependent on FcγR-mediated clearance by myeloid cells, which can be prevented by pretreatment with hIVIg (human intravenous immunoglobulin)[39]. We did not observe differences in half-life of IgA antibodies between NSG and Balb/c mice, implying that there is no similar mechanism for CD89-mediated clearance of IgA in NSG mice. For more accurate estimations of IgA3.0 ch14.18 half-life in humans, we could use cynomolgus monkeys. Since we found that they express CD89 similar to humans and perform comparable ADCC of IMR32 neuroblastoma cells, this animal model is well suitable for future toxicokinetic and PK studies.

Despite the short half-life of IgA in mice, we showed that IgA3.0 ch14.18 is significantly reducing tumor outgrowth in two different mouse tumor models, but it is not curative. It must be noted that both in our hands (**Supplemental Figure 6C–E**) and in other studies (among which two studies on which Food and Drug Administration/European Medicines Agency approval was based) the effect of IgG1 ch14.18 in treating mouse neuroblastoma models is modest and high doses of IgG1 ch14.18 are required for a treatment effect[40,51,52]. IgG1 ch14.18 is proven effective in patients, hence this suggests that mouse neuroblastoma models are relatively hard to treat with anti-GD2 antibody therapy and that the therapeutic potential is underestimated in mouse experiments. As we demonstrated, this may be explained by the fact that murine neutrophils do not kill neuroblastoma cells as well as human neutrophils (**Figure 6A**). Neutrophil numbers and activation might be lower due to the relative germ-free environment of laboratory mice as was demonstrated by Zhang *et al*[53]. However, neutrophils do seem to be required for the IgA3.0-mediated antitumor effect, since we observed a more significant treatment effect in the 9464D-GD2 tumors compared with the IMR32 tumors, which are relatively devoid of myeloid cells. Hence, it will be important to investigate whether neutrophil phenotype and/or tumor infiltration prior to treatment could be predictive for treatment response. Currently, we might also be underestimating the therapeutic potential of IgA3.0 relative to IgG1 ch14.18 in our *in vitro* assays, since most experiments were performed with healthy donor effector cells. However, we observed that patient PBMC (most importantly NK cells) are not as

functional as PBMC from healthy individuals, while patient neutrophils are still efficiently killing tumor cells with IgA3.0 ch14.18.

With this study, we brought IgA3.0 ch14.18 immunotherapy forward to clinical application. Even though IgA antibody therapy is hard to study in mice due to the lack of CD89, development of mouse anti-human antibodies in long-term syngeneic models and low numbers of rather 'lazy' neutrophils, we demonstrated clear antitumor effects *in vivo*. Furthermore, considering that IgG1 ch14.18 is inducing less ADCC by neuroblastoma patient-derived effector cells than by healthy donor effector cells, we might underestimate the efficacy of IgA3.0 ch14.18 in this study. Still some outstanding questions will need to be investigated before clinical studies are initiated. For example, currently anti-GD2 immunotherapy is combined with the administration of GM-CSF, which is proven to enhance macrophage-mediated and neutrophil-mediated killing of neuroblastoma cells[54]. However, currently GM-CSF is not available in Europe, but recently G-CSF was found to be a suitable alternative (*in vitro*)[55]. It will be paramount to determine if one or both of these cytokines will enhance IgA3.0 ch14.18 therapy, because this is a plausible combination considering the mechanism of action. Similarly, the combination of IgA3.0 ch14.18 with 13-*cis* retinoic acid should be validated[4]. Preliminary *in vitro* studies already showed that combining IgA ch14.18 with GM-CSF and 13-*cis* retinoic acid enhanced ADCC of neuroblastoma cells[13]. Other combination strategies, for example, with myeloid checkpoint inhibitors like anti-CD47 antibodies could further enhance IgA3.0 ch14.18 in the future. In summary, IgA3.0 ch14.18 is a promising new therapeutic candidate to treat neuroblastoma patients, showing (1) increased half-life compared with natural IgA antibodies, (2) increased protein stability, (3) potent CD89-mediated tumor killing *in vitro* by healthy subjects and patients with neuroblastoma and (4) anti-tumor efficacy in long-term mouse neuroblastoma models.

Acknowledgments

We would like to thank Juliet Gray for providing us with 9464D mouse neuroblastoma cells. We thank TigaTx for the use of their preclinical IgA3.0 ch14.18 antibody batch. We thank the flow cytometry facility and MDD in the UMCU for their service and the GDL laboratory for excellent care of the laboratory animals.

Author contributions

FM-W and JL contributed equally.

Conceptualization: MS, ME, JL and FM-W. Methodology: MS, MN, KRR, MJD, SK, RR. Formal Analysis: MS, ME, SK. Investigation: MS, MN, KRR, MJD, AJRH, SK, RR, GCK, RdR, ES, MJ, CC, GvT. Resources: AMC, MPD, GvT. Writing—Original Draft: MS, ME, GvT, JL, FM-W. Writing—Review and Editing: MS, ME, JL, FM-W, KRR, RR, AMC, MdB, TV and GvT. Supervision and Funding Acquisition: JL, FM-W. Guarantor: JL.

Funding

MS and MN are funded by Villa Joep (project 17 IgA and anti-GD2). ME and MJ are funded by The Dutch Cancer Association: Grant number 7650. ME, MN, ES, MJ, MdB, GvT and JL were (partially) employed by TigaTx. TV is supported by the German Research Organisation (DFG, KFO 5010). KRR, MJD and AJRH acknowledge support from the Netherlands Organization for Scientific Research (NWO) through the X-omics Road Map program (Project 184.034.019) and KRR further acknowledges NWO Veni grant VI.Veni.192.058.

Competing interests

JL and MdB are co-founder of TigaTx and JL is principal investigator on a research collaboration partially funded by TigaTx. ME, MN, ES, MJ and GvT were (partially) employed by TigaTx during the project and SK and RR are/were employed by Milabs. JL, GvT, ME are inventors on patent applications WO2019059771 and WO2020197400.

Ethical approval

This study involves human participants and was approved by UMC Utrecht 07–125/ OPrincess Maxima Center - General Biobank approval. Participants gave informed consent to participate in the study before taking part.

REFERENCES

1. Preter, K. De *et al.* Human fetal neuroblast and neuroblastoma transcriptome analysis confirms neuroblast origin and highlights neuroblastoma candidate genes. *Genome Biol.* **7**, R84-r84. (2006).

2. Matthay, K. K. *et al.* Treatment of high-risk neuroblastoma with intensive chemotherapy, radiotherapy, autologous bone marrow transplantation, and 13-cis-retinoic acid. Children's Cancer Group. *N. Engl. J. Med.* **341**, 1165–1173 (1999).

3. Berthold, F. *et al.* Myeloablative megatherapy with autologous stem-cell rescue versus oral maintenance chemotherapy as consolidation treatment in patients with high-risk neuroblastoma: a randomised controlled trial. *Lancet. Oncol.* **6**, 649–658 (2005).

4. Yu, A. L. *et al.* Anti-GD2 antibody with GM-CSF, interleukin-2, and isotretinoin for neuroblastoma. *N. Engl. J. Med.* **363**, 1324–1334 (2010).

5. Mueller, I. *et al.* Tolerability, response and outcome of high-risk neuroblastoma patients treated with long-term infusion of anti-GD(2) antibody ch14.18/CHO. *MAbs* **10**, 55–61 (2018).

6. Bruchelt, G. *et al.* Effects of granulocytes on human neuroblastoma cells measured by chemiluminescence and chromium-51 release assay. *J. Biolumin. Chemilumin.* **3**, 93–96 (1989).

7. Cheung, N. K. *et al.* FCGR2A polymorphism is correlated with clinical outcome after immunotherapy of neuroblastoma with anti-GD2 antibody and granulocyte macrophage colony-stimulating factor. *J. Clin. Oncol.* **24**, 2885–2890 (2006).

8. Cheung, I. Y., Hsu, K. & Cheung, N. K. Activation of peripheral-blood granulocytes is strongly correlated with patient outcome after immunotherapy with anti-GD2 monoclonal antibody and granulocyte-macrophage colony-stimulating factor. *J. Clin. Oncol.* **30**, 426–432 (2012).

9. Cheung, N. K. *et al.* Key role for myeloid cells: phase II results of anti-G(D2) antibody 3F8 plus granulocyte-macrophage colony-stimulating factor for chemoresistant osteomedullary neuroblastoma. *Int. J. cancer* **135**, 2199–2205 (2014).

10. Barker, E. *et al.* Effect of a chimeric anti-ganglioside GD2 antibody on cell-mediated lysis of human neuroblastoma cells. *Cancer Res.* **51**, 144–149 (1991).

11. Sorkin, L. S. *et al.* Anti-GD(2) with an FC point mutation reduces complement fixation and decreases antibody-induced allodynia. *Cancer Res.* **149**, 362–367 (2010).

12. Furman, W. L. *et al.* A Phase II Trial of Hu14.18K322A in Combination with Induction Chemotherapy in Children with Newly Diagnosed High-Risk Neuroblastoma. *Clin. cancer Res. an Off. J. Am. Assoc. Cancer Res.* **25**, 6320–6328 (2019).

13. Evers, M. *et al.* Anti-GD2 IgA kills tumors by neutrophils without antibody-associated pain in the preclinical treatment of high-risk neuroblastoma. *J. Immunother. cancer* **9**, (2021).

14. Tsuzukida, Y., Wang, C. C. & Putnam, F. W. Structure of the A2m(1) allotype of human IgA--a recombinant molecule. *Proc. Natl. Acad. Sci. U. S. A.* **76**, 1104–1108 (1979).

15. Chintalacharuvu, K. R., Raines, M. & Morrison, S. L. Divergence of human alpha-chain constant region gene sequences. A novel recombinant alpha 2 gene. *J. Immunol.* **152**, 5299–5304 (1994).

16. Mattu, T. S. *et al.* The glycosylation and structure of human serum IgA1, Fab, and Fc regions and the role of N-glycosylation on Fcα receptor interactions. *J. Biol. Chem.* **273**, 2260–2272 (1998).

17. Blaese, R. M., Strober, W., Levy, A. L. & Waldmann, T. A. Hypercatabolism of IgG, IgA, IgM, and albumin in the Wiskott-Aldrich syndrome. A unique disorder of serum protein metabolism. *J. Clin. Invest.* **50**, 2331–2338 (1971).

18. Delacroix, D. L. *et al.* Changes in size, subclass, and metabolic properties of serum immunoglobulin A in liver diseases and in other diseases with high serum immunoglobulin A. *J. Clin. Invest.* **71**, 358–367 (1983).

19. Ovacik, M. & Lin, K. Tutorial on Monoclonal Antibody Pharmacokinetics and Its Considerations in Early Development. *Clin. Transl. Sci.* **11**, 540–552 (2018).

20. Schiff, R. I. & Rudd, C. Alterations in the half-life and clearance of IgG during therapy with intravenous gamma-globulin in 16 patients with severe primary humoral immunodeficiency. *J. Clin. Immunol.* **6**, 256–264 (1986).

21. Mankarious, S. *et al.* The half-lives of IgG subclasses and specific antibodies in patients with primary immunodeficiency who are receiving intravenously administered immunoglobulin. *J. Lab. Clin. Med.* **112**, 634–640 (1988).

22. Boross, P. *et al.* IgA EGFR antibodies mediate tumour killing in vivo. 1213–1226 (2013) doi:10.1002/emmm.201201929.

23. Stockert, R. J., Kressner, M. S., Collins, J. C., Sternlieb, I. & Morell, A. G. IgA interaction with the asialoglycoprotein receptor. *Proc. Natl. Acad. Sci. U. S. A.* **79**, 6229–6231 (1982).

24. Rifai, A., Fadden, K., Morrison, S. L. & Chintalacharuvu, K. R. The N-glycans determine the differential blood clearance and hepatic uptake of human immunoglobulin (Ig)A1 and IgA2 isotypes. *J. Exp. Med.* **191**, 2171–2182 (2000).

25. Lee, S. J. *et al.* Mannose receptor-mediated regulation of serum glycoprotein homeostasis. *Science* **295**, 1898–1901 (2002).

26. Goetze, A. M. *et al.* High-mannose glycans on the Fc region of therapeutic IgG antibodies increase serum clearance in humans. *Glycobiology* **21**, 949–959 (2011).

27. BRAMBELL, F. W., HEMMINGS, W. A. & MORRIS, I. G. A THEORETICAL MODEL OF GAMMA-GLOBULIN CATABOLISM. *Nature* **203**, 1352–1354 (1964).

28. Junghans, R. P. & Anderson, C. L. The protection receptor for IgG catabolism is the beta2-microglobulin-containing neonatal intestinal transport receptor. *Proc. Natl. Acad. Sci. U. S. A.* **93**, 5512–5516 (1996).

29. Roopenian, D. C. & Akilesh, S. FcRn: the neonatal Fc receptor comes of age. *Nat. Rev. Immunol.* **7**, 715–725 (2007).

30. Lohse, S. *et al.* Characterization of a mutated IgA2 antibody of the m(1) allotype against the epidermal growth factor receptor for the recruitment of monocytes and macrophages. *J. Biol. Chem.* **287**, 25139–25150 (2012).

31. Brunke, C. *et al.* Effect of a tail piece cysteine deletion on biochemical and functional properties of an epidermal growth factor receptor-directed IgA2m(1) antibody. *MAbs* **5**, 936–945 (2013).

32. Lohse, S. *et al.* An Anti-EGFR IgA That Displays Improved Pharmacokinetics and Myeloid Effector Cell Engagement In Vivo. *Cancer Res.* **76**, 403–417 (2016).

33. Kiryluk, K. & Novak, J. The genetics and immunobiology of IgA nephropathy. *J. Clin. Invest.* **124**, 2325–2332 (2014).

34. Atkin, J. D., Pleass, R. J., Owens, R. J. & Woof, J. M. Mutagenesis of the human IgA1 heavy chain tailpiece that prevents dimer assembly. *J. Immunol.* **157**, 156–159 (1996).

35. Brandsma, A. M. *et al.* Simultaneous Targeting of FcγRs and FcαRI Enhances Tumor Cell Killing. *Cancer Immunol. Res.* **3**, 1316–1324 (2015).

36. van Egmond, M. *et al.* Human immunoglobulin A receptor (FcalphaRI, CD89) function in transgenic mice requires both FcR gamma chain and CR3 (CD11b/CD18). *Blood* **93**, 4387–4394 (1999).

37. Hamre, R., Farstad, I. N., Brandtzaeg, P. & Morton, H. C. Expression and modulation of the human immunoglobulin A Fc receptor (CD89) and the FcR gamma chain on myeloid cells in blood and tissue. *Scand. J. Immunol.* **57**, 506–516 (2003).

38. Huang, X., Li, Y., Fu, M. & Xin, H.-B. Polarizing Macrophages In Vitro. *Methods Mol. Biol.* **1784**, 119–126 (2018).

39. Li, F. *et al.* Mouse Strains Influence Clearance and Efficacy of Antibody and Antibody-Drug Conjugate Via Fc-FcγR Interaction. *Mol. Cancer Ther.* **18**, 780–787 (2019).

40. Mujoo, K., Cheresh, D. A., Yang, H. M. & Reisfeld, R. A. Disialoganglioside GD2 on human neuroblastoma cells: target antigen for monoclonal antibody-mediated cytolysis and suppression of tumor growth. *Cancer Res.* **47**, 1098–1104 (1987).

41. Zeng, Y. *et al.* Anti-neuroblastoma effect of ch14.18 antibody produced in CHO cells is mediated by NK-cells in mice. *Mol. Immunol.* **42**, 1311–1319 (2005).

42. Siebert, N. *et al.* Reduction of CD11b(+) myeloid suppressive cells augments anti-neuroblastoma immune response induced by the anti-GD(2) antibody ch14.18/CHO. *Oncoimmunology* **9**, 1836768 (2020).

43. Göritzer, K., Maresch, D., Altmann, F., Obinger, C. & Strasser, R. Exploring Site-Specific N-Glycosylation of HEK293 and Plant-Produced Human IgA Isotypes. *J. Proteome Res.* **16**, 2560–2570 (2017).

44. Göritzer, K. *et al.* Distinct Fcα receptor N-glycans modulate the binding affinity to immunoglobulin A (IgA) antibodies. *J. Biol. Chem.* **294**, 13995–14008 (2019).

45. Zhong, X. *et al.* Transient CHO expression platform for robust antibody production and its enhanced N-glycan sialylation on therapeutic glycoproteins. *Biotechnol. Prog.* **35**, e2724 (2019).

46. Rouwendal, G. J. *et al.* A comparison of anti-HER2 IgA and IgG1 in vivo efficacy is facilitated by high N-glycan sialylation of the IgA. *MAbs* **8**, 74–86 (2016).

47. Steffen, U. *et al.* IgA subclasses have different effector functions associated with distinct glycosylation profiles. *Nat. Commun.* **11**, 120 (2020).

48. Snoeck, V., Peters, I. R. & Cox, E. The IgA system: a comparison of structure and function in different species. *Vet. Res.* **37**, 455–467 (2006).

49. Andersen, J. T., Daba, M. B., Berntzen, G., Michaelsen, T. E. & Sandlie, I. Cross-species binding analyses of mouse and human neonatal Fc receptor show dramatic differences in immunoglobulin G and albumin binding. *J. Biol. Chem.* **285**, 4826–4836 (2010).

50. Sharma, S. K. *et al.* Fc-Mediated Anomalous Biodistribution of Therapeutic Antibodies in Immunodeficient Mouse Models. *Cancer Res.* **78**, 1820–1832 (2018).

51. Kendra, K., Malkovska, V., Allen, M., Guzman, J. & Albertini, M. In vivo binding and antitumor activity of Ch14.18. *J. Immunother.* **22**, 423–430 (1999).

52. Barry, W. E. *et al.* Activated Natural Killer Cells in Combination with Anti-GD2 Antibody Dinutuximab Improve Survival of Mice after Surgical Resection of Primary Neuroblastoma. *Clin. cancer Res. an Off. J. Am. Assoc. Cancer Res.* **25**, 325–333 (2019).

53. Zhang, D. *et al.* Neutrophil ageing is regulated by the microbiome. *Nature* **525**, 528–532 (2015).

54. Batova, A., Kamps, A., Gillies, S. D., Reisfeld, R. A. & Yu, A. L. The Ch14.18-GM-CSF fusion protein is effective at mediating antibody-dependent cellular cytotoxicity and complement-dependent cytotoxicity in vitro. *Clin. Cancer Res.* **5**, 4259–63 (1999).

55. Martinez Sanz, P. *et al.* G-CSF as a suitable alternative to GM-CSF to boost dinutuximab-mediated neutrophil cytotoxicity in neuroblastoma treatment. *J. Immunother. cancer* **9**, (2021).

SUPPLEMENTAL INFORMATION

Mass spectrometry for glycosylation analysis

Unless otherwise stated, chemicals and reagents were acquired from Sigma Aldrich. 10 µg of antibody was denatured, reduced and alkylated by adding 100 µL of 150 mM Tris, 5mM TCEP, 30 mM CAA, 1% SDC, at pH 8,5. Next, 100 ng GluC (Roche) was added and the sample was incubated at 37 °C for 4 h. Hereafter, 100 ng of trypsin was added and the sample was incubated overnight at 37 °C. The samples where then acidified by adding TFA to a concentration of 0.5%, causing SDC to precipitate, followed by solid phase extraction (SPE) using an Oasis HBL µ-elution plate (Waters Chromatography). After SPE, the samples where dried with a vacuum centrifuge. Subsequently the sample was reconstituted in 2% FA.

Samples were analyzed on a Fusion Lumos mass spectrometer (ThermoFischer) connected to a UHPLC 3000 system (ThermoFischer). Approximately 100 ng of reconstituted peptides were trapped on a precolumn and then separated on a 50 cm x 75 µm Poroshell EC-C18 analytical column (2.7 µm) temperature controlled at 40 °C. Solvent A consisted of 0.1% formic acid, solvent B of 0.1% formic acid in 80% acetonitrile. Trapping was performed for 2 min in 9% solvent B. Peptides were separated by a 40 min gradient of 9–44% buffer B followed by 44–99% B in 4 min, 99% B for 10 min. MS data were obtained in data-dependent acquisition mode with three separate fragmentation modes: higher-energy collisional dissociation (HCD), HCD-product-dependent stepping collision energy HCD (HCD-pd-sHCD) and HCD-product-dependent electron-transfer/higher-energy collision dissociation (HCD-pd-EtHCD). For all three methods, full scans were acquired in the *m/z* range of 350-2000 at a resolution of 120,000 (at *m/z* 400) with AGC target $3*10^6$. In the runs the most intense precursor ions were selected for HCD fragmentation performed at a normalized collision energy (NCE) of 29%, after accumulation to target value of $1*10^5$. MS/MS acquisition was performed at a resolution of 60,000, recording within an *m/z* window from 120-4000. Product-dependent fragmentation methods were initiated when at least three of the following ions (± 20 ppm) were detected from the preceding HCD scan: 127.0390, 138.0550, 145.0495, 163.0601, 168.0655, 186.0761, 204.0867, 243.0264, 274.0921, 292.1027, 366.1395, 405.0793, 407.1660, 512.1974, or 657.2349. HCD-pd-sHCD was performed with NCEs at 10%, 25% and 40%, whereas HCD-pd-EThcD made use of supplemental activation at 25%.

The MS data were searched using Byonic v4.1.10 (Protein Metrics Inc), with a fully specific search for C-terminal cleavage at Arg, Lys, Glu and Asp, with a maximum of three missed cleavages. Precursor mass tolerance was set at 10 ppm and fragment mass tolerance (both HCD and EThcD) at 20 ppm. Cys carbamidomethylation was set as fixed modification, with variable modifications including oxidation, pyroglutamic acid formation and phosphorylation, in addition to 279 potential *N*-glycan species. Detections were filtered for having a Byonic score ≥150 and a |log| peptide probability score ≥1.5. Subsequently,

we used Skyline (21.1.0.146) to integrate the MS1 areas of the resulting list of glycan composition for the most frequently occurring peptide sequences. For this, we allowed a 5 ppm mass accuracy for the glycopeptide combination and filtered on having a dotp of 0.8 for the best replicate. Integration windows were manually adjusted to capture the whole peak area for a signal, and to have overlapping retention times in the MS1 replicates. Integrated areas were normalized to the sum of intensities per peptide. For visualization of glycans recommendations of the Consortium for Functional Glycomics were followed and glycan cartoons were constructed using GlycoWorkbench (v2.1 build 146).

Indium-111 labeling and biodistribution SPECT/CT scans

IgG1 and IgA3.0 ch14.18 (500ug, 1mg/mL) were transferred to 0.1 M sodium bicarbonate (pH 8.2) buffer using 30kDa Amicon Ultra 0.5 mL centrifugal filters (Merck). A 20-fold molar excess of p-SCN-Bn-DTPA metal linker (2 mg/mL in dry DMSO, Macrocyclics) was added and incubated for 1 h at 37 °C. Samples were passed through a G50 Sephadex column, eluted with 0.5 M MES (2-(*N*-morpholino)ethanesulfonic acid) buffer (pH 5.4, Sigma) and fractions containing BnDTPA-antibody conjugates were collected. BnDTPA-antibodies were transferred to 0.5 M MES buffer using 30 kDa centrifugal filters as above. 150 µL Indium-111 (activity of 370 MBq/mL, Mallinckrodt) was added per 150 µg BnDTPA-antibody sample and incubated for 1 h at RT. Samples were passed through a G50 column, eluted with PBS (pH 7.4) and fractions containing ^{111}In-labeled antibody were collected. Purity was assessed by running samples with 0.1 M citrate buffer on an iTLC (instant Thin-Layer Chromatography) strip (Agilent) followed by radio-TLC scanning. Purity for both IgA3.0 and IgG1 was over 97% (**Supplemental Figure 4D**).

NSG mice with s.c. IMR32 tumors (+/- 1500 mm3) were injected i.v. with either 1.6 MBq ^{111}In-labeled IgG1 or 3.2 MBq ^{111}In-labeled IgA3.0 ch14.18. SPECT/CT images were acquired in list-mode at 24 h and 48 h post-injection using a VECTor6CT (MILabs B.V., Utrecht, NL). All animals were anaesthetized using 4% isoflurane and maintained at 2% and 37 °C throughout the imaging session. Image acquisition was performed using the HE-UHR-M collimator (0.75 mm pinhole size) for approximately 1 h. Total-body CT images were acquired for anatomical reference and attenuation correction (50 kvP, 0.21 mA, 75 ms). Reconstruction of SPECT images was performed using the SROSEM algorithm (5 iterations, 128 subsets, and 0.2 mm voxel size) and an automatic triple energy window for scatter correction at both photopeaks of ^{111}In. Reconstruction of CT images was performed at 100 µm as per manufacturers' default settings. To allow quantification of SPECT data, calibration factors derived from ^{111}In phantoms were used and for attenuation correction the SPECT data was registered to the CT data. Image post-processing was performed using the volume-of-interest analyses with the PMOD software package (Version 4.1, PMOD Technologies) to calculate the % injected dose per mL of tissue (% ID/mL).

Marker	Fluorochrome	Clone	Dilution	Company
CD45	BV510	HI30	1:200	Biolegend
CD14	FITC	TÜK4	1:50	Miltenyi
CD3	PB	UCHT1	1:50	BD
CD20	APC-H7	2H7	1:100	BD
CD56	PE-Cy7	NCAM 16.2	1:200	BD
CD16	PE	3G8	1:100	BD

Table S1 | Panel of fluorophore-conjugated antibodies for human PBMC analysis

Marker	Fluorochrome	Clone	Dilution	Company
CD45	BV510	HI30	1:200	Biolegend
CD66b	AF647	G10F5	1:400	Biolegend
CD89	PerCP-Cy5.5	A59	1:80	Biolegend
LOX-1	PE	15C4	1:50	Biolegend
CD11b	APC-Cy7	ICRF44	1:100	Biolegend

Table S2 | Panel of fluorophore-conjugated antibodies for human PMN analysis

Marker	Fluorochrome	Clone	Dilution	Company
c-kit	BV711	2B8	1:50	BD
CD45	BV510	30-F11	1:200	Biolegend
CD11b	FITC	M1/70	1:50	BD
F4/80	BV781	BM8	1:200	Biolegend
Human CD89	PE	A59	1:50	BD
Ly6C	PerCP-Cy5.5	HK1.4	1:100	Biolegend
Ly6G	PE-Cy7	1A8	1:200	Biolegend
Siglec F (CD170)	BV421	S17007L	1:50	Biolegend

Table S3 | Panel of fluorophore-conjugated antibodies for mouse tissue analysis with flow cytometry

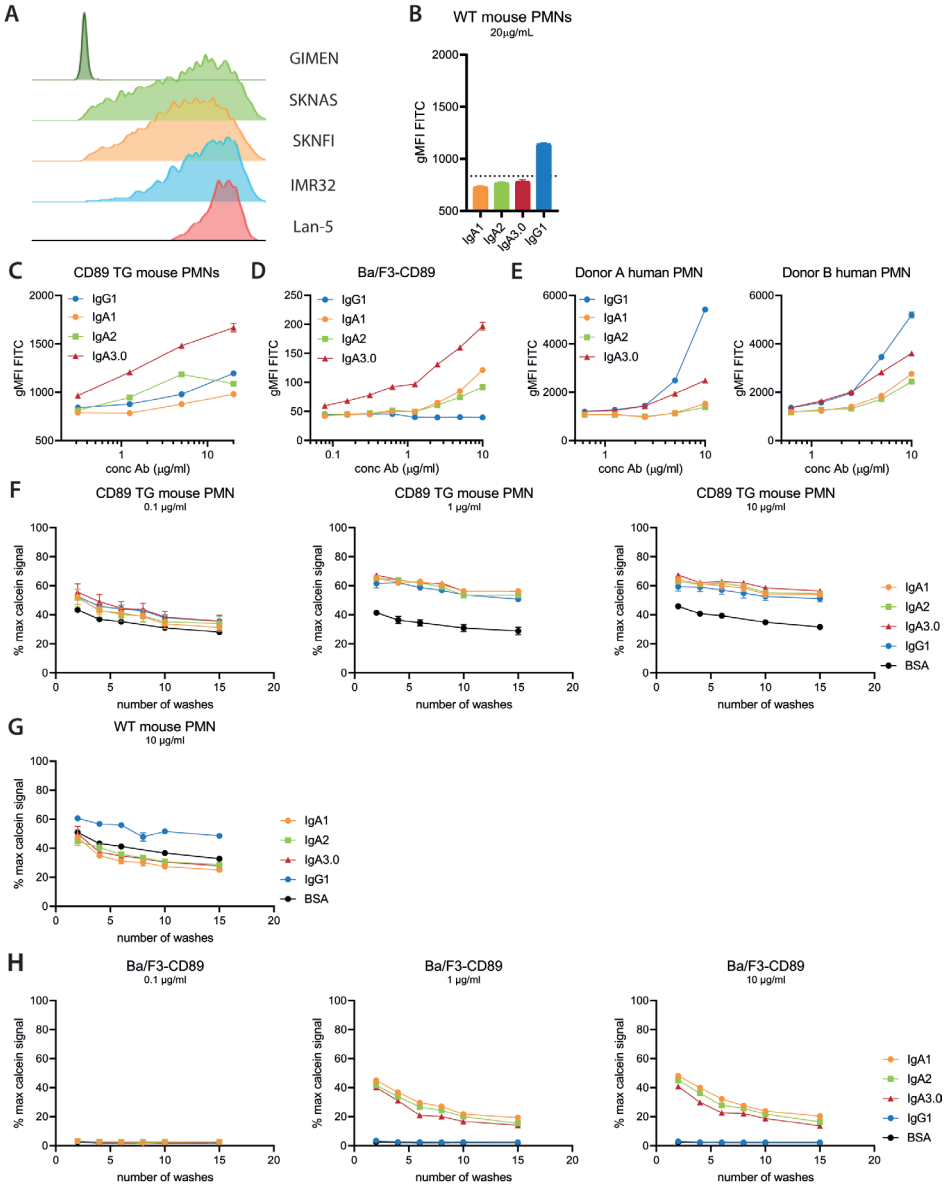

Figure S1 | GD2 expression and ch14.18 antibody binding (**A**) GD2 expression on neuroblastoma cell lines determined with flow cytometry. Monomeric Fc-binding to CD89 was assessed by incubating ch14.18 antibodies with (**B**) WT mouse PMN, (**C**) CD89 transgenic mouse neutrophils, (**D**) Ba/F3-CD89 cells or (**E**) human PMN followed by detection with FITC anti-human kappa antibody. Binding of complexed IgA to CD89 was assessed by incubating calcein-labeled (**F**) CD89 transgenic mouse PMN, (**G**) wild type mouse PMN or (**H**) Ba/F3-CD89 cells with antibody-coated plates and measuring remaining fluorescence during 10 washes. PMN = polymorphonuclear leukocytes.

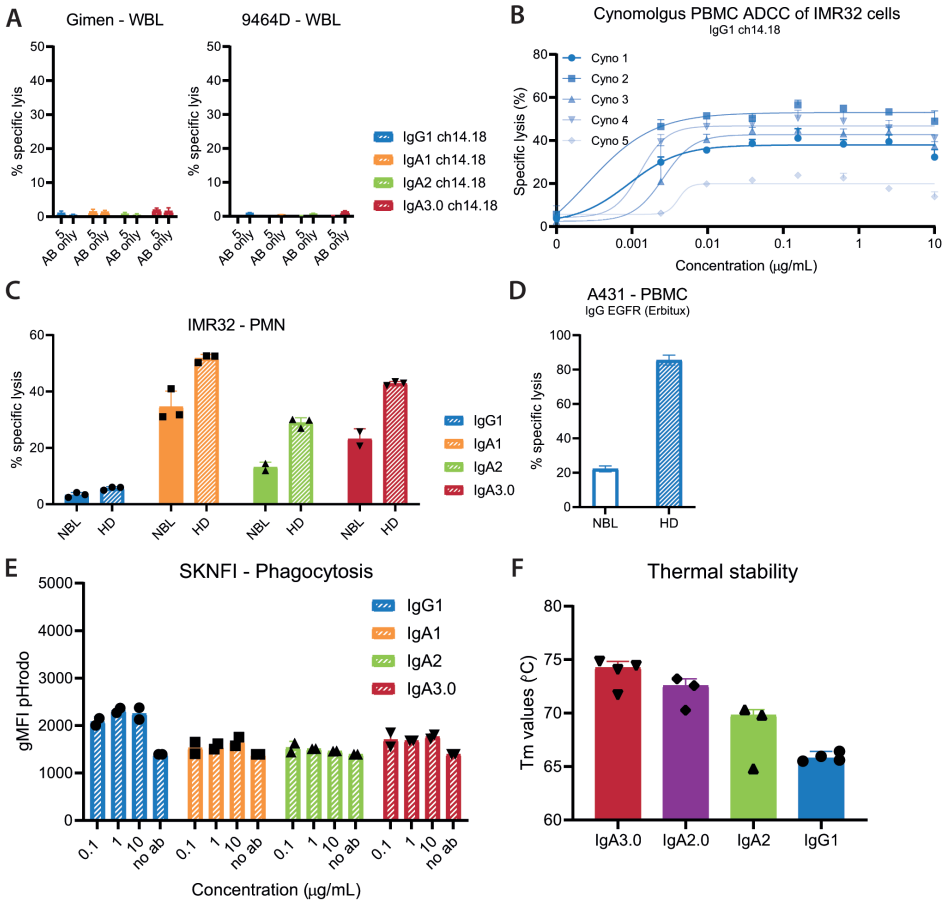

Figure S2 | ADCC and ADCP experiments and Tm values in thermal stability assays. (**A**) ADCC against GD2-negative neuroblastoma target cells was studied in ^{51}Cr-release assays with WBL as effector cells. (**B**) ^{51}Cr-release assays with cynomolgus PBMC as effector cells. (**C**) Comparison of neuroblastoma patient-derived PMN and healthy donor PMN ADCC against IMR32 cells upon IgA3.0 ch14.18 stimulation in ^{51}Cr-release assays. (**D**) Comparison of neuroblastoma patient-derived PBMC and healthy donor PBMC ADCC against A431 cells upon IgG EGFR (Erbitux) stimulation in ^{51}Cr-release assays. (**E**) The efficiency of antibodies in inducing ADCP against pHrodo-labeled human neuroblastoma target cells was assessed with monocyte-derived macrophages differentiated with M-CSF as effector cells. (**F**) Average Tm values as determined by Sypro orange thermal shift assays for different isotypes of 2D11 (anti-CD47), Obinutuzumab (anti-CD20), Rituximab (anti-CD20), Dinutuximab (anti-GD2), Trastuzumab (anti-Her2) and Cetuximab (anti-EGFR) antibodies. PMN = polymorphonuclear leukocytes, PBMC = peripheral blood mononuclear cells, WBL = whole blood leukocytes.

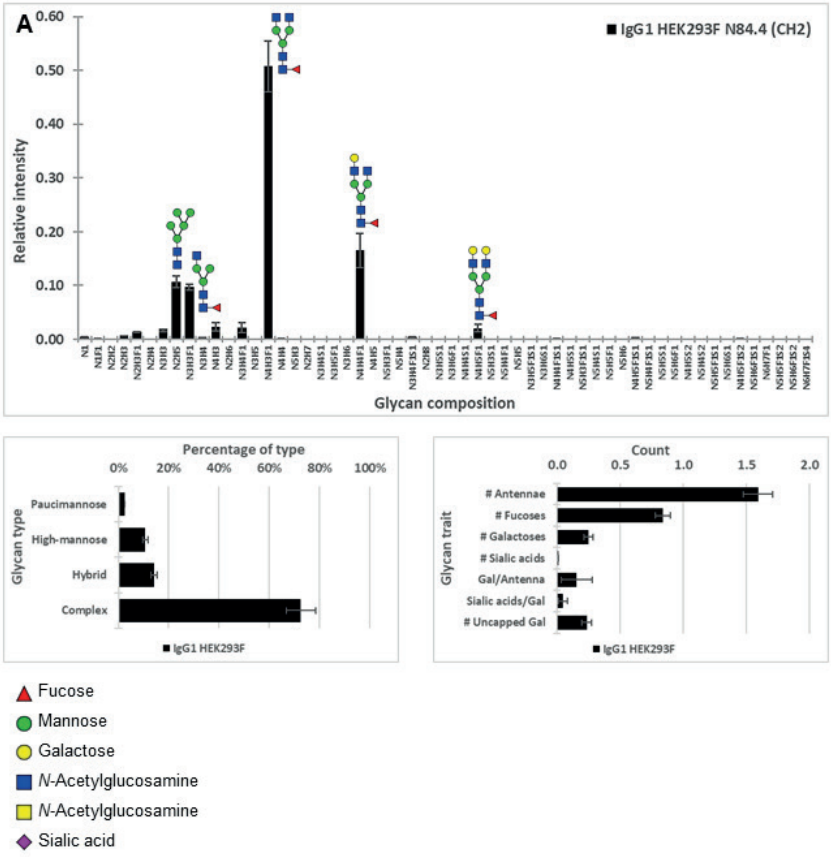

Figure S3 | Glycosylation analysis. Complete glycosylation profiles of IgG1 (**A**), IgA1 (**B**), IgA2 (**C**) and IgA3.0 (**D**) ch14.18 antibodies.

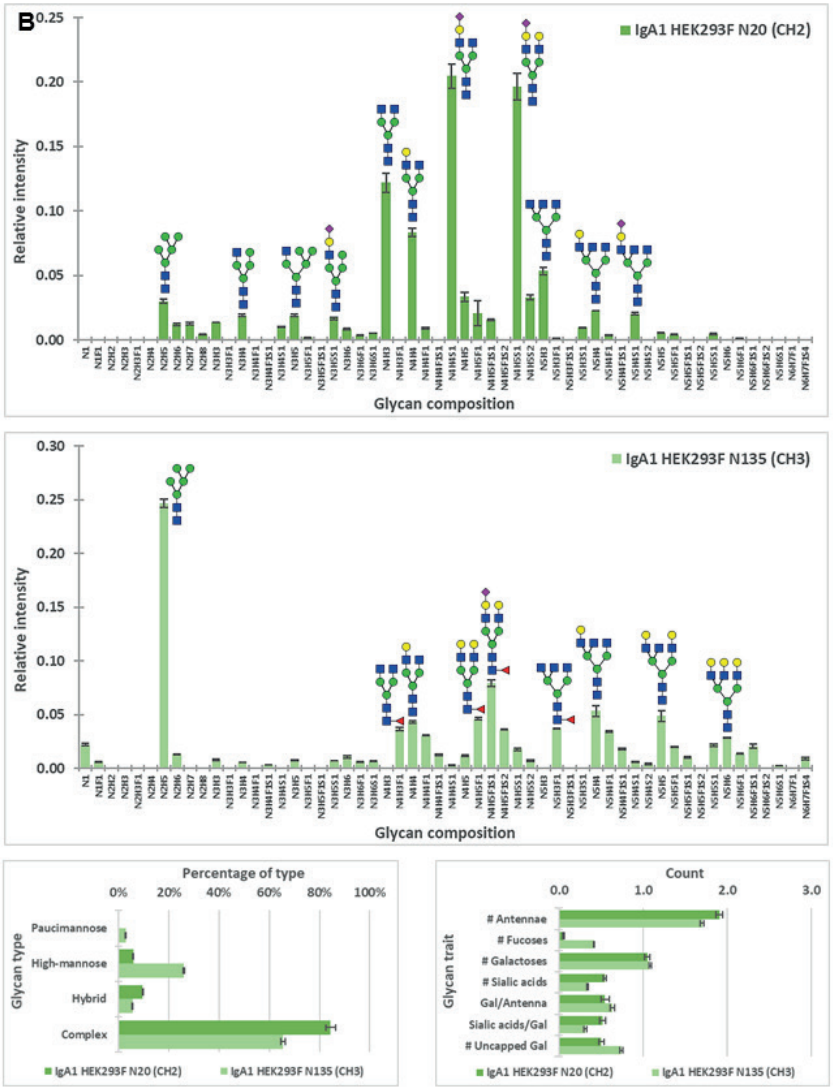

Figure S3 | Glycosylation analysis. Complete glycosylation profiles of IgG1 (**A**), IgA1 (**B**), IgA2 (**C**) and IgA3.0 (**D**) ch14.18 antibodies.

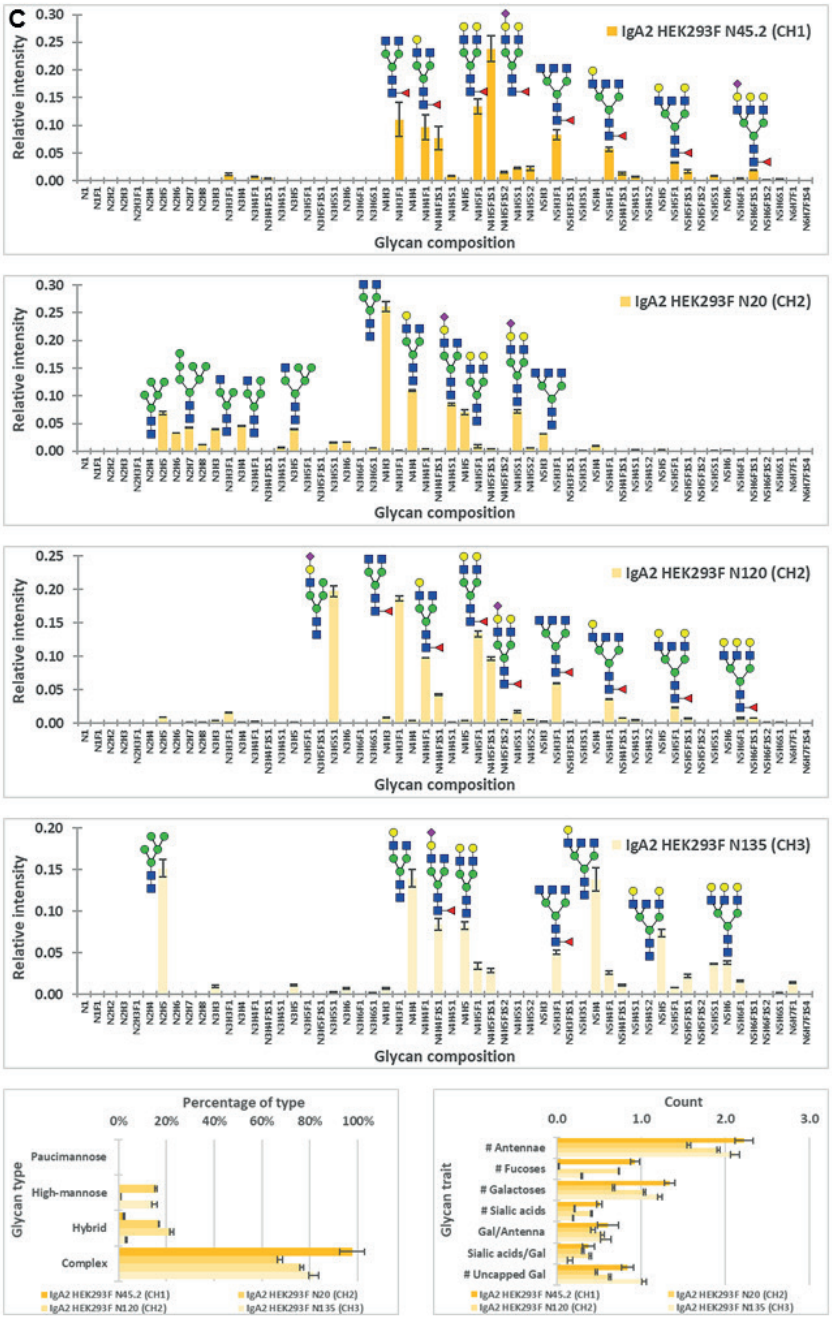

Figure S3 | Glycosylation analysis. Complete glycosylation profiles of IgG1 (**A**), IgA1 (**B**), IgA2 (**C**) and IgA3.0 (**D**) ch14.18 antibodies.

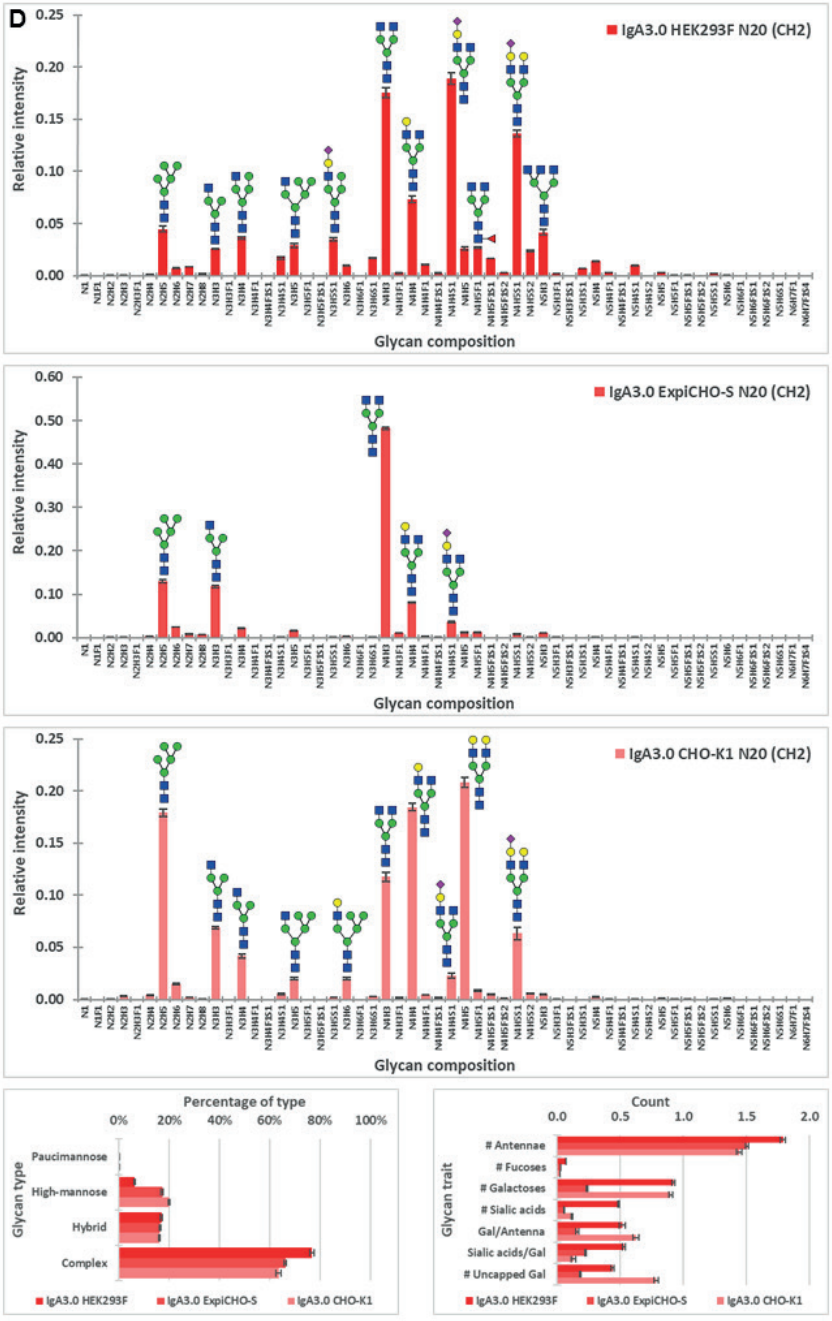

Figure S3 | Glycosylation analysis. Complete glycosylation profiles of IgG1 (**A**), IgA1 (**B**), IgA2 (**C**) and IgA3.0 (**D**) ch14.18 antibodies.

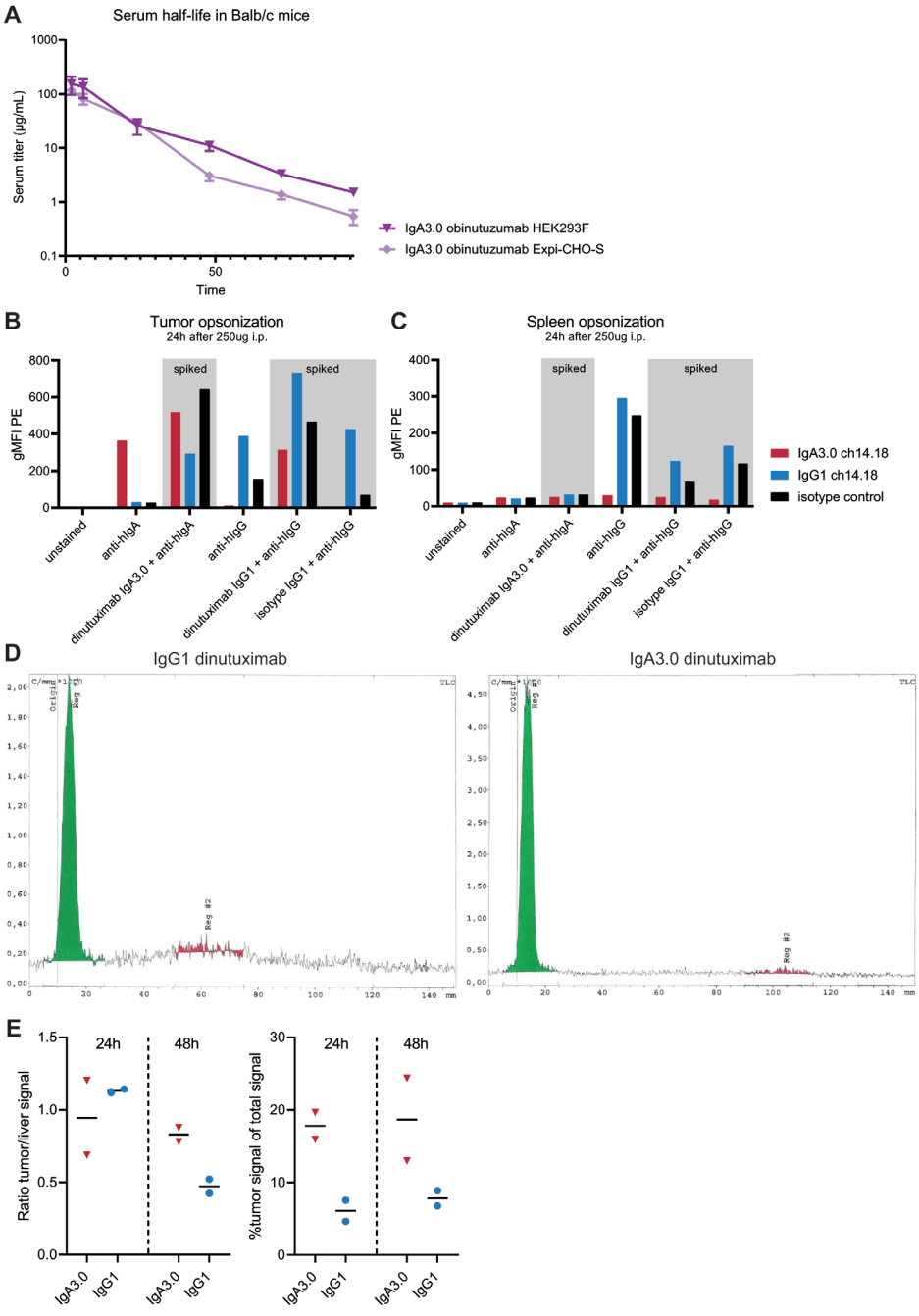

Figure S4 | PK studies and biodistribution analysis. (**A**) Balb/c and NSG mice were injected i.v. with 5 mg/kg anti-CD20 antibodies produced in either HEK293F or Expi-CHO-S. Serum concentrations over time were determined using ELISA on blood samples collected from the submandibular vein. (**B**) Tumor and (**C**) spleen of mice treated with antibody variants were isolated and stained with anti-hIgA or anti-hIgG antibodies to determine opsonization. (**D**) Purity of ^{111}In-labeled antibodies assessed using iTLC followed by radio-TLC scanning showed that samples have a purity of over 97%. (**E**) Quantification of SPECT signal in tumor compared to liver or total signal using volume-of-interest analyses tool in PMOD software.

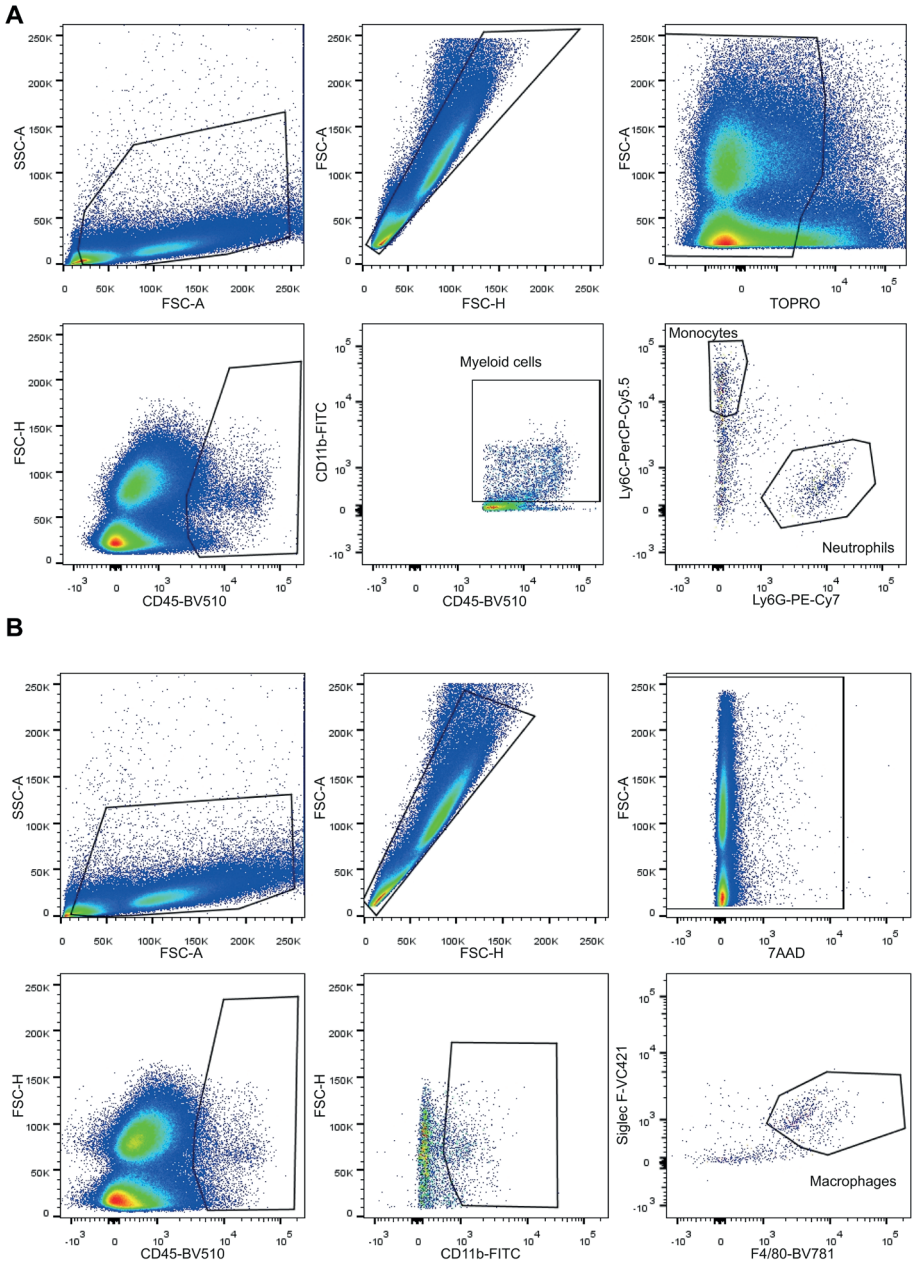

Figure S5 | Gating strategies for immune cell populations in IMR32 tumors. (**A**) Gating strategy for CD11b^{+} myeloid cells, Ly6G^{+} Ly6C^{int} neutrophils and Ly6C^{high} monocytes in IMR32 tumors. (**B**) Gating strategy for F4/80^{+} macrophages in IMR32 tumors.

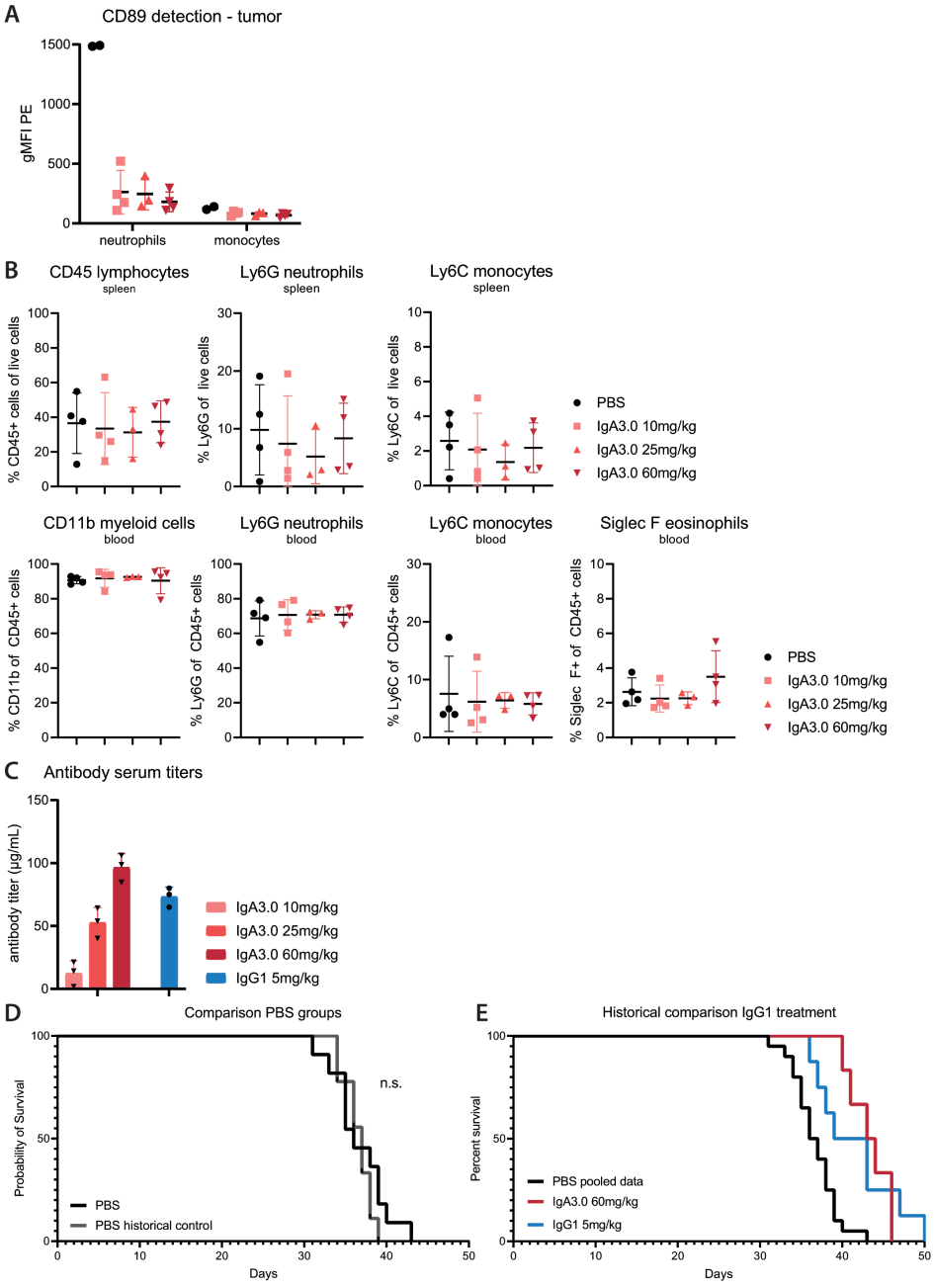

Figure S6 | TME analysis, serum antibody titers in IMR32 tumor bearing mice and historical comparison of IgA3.0 ch14.18 with IgG1 ch14.18 therapy. (**A**) CD89 staining on neutrophils and monocytes in tumor samples. (**B**) Spleen and blood immune cell composition of IMR32 tumor bearing mice. (**C**) Serum concentrations were determined using ELISA on blood samples collected from the submandibular vein. (**D**) Historical comparison of PBS groups from 2 different experiments shows similar outgrowth of IMR32 tumors in NSG mice. (**E**) Historical comparison of treatment with 60 mg/kg IgA3.0 ch14.18 or 5 mg/kg IgG1 ch14.18 showed similar therapeutic effects of antibodies.

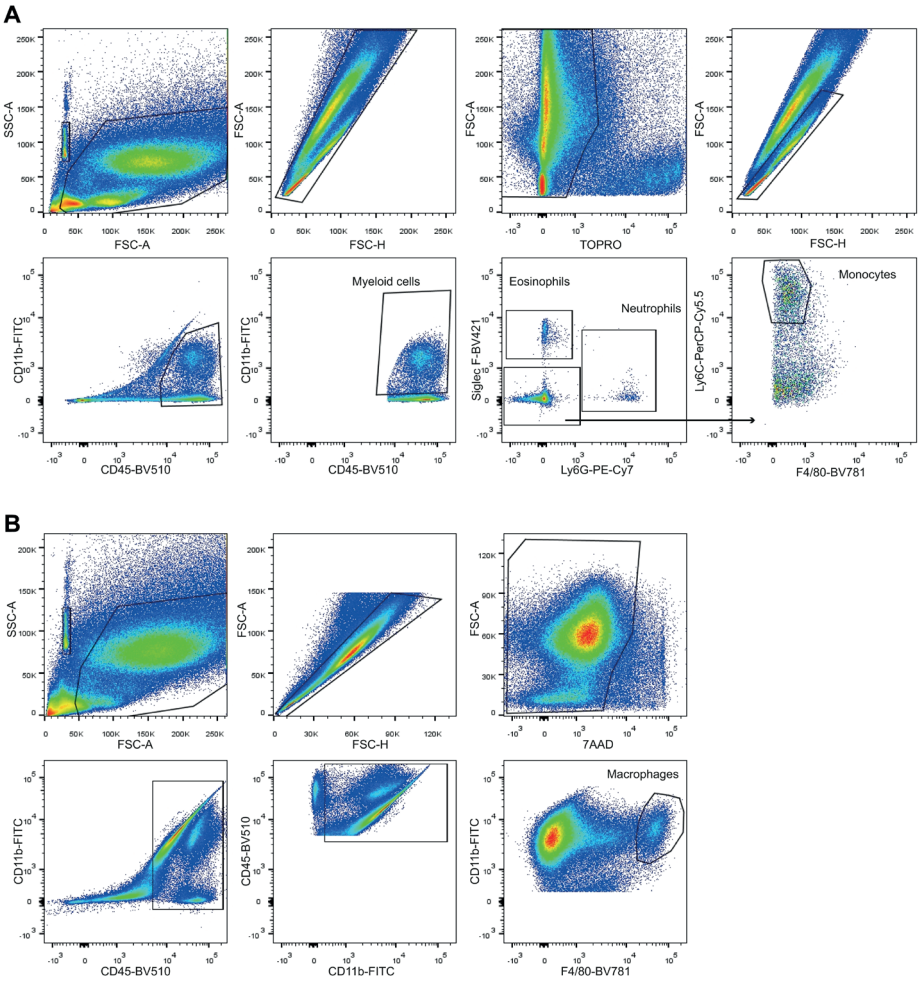

Figure S7 | Gating strategies for immune cell populations in 9464D-GD2 tumors. (**A**) Gating strategy for CD11b^{+} myeloid cells, Ly6G^{+} Ly6C^{int} neutrophils, Siglec F^{+} eosinophils and Ly6C^{high} monocytes in 9464D-GD2 tumors. (**B**) Gating strategy for F4/80^{+} macrophages in 9464D-GD2 tumors.

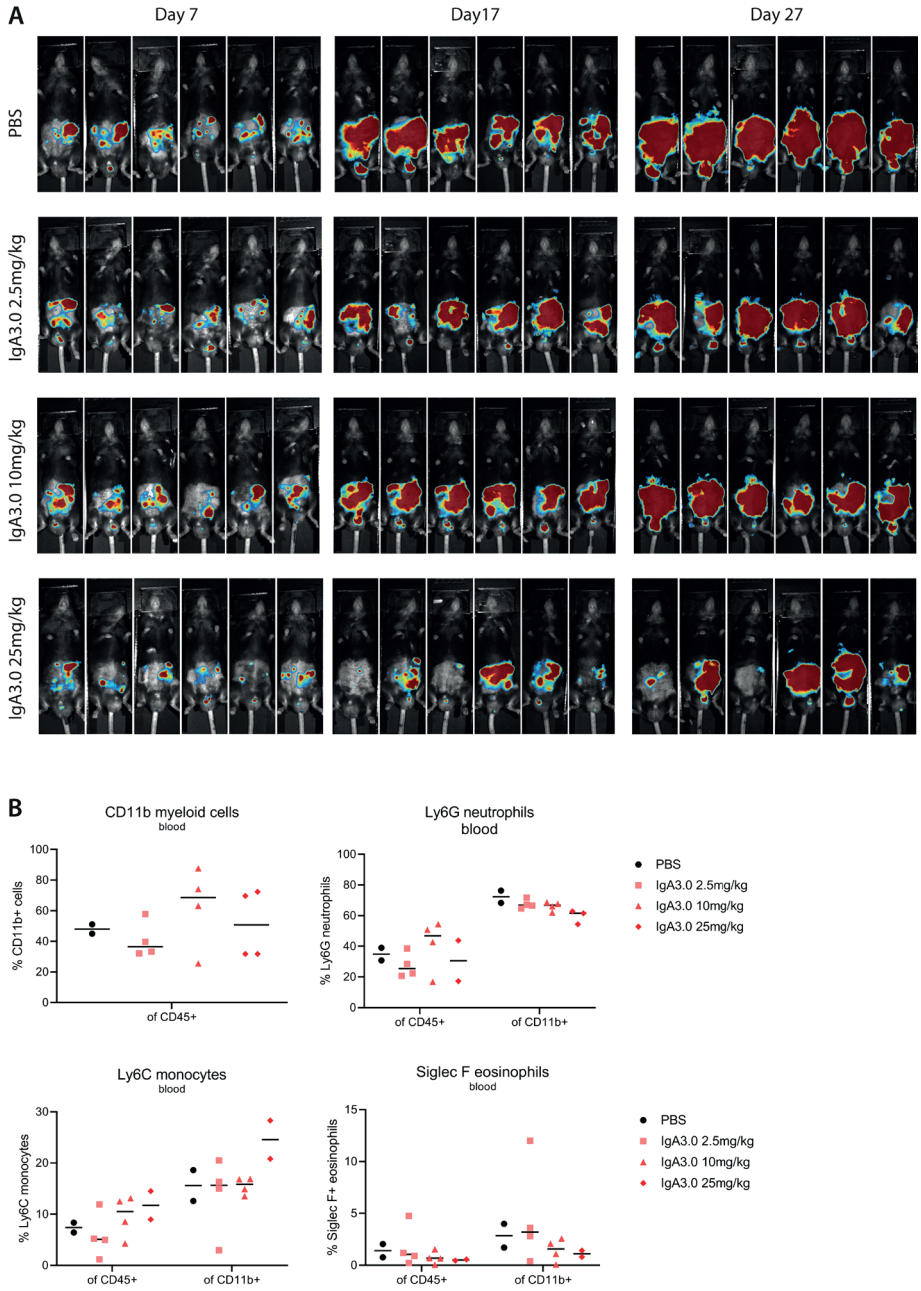

Figure S8 | BLI scans of 9464D-GD2 tumor outgrowth, TME analysis, serum antibody titers and historical comparison of IgA3.0 ch14.18 with IgG1 ch14.18 therapy. (**A**) BLI scans with photo overlay of 9464D-GD2 tumor outgrowth in C57Bl/6 mice. (**B**) Blood immune cell composition of 9464D-GD2 tumor bearing mice. (**C**) T cell quantification in blood, peritoneal lavage and tumor samples of 9464D-GD2 tumor bearing mice. (**D**) CD89 staining on neutrophils, monocytes and eosinophils in tumor and peritoneal lavage samples. (**E**) Serum concentrations were determined using ELISA on blood samples collected from the submandibular vein (**F**) Historical comparison of PBS groups from 2 different experiments shows similar outgrowth of

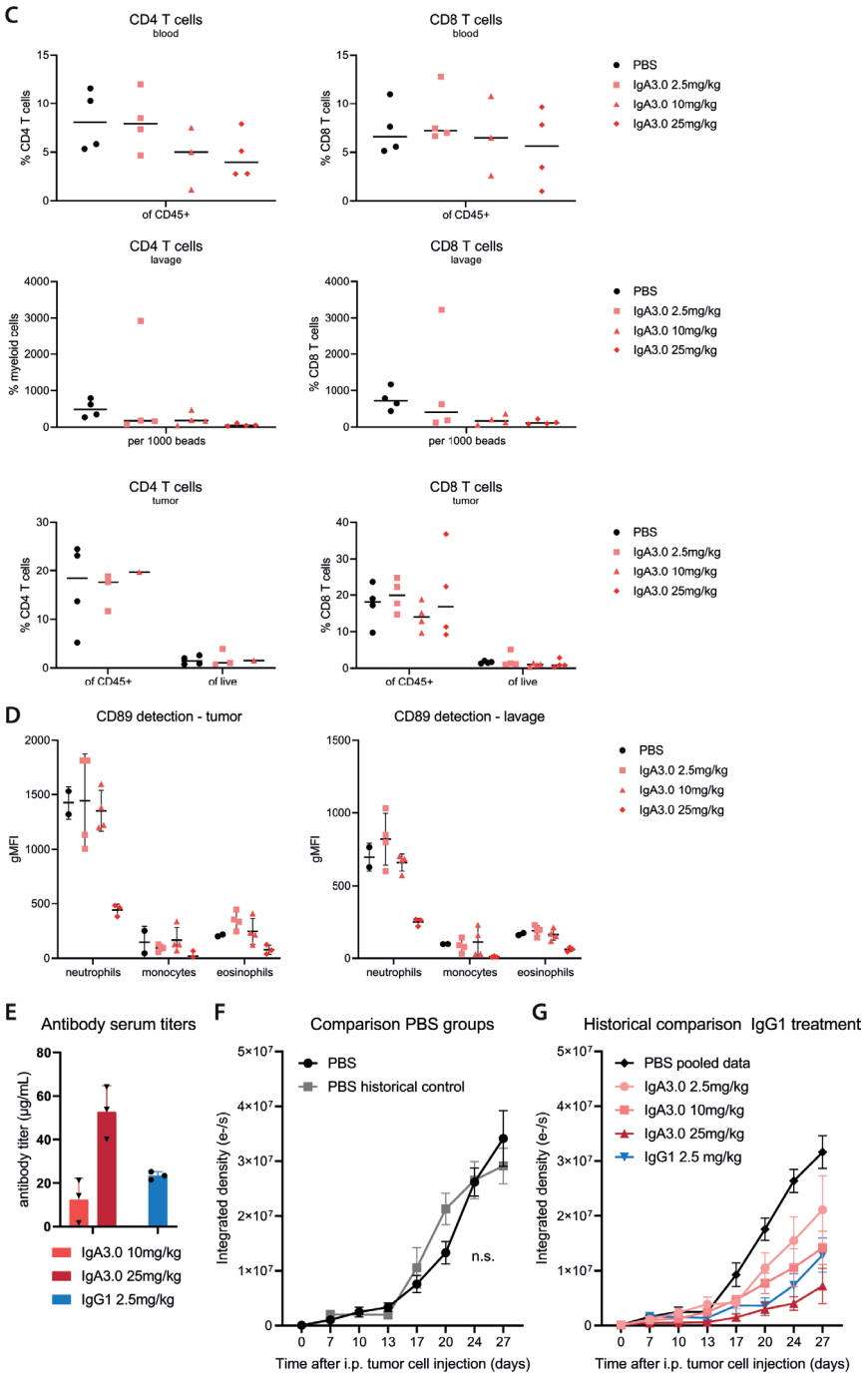

9464D-GD2 tumors in C57BL/6 mice. (**G**) Historical comparison of treatment with IgA3.0 and IgG1 ch14.18 showed similar therapeutic efficacy.


6

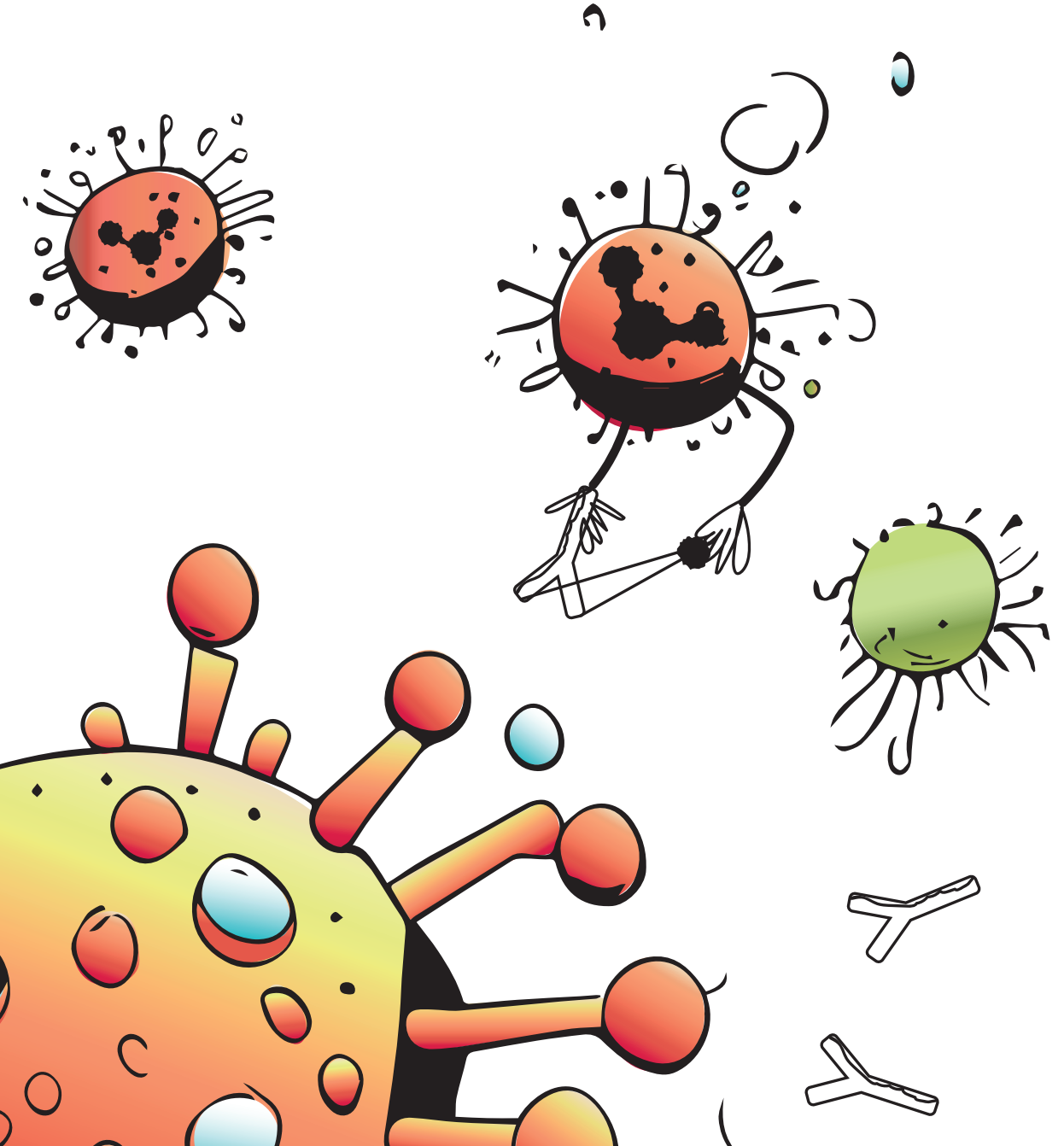

Chapter 7.

Enhancing IgA-mediated neutrophil cytotoxicity against neuroblastoma by CD47 blockade

Chilam Chan[1], Marjolein C. Stip[1], Maaike Nederend[1], J.H. Marco Jansen[1], Elsemieke M. Passchier[1], Femke van den Ham[3], Judith Wienke[3], Geert van Tetering[1], Jeanette H.W. Leusen[1]

Affiliations

1. Center for Translational Immunology, University Medical Center Utrecht, The Netherlands
2. Princess Máxima Center for Pediatric Oncology, Utrecht, the Netherlands

Under revision for publication in Journal for Immunotherapy of Cancer, 2024

ABSTRACT

Approximately half of the neuroblastoma patients develop high-risk neuroblastoma. Current treatment involves a multimodal strategy, including immunotherapy with dinutuximab (IgG ch14.18) targeting GD2. Despite achieving promising results, the recurrence rate remains high and poor survival persists. The therapeutic efficacy of dinutuximab is compromised by suboptimal activation of neutrophils and severe neuropathic pain, partially induced by complement activation. To enhance neutrophil cytotoxicity, IgG ch14.18 was converted to the IgA isotype, resulting in potent neutrophil-mediated ADCC, without complement activation. However, myeloid checkpoint molecules hamper neutrophil cytotoxicity, for example through CD47 that is overexpressed on neuroblastomas and orchestrates an immunosuppressive environment upon ligation to SIRPα expressed on neutrophils. In this study, we combined IgA therapy with CD47 blockade. *In vitro* killing assays showed enhanced IgA-mediated ADCC by neutrophils targeting neuroblastoma cell lines and organoids in comparison to IgG. Notably, when combined with CD47 blockade, both IgG and IgA therapy were enhanced, though the combination with IgA resulted in the greatest improvement of ADCC. Furthermore, in a neuroblastoma xenograft model, we systemically blocked CD47 with a SIRPα fusion protein containing an ablated IgG1 Fc, and compared IgA therapy to IgG therapy. Only IgA therapy combined with CD47 blockade increased neutrophil influx to the tumor microenvironment. Moreover, the IgA combination strategy hampered tumor outgrowth most effectively and prolonged tumor-specific survival. These promising results highlight the potential to enhance immunotherapy efficacy against high-risk neuroblastoma through improved neutrophil cytotoxicity by combining IgA therapy with CD47 blockade.

Keywords

Neuroblastoma, GD2, Neutrophils, IgA, CD47/SIRPα, Checkpoint inhibition

INTRODUCTION

Neuroblastoma is the most prevalent extracranial solid tumor in childhood, often diagnosed before the age of five[1]. Neuroblastoma emerges from neural crest cells forming the sympathetic nervous system and typically develops in the adrenal medulla or paraspinal ganglia[2]. Neuroblastomas are highly heterogenous, with some tumors regressing spontaneously, while up to 50% of neuroblastoma patients develop high-risk neuroblastoma, with a 5-year survival rate of only 45%[3,4].

The current standard treatment for high-risk neuroblastoma involves surgery, chemotherapy with hematopoietic stem-cell rescue, radiation therapy, and immunotherapy[5]. In 2015,

the US FDA approved dinutuximab (IgG ch14.18) for immunotherapy treatment of these patients. Dinutuximab is an antibody directed against the end-terminal penta-oligosaccharide of GD2, a disialoganglioside expressed on the cell surface. GD2 is expressed at low levels on normal tissues of the central nervous system and peripheral nerves, but is highly expressed on many tumors of neuroectodermal origin, including neuroblastoma[6,7]. GD2 is overexpressed in nearly all neuroblastoma patients, making it an attractive target for immunotherapy[8].

Dinutuximab activates NK cells, macrophages and granulocytes against the tumor by Fc gamma receptor- (FcγR) mediated effector functions, including antibody-dependent cell-mediated cytotoxicity (ADCC), antibody-dependent cellular phagocytosis (ADCP) and trogocytosis[9]. While immunotherapy has shown promise, the increase in event-free survival at two years has only been 20%[10]. This could be in part explained by the severe side effects, such as neuropathic pain, which limits the dose administered[11]. A single point mutation, K332A in the Fc region of dinutuximab disrupted C1q binding and reduced neuropathic pain in some patients, suggesting complement activation is at least partly associated with these side effects[11,12]. The neuropathic pain and high relapse rate, highlight the need for enhancement in current treatment strategies[13,14].

While often overlooked, granulocytes can be important effector cells in immunotherapy, as it is the most abundant leukocyte population in blood[15]. Granulocytes, consisting mostly of neutrophils, are activated by dinutuximab via FcγRIIa, and induces cytotoxicity against neuroblastomas[16–18]. However, neutrophils express to a much higher level, FcγRIIIb, which is a GPI-linked receptor and therefor will not activate neutrophils, but can act as a sink for IgG antibodies[19]. To improve the activation of neutrophils, we previously converted IgG ch14.18 into the IgA isotype[20]. IgA ch14.18 demonstrated robust neutrophil-mediated ADCC through the activation of the Fc alpha receptor (FcαRI, CD89) and does not bind to FcγRs. Additionally, IgA does not activate the complement system and therefore the isotype switch alleviated the neuropathic pain as demonstrated in mouse models. Subsequently, IgA ch14.18 was further engineered into IgA3.0 ch14.18 to enhance its stability and manufacturability, making it more suitable for potential clinical applications[21]. Neuroblastoma is regarded as an immunologically cold tumor, distinguished by limited lymphocyte infiltration and a suppressive tumor microenvironment (TME)[22,23]. Nevertheless, IgA ch14.18 showed encouraging results in extending survival in neuroblastoma-bearing mice, but analysis of the tumor microenvironment showed very poor attraction of myeloid cells upon IgA therapy, implying that the TME is immunological suppressed[21]. Checkpoint molecules, play a crucial role in inhibiting the immune response within the TME. CD47 is a myeloid checkpoint molecule, overexpressed on the surface of tumor cells, including neuroblastoma and interacts with signal regulatory protein alpha (SIRPα) on neutrophils, monocytes and macrophages. This interaction promotes immunosuppression and shields the tumor from immunosurveillance[24–27]. The CD47/SIRPα axis is commonly referred to as a

"Don't eat me" signal in macrophages, as it suppresses phagocytosis of the tumor cells[26,28]. Similarly, engagement of CD47 with SIRPα on neutrophils has been shown to suppress ADCC and trogocytosis[29,30]. Neutrophils are regulated by various stimulatory signals and inhibitory checkpoint molecules, which together dictate the fate of the neutrophil. Blocking CD47 removes a suppressive signal, shifting the balance towards a more anti-tumor phenotype, allowing neutrophils to become more actively engaged in tumor cell killing. IgG ch14.18 in combination with CD47 blockade enhanced the cytotoxicity against neuroblastoma by neutrophils[27]. However, additional GM-CSF was required to stimulate granulocytes and achieve an optimal anti-tumor response, possibly due to suboptimal activation of neutrophils by IgG ch14.18[16,27]. Currently, the combination of IgA ch14.18 and CD47 blockade in neuroblastoma has not been studied.

We hypothesize that IgA therapy in combination with CD47 blockade could be a novel strategy to tackle high-risk neuroblastoma. First of all, IgA activates neutrophils more effectively and outperforms IgG in neutrophil-mediated cytotoxicity[20]. Secondly, the lack of a C1q-binding site in IgA prevents complement associated neuropathic pain[20]. Finally, in various other cancer models, such as breast cancer, leukemia and lymphoma, the combination of IgA with CD47 blockade demonstrated superior efficacy compared to the combination of IgG with CD47 blockade[30–32]. In our study, we aimed to investigate the effect of CD47 blockade on the efficacy of IgA antibody therapy targeting GD2 in neuroblastoma.

METHODS

Antibodies

IgG and IgA3.0 (hereafter called IgA) antibodies targeting GD2 (ch14.18, dinutuximab) were produced by WuXi Biologics in CHO-K1 cells. To block CD47, we either used an engineered human SIRPα D1 domain with high affinity for both mouse and human CD47 fused to IgG1 L234A/L235A/P329G (LALAPG) as described in Chernyavska et al., 2022[33] or an IgG1 LALAPG anti-CD47 (Clone 2.3D11) produced and purified in-house. Antibodies were produced and purified as described previously[20,34]. In short, antibodies were produced through transient transfection of Expi-CHO-S cells (Thermo Fisher Scientific). Subsequently, supernatant containing the antibody was affinity purified using a HiTrap® Protein A column (Cytiva) for IgG antibodies or a HiTrap® KappaSelect column (Cytiva) for IgA antibodies, coupled to a ÄKTA liquid chromatography system (Cytiva). The captured IgG was eluted and subsequently dialyzed against PBS, while IgA was additionally purified by size exclusion chromatography. The eluate was filtered using a 0.22 µm filter and the antibody concentration was measured by UV absorbance at 280 nm using the corresponding extinction coefficient (ε280).

Cell lines

The human neuroblastoma cell lines IMR32, SKNFI, SKNAS, LAN-5, GIMEN, were obtained from the American Type Culture Collection (ATCC). All cells were maintained in DMEM (Dulbecco's Modified Eagle Medium, Thermo Fisher Scientific) supplemented with 10% fetal calf serum (FCS), 100 U/mL penicillin-streptomycin (Pen/Strep, Gibco, life technologies), and 2% MEM non-essential amino acids solution (NEAA, Thermo Fisher Scientific), hereafter called complete DMEM. All cell lines were grown at 37°C in a humidified incubator containing 5% CO_2. ExpiCHO-S cells (Thermo Fisher Scientific) were cultured in ExpiCHO Expression Medium (Gibco) at 37°C, 8% CO_2, shaking at 125 rpm. Cells were not cultured past 20 passages, and they were regularly tested for mycoplasma contamination by a Mycoalert mycoplasma detection kit (Lonza).

AMC691B organoids

Patient-derived organoids AMC691B were kindly provided by Prof. Jan Molenaar and generated as described previously[35]. The organoids were cultured in neuroblastoma organoid medium, consisting of DMEM with low glucose and Glutamax™, supplemented with 20% Ham's F-12 Nutrient Mix, B-27 supplement minus vitamin A (50×), N-2 supplement (100×), 100 U/mL penicillin, 100 µg/mL streptomycin, 20 ng/mL animal-free recombinant human EGF, 40 ng/mL recombinant human FGF-basic, 200 ng/mL recombinant human IGF-I, 10 ng/mL recombinant human PDGF-AA and 10 ng/mL recombinant human PDGF-BB (see **Table 1**) at 37 °C with 5% CO_2 and were subcultured once or twice per week depending on growth rate. AMC691B transduced with GFP-luciferase constructs were generated previously[36].

DMEM with low glucose and Glutamax™	Thermo Fisher	Cat#21885-108
Ham's F-12 Nutrient Mix	Thermo Fisher	Cat#31765027
B-27 supplement minus vitamin A (50×)	Thermo Fisher	Cat#12587010
N-2 supplement (100×)	Thermo Fisher	Cat#17502048
Recombinant human EGF	Peprotech	Cat#AF-100-15
Recombinant human FGF-2	Peprotech	Cat#100-18B
Recombinant human IGF-1	R&D	Cat#100-11
Recombinant human PDGF-AA	Peprotech	Cat#100-13A
Recombinant human PDGF-BB	Peprotech	Cat#100-14B

Table 1 | Composition of the organoid medium

ADCC assays

^{51}Cr release ADCC assays were performed as previously described[37]. In brief, target cells were labeled with 100 µCi chromium-51 (PerkinElmer) per million cells for at least 2 hours at 37 °C and 5% CO_2. Labeled cells were washed three times with medium, before being pre-treated with 10 µg/mL of SIRPα fusion protein for 30 minutes at room temperature to block CD47. Human polymorphonuclear leukocytes (PMNs) and peripheral blood mononuclear cells (PBMCs) were isolated from peripheral blood from healthy donors at the UMC Utrecht by Ficoll density gradient centrifugation. After collecting the PBMC layer, the remaining pellet was subjected to erythrocyte lysis using RBC Lysis Buffer (Biolegend) and PMNs were collected. Whole leukocytes were obtained by lysing the red blood cells from peripheral blood, followed by resuspending the remaining leukocytes in the original volume. The effector to target (E:T) ratio used for PMNs and PBMCs was 40:1 and 100:1, respectively. For whole leukocytes, a volume of 50 µL was added to the target cells in a final volume of 200 µL. Antibodies were added at the concentrations specified in each experiment. After 4 hours of incubation at 37 °C in a humidified incubator containing 5% CO_2, the plate was centrifuged, and the supernatant was transferred to a lumaplate (PerkinElmer) to be measured on a beta-gamma counter for radioactive scintillation (in cpm) (PerkinElmer). Specific lysis was calculated using the formula: ((Experimental cpm – basal cpm)/(maximal cpm – basal cpm))*100. The maximum cpm was determined by treating target cells with 5% Triton X-100 (Sigma-Aldrich), and the baseline cpm was determined by chromium release from target cells in the absence of antibodies and effector cells.

A luciferase-based ADCC assay was performed to measure ADCC against AMC691B organoids. Three days prior to the assay, organoids were dissociated into single cells, and 5000 cells were seeded in organoid medium into a solid white flat bottom 96-well plate (Corning). PBMCs and PMNs were freshly isolated from healthy donor blood on the day of the assay as described above. Effector cells were added to the wells at an E:T ratio of 40:1 for PMNs and 100:1 for PBMCs (5-20% of the PBMCs are NK cells). CD47 was blocked by adding SIRPα fusion protein at a final concentration of 10 µg/mL. Subsequently, the plate was incubated for 4 hours at 37 °C in a humidified incubator containing 5% CO_2. Five minutes before luminescence measurement, IVISbrite D-luciferin (XenoLight, Perkin Elmer) was added to the wells at a final concentration of 150 µg/mL. Luminescence was measured on the Spectramax M3 (Molecular Devices) with a measurement interval of 1 sec and a settling time of 0.1 sec. Specific lysis was calculated as: 100 - (((Experimental luminescence - Basal luminescence) / Maximal luminescence) * 100), where basal luminescence was obtained from medium-only controls and maximal luminescence was obtained from organoids-only controls.

Flow cytometry

For the FACS staining, 100,000 cells were seeded and stained with the indicated antibodies in FACS buffer (PBS, 0.01% bovine serum albumin, 0.01% sodium-azide) for 45 min on ice. Expression level of SIRPα (15-414, Biolegend) on various immune cell subsets within whole peripheral blood was determined using the following antibodies to determine different immune cell subsets: Anti-CD45 (HI30, Biolegend), anti-CD19 (SJ25C1, BD Biosciences), anti-CD3 (UCHT1, Biolegend), anti-CD14 (MΦP9, BD Biosciences), anti-CD56 (NCAM16.2, BD Biosciences) and anti-CD66b (G10F5, BD Biosciences).

Surface expression of GD2 on neuroblastoma cell lines was determined using an anti-GD2 antibody (14G2a, Biolegend), while CD47 expression was measured using anti-CD47 (CC2C6, Biolegend) antibody.

To quantify the number of CD47 molecules per cell, we performed a QIFIKIT (Agilent/Dako) analysis according to the manufacturer's instructions. Cells were stained with a saturating concentration of 10 µg/mL unconjugated mouse IgG monoclonal antibody directed against CD47 (CC2C6, Biolegend). Measurements were performed using a BD FACS Canto II flow cytometer.

Trogocytosis

Neuroblastoma cells were labeled with 5 µM DiO (Molecular Probes) according to manufacturer's instructions. Labeled cells were co-cultured with PMNs at an E:T ratio of 10:1 in complete DMEM for up to 4 hours with 10 µg/mL IgG or IgA (ch14.18) and 10 µg/mL IgG1 LALAPG SIRPα in indicated experiments at 37 °C in a humidified incubator containing 5% CO_2. After co-culture, cells were washed with PBS, and stained with anti-CD66b-V450 (G10F5, BD Biosciences). The frequency of DiO^+ neuroblastoma/target cells taken up by $CD66b^+$ neutrophils was measured by flow cytometry using a BD FACS Canto II flow cytometer.

CRISPR/Cas9 of CD47

CD47 was knocked out using CRISPR/Cas9 technology. A single guide RNA (sgRNA, AGCAACAGCGCCGCUACCAG, IDT) targeting *CD47* or a scrambled negative control (IDT) was used to guide the Cas9 nuclease to the target site. IMR32 cells were prepared for electroporation with the Neon Transfection System (Thermo Fisher) following the manufacturer's instructions. Three pulses were delivered at 1200 V and 20 ms to introduce the sgRNA and Cas9 complex into the cells. Knock out efficiency was determined by flow cytometry, and the IMR32-CD47KO population was enriched by sorting the CD47 negative cells using the BD FACSAria II cell sorter.

Live cell imaging

One day prior to the live cell imaging experiment, SKNAS cells were seeded in an 8 well µ-slide (Ibidi). Tumor cells were labeled with 1 µM CellTrace CFSE according to the manufacturer's protocol (Thermo Fisher Scientific). Next, 10 µg/mL of IgA ch14.18 in the absence or presence of 10 µg/mL of IgG1 LALAPG SIRPα fusion protein and 1 µM TO-PRO-3 (Thermo Fisher Scientific) were added to the target cells. After 15 minutes, primary PMNs were added. Cells were kept in an enclosed incubation chamber at 37 °C and 5% CO_2 on a Deltavision RT widefield microscope (GE Healthcare) equipped with an Olympus 40×/1.35 NA oil immersion objective and a Cascade II 1K EMCCD/E2V CCD-201 camera. Recordings were made at 25-second intervals for 2 hours.

AMC691B organoids were seeded as single cells in an 8 well µ-slide, three days prior to the experiment. PMNs were freshly isolated and stained with 1 µM eFluor 450 dye (Thermo Fisher Scientific) according to manufacturer's instructions. For the experiment, 10 µg/mL of IgA ch14.18 in the absence or presence of 10 µg/mL of IgG1 LALAPG SIRPα fusion protein was added to the organoids. Additionally, 1 µM propidium iodide nucleic acid stain (Thermo Fisher Scientific) was added to visualize cell death. Live cell imaging (xyzt) was performed within an incubation chamber maintained at 37 °C and 5% CO_2 using a Stellaris 5 confocal microscope (Leica) equipped with an HC PL APO 20x/0.75 dry objective (Leica) and power HyD S detectors (410-850 nm). Recordings were made at 32-second intervals for 4 hours. Image analysis was performed in LAS X (Leica) and Imaris (Bitplane).

Subcutaneous IMR32 mouse model

Human FcαRI (CD89) transgenic (Tg) mice were previously generated at the UMC Utrecht and backcrossed on a SCID (NOD.CB-17/Icr-*Prkdc*$^{scid/scid}$/Rj) background[38]. All mice were bred and maintained at Janvier Labs in Paris, France, before being transported to the University of Utrecht's Central Laboratory Animal Research Facility for the experiment. Here, mice were housed in a controlled environment with a 12:12 hr light-dark cycle with access to food and water ad libitum. We used male transgene-negative (nTg) littermates for the solvent (PBS) control, IgG treatment and CD47 blockade only treatment groups. These treatment groups do not receive IgA and thus do not require the presence of CD89. Importantly, no differences in terms of tumor outgrowth are reported between the CD89 Tg mice and the non-Tg littermates, allowing combined use in the same experiment[39]. We used male mice ranging in age from 10 to 32 weeks in this experiment. Mice were acclimatized for at least one week prior to the experiment and randomized based on weight and age. The treatment and analysis were both double-blind.

IMR32 cells were mixed in a 1:1 solution of PBS and high concentration matrigel (Corning). 2.5 million cells in 150 µL were injected subcutaneously and tumor growth was monitored using a caliper to measure length, width, and height until the tumor size reached 1500 mm^3 (humane end-point). Starting from day 2 after tumor cell injection, the neutrophil-depleting

agent, mouse anti-Ly6G (clone 1A8, mIgG2a, Absolute Antibody), was administered intraperitoneally (i.p.) three times a week at a dose of 100 µg per mouse[40]. Treatment was started from day 4 and was given intraperitoneally. IgG ch14.18 was administered once a week at a dosage of 5 mg/kg, IgA ch14.18 three times a week at 25 mg/kg. A higher IgA dose was administered to compensate for its shorter half-life. These doses were tested previously and showed comparable serum titers over time[20,21]. Additionally, IgG1 LALAPG SIRPα was injected i.p. every 9 days at 30 mg/kg. As a solvent control, mice received PBS.

Analysis of the tumor microenvironment

When the tumor reached a size of 1500 mm^3, mice were euthanized, and their tumor was collected in ice-cold PBS. Additionally, blood samples were obtained using the cheek puncture method and collected in lithium-heparin tubes (Sarstedt) for further analysis. Following tumor collection, the tumors were cut into smaller pieces and digested using the mouse tumor dissociation kit from Miltenyi. Up to 1 gram of tumor tissue was processed following the manufacturer's protocol. The dissociation was carried out using the 37C_m_TDK_1 program on a gentleMACS Octo Dissociator (Miltenyi). After the dissociation process, the samples were passed through a 100 µm cell strainer to obtain a single-cell suspension. Subsequently, both the blood samples (**Supplemental Table 1**) and 2.5 million tumor cells (**Supplemental Table 2**) were stained for FACS analysis.

Data processing and statistical analyses

Flow cytometry data was analyzed using FlowJo software (TreeStar). Statistical analyses were performed using GraphPad Prism 9.3.0 (GraphPad Software Inc.). Specific statistical tests performed for each experiment are indicated in the corresponding figure legends. Data are presented as mean ± standard deviation (SD) or standard error of mean (SEM) and a p-value of less than 0.05 was considered statistically significant. Graphs and figures were generated using the aforementioned software, Adobe Illustrator and Biorender. Imaging data was analyzed using Imaris (Bitplane).

RESULTS

Neuroblastoma cell lines express high levels of GD2 and CD47

The current standard treatment regimen for treating high-risk neuroblastoma with immunotherapy uses dinutuximab (IgG ch14.18). To determine whether a combination therapy using IgA ch14.18 and CD47 blockade would be beneficial, we first assessed the expression levels of GD2 in a panel of commonly used neuroblastoma cell lines (**Figure 1A**). Additionally, to investigate whether the CD47/SIRPα axis could play a role in neuroblastoma, we quantified CD47 expression levels using QIFIKIT analysis (**Figure**

1B). Flow cytometry analysis revealed high expression levels of GD2 as compared to the GD2-negative GIMEN cells. Moreover, all neuroblastoma cell lines expressed high levels of CD47. Next, we assessed the expression of SIRPα, the receptor for CD47, in immune cell subsets in the blood. SIRPα was only expressed in monocytes and neutrophils (**Figure 1C**), confirming that SIRPα expression is limited to the myeloid compartment. These findings suggest that targeting GD2 using IgA and simultaneously blocking CD47 may be an effective therapeutic strategy in neuroblastoma.

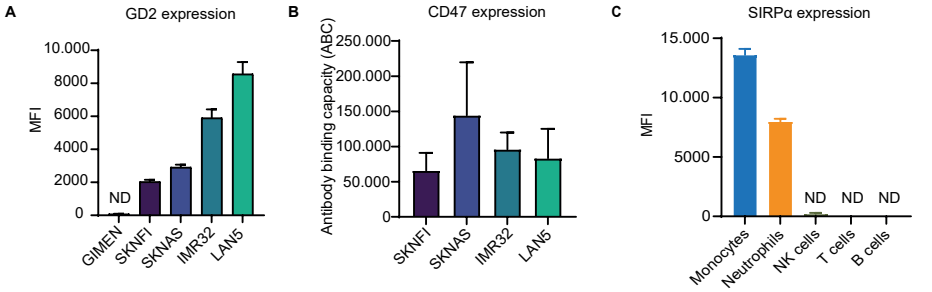

Figure 1 | Expression levels of GD2 and CD47 in neuroblastoma cells and SIRPα in leukocytes. (**A**) The expression level of GD2 on various neuroblastoma cell lines was determined using flow cytometry. Data is shown as MFI ± SD. (**B**) The absolute expression level of CD47 was determined through QIFIKIT analysis using 10 µg/mL anti-CD47 antibody (Clone: CC2C6). ABC for *n* = 3 experiments is shown as mean ± SD. (**C**) The expression level of SIRPα on leukocytes in blood from healthy donors was evaluated. MFI values of one representative donor are depicted as mean ± SD. At least three different donors were tested; ND, not detected; MFI, mean fluorescence intensity; ABC, antibody binding capacity.

CD47 blockade enhanced ADCC by neutrophils

To investigate whether the CD47/SIRPα axis suppresses neutrophil function in IgA-mediated killing, we tested three different methods that disrupt this myeloid checkpoint: 1) an engineered human SIRPα domain 1 protein fused to an inactivated IgG1 Fc, hereafter SIRPα fusion protein, 2) an anti-CD47 antibody (Clone: 2.3D11), or 3) CD47 knockout (**Supplemental Figure 1**) of the neuroblastoma cell line IMR32. ADCC induction by IgA in combination with either of these blocking strategies was tested in a ^{51}Cr release assay. IgA ch14.18 alone induced a modest killing efficiency of up to 25% with whole leukocytes as effector cells, but this was significantly improved by disrupting the CD47 axis, which increased killing by more than two-fold from 25% to over 50% (**Figure 2A**). All three strategies disrupting the CD47/SIRPα axis showed comparable results, but we chose to continue with the SIRPα fusion protein due to its versatility in binding both human and mouse CD47, making it convenient for both *in vitro* and *in vivo* studies.

When PBMCs were used as effector cells, we did not observe any improvement of either IgA or IgG ch14.18 upon CD47 blockade (**Figure 2B**), consistent with the fact that PBMC-mediated lysis is primarily driven by natural killer cells that lack SIRPα expression in our

hands (**Figure 1C**). In contrast, CD47 blockade enhanced both IgA and IgG ch14.18-induced lysis of all tested neuroblastoma cells when PMNs were used as effector cells (**Figure 2C**). IgA was more effective in inducing PMN-mediated ADCC than IgG. CD47 blockade improved both IgG-mediated and IgA-mediated lysis, but the combination with IgA resulted in the highest lysis. Using whole leukocytes as effector cells, we observed similar if not higher lysis mediated by IgA compared to IgG in the presence of the SIRPα fusion protein (**Figure 2D**). In this assay, IgA-mediated lysis was primarily induced by neutrophils, and to a lesser degree monocytes, while IgG-mediated lysis was induced by NK cells, neutrophils and possibly monocytes. Moreover, the fold increase in lysis as a result of CD47 blockade was higher for IgA compared to IgG (**Figure 2E**), showing that IgA can benefit more from CD47 checkpoint inhibition, likely due to the high SIRPα expression on neutrophils.

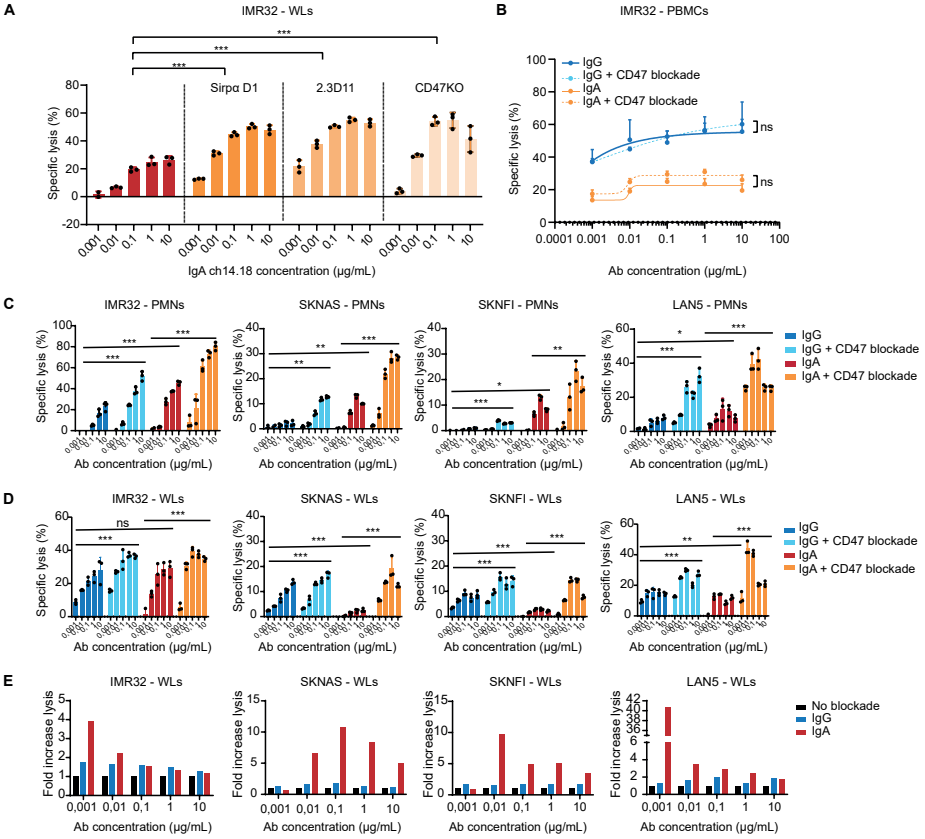

Figure 2 | CD47 blockade enhanced ADCC capacity by neutrophils. (**A**) The specific lysis of IMR32 (-CD47KO) cells was evaluated in a ^{51}Cr release assay using whole leukocytes. IgA ch14.18 was added in titrated concentrations in the presence or absence of 10 µg/mL CD47 blocking antibody (IgG1 LALAPG SIRPα or IgG1 LALAPG 2.3D11). (**B**) PBMC-mediated ADCC (E:T 100:1) of IMR32 cells was determined using IgG or IgA ch14.18 at different concentrations (0,001 µg/mL to 10 µg/mL) in the presence or absence of 10

µg/mL IgG1 LALAPG SIRPα. (**C**) Specific lysis of neuroblastoma cell lines was evaluated in an ADCC assay using PMNs (E:T 40:1) and (**D**) whole leukocytes using IgA or IgG ch14.18 with or without pre-incubation with 10 µg/mL IgG1 LALAPG SIRPα. (**E**) The fold increase in ADCC capacity upon CD47 blockade. In all ^{51}Cr release ADCC assays, the lysis was evaluated after a 4-hour incubation. PMNs, PBMCs, and whole leukocytes were isolated from healthy donors' blood. The mean ± SD specific lysis of a technical triplicate of a single donor is shown. Representative graphs of at least 3 independent experiments. ns > 0.05, * = $p < 0.05$, ** = $p < 0.01$ and *** = $p < 0.001$, determined by two-way ANOVA followed by Tukey's post-hoc test; PMNs, polymorphonuclear leukocytes; PBMCs, peripheral blood mononuclear cells; WLs, whole leukocytes; Ab, antibody.

IgG- and IgA-induced trogocytosis of neuroblastoma cells

To characterize the tumor cell killing mechanism induced by the combination of GD2-targeting antibodies and CD47 blockade, we used DiO-labeled neuroblastoma cells to identify the interaction between the tumor cells and PMNs. DiO, a lipophilic dye that incorporates into the cell membrane, allowed us to visualize the process of trogocytosis, whereby PMNs ingest pieces of the tumor cells (**Figure 3A**). We observed that PMNs gradually became DiO-positive over time after incubation with the tumor cells, indicating the uptake of tumor cell fragments by trogocytosis (**Figure 3B**). We observed increasing levels of trogocytosis over time in all experimental conditions. Surprisingly, IgG and IgA induced similar trogocytosis by PMNs against IMR32 cells. With SKNAS cells, IgA induced more trogocytosis compared to IgG. When combined with CD47, the trogocytosis capacity was increased for both IgG and IgA. This process ultimately led to tumor cell death, as shown in the ADCC assays (**Figure 2**).

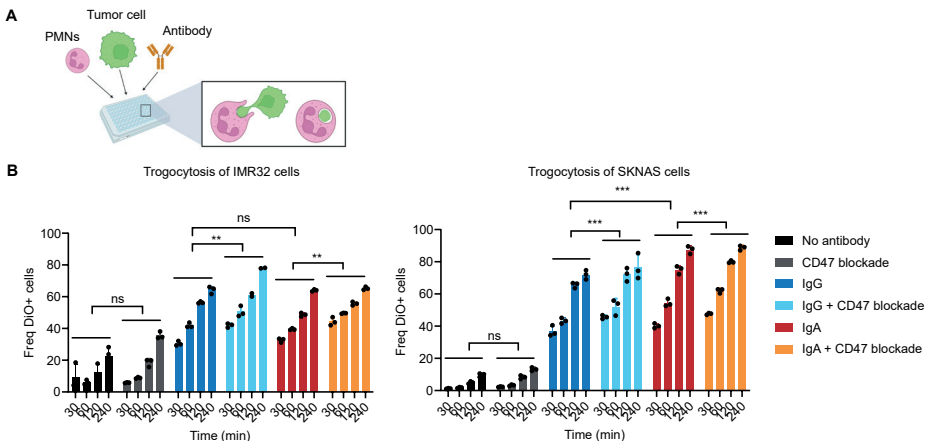

Figure 3 | IgG and IgA-induced trogocytosis of neuroblastoma cells. (**A**) Neuroblastoma cells were labeled with DiO and co-cultured with IgG or IgA ch14.18 and PMNs (E:T 10:1) for up to 4 hours. PMNs were isolated from healthy donors' blood. Trogocytosis was quantified by the frequency of uptake of DiO+ staining by $CD66b^+$ neutrophils. (**B**) Trogocytosis of IMR32 (left) and SKNAS (right) cells using 10 µg/mL IgG or IgA ch14.18 in the presence or absence of 10 µg/mL IgG1 LALAPG SIRPα was measured for up to 4 hours. The mean ± SD of a technical triplicate of a single donor is presented. One representative graph represents at least $n = 3$ independent experiments. The statistical analysis was performed using two-way ANOVA followed by Tukey's post-hoc test. ns > 0.05, * = $p < 0.05$, ** = $p < 0.01$ and *** = $p < 0.001$; PMNs, polymorphonuclear leukocytes; Freq, frequency.

IgA in combination with CD47 blockade induced swarming of neutrophils and killing of neuroblastoma cells

In the previous ^{51}Cr release ADCC assays (**Figure 2C, E**), SKNAS showed the highest resistance to IgA-induced lysis. Moreover, CD47 blockade on these cells resulted in the highest increase in IgA-mediated lysis by PMNs. Following that, we visualized the process of tumor cell killing by IgA-activated PMNs in a live imaging assay using widefield microscopy (**Figure 4A**). CFSE-labeled SKNAS neuroblastoma cells (green) were treated with IgA and SIRPα fusion protein, which efficiently induced tumor cell death by PMNs as marked by red TO-PRO-3 staining (**Figure 4B, Supplemental Video 1** (online)). Notably, the addition of CD47 blockade to IgA resulted in neutrophil swarming directed towards the tumor cells within a couple of minutes, characterized by increased migration (**Figure 4C**). The combination treatment showed tumor cell killing after 30 minutes of incubation, while IgA alone only induced minor cell death and CD47 block alone did not result in any cell death. These live cell imaging results emphasize the significance of disrupting the CD47/SIRPα axis, enabling strong activation of neutrophils by IgA. This is characterized by the swarming behavior, ultimately leading to the effective killing of tumor cells.

Enhanced IgA-mediated killing of neuroblastoma organoids by CD47 blockade.

In addition to ADCC assays using cell lines, we evaluated the efficacy of our approach in a more complex 3D model representative of neuroblastoma by performing killing assays with patient-derived organoids (AMC691B) (**Figure 5A**). Organoids provide a three-dimensional tumor model mimicking the bulkiness of solid tumors. AMC691B organoids have comparable GD2, but lower CD47 expression than IMR32 cells (**Figure 5B**). IgG-mediated cytotoxicity against AMC691B organoids was low when PMNs were used as effector cells, whereas IgA was more effective, achieving up to 40% lysis at the highest antibody concentration (**Figure 5C**). When PBMCs were used as effector cells, IgG killing was more effective, resulting in comparable lysis to IgA in a PMN ADCC. Consistent with our findings using cell lines, CD47 blockade enhanced antibody-mediated killing by PMNs of AMC691B organoids, but no improvement was observed with antibody-mediated killing by PBMCs. Moreover, among all tested conditions, the combination of IgA and CD47 blockade was the most effective in inducing tumor cell killing by PMNs, achieving lysis as high as 70%. Neutrophil cytotoxicity against the organoid was further assessed with live cell imaging (**Figure 5D, Supplemental Video 2** (online)). Addition of IgA rapidly induced killing of the organoid, however, efficient killing only lasted for 20 minutes (**Figure 5E**). When the CD47 checkpoint inhibitor was added, IgA cytotoxicity was more persistent and effective killing was observed for 90 minutes. Overall, the combination strategy induced more lysis of the tumor cells, which was accompanied by increased swarming of neutrophils, as also observed with SKNAS cells. Our observations that IgA ch14.18 with CD47 blockade can enhance immune responses even against 3D tumor structures further support the therapeutic potential of this combination strategy.

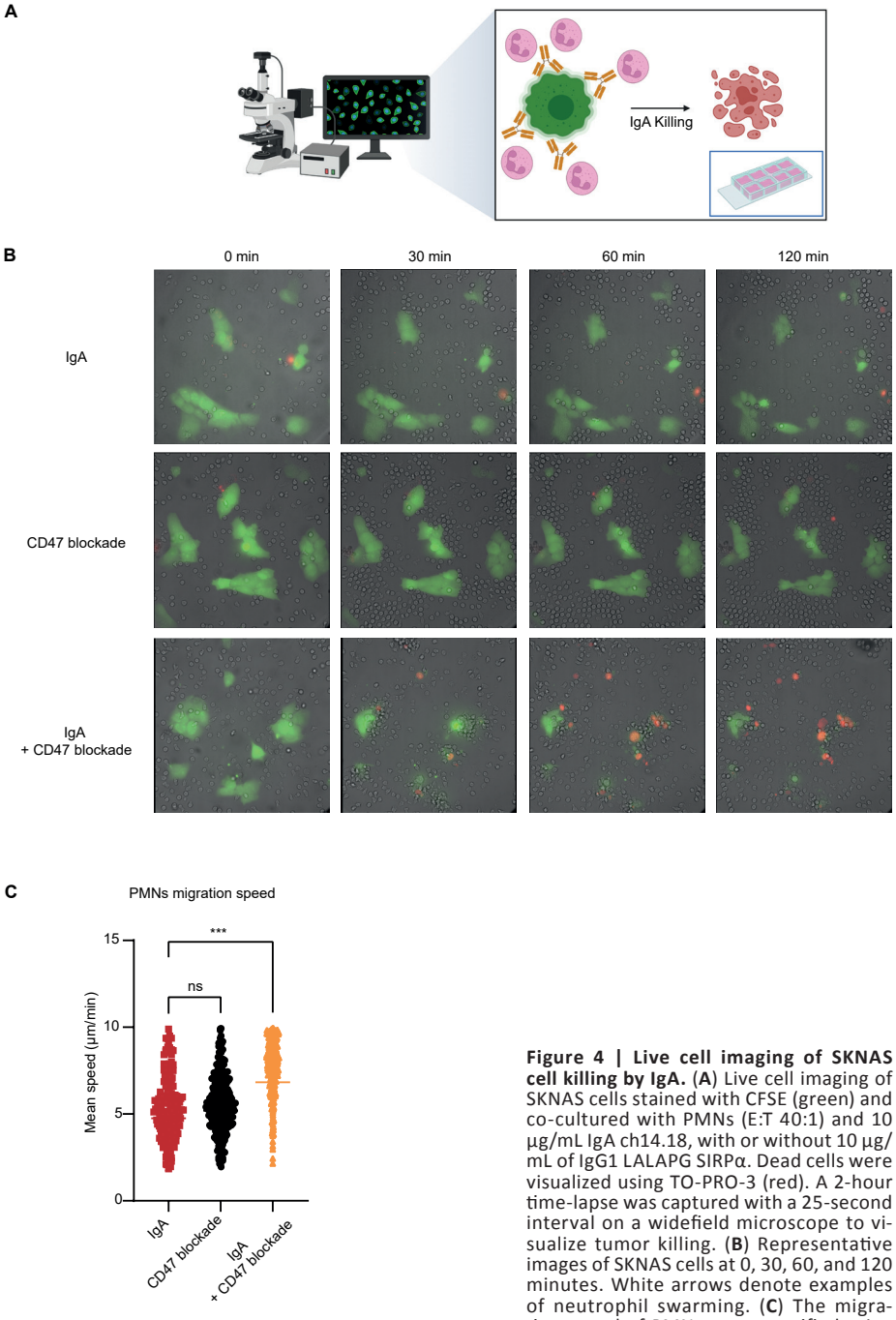

Figure 4 | Live cell imaging of SKNAS cell killing by IgA. (**A**) Live cell imaging of SKNAS cells stained with CFSE (green) and co-cultured with PMNs (E:T 40:1) and 10 µg/mL IgA ch14.18, with or without 10 µg/mL of IgG1 LALAPG SIRPα. Dead cells were visualized using TO-PRO-3 (red). A 2-hour time-lapse was captured with a 25-second interval on a widefield microscope to visualize tumor killing. (**B**) Representative images of SKNAS cells at 0, 30, 60, and 120 minutes. White arrows denote examples of neutrophil swarming. (**C**) The migration speed of PMNs was quantified using IMARIS analysis software. Statistical analysis was performed using a one-way ANOVA followed by Dunnett's post-hoc test, ns > 0.05 and *** = $p < 0.001$; PMNs, polymorphonuclear leukocytes; min, minutes.

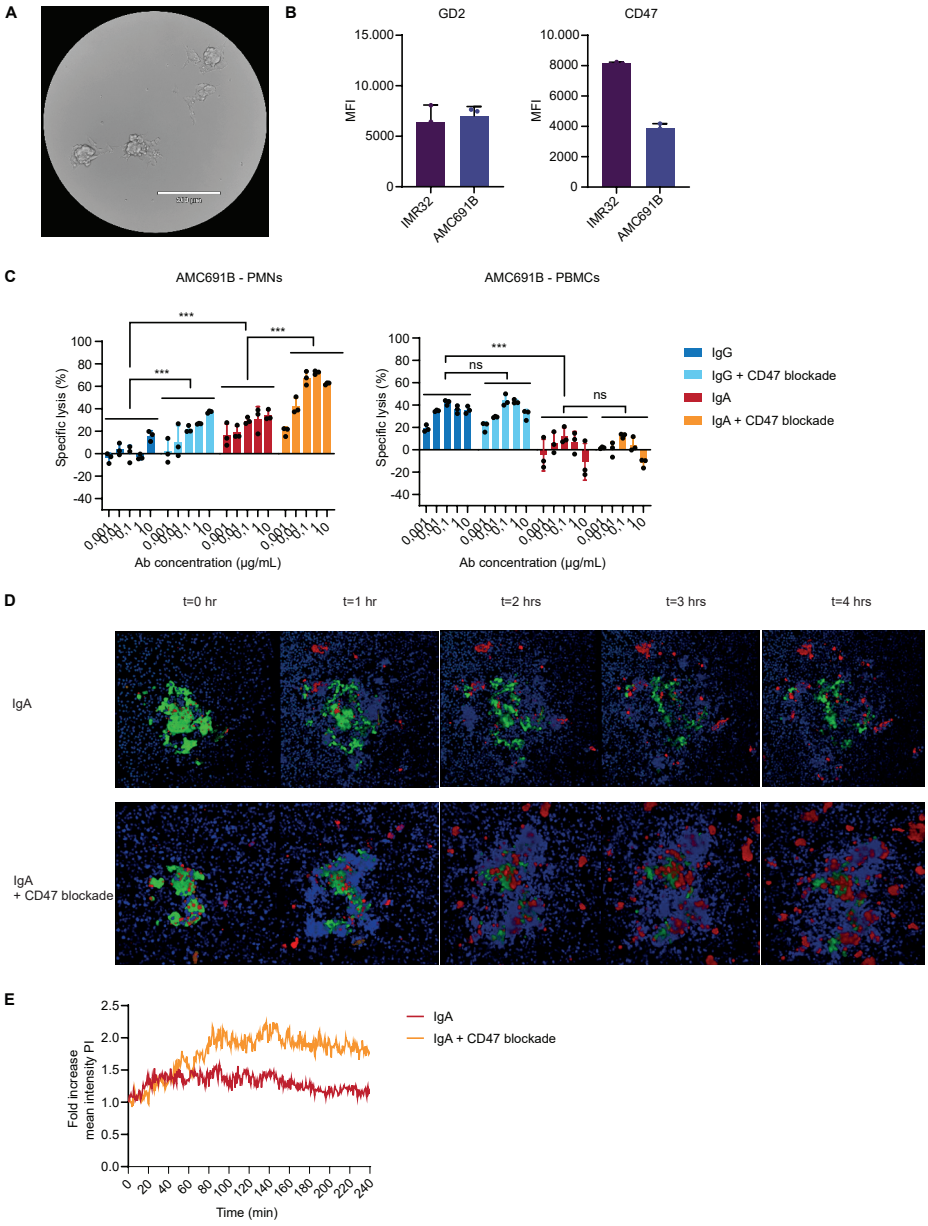

Figure 5 | Enhanced IgA-mediated killing of neuroblastoma organoids by CD47 blockade. (**A**) Representative image of neuroblastoma organoid line AMC691B three days after seeding. (**B**) Flow cytometric analysis of GD2 and CD47 expression levels on AMC691B compared to IMR32 cells. Expression was shown as MFI value ± SD. (**C**) Specific lysis of neuroblastoma organoids determined in a 4-hour luciferase-based ADCC assay using PMNs (E:T 40:1) or PBMCs (E:T 100:1) from healthy donors. A concentration range of IgA or IgG ch14.18 was added in the presence or absence of 10 µg/mL SIRPα fusion protein. The mean ± SD specific lysis of a technical triplicate of a single donor is shown. One representative graph represents at least n = 3 independent experiments. Significance levels are indicated as ns > 0.05, * = $p < 0.05$, ** = $p < 0.01$ and *** = $p < 0.001$, determined by two-way ANOVA followed by Tukey's post-hoc test. (**D**) Live cell imaging of AMC691B-GFP$^+$. Organoids were co-cultured with eFluor 450 (blue) stained PMNs (E:T 40:1). IgA-mediated lysis was recorded after addition of 10 µg/mL IgA ch14.18 and 10 µg/mL SIRPα fusion protein. Cell lysis

was visualized using Propidium Iodide (red). A 4-hour time-lapse was captured with a 32-second interval on the Stellaris 5 confocal microscope. Representative images at 0, 1, 2, 3 and 4 hours. (**E**) Cell lysis was determined as means of total Propidium Iodide intensity. Fold changes from the intensity measured at t= 0 hr are calculated and shown; MFI, mean fluorescence intensity; PMNs, polymorphonuclear leukocytes; PBMCs, peripheral blood mononuclear cells; Ab, antibody; hr, hour

Checkpoint inhibition prolonged survival of IMR32 tumor-bearing mice

To assess whether the enhanced tumor cell killing upon CD47 blockade could be translated into the *in vivo* setting, we performed a mouse experiment using CD89 transgenic SCID mice inoculated with IMR32 tumor cells. Previously, we could delay tumor outgrowth in this tumor model with a dose of 60 mg/kg of IgA ch14.18[21]. In the present experiment, we administered a suboptimal dose of 25 mg/kg IgA ch14.18, which previously failed to improve survival in tumor-bearing mice, and again it showed no observable differences in tumor outgrowth when compared to the solvent group (**Figure 6A**). In comparison, 5 mg/kg IgG slightly delayed tumor outgrowth in these mice. To explore the therapeutic potential of CD47 blockade in mice, we intraperitoneally administered the SIRPα fusion protein at a dose of 30 mg/kg. Combining 25 mg/kg IgA with CD47 blockade resulted in significant suppression of tumor outgrowth, which corresponded to significantly prolonged survival of the tumor-bearing mice (**Figure 6B**). Remarkably, by day 60, 50% of the mice in the IgA and CD47 blockade combination group were still alive, compared to survival rates of 0% and 27% in the IgG and IgG + CD47 blockade treatment groups, respectively. To assess the contribution of neutrophils to the IgA-mediated anti-tumor response, we depleted neutrophils in the IgA and CD47 blockade combination treatment group with i.p. injections of 100 µg mouse anti-Ly6G thrice a week (**Supplemental Figure 2B**). The therapeutic effect was completely lost when neutrophils were depleted, and tumor outgrowth matched that of the solvent control group, highlighting the essential role of neutrophils for IgA-mediated therapy.

Given the myeloid checkpoint inhibitor's high affinity for both human and mouse CD47, it effectively replicates the antibody sink challenge currently encountered by clinically applied anti-CD47 antibodies like magrolimab. Therefore, our model provides a realistic representation of the clinical setting. Despite the high affinity for CD47, administration of the SIRPα fusion protein alone did not show any therapeutic effect due to the Fc dead tail. Moreover, in an earlier pilot study, administration of the SIRPα fusion protein did not affect the red blood cell count in mice (**Supplemental Figure 2A**), which is vital since red blood cell-related toxicities are a major concern with CD47 checkpoint inhibitors.

To examine the effect of our treatment strategies on the immune cell composition we used flow cytometry to analyze both blood and the tumor. (**Figure 6C, D**) There were no significant differences in immune cell composition in the blood upon the different treatment regimens. In the tumor, IgA treatment slightly elevated the number of myeloid cells, albeit not significant. More notably, IgA in combination with CD47 blockade triggered a surge in the myeloid cell count in the tumor (**Figure 6D**). Neutrophil, monocyte, eosinophil

and macrophage counts were all significantly elevated, with increases ranging from 7-fold to 20-fold compared to PBS control. The majority of myeloid cells were neutrophils, which accounted for more than half of the total myeloid cell population. Our data implies that by disrupting the CD47/SIRPα axis, the immunosuppressive environment is relieved, allowing IgA to effectively activate and recruit neutrophils and other myeloid cells to the tumor.

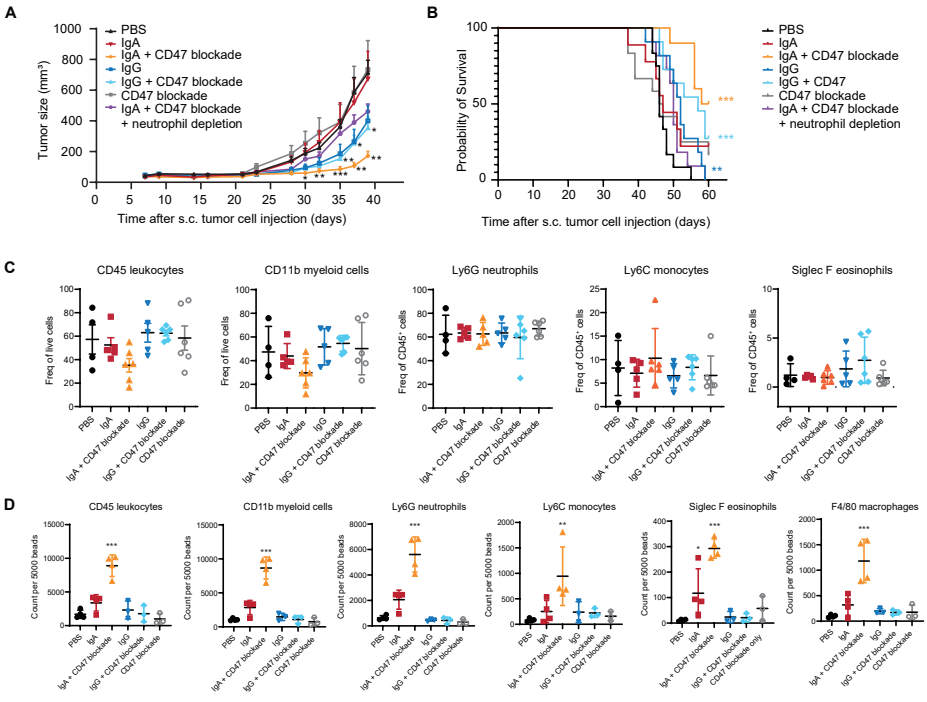

Figure 6 | Combination of IgA and CD47 blockade suppressed subcutaneous IMR32 tumor outgrowth in SCID mice. (**A**) Male SCID mice were subcutaneously injected with 2.5 million IMR32 tumor cells on day 0. Neutrophil depletion was started on day 2, and treatment began on day 4, following the treatment scheme outlined in the methods section. Tumor progression was monitored over time by measuring subcutaneous tumor dimensions with a caliper. Mice were euthanized once tumors reached a volume of 1500 mm^3. Tumor growth data is presented up to the day when the first mice reached the humane end-point, which occurred on day 39. Tumor sizes are shown as mean ± SEM of 9-13 mice per treatment group. * = $p < 0.05$, ** = $p < 0.01$ and *** = $p < 0.001$, using two-way ANOVA. Asterisks indicated significance compared to solvent control group. (**B**) Kaplan-Meier survival plot of IMR32 tumor-bearing mice. ** = $p < 0.01$ and *** = $p < 0.001$ as determined with the log-rank (Mantel-Cox) test. Asterisks indicated significance compared to solvent control group. (**C**) Immune cell composition in blood was obtained through a cheek puncture on day 16 and 33, and subsequently analyzed using flow cytometry. Data from both days are pooled and shown as mean ± SD of 4-6 mice per group. No significant differences were measured as analyzed with one-way ANOVA. (**D**) Immune cell composition within the tumor was assessed using flow cytometry at the humane end-point. Data is shown as mean ± SD of 3-4 mice per treatment group. * = $p < 0.05$, ** = $p < 0.01$ and *** = $p < 0.001$, using one-way ANOVA. Asterisks indicated significance compared to solvent control group; s.c., subcutaneous; Freq, frequency.

DISCUSSION

This study demonstrates a superior therapy combining IgA ch14.18 with CD47 blockade compared to the original IgG ch14.18 therapy in a preclinical neuroblastoma mouse model. The isotype switch of dinutuximab from IgG to IgA resulted in improved neutrophil recruitment and activation of ADCC. Despite effective neutrophil activation by IgA, neuroblastoma, like many other cancers, overexpresses checkpoint molecules as an evasion strategy. All of the neuroblastoma cell lines included here, which were originally derived from high-risk patients, showed CD47 overexpression. The interaction of CD47 on the tumor cells with SIRPα on neutrophils reduced the ADCC capacity as shown in chromium release assays. Notably, SKNAS and SKNFI, which had lower GD2 levels, benefited the most from the combination of IgA therapy and CD47 blockade. Presumably, the relatively weaker IgA-mediated neutrophil activation due to the lower antigen abundance made these cells more sensitive to CD47/SIRPα resistance. This emphasizes the importance of checkpoint inhibition, particularly in neuroblastoma patients with low GD2 expression[41,42].

Our findings demonstrated that disrupting the CD47/SIRPα axis enhanced neutrophil-mediated ADCC by both IgG and IgA. However, ADCC by PBMCs was not improved, probably due to the lack of SIRPα expression on NK cells, the most important effector cell of IgG antibody therapy in the PBMC fraction. Both IgG and IgA ch14.18 induced significant trogocytosis, which was further improved by CD47 blockade. Surprisingly, despite the similar frequency of trogocytosis induced by IgG and IgA, it did not translate to comparable ADCC by neutrophils, especially evident when targeting IMR32 cells. Specifically, IgG-mediated lysis of IMR32 cells by neutrophils was lower than that of IgA. These observations suggest that IgG-activated neutrophils like IgA-activated neutrophils take small bites of the cell membrane, however with insufficient strength to disrupt the membrane's integrity and induce cell death. This could be explained by weaker ITAM signaling as a result of the 1:1 stoichiometry observed with IgG versus the 1:2 stoichiometry observed with IgA. Consequently, IgA activates four ITAMs as opposed to the two ITAMs activated by IgG[19]. Furthermore, when trogocytosis does not result in induced cell death, the cell membrane may be repaired via repair mechanisms and antibody-bound antigen is shaved from the cell surface, as seen with CD20[43,44]. It would not be surprising if GD2 experienced something comparable, eventually leading to relapse in patients[41,45].

The combination of IgA ch14.18 and CD47 blockade significantly increased neutrophil cytotoxicity against neuroblastoma cell lines and organoids, which was underscored by data from our *in vivo* study. In our subcutaneous IMR32 tumor model, combining IgA therapy with CD47 blockade hampered tumor outgrowth, contributing to a significant improved survival rate of tumor-bearing mice. The therapeutic response was primarily attributed to the presence of neutrophils, as the depletion of neutrophils abolished the observed therapeutic effect. The combination of IgA therapy and CD47 blockade could

essentially maintain a positive feedback loop in which robust neutrophil activation triggers the release of cytokines and chemokines, which attract more immune cells directed against the tumor cells.

We used an in house produced CD47 blocking protein consisting of an engineered SIRPα D1 domain fused to IgG1 with LALAPG mutations to ablate Fc functions[33,46]. The SIRPα fusion is able to target human CD47 on the IMR32 tumor as well as the ubiquitously expressed mouse CD47 on healthy murine cells. Since CD47 is widely expressed on healthy cells, including red blood cells, CD47 antibodies are rapidly captured, requiring a high dose to achieve effective concentrations at the tumor site, which is known as the CD47 "sink" effect[47]. As a result, a relatively high dose of 30 mg/kg was required as determined by Kauder et al., 2018[48]. It's worth noting that, despite the high dose given to the mice, there was no decrease in red blood cell count, implying that including an Fc dead tail in the CD47 targeting strategy mitigated potential side effects such as anemia. Furthermore, CD47 block alone did not induce apparent differences in leukocyte composition in blood and within the tumor. To improve clinical application, the problems caused by the CD47 "sink" effect could be circumvented by using novel targeting strategies, such as bispecific antibodies or QPCTL inhibitors[24,49].

Although the addition of dinutuximab to the treatment protocol for high-risk neuroblastoma patients has improved 5-year survival rates, recurrences remain a challenge[13]. Dinutuximab has been shown to promote macrophage-induced phagocytosis as well as neutrophil-mediated ADCC[16,20,21,50,51]. However, the efficacy of IgG in activating myeloid cells remains suboptimal, leaving room for improvement. As a result, combination strategies involving CD47 blockade were investigated, leading to the initiation of a phase 1 clinical trial (NCT04751383) examining the use of dinutuximab and the CD47 monoclonal antibody, magrolimab, for pediatric neuroblastoma and osteosarcoma patients[26,27]. Unfortunately, due to unexpected toxicities, this trial had to be suspended. The specific clinical implications of this outcome are unknown. Alternatively, using IgA in combination with CD47 blockade was found to be more effective in our study in extending tumor-specific survival than using IgG alone or IgG in combination with CD47 blockade. This suggests that IgA therapy in combination with CD47 checkpoint inhibition may be a more effective treatment option than IgG.

Additionally, infiltration of myeloid cells is often associated with restricted lymphocyte responses. However, CD47 blockade indirectly modulates the adaptive immune system by enhancing cross-priming of cytotoxic T cells by myeloid cells[52]. Disruption of the CD47/SIRPα axis promotes tumor cell engulfment by dendritic cells and macrophages, followed by antigen presentation[48,53,54]. Moreover, there is emerging evidence suggesting that neutrophils might engage in antigen presentation upon taking up antigens through trogocytosis[52,55]. In essence, targeting the CD47/SIRPα axis serves as a bridge connecting the innate and adaptive immune system, facilitating the infiltration of immune cells into

the immunologically "cold" neuroblastoma. Furthermore, CD47 can directly hinder T cell activation by interacting with the checkpoint molecule thrombospondin-1 on T cells[56]. However, due to the limitations of our immunocompromised mouse model, we were unable to investigate the effect of CD47 blockade on the adaptive immune system. Exploring the effect of CD47 blockade on the adaptive immune response in immunocompetent mouse models would be a valuable direction for future research.

In conclusion, our study showed a promising interplay between IgA-mediated therapy and CD47 blockade, providing improved immune responses against neuroblastoma. Our results demonstrated that a combined strategy significantly improved immune cell infiltration in an otherwise immune-suppressed tumor microenvironment. *In vivo*, strong induction and activation of neutrophils by IgA restrained tumor growth and prolonged survival. The combination of IgA ch14.18 and CD47 blockade emerges as a potent therapeutic option for high-risk neuroblastoma patients.

Author contributions

GvT and JL contributed equally.

Funding

CC and JHMJ are funded by grant #11944 from The Dutch Cancer Society (KWF). MCS and MN are funded by Villa Joep (project 17 IgA and anti-GD2)

Competing interests

CC, MCS, MN, JHMJ, EMP, FH, JW, GT have nothing to disclose. JHWL is the scientific founder and shareholder of TigaTx.

Ethical approval

This study involves human participants and was approved by UMC Utrecht 07–125. Participants gave informed consent to participate in the study before taking part. All animal experiments followed international guidelines and were approved by the national Central Authority for Scientific Procedures on Animals (CCD) and the local experimental animal welfare organization (AVD115002016410).

REFERENCES

1. Smith, M. A. *et al.* Outcomes for children and adolescents with cancer: challenges for the twenty-first century. *J. Clin. Oncol. Off. J. Am. Soc. Clin. Oncol.* **28**, 2625–2634 (2010).

2. Aygun, N. Biological and Genetic Features of Neuroblastoma and Their Clinical Importance. *Curr. Pediatr. Rev.* **14**, 73–90 (2018).

3. Cheung, N.-K. V & Dyer, M. A. Neuroblastoma: developmental biology, cancer genomics and immunotherapy. *Nat. Rev. Cancer* **13**, 397–411 (2013).

4. Neuroblastoma - Childhood: Statistics. vol. 2020 (2019).

5. Chung, C. *et al.* Neuroblastoma. *Pediatr. Blood Cancer* **68 Suppl 2**, e28473 (2021).

6. Sait, S. & Modak, S. Anti-GD2 immunotherapy for neuroblastoma. *Expert Rev. Anticancer Ther.* **17**, 889–904 (2017).

7. Ladenstein, R. *et al.* Interleukin 2 with anti-GD2 antibody ch14.18/CHO (dinutuximab beta) in patients with high-risk neuroblastoma (HR-NBL1/SIOPEN): a multicentre, randomised, phase 3 trial. *Lancet Oncol.* **19**, 1617–1629 (2018).

8. Paret, C. *et al.* GD2 Expression in Medulloblastoma and Neuroblastoma for Personalized Immunotherapy: A Matter of Subtype. *Cancers (Basel).* **14**, (2022).

9. Morandi, F., Sabatini, F., Podestà, M. & Airoldi, I. Immunotherapeutic Strategies for Neuroblastoma: Present, Past and Future. *Vaccines* **9**, (2021).

10. Yu, A. L. *et al.* Anti-GD2 antibody with GM-CSF, interleukin-2, and isotretinoin for neuroblastoma. *N. Engl. J. Med.* **363**, 1324–1334 (2010).

11. Navid, F. *et al.* Phase I trial of a novel anti-GD2 monoclonal antibody, hu14.18K322A, designed to decrease toxicity in children with refractory or recurrent neuroblastoma. *J. Clin. Oncol.* **32**, 1445–1452 (2014).

12. Sorkin, L. S. *et al.* Anti-GD(2) with an FC point mutation reduces complement fixation and decreases antibody-induced allodynia. *Cancer Res.* **149**, 362–367 (2010).

13. Finklestein, J. Z. & Gilchrist, G. S. Recent advances in neuroblastoma. *Calif. Med.* **116**, 27–36 (1972).

14. London, W. B. *et al.* Clinical and biologic features predictive of survival after relapse of neuroblastoma: a report from the International Neuroblastoma Risk Group project. *J. Clin. Oncol. Off. J. Am. Soc. Clin. Oncol.* **29**, 3286–3292 (2011).

15. Rosales, C. Neutrophil: A Cell with Many Roles in Inflammation or Several Cell Types? *Front. Physiol.* **9**, 113 (2018).

16. Chen, R. L., Reynolds, C. P. & Seeger, R. C. Neutrophils are cytotoxic and growth-inhibiting for neuroblastoma cells with an anti-GD2 antibody but, without cytotoxicity, can be growth-stimulating. *Cancer Immunol. Immunother.* **48**, 603–612 (2000).

17. Cheung, N. K. *et al.* FCGR2A polymorphism is correlated with clinical outcome after immunotherapy of neuroblastoma with anti-GD2 antibody and granulocyte macrophage colony-stimulating factor. *J. Clin. Oncol.* **24**, 2885–2890 (2006).

18. Metelitsa, L. S. *et al.* Antidisialoganglioside/granulocyte macrophage-colony-stimulating factor fusion protein facilitates neutrophil antibody-dependent cellular cytotoxicity and depends on FcgammaRII (CD32) and Mac-1 (CD11b/CD18) for enhanced effector cell adhesion and azuroph. *Blood* **99**, 4166–4173 (2002).

19. Brandsma, A. M. *et al.* Potent Fc Receptor Signaling by IgA Leads to Superior Killing of Cancer Cells by Neutrophils Compared to IgG. *Front. Immunol.* **10**, 704 (2019).

20. Evers, M. *et al.* Anti-GD2 IgA kills tumors by neutrophils without antibody-associated pain in the preclinical treatment of high-risk neuroblastoma. *J. Immunother. cancer* **9**, (2021).

21. Stip, M. C. *et al.* IgA antibody immunotherapy targeting GD2 is effective in preclinical neuroblastoma models. *Jitc* **11**, (2023).

22. Voeller, J. *et al.* Combined innate and adaptive immunotherapy overcomes resistance of immunologically cold syngeneic murine neuroblastoma to checkpoint inhibition. *J. Immunother. cancer* **7**, 344 (2019).

23. Masih, K. E., Wei, J. S., Milewski, D. & Khan, J. Exploring and Targeting the Tumor Immune Microenvironment of Neuroblastoma. *J. Cell. Immunol.* **3**, 305–316 (2021).

24. Chan, C. *et al.* Targeting Myeloid Checkpoint Molecules in Combination With Antibody Therapy: A Novel Anti-Cancer Strategy With IgA Antibodies? *Front. Immunol.* **13**, 932155 (2022).

25. Jaiswal, S. *et al.* CD47 is upregulated on circulating hematopoietic stem cells and leukemia cells to avoid phagocytosis. *Cell* **138**, 271–285 (2009).

26. Theruvath, J. *et al.* Anti-GD2 synergizes with CD47 blockade to mediate tumor eradication. *Nat. Med.* **28**, 333–344 (2022).

27. Martínez-Sanz, P. *et al.* CD47-SIRPα Checkpoint Inhibition Enhances Neutrophil-Mediated Killing of Dinutuximab-Opsonized Neuroblastoma Cells. *Cancers (Basel).* **13**, (2021).

28. Willingham, S. B. *et al.* The CD47-signal regulatory protein alpha (SIRPa) interaction is a therapeutic target for human solid tumors. *Proc. Natl. Acad. Sci. U. S. A.* **109**, 6662–6667 (2012).

29. Matlung, H. L. *et al.* Neutrophils Kill Antibody-Opsonized Cancer Cells by Trogoptosis. *Cell Rep.* **23**, 3946-3959.e6 (2018).

30. Treffers, L. W. *et al.* IgA-Mediated Killing of Tumor Cells by Neutrophils Is Enhanced by CD47-SIRPα Checkpoint Inhibition. *Cancer Immunol. Res.* **8**, 120–130 (2020).

31. Baumann, N. *et al.* Myeloid checkpoint blockade improves killing of T-acute lymphoblastic leukemia cells by an IgA2 variant of daratumumab. *Front. Immunol.* **13**, 949140 (2022).

32. Evers, M. *et al.* The selection of variable regions affects effector mechanisms of IgA antibodies against CD20. *Blood Adv.* **5**, 3807–3820 (2021).

33. Chernyavska, M. *et al.* Evaluation of immunotherapies improving macrophage anti-tumor response using a microfluidic model. *Organs-on-a-Chip* **4**, 100019 (2022).

34. Meyer, S. *et al.* Improved in vivo anti-tumor effects of IgA-Her2 antibodies through half-life extension and serum exposure enhancement by FcRn targeting. *MAbs* **8**, 87–98 (2016).

35. Bate-Eya, L. T. *et al.* Newly-derived neuroblastoma cell lines propagated in serum-free media recapitulate the genotype and phenotype of primary neuroblastoma tumours. *Eur. J. Cancer* **50**, 628–637 (2014).

36. M Kholosy, W. *et al.* Neuroblastoma and DIPG Organoid Coculture System for Personalized Assessment of Novel Anticancer Immunotherapies. *J. Pers. Med.* **11**, (2021).

37. Brandsma, A. M. *et al.* Simultaneous Targeting of FcγRs and FcαRI Enhances Tumor Cell Killing. *Cancer Immunol. Res.* **3**, 1316–1324 (2015).

38. van Egmond, M. *et al.* Human immunoglobulin A receptor (FcalphaRI, CD89) function in transgenic mice requires both FcR gamma chain and CR3 (CD11b/CD18). *Blood* **93**, 4387–4394 (1999).

39. Stip, M. C. *et al.* Characterization of human Fc alpha receptor transgenic mice: comparison of CD89 expression and antibody-dependent tumor killing between mouse strains. *Cancer Immunol. Immunother.* (2023) doi:10.1007/s00262-023-03478-4.

40. Olofsen, P. A. *et al.* Effective, Long-Term, Neutrophil Depletion Using a Murinized Anti-Ly-6G 1A8 Antibody. *Cells* **11**, (2022).

41. Schumacher-Kuckelkorn, R. *et al.* Lack of immunocytological GD2 expression on neuroblastoma cells in bone marrow at diagnosis, during treatment, and at recurrence. *Pediatr. Blood Cancer* **64**, 46–56 (2017).

42. Schumacher-Kuckelkorn, R., Hero, B., Ernestus, K. & Berthold, F. Lacking immunocytological GD2 expression in neuroblastoma: report of 3 cases. *Pediatr. Blood Cancer* **45**, 195–201 (2005).

43. van Rees, D. J. *et al.* Cancer cells resist antibody-mediated destruction by neutrophils through activation of the exocyst complex. *J. Immunother. cancer* **10**, (2022).

44. Beum, P. V *et al.* Loss of CD20 and bound CD20 antibody from opsonized B cells occurs more rapidly because of trogocytosis mediated by Fc receptor-expressing effector cells than direct internalization by the B cells. *J. Immunol.* **187**, 3438–3447 (2011).

45. Tibbetts, R. *et al.* Anti-disialoganglioside antibody internalization by neuroblastoma cells as a mechanism of immunotherapy resistance. *Cancer Immunol. Immunother.* **71**, 153–164 (2022).

46. Weiskopf, K. *et al.* Engineered SIRPα variants as immunotherapeutic adjuvants to anticancer antibodies. *Science* **341**, 88–91 (2013).

47. Bouwstra, R., van Meerten, T. & Bremer, E. CD47-SIRPα blocking-based immunotherapy: Current and prospective therapeutic strategies. *Clin. Transl. Med.* **12**, e943 (2022).

48. Kauder, S. E. *et al.* ALX148 blocks CD47 and enhances innate and adaptive antitumor immunity with a favorable safety profile. *PLoS One* **13**, e0201832 (2018).

49. Logtenberg, M. E. W. *et al.* Glutaminyl cyclase is an enzymatic modifier of the CD47- SIRPα axis and a target for cancer immunotherapy. *Nat. Med.* **25**, 612–619 (2019).

50. Michon, J. *et al.* In vitro killing of neuroblastoma cells by neutrophils derived from granulocyte colony-stimulating factor-treated cancer patients using an anti-disialoganglioside/anti-Fc gamma RI bispecific antibody. *Blood* **86**, 1124–1130 (1995).

51. Chan, G. C.-F. & Chan, C. M. Anti-GD2 Directed Immunotherapy for High-Risk and Metastatic Neuroblastoma. *Biomolecules* **12**, (2022).

52. van Duijn, A., Van der Burg, S. H. & Scheeren, F. A. CD47/SIRPα axis: bridging innate and adaptive immunity. *J. Immunother. cancer* **10**, (2022).

53. Liu, X. *et al.* CD47 blockade triggers T cell-mediated destruction of immunogenic tumors. *Nat. Med.* **21**, 1209–1215 (2015).

54. Xu, L., Wang, S., Li, J. & Li, B. CD47/SIRPα blocking enhances CD19/CD3-bispecific T cell engager antibody-mediated lysis of B cell malignancies. *Biochem. Biophys. Res. Commun.* **509**, 739–745 (2019).

55. Lin, A. & Loré, K. Granulocytes: New Members of the Antigen-Presenting Cell Family. *Front. Immunol.* **8**, 1781 (2017).

56. Schwartz, A. L. *et al.* Antisense targeting of CD47 enhances human cytotoxic T-cell activity and increases survival of mice bearing B16 melanoma when combined with anti-CTLA4 and tumor irradiation. *Cancer Immunol. Immunother.* **68**, 1805–1817 (2019).

SUPPLEMENTAL INFORMATION

Target	Fluorophore	Clone	Manufacturer	Dilution
CD45	BV510	30-F11	Biolegend	1:30
CD11b	FITC	M1/70	Pharmingen	1:50
Ly6C	PerCP-Cy5.5	HK1.4	Biolegend	1:100
Ly6G/C	PE-Cy7	RB6-8C5	Pharmingen	1:200
Siglec F (CD170)	BV421	S17007L	Biolegend	1:50
hCD89	APC	A59	Biolegend	1:50
SIRPα (CD172)	PE	P84	Thermo Fisher	1:100

Table S1 | Antibody panel for blood analysis

Target	Fluorophore	Clone	Manufacturer	Dilution
CD45	BV510	30-F11	Biolegend	1:200
CD11b	FITC	M1/70	Pharmingen	1:50
Ly6C	APC-Cy7	HK1.4	Biolegend	1:200
Ly6G/C	PE-Cy7	RB6-8C5	Pharmingen	1:400
Siglec F (CD170)	BV421	S17007L	Biolegend	1:50
F4/80	BV785	BM8	Biolegend	1:50
hCD89	APC	A59	Biolegend	1:50
SIRPα (CD172)	PE	P84	Thermo Fisher	1:100
Live/dead marker 7-AAD	-	-	Pharmingen	1:20

Table S2 | Antibody panel for tumor analysis

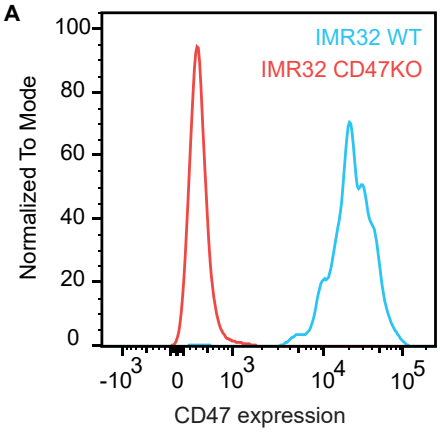

Figure S1 | CD47 expression on IMR32 WT and IMR32 CD47 KO cells. (**A**) Histogram depicting the expression levels of CD47 as measured by flow cytometry; WT, wildtype; KO, knockout

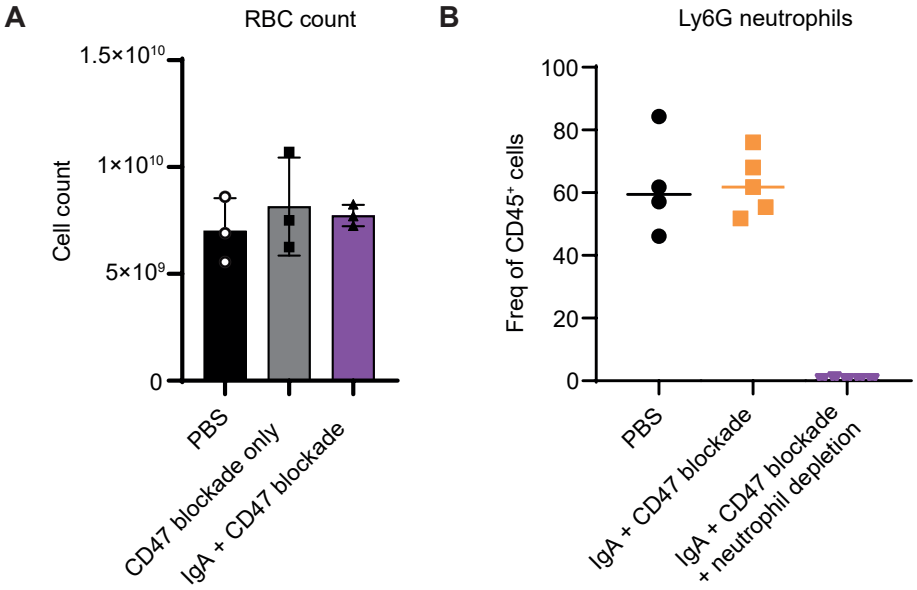

Figure S2 | Red blood cell and neutrophil count in tumor-bearing mice. (**A**) Blood samples were collected through a cheek puncture from C57Bl/6 mice that received different treatments: CD47 blockade (30 mg/kg), a combination treatment of IgA (10 mg/kg) and CD47 blockade (30 mg/kg), and a solvent control. The red blood cells count was measured in the collected blood samples. (**B**) Neutrophils were depleted through i.p. injections of mouse anti-Ly6G (100 µg), administered three times a week starting from day 2 of the experiment. Blood samples were collected via cheek puncture on day 16 and day 33. The presence of neutrophils in the obtained blood samples was measured by flow cytometry. The data from both days were combined resulting in a total of 4-6 mice per group; Freq, frequency; RBC, red blood cell


7

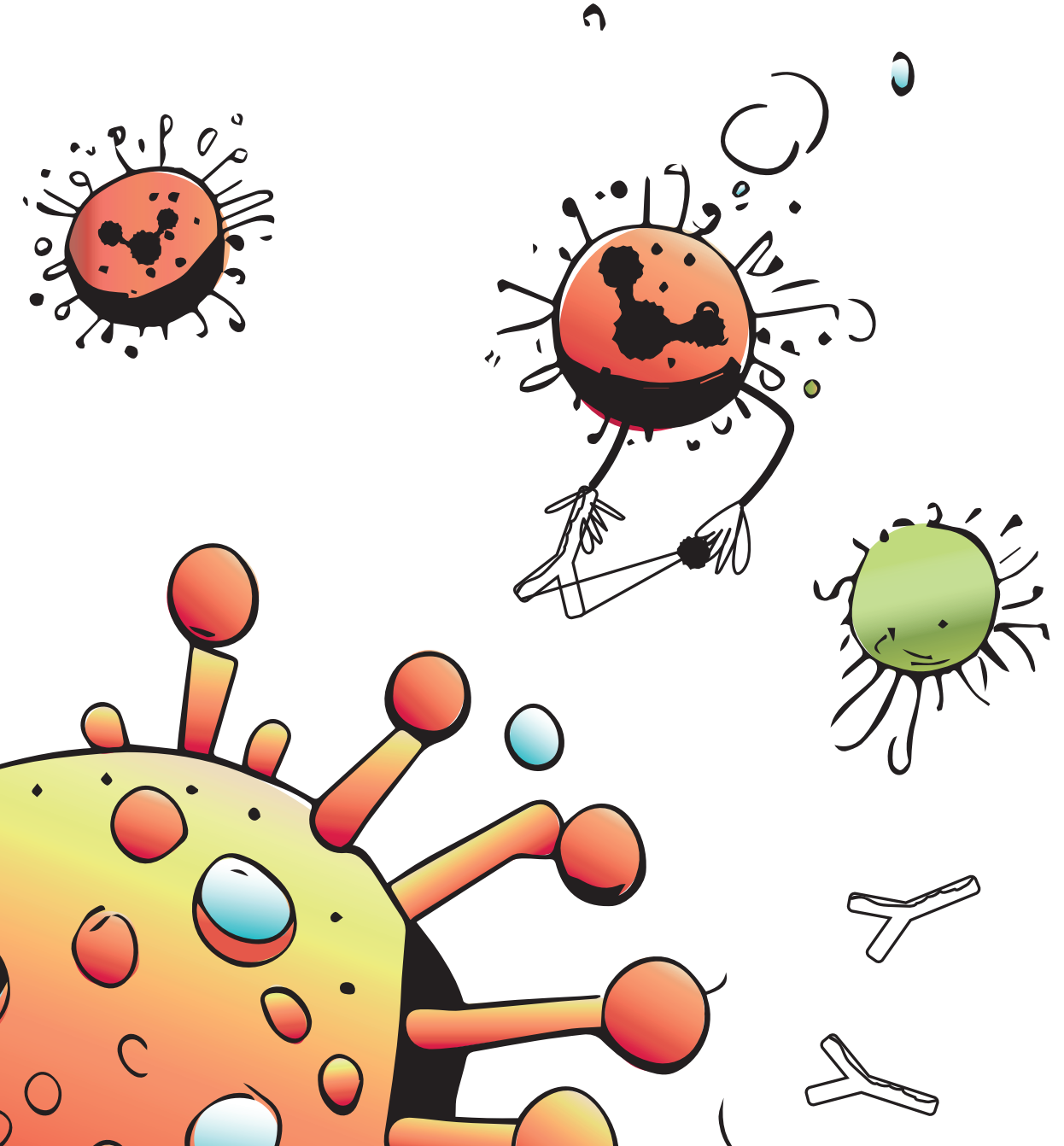

Chapter 8.

General discussion

IgA antibody therapy emerges as a promising therapeutic for cancer, displaying several advantages compared to IgG antibody therapy. Research in this thesis brings the application of IgA anti-GD2 antibody therapy for neuroblastoma to the brink of clinical application. However, there are some final steps to be taken and small improvements or combination strategies to be further developed. Additionally, preclinical evidence for efficacy of IgA antibody therapy could be solidified by evaluating IgA in more different (animal) models, since there are some limitations to the CD89 transgenic mice used in our studies.

POSSIBILITIES AND LIMITATIONS OF THE CD89 TRANSGENIC MOUSE MODEL

The CD89 transgenic mice generated in our laboratory are indispensable for evaluating the efficacy and underlying mechanisms of IgA antibody therapy. Investigations employing this murine model have yielded novel insights in FcαRI biology, such as the release of intracellular free calcium levels upon FcαRI crosslinking and the requirement of Mac-1 (CD11b in complex with CD18) for secretory IgA binding to FcαRI[1,2]. Additionally, in this thesis we observe that CD89 expression is upregulated in tumor-bearing mice, both within the systemic circulation and, more pronouncedly, in the tumor microenvironment (TME). Nevertheless, there are several noteworthy limitations inherent to the CD89 transgenic mouse model, when considering its translational relevance to humans.

While we observed that our model expressing CD89 under the endogenous human promoter most closely recapitulates the human expression pattern compared to all CD89 transgenic mouse models available (**Chapter 2**), one dissimilarity persists. Specifically, CD89 expression is absent on monocytes of healthy mice, though it can be slightly induced under inflammatory conditions. This contrasts with human monocytes, wherein CD89 is expressed constitutively. Laboratory mice are kept under sterile conditions, whereas humans are constantly challenged by pathogens. Possibly, infections induce CD89 expression on monocytes, explaining the lack of CD89 in unstimulated transgenic mice.

Secondly, in our CD89 transgenic mice it is difficult to compare the efficacy of IgA to IgG antibody therapy, which currently serves as the gold standard in the clinic. The extremely short half-life of human IgA in mice – merely 15h – stands in stark contrast to its half-life in humans, spanning 4 to 7 days[3–5]. Though the half-life of human monoclonal IgG antibodies in mice is shorter as well – measuring 4 to 9 days in mice and 21 days in humans – the relative difference is much smaller (**Table 1**)[6–9]. Therefore, in experimental studies we need substantially higher quantities of IgA to discern treatment benefits, as was the case in the neuroblastoma mouse models in **Chapter 6**. Currently, we strive to compare IgA and IgG based on similar serum concentrations, meaning we have to dose IgA and IgG differently, which remains challenging. The relatively long half-life of human IgG1 in

mice can be partially explained by its artificially high binding affinity for mouse FcRn in comparison to mouse IgG[10]. Furthermore, it is noteworthy that the human and murine IgG antibody isotypes and Fcγ receptor systems are incongruent as well. Finally, disparities in the cellular expression pattern of FcγRs further limit the translational value of mouse models for studying human IgG[11].

	IgA	IgG
Human	4-7 days	21 days
Mouse	15h	4-9 days
Relative difference	6.4-11.2-fold	2.33-5.25-fold

Table 1 | Difference of half-life of human IgA and IgG antibodies in mice and men.

In **Chapters 2 and 6** we describe that the primary effector cells of IgA therapy in humans, neutrophils, are not effective in mice in performing ADCC upon IgA stimulation. Moreover, neutrophils make up only ~10% of circulating leukocytes in mice, whereas this proportion ranges from 50 to 70% in humans. IgA-mediated ADCC was even poorer in neutrophils derived from immunocompromised mice (SCID and NSG), though we often need these mice to study IgA in human xenograft tumor models.

While the CD89 transgenic mice have proven to be an essential model for our research, it is prudent to consider alternative *in vivo* models in the future, either as a supplementary resource or as a potential replacement. First of all, mice with a comprehensive human Fc receptor repertoire could be used, to be able to properly compare IgA and IgG. Presently, such models have been established for human FcγRs, but these mice do not yet co-express human FcRn or FcαRI[12]. Consequently, a crossbreeding step with human FcRn transgenic mice (for example with the mouse model described by Low et al.[13]) and with our own CD89 transgenic mice would be required. However, a more optimal and easily accessible option is to use MISTRG mice (M-CSF$^{h/h}$ IL-3/GM-CSF$^{h/h}$ hSIRPAtg TPO$^{h/h}$ Rag2$^{-/-}$ IL2Rγ$^{-/-}$). These highly immunodeficient mice are capable of supporting the engraftment of human CD34^{+} hematopoietic stem cells, fostering the development of a fully human immune system including functional neutrophils[14]. This model effectively resolves the problem of inert mouse neutrophils and additionally, the reconstituted immune cells express human FcRs. An additional advantage of this model is that tumor outgrowth rate and immune cell infiltration more faithfully recapitulate human tumors[15].

Other relevant species to study IgA immunotherapy include rats and non-human primates (NHP). Rats and NHP are commonly used for preclinical studies and both inherently express an FcαRI[16,17]. In **Chapter 6** we observe that the FcαRI expression pattern is very similar between humans and NHP. Neutrophils from Cynomolgus monkeys demonstrated IgA-mediated ADCC, indicating cross-reactivity of their FcαRI with human IgA. Moreover,

neutrophils constitute ~50% of circulating leukocytes in NHP, mirroring the composition in humans[18,19]. NHP models will be especially valuable in preclinical safety and dosing studies, as a final step before introducing IgA immunotherapy in the clinic.

THE APPLICATION OF IGA ANTIBODY THERAPY IN NEUROBLASTOMA

In **Chapter 4**, we highlight the critical importance of targeting myeloid cells in neuroblastoma. Especially MDSC and TAMs play a pivotal role in establishing a complex immunosuppressive milieu within the TME, thereby inhibiting the adaptive immune system. This is considered one of the reasons that T cell-based therapies, such as CAR T cells and PD1/PD-L1 checkpoint inhibitors, have failed to be effective against neuroblastoma. For example, Tumino et al. demonstrated that during GD2.CAR T-cell therapy in neuroblastoma circulating PMN-MDSC increase, which mediate resistance to the CAR T cell therapy. In *in vitro* and *in vivo* models for pediatric sarcomas, Long and colleagues showed that administration of ATRA eradicated M-MDSCs and attenuated the suppressive capabilities of PMN-MDSCs, thus improving the efficacy of GD2.CAR T-cell therapy[20]. These studies suggest that the reduction of immunosuppression by myeloid cells is a prerequisite for T cell reactivation in neuroblastoma.

At the moment, the majority of strategies targeting myeloid cells in cancer are focusing on depleting these cells from the TME or on reprogramming their functional characteristics. However, with IgA antibody therapy, we seek to not only neutralize the suppressive effects exerted by myeloid cells but to harness their potential to combat the tumor as well. By doing so, the therapy has a two-pronged approach: it abrogates the immunosuppressive activity of myeloid cells and makes them attack the tumor.

IgA antibody therapy could be effective in a broad spectrum of cancer types, but especially for neuroblastoma IgA appears to be suitable. First of all, we and others have observed that a high target density is improving neutrophil-mediated tumor cell killing[21]. Due to the nature of GD2 – being a glycolipid rather than a protein – it can be extremely highly expressed. In neuroblastoma, average GD2 expression has been approximated at 5 to 10 million molecules per cell[22,23]. Expression of GD2 in neuroblastoma is more than a 100-fold greater compared to other conventional antibody targets in cancer, such as HER2 or CD20[24,25]. This high target density in neuroblastoma could be beneficial for IgA therapy efficacy.

Secondly, the timing of immunotherapy within the existing treatment regimen in neuroblastoma aligns particularly favorably with the mechanism of action of IgA antibody therapy. Currently, immunotherapy is administered shortly after tandem HSCT and at that moment only 23% of the NK cell population has recovered[26]. Additionally, the phenotype

of recovered NK cells is different, marked by a decreased ratio of cytotoxic ($CD56^{dim}CD16^{+}$) to cytokine-releasing NK cells ($CD56^{bright}CD16^{+/-}$) at the start of immunotherapy. Given that cytotoxic NK cells are the most important effector cells of IgG anti-GD2 therapy, it can be expected that therapeutic efficacy is suboptimal. As evident in **Chapter 6**, the efficacy of IgG1 ch14.18 is indeed compromised when employing effector cells derived from neuroblastoma patients, in contrast to effector cells from healthy donors. On the other hand, up to 79% of the neutrophil numbers are recovered from HSCT by the onset of immunotherapy and the efficacy of IgA3.0 ch14.18 is not much reduced with patient-derived effector cells (neutrophils)[26]. Since most *in vitro* experiments in this thesis were performed with healthy donor effector cells and fixed numbers of effector cells, we might be underestimating the therapeutic potential of IgA3.0 relative to IgG1 ch14.18.

Finally, we observe in **Chapter 5** that changing the isotype of the ch14.18 antibody from IgG to IgA alleviates neuropathic pain in mice. Since GD2 is not only expressed on neuroblastoma cells, but on sensory nerve fibers as well, IgG1 ch14.18 activates the complement system via its C1q binding domain. Eventually this leads to the generation of anaphylatoxins, such as C5a, which subsequently activates sensory neurons and elicits the sensation of pain (reviewed in [27]). We have previously noted that the K322A mutation in IgG1 ch14.18 abolished the induction of pain in rats[28], although it still provokes neuropathic pain in patients. We postulated that this mutation might not entirely disrupt the C1q binding, leading to residual complement activation. Results described in **Chapter 5** confirm this, showing *in vitro* that with IgG1 ch14.18 K322A C5a induction is not fully abrogated. This aligns with the findings from Sorkin et al., who reported that systemic administration of hu14.18 K322A in rats reduced pain as measured by the Von Frey test, but not completely abrogated it[28]. As anticipated, IgA ch14.18 did not induce any C5a production *in vitro* and therefore neuropathic pain in mice was absent. Moreover, no complement deposition on mouse sciatic nerves was observed after IgA injection *in vivo*. Collectively, this body of evidence points suggests that IgA anti-GD2 antibodies will not induce pain in neuroblastoma patients, which would be a significant improvement compared to IgG anti-GD2 antibodies.

TACKLING LIMITATIONS OF IGA ANTIBODY THERAPY WITH IGA3.0

The shorter half-life of IgA compared to IgG antibodies has been acknowledged as a potential limitation for IgA antibody therapy. However, when placing this in the context of other clinically approved drugs, the half-life of IgA (4-7 days) is still relatively long. This characteristic has advantages as well, as it affords greater flexibility in adapting dosing regimens during the course of treatment or in response to adverse patient reactions.

In **Chapter 6** we improve the half-life of IgA ch14.18 by introducing mutations resulting in the IgA3.0 molecule. In murine models, IgA3.0 ch14.18 exhibited a significant longer half-life, potentially attributed to reduced degradation by the ASGPR and mannose receptor. While the precise translation of this prolonged half-life from mice to humans remains uncharted, it is conceivable that the half-life of IgA3.0 will be longer in humans as well. Clinical studies will have to be performed to reveal the exact half-life of IgA3.0 in humans. If it turns out that the half-life of IgA3.0 is still not satisfactory in patients, there are strategies described previously to extend the half-life of IgA, such as the addition of an albumin-binding domain[29]. The addition of an albumin-binding domain facilitates the recycling of IgA through the FcRn, extending its half-life up to 4 days in mice.

Another limitation of IgA, its extensive glycosylation, has been effectively mitigated through the IgA3.0 design, which eliminates 3 out of 4 *N*-glycosylation sites. Studies investigating IgA glycosylation have largely indicated that the removal of *N*-glycans (either enzymatic or using mutations) does not impact FcαRI binding[30,31]. However, Lombana and colleagues observed a loss off binding to FcαRI upon complete removal of all *N*-glycosylation sites[32]. Notably, they only evaluated polymeric IgA, which could explain the different outcome of these studies. In our lab, we recently created the IgA4.0 molecule, which is similar to IgA3.0, but featuring an additional mutation to remove the final glycosylation site (**Figure 1**). Preliminary data suggests that IgA4.0 behaves very similar compared to IgA3.0 and maintains its affinity for FcαRI (unpublished data). These conflicting results underscore that the field studying glycosylation of IgA is still quite immature, especially compared to the knowledge that is available about IgG glycosylation. For example, most studies in IgA glycosylation focus on the absence or presence of glycosylation in general, with limited exploration into the impact of specific glycosylation patterns on Fc binding, such as the presence of terminal sialylation, uncapped mannoses or galactoses and core fucosylation.

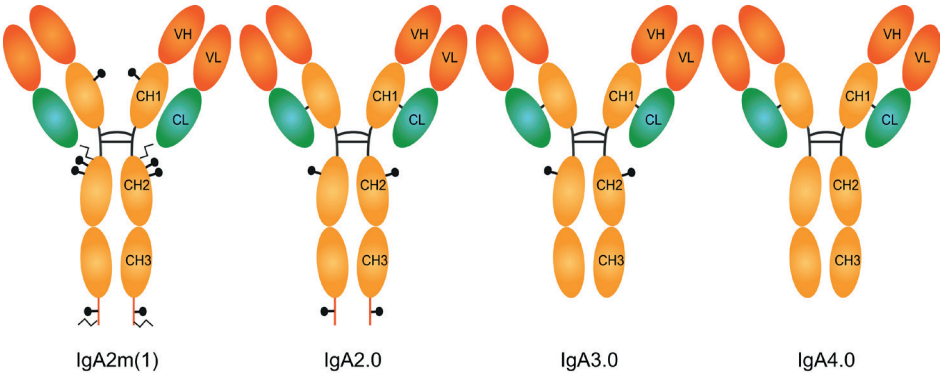

Figure 1 | Engineered IgA formats IgA2.0, IgA3.0 and IgA4.0 are based the naturally occurring IgA2m(1) allotype.

Interestingly, in **Chapter 6** we document that the Fc tail of IgA3.0 has a modestly higher affinity for FcαRI compared to IgA1 and IgA2 *in vitro*, which was never reported for IgA2.0 (**Figure 1**)[33]. Therefore, the increased affinity can likely be attributed to the removal of the glycan structure at N135 or to the removal of the whole tail piece. IgA antibodies produced in plants lacking the enzymes for *N*-glycan synthesis, do not exhibit increased Fc tail affinity for FcαRI[34,35]. This suggests that deletion of the entire tail piece is underlying the small increase in Fc affinity. It will be interesting to elucidate this further in future research.
In the same chapter we observe a divergence in the glycosylation pattern of IgA3.0 ch14.18, when produced in CHO or HEK293F platforms. IgA3.0 ch14.18 synthesized in HEK293F cells harboured a more mature, terminally sialylated glycosylation pattern at the N20 site compared to IgA3.0 ch14.18 produced in CHO cells, which translated into a small increase of half-life in mice. However, in general the CHO system is considered to have a higher sialylation capacity then HEK293F[36,37]. Currently, CHO cells are the predominant choice for the production of clinical-grade antibodies and are used for generating 60% of all biotherapeutics. Additionally, the CHO system is characterised extensively and generally has higher protein yields compared to HEK293F (reviewed in [37]). Before proceeding to clinical batch production, the choice of production system must be well considered and investigated first. Even the production of IgA in bacteria such as *E. Coli* or yeast systems could be considered, since thus far we have not observed reduced function of completely unglycosylated IgA (unpublished data). Such platforms would be cheaper and faster in production compared to mammalian cells and therefore reduce healthcare costs.

PROMISING COMBINATION THERAPIES FOR IGA ANTIBODY THERAPY

In **Chapter 7** we explore a combination therapy with IgA for the treatment of neuroblastoma, by blocking the CD47/SIRPα axis and administering IgA3.0 ch14.18 simultaneously. In this proof-of-concept study, we used an engineered human SIRPα D1 domain fused to IgG1 LALAPG to inhibit the CD47/ SIRPα axis. The human SIRPα D1 domain was engineered as described by Weiskopf et al to enhance its affinity for both mouse and human CD47[38,39]. Though beforehand we had concerns regarding on-target toxicity of the SIRPα fusion protein, we did not observe any toxicity in our mouse models thus far. However, this molecule still won't be suitable for clinical application, due to the widely distributed expression of CD47 on healthy cells acting as a large antibody sink.
An elegant strategy to bring this combination therapy to the clinic, would be to develop a bispecific antibody recognizing both GD2 and CD47, combining a high-affinity arm for GD2 and a low affinity arm for CD47. In this way, the antibody only binds CD47 upon recognition of GD2, thus circumventing the sink effect. Recently, a new heterodimeric

IgA Fc platform was developed by Heinkel and colleagues, which could be applied to generate this bispecific antibody[40]. Other strategies targeting the CD47/SIRPα axis that are already in development are SIRPα blocking antibodies (NCT04653142 and NCT05168202) and inhibitors of glutaminyl-peptide cyclotransferase-like protein (QPCTL), an enzyme crucially involved in the recognition of CD47 by SIRPα[41–43]. Combinations of these molecules with IgA anti-GD2 antibody therapy could be considered as well.

Given that IgA exerts its therapeutic effect mainly via myeloid cells, a strong rationale emerges for the synergistic combination of IgA with other myeloid-targeting drugs. Concomitant targeting of other myeloid checkpoint inhibitors, such as the Siglec receptor family or leukocyte immunoglobulin-like receptor subfamily B 1 and 2 (LILRB1/2) could invigorate IgA antibody therapy (reviewed in [44]). Furthermore, IgA could be combined with radiotherapy. As observed in many types of cancer, radiotherapy increases neutrophil and MDSC infiltration in the TME[45–47] and therapies targeting neutrophils or MDSC after radiotherapy can enhance its efficacy[48]. Thus, radiotherapy followed by IgA antibody therapy could prove an excellent combination strategy for the treatment of neuroblastoma.

Another strategy previously explored is the simultaneous use of both IgA and IgG antibodies[49]. Combining IgA and IgG amplifies cytotoxicity, but only when different targets are engaged. In the context of neuroblastoma, IgA antibodies targeting GD2 could be paired with IgG antibodies targeting B7-H3, a commonly expressed marker on neuroblastoma cells[50,51]. Others have attempted to engineer hybrid molecules combining both IgA and IgG effector functions within a single antibody construct[52,53]. Though these molecules indeed have multiple effector functions, their therapeutic efficacy did not surpass that of conventional IgG or IgA antibodies alone. Similarly, IgA and IgE antibodies could be combined. IgE antibodies are particularly effective in activating macrophages and an initial phase I clinical trial has been completed (NCT02546921)[54,55]. Since IgA primarily activates granulocytes, these isotypes together activate the entire myeloid compartment of the immune system.

It will be important to study these and other combination therapies that can enhance IgA efficacy or synergize with IgA. Though IgA antibody therapy presents a potent new avenue, achieving curative outcomes with IgA alone will be unlikely, as has been observed for many other antibody therapeutics.

MOVING FORWARD TO CLINICAL APPLICATION OF IGA ANTIBODY THERAPY FOR NEUROBLASTOMA

In 2009 GD2 was ranked as the 12th most important cancer antigen by the National Cancer Institute based on therapeutic function, immunogenicity, role of the antigen in oncogenicity, specificity, expression level and percent of antigen-positive cells, stem

cell expression, number of patients with antigen-positive cancers, number of antigenic epitopes, and cellular location of antigen expression[56]. However, the currently approved IgG anti-GD2 antibodies induce neuropathic pain, which is dose-limiting in neuroblastoma patients and restricts the application of anti-GD2 antibody therapy across other cancer types. This thesis has addressed these issues and described a viable alternative with IgA anti-GD2 antibody therapy and has propelled it towards clinical application.

Some final steps are warranted before clinical application of IgA anti-GD2 antibody therapy. Ideally, the efficacy of IgA antibody therapy should be evaluated in more sophisticated, translational models, such as in transgenic mice with a full array of human Fc receptors, in MISTRG mice or in rats that naturally express CD89. Secondly, preclinical safety and dosing studies, including the assessment of neuropathic pain, should be performed in NHP. Additionally, other behavioural pain tests could be performed in mouse models, such as the Burrowing test[57]. Thirdly, it would be valuable to evaluate the cytotoxic efficacy of IgA anti-GD2 with more primary, patient-derived samples, since the number of samples we studied is still limited. Finally, the optimal production cell line for clinical batch production should be determined, since it is not completely clear whether CHO cells are the optimal production platform for IgA anti-GD2 antibodies. I believe that the application of IgA anti-GD2 antibody therapy in neuroblastoma is not far away and I hope it will contribute to improving neuroblastoma patient care in the imminent future.

REFERENCES

1. Stockmeyer, B. *et al.* Triggering Fc alpha-receptor I (CD89) recruits neutrophils as effector cells for CD20-directed antibody therapy. *J. Immunol.* **165**, 5954–5961 (2000).

2. Van Spriel, A. B., Leusen, J. H. W., Vilé, H. & Van De Winkel, J. G. J. Mac-1 (CD11b/CD18) as accessory molecule for Fc alpha R (CD89) binding of IgA. *J. Immunol.* **169**, 3831–3836 (2002).

3. Boross, P. *et al.* IgA EGFR antibodies mediate tumour killing in vivo. 1213–1226 (2013) doi:10.1002/emmm.201201929.

4. Blaese, R. M., Strober, W., Levy, A. L. & Waldmann, T. A. Hypercatabolism of IgG, IgA, IgM, and albumin in the Wiskott-Aldrich syndrome. A unique disorder of serum protein metabolism. *J. Clin. Invest.* **50**, 2331–2338 (1971).

5. Delacroix, D. L. *et al.* Changes in size, subclass, and metabolic properties of serum immunoglobulin A in liver diseases and in other diseases with high serum immunoglobulin A. *J. Clin. Invest.* **71**, 358–367 (1983).

6. Schiff, R. I. & Rudd, C. Alterations in the half-life and clearance of IgG during therapy with intravenous gamma-globulin in 16 patients with severe primary humoral immunodeficiency. *J. Clin. Immunol.* **6**, 256–264 (1986).

7. Mankarious, S. *et al.* The half-lives of IgG subclasses and specific antibodies in patients with primary immunodeficiency who are receiving intravenously administered immunoglobulin. *J. Lab. Clin. Med.* **112**, 634–640 (1988).

8. Zuckier, L. S., Georgescu, L., Chang, C. J., Scharff, M. D. & Morrison, S. L. The use of severe combined immunodeficiency mice to study the metabolism of human immunoglobulin G. *Cancer* **73**, 794–799 (1994).

9. Unverdorben, F. *et al.* Pharmacokinetic properties of IgG and various Fc fusion proteins in mice. *MAbs* **8**, 120–128 (2016).

10. Andersen, J. T., Daba, M. B., Berntzen, G., Michaelsen, T. E. & Sandlie, I. Cross-species binding analyses of mouse and human neonatal Fc receptor show dramatic differences in immunoglobulin G and albumin binding. *J. Biol. Chem.* **285**, 4826–4836 (2010).

11. Bruhns, P. Properties of mouse and human IgG receptors and their contribution to disease models. *Blood* **119**, 5640–5649 (2012).

12. Smith, P., DiLillo, D. J., Bournazos, S., Li, F. & Ravetch, J. V. Mouse model recapitulating human Fcγ receptor structural and functional diversity. *Proc. Natl. Acad. Sci. U. S. A.* **109**, 6181–6186 (2012).

13. Low, B. E., Christianson, G. J., Lowell, E., Qin, W. & Wiles, M. V. Functional humanization of immunoglobulin heavy constant gamma 1 Fc domain human FCGRT transgenic mice. *MAbs* **12**, 1829334 (2020).

14. Martinez-Sanz, P. *et al.* Humanized MISTRG as a preclinical in vivo model to study human neutrophil-mediated immune processes. *Front. Immunol.* **14**, 1105103 (2023).

15. Rongvaux, A. *et al.* Development and function of human innate immune cells in a humanized mouse model. *Nat. Biotechnol.* **32**, 364–372 (2014).

16. Maruoka, T., Nagata, T. & Kasahara, M. Identification of the rat IgA Fc receptor encoded in the leukocyte receptor complex. *Immunogenetics* **55**, 712–716 (2004).

17. Rogers, K. A., Scinicariello, F. & Attanasio, R. Identification and characterization of macaque CD89 (immunoglobulin A Fc receptor). *Immunology* **113**, 178–186 (2004).

18. Choi, K. *et al.* Reference values of hematology, biochemistry, and blood type in cynomolgus monkeys from cambodia origin. *Lab. Anim. Res.* **32**, 46–55 (2016).

19. Koo, B.-S. *et al.* Reference values of hematological and biochemical parameters in young-adult cynomolgus monkey (Macaca fascicularis) and rhesus monkey (Macaca mulatta) anesthetized with ketamine hydrochloride. *Lab. Anim. Res.* **35**, 7 (2019).

20. Long, A. H. *et al.* Reduction of MDSCs with All-trans Retinoic Acid Improves CAR Therapy Efficacy for Sarcomas. *Cancer.Immunol.Res.* **4**, 869–880 (2016).

21. Derer, S. *et al.* Impact of epidermal growth factor receptor (EGFR) cell surface expression levels on effector mechanisms of EGFR antibodies. *J. Immunol.* **189**, 5230–5239 (2012).

22. Wu, Z. L., Schwartz, E., Seeger, R. & Ladisch, S. Expression of GD2 ganglioside by untreated primary human neuroblastomas. *Cancer Res.* **46**, 440–443 (1986).

23. Nazha, B., Inal, C. & Owonikoko, T. K. Disialoganglioside GD2 Expression in Solid Tumors and Role as a Target for Cancer Therapy. *Front. Oncol.* **10**, 1000 (2020).

24. Olejniczak, S. H., Stewart, C. C., Donohue, K. & Czuczman, M. S. A quantitative exploration of surface antigen expression in common B-cell malignancies using flow cytometry. *Immunol. Invest.* **35**, 93–114 (2006).

25. Ho-Pun-Cheung, A. *et al.* Quantification of HER1, HER2 and HER3 by time-resolved Förster resonance energy transfer in FFPE triple-negative breast cancer samples. *Br. J. Cancer* **122**, 397–404 (2020).

26. Nassin, M. L. *et al.* Immune Reconstitution Following Autologous Stem Cell Transplantation in Patients with High-Risk Neuroblastoma at the Time of Immunotherapy. *Biol. blood marrow Transplant. J. Am. Soc. Blood Marrow Transplant.* **24**, 452–459 (2018).

27. Quadros, A. U. & Cunha, T. M. C5a and pain development: An old molecule, a new target. *Pharmacol. Res.* **112**, 58–67 (2016).

28. Sorkin, L. S. *et al.* Anti-GD(2) with an FC point mutation reduces complement fixation and decreases antibody-induced allodynia. *Cancer Res.* **149**, 362–367 (2010).

29. Mester, S. *et al.* Extended plasma half-life of albumin-binding domain fused human IgA upon pH-dependent albumin engagement of human FcRn in vitro and in vivo. *MAbs* **13**, 1893888 (2021).

30. Mattu, T. S. *et al.* The glycosylation and structure of human serum IgA1, Fab, and Fc regions and the role of N-glycosylation on Fcα receptor interactions. *J. Biol. Chem.* **273**, 2260–2272 (1998).

31. Gomes, M. M. *et al.* Analysis of IgA1 N-glycosylation and its contribution to FcalphaRI binding. *Biochemistry* **47**, 11285–11299 (2008).

32. Lombana, T. N. *et al.* Production, characterization, and in vivo half-life extension of polymeric IgA molecules in mice. *MAbs* **11**, 1122–1138 (2019).

33. Lohse, S. *et al.* An Anti-EGFR IgA That Displays Improved Pharmacokinetics and Myeloid Effector Cell Engagement In Vivo. *Cancer Res.* **76**, 403–417 (2016).

34. Göritzer, K., Maresch, D., Altmann, F., Obinger, C. & Strasser, R. Exploring Site-Specific N-Glycosylation of HEK293 and Plant-Produced Human IgA Isotypes. *J. Proteome Res.* **16**, 2560–2570 (2017).

35. Göritzer, K. *et al.* Distinct Fcα receptor N-glycans modulate the binding affinity to immunoglobulin A (IgA) antibodies. *J. Biol. Chem.* **294**, 13995–14008 (2019).

36. Croset, A. *et al.* Differences in the glycosylation of recombinant proteins expressed in HEK and CHO cells. *J. Biotechnol.* **161**, 336–348 (2012).

37. Goh, J. B. & Ng, S. K. Impact of host cell line choice on glycan profile. *Crit. Rev. Biotechnol.* **38**, 851–867 (2018).

38. Weiskopf, K. *et al.* Engineered SIRPα variants as immunotherapeutic adjuvants to anticancer antibodies. *Science* **341**, 88–91 (2013).

39. Chernyavska, M. *et al.* Evaluation of immunotherapies improving macrophage anti-tumor response using a microfluidic model. *Organs-on-a-Chip* **4**, 100019 (2022).

40. Heinkel, F. *et al.* Engineering a pure and stable heterodimeric IgA for the development of multispecific therapeutics. *MAbs* **14**, 2141637 (2022).

41. Strati, P. *et al.* Interim Results from the First Clinical Study of CC-95251, an Anti-Signal Regulatory Protein-Alpha (SIRPα) Antibody, in Combination with Rituximab in Patients with Relapsed and/or Refractory Non-Hodgkin Lymphoma (R/R NHL). *Blood* **138**, 2493 (2021).

42. Champiat, S. *et al.* Safety, pharmacokinetics, efficacy, and preliminary biomarker data of first-in-class BI 765063, a selective SIRPα inhibitor: Results of monotherapy dose escalation in phase 1 study in patients with advanced solid tumors. *J. Clin. Oncol.* **39**, 2623 (2021).

43. Logtenberg, M. E. W. *et al.* Glutaminyl cyclase is an enzymatic modifier of the CD47- SIRPα axis and a target for cancer immunotherapy. *Nat. Med.* **25**, 612–619 (2019).

44. Chan, C. *et al.* Targeting Myeloid Checkpoint Molecules in Combination With Antibody Therapy: A Novel Anti-Cancer Strategy With IgA Antibodies? *Front. Immunol.* **13**, 932155 (2022).

45. Takeshima, T. *et al.* Key role for neutrophils in radiation-induced antitumor immune responses: Potentiation with G-CSF. *Proc. Natl. Acad. Sci. U. S. A.* **113**, 11300–11305 (2016).

46. Liu, Q. *et al.* Radiotherapy programs neutrophils to an antitumor phenotype by inducing mesenchymal-epithelial transition. *Transl. lung cancer Res.* **10**, 1424–1443 (2021).

47. Shinde-Jadhav, S. *et al.* Role of neutrophil extracellular traps in radiation resistance of invasive bladder cancer. *Nat. Commun.* **12**, 2776 (2021).

48. Oweida, A. J. *et al.* Response to radiotherapy in pancreatic ductal adenocarcinoma is enhanced by inhibition of myeloid-derived suppressor cells using STAT3 anti-sense oligonucleotide. *Cancer Immunol. Immunother.* **70**, 989–1000 (2021).

49. Brandsma, A. M. *et al.* Simultaneous Targeting of FcγRs and FcαRI Enhances Tumor Cell Killing. *Cancer Immunol. Res.* **3**, 1316–1324 (2015).

50. Castriconi, R. *et al.* Identification of 4Ig-B7-H3 as a neuroblastoma-associated molecule that exerts a protective role from an NK cell-mediated lysis. *Proc. Natl. Acad. Sci. U. S. A.* **101**, 12640–12645 (2004).

51. Dondero, A. *et al.* Multiparametric flow cytometry highlights B7-H3 as a novel diagnostic/therapeutic target in GD2neg/low neuroblastoma variants. *J. Immunother. cancer* **9**, (2021).

52. Kelton, W. *et al.* IgGA: a 'cross-isotype' engineered human Fc antibody domain that displays both IgG-like and IgA-like effector functions. *Chem. Biol.* **21**, 1603–1609 (2014).

53. Borrok, M. J. *et al.* Enhancement of antibody-dependent cell-mediated cytotoxicity by endowing IgG with FcαRI (CD89) binding. *MAbs* **7**, 743–751 (2015).

54. Josephs, D. H. *et al.* Anti-Folate Receptor-α IgE but not IgG Recruits Macrophages to Attack Tumors via TNFα/MCP-1 Signaling. *Cancer Res.* **77**, 1127–1141 (2017).

55. Chauhan, J. *et al.* Anti-cancer pro-inflammatory effects of an IgE antibody targeting the melanoma-associated antigen chondroitin sulfate proteoglycan 4. *Nat. Commun.* **14**, 2192 (2023).

56. Cheever, M. A. *et al.* The prioritization of cancer antigens: a national cancer institute pilot project for the acceleration of translational research. *Clin. cancer Res. an Off. J. Am. Assoc. Cancer Res.* **15**, 5323–5337 (2009).

57. Deacon, R. M. J. Burrowing: a sensitive behavioural assay, tested in five species of laboratory rodents. *Behav. Brain Res.* **200**, 128–133 (2009).


8

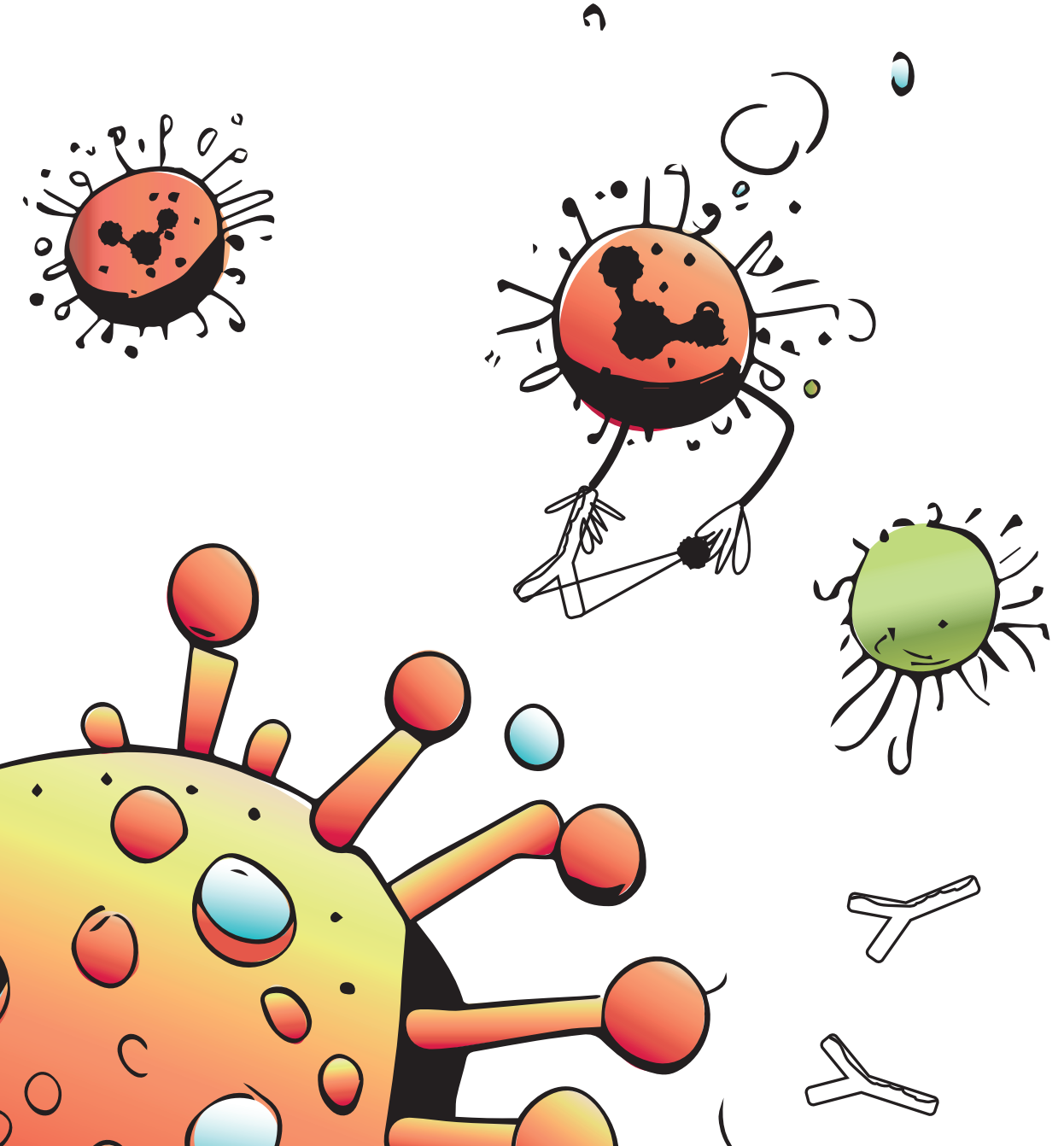

Chapter 9.

Nederlandse samenvatting

NEUROBLASTOOM EN ANTI-GD2 ANTISTOFTHERAPIE

Neuroblastoom is een van de meest voorkomende tumoren bij kinderen en verantwoordelijk voor ongeveer 15% van de sterfgevallen door kinderkanker. Deze tumor ontstaat tijdens de embryonale ontwikkeling en primaire tumoren bevinden zich meestal in de bijnier of in de sympathische neurale ganglia in de buik. Bij laag risicopatiënten kunnen tumoren spontaan in remissie gaan en anders is operationele verwijdering meestal afdoende. Echter, tot 50% van de neuroblastoompatiënten wordt geclassificeerd als hoog risicopatiënt, waarbij de 5-jaars overlevingskans slechts rond de 45% is.

Patiënten met hoog risiconeuroblastoom komen in aanmerking voor chemotherapie, operationele verwijdering van de primaire tumor, intensieve chemotherapie in combinatie met een dubbele autologe stamceltransplantatie en radiotherapie. Daarnaast krijgen hoog risicopatiënten op het moment anti-disialoganglioside (GD2) immunotherapie in combinatie met *13-cis*-retinoïnezuur. Anti-GD2-antistoffen doden tumorcellen door middel van antigeenafhankelijke cellulaire cytotoxiciteit (ADCC) van NK-cellen, macrofagen en neutrofielen. Hoewel de immunotherapie effectief is, veroorzaakt het ernstige, dosisbeperkende neuropathische pijn, die waarschijnlijk wordt veroorzaakt door complementactivatie op GD2-positieve sensorische neuronen. Op dit moment zijn er twee anti-GD2-antistoffen goedgekeurd voor klinische toepassing: dinutuximab (beta) en naxitamab. Dinutuximab (ch14.18) was de eerste anti-GD2-antistof die werd goedgekeurd voor klinische toepassing en deze antistofkloon vormt de basis voor de anti-GD2 IgA-immunotherapie die we in dit proefschrift ontwikkelen.

Antistoffen bestaan uit 5 isotypen (IgM, IgD, IgG, IgE en IgA), maar op het moment zijn alleen IgG-antistoffen goedgekeurd voor toepassing in de kliniek. IgG antistoffen zijn makkelijk toepasbaar vanwege de uitgebreide reeks effectormechanismen, de lange halfwaardetijd (door recycling via de neonatale Fc-receptor (FcRn)) en het eenvoudige glycosyleringsprofiel van IgG. Er zijn vier IgG-subklassen (IgG1, IgG2, IgG3 en IgG4), die allemaal zijn gebruikt in antistoftherapie. Echter, ze kunnen volledig verschillende werkingsmechanismen hebben, onder andere door hun variërende affiniteit voor de verschillende Fc gamma receptoren (FcγRs). Dinutuximab en naxitamab zijn van het IgG1-isotype, dat een hoge affiniteit voor activerende FcγRs heeft en daarom is de werkzaamheid voornamelijk gebaseerd op het induceren van ADCC.

Er zijn echter – naast het opwekken van neuropathische pijn – ook beperkingen aan anti-GD2 IgG-antistoftherapie. Ondanks de effectiviteit van immunotherapie zal nog steeds 50% van de patiënten recidiveren en aan de ziekte overlijden. IgG-antistoffen activeren vooral NK-cellen en macrofagen, maar andere myeloïde cellen, zoals neutrofielen en het adaptieve immuunsysteem worden niet (volledig) geactiveerd door IgG. De effectiviteit van anti-GD2 IgG-antistoffen wordt verder gehinderd doordat IgG niet alleen bindt aan activerende FcγRs, maar ook aan de remmende (FcγRIIb) en neutrale (FcγRIIIb) receptoren, wat de

activatie van immuuncellen belemmert. Om de immunotherapie voor neuroblastoom te verbeteren, hebben we in dit proefschrift anti-GD2 antistoffen van het IgA isotype ontwikkeld.

IgA-antistoffen activeren immuuncellen via de FcαRI, die exclusief tot expressie komt op myeloïde cellen. Neutrofielen en macrofagen zijn de belangrijkste effectorcellen voor IgA-antistoftherapie, hoewel de FcαRI ook tot expressie komt (of induceerbaar is) op eosinofielen, monocyten, subpopulaties van dendritische cellen en Kupffer-cellen. Na binding aan GD2 kan IgA clusteren met de FcαRI en specifieke effectormechanismen in myeloïde cellen activeren, zoals ADCC, fagocytose (ADCP), antigeenpresentatie en de vorming van neutrofiel-extracellulaire vangnetten (NET). IgA mist het C1q-bindende domein dat betrokken is bij de activatie van complement door IgG-antistoffen. Vanwege deze eigenschappen verwachtten we dat anti-GD2 IgA-antistoffen geen complement-gemedieerde pijn opwekken, neutrofielen direct activeren en alleen binden aan een activerende Fc-receptor: de Fc alfareceptor I (FcαRI of CD89).

DEEL I: HET ONTWIKKELEN VAN MUISMODELLEN OM IGA-ANTISTOFTHERAPIE TE BESTUDEREN

Voordat we de ontwikkeling van anti-GD2 IgA-antistoffen voor neuroblastoom beschrijven in het tweede deel van dit proefschrift, worden in het eerste deel twee belangrijke tools voor *in vivo* onderzoek beschreven. Deze tools worden vervolgens gebruikt in de studies naar IgA-antistoftherapie voor neuroblastoom in het tweede deel.

In het verleden werd het onderzoek naar IgA-antistoftherapie in muismodellen belemmerd, omdat muizen van nature geen equivalent van de humane FcαRI tot expressie brengen. Tijdens de evolutie is de FcαRI verloren gegaan in muizen als gevolg van concurrentie met bacteriële decoy-eiwitten voor IgA. Daarom zijn er verschillende transgene muizen met humaan CD89 gegenereerd, waaronder het model dat in dit proefschrift wordt gebruikt. **Hoofdstuk 2** beschrijft de ontwikkeling en kenmerken van een transgeen muismodel, dat humaan CD89 tot expressie brengt onder de endogene promotor.

Dit transgene muismodel voor CD89 is gegenereerd op FVB/N muizen en later ingekruist op vier verschillende achtergronden (C57BL/6, BALB/c, SCID en NXG). Met behulp van Targeted Locus Amplification hebben we vastgesteld dat het hCD89-transgen in chromosoom 4 is geïntegreerd. In alle muizenstammen is de CD89-expressie het hoogst in neutrofielen, gematigd op andere myeloïde cellen zoals eosinofielen en dendritische cel-subpopulaties, en induceerbaar op onder andere monocyten, macrofagen en Kupffer-cellen. Er zijn verschillen in CD89 expressie tussen de muizenstammen: CD89-niveaus zijn het hoogst in BALB/c en SCID, lager in C57BL/6 en het laagst in NXG-muizen. Onverwachts vonden we dat CD89 is verhoogd op myeloïde cellen van muizen met tumoren, zowel in het bloed als in de

tumor. Dit is een extra reden om onderzoek te doen naar IgA-antistoftherapie voor kanker, omdat verwacht kan worden dat hogere CD89-expressie gunstig is voor de effectiviteit.
Vervolgens vergelijken we zowel de samenstelling en het fenotype van immuuncellen als de expressie van myeloïde activatiemarkers en FcγRs tussen wildtype en CD89-transgene muizen. Hier werd geen verschil gevonden en wildtype en transgene dieren kunnen daarom in de toekomst ook in hetzelfde experiment worden gebruikt. Wildtype muizen kunnen bijvoorbeeld ingezet worden in controlegroepen of in groepen behandeld met IgG antistoffen. Op deze manier zijn er in totaal minder proefdieren nodig.
Tot slot bestuderen we IgA/CD89-gemedieerde ADCC van alle CD89-transgene muizenstammen. IgA-gemedieerde ADCC van tumorcellen is het krachtigst met geïsoleerde neutrofielen van BALB/c en C57BL/6 en minder met neutrofielen van SCID en NXG-muizen. Echter, wanneer effectorcellen uit een vast volume van volledig bloed worden gebruikt, zijn SCID- en BALB/c-stammen het meest efficiënt, omdat deze een veel hoger aantal neutrofielen hebben. Hoewel er dus verschillen bestaan tussen de stammen, bieden CD89-transgene muizen een krachtig model om de werkzaamheid van IgA-immunotherapie tegen infectieziekten en kanker te testen.
In **hoofdstuk 3** wordt een nieuwe methode ontwikkeld voor langdurige depletie van neutrofielen in muizen. Op het moment worden hiervoor meestal anti-Ly-6G (kloon 1A8) of anti-Gr-1 (kloon RB6-8C5) antistoffen gebruikt. In de loop der jaren is duidelijk geworden dat depletie door middel van deze antistoffen slechts gedeeltelijk of alleen tijdelijk effectief is. Terwijl Ly-6G specifiek tot expressie komt op neutrofielen, komt Ly-6C (de andere receptor die wordt herkend door de Gr-1-antistof), ook voor op subpopulaties van monocyten, macrofagen, dendritische cellen en lymfocyten. Hierdoor depleteert de anti-Gr-1 antistof niet alleen neutrofielen, maar ook deze andere myeloïde cellen. De anti-Ly-6G antistof is wel specifiek, maar zowel de anti-Ly-6G als de anti-Gr-1 antistoffen zijn van het rat IgG2a-isotype, waardoor de neutrofieldepletie minder efficiënt is. Deze rattenantistoffen worden namelijk al na één week behandeling door muis-anti-rat-antistoffen geklaard, wat resulteert in een verminderde werkzaamheid op langere termijn. Om deze problemen op te lossen, beschrijven we in **hoofdstuk 3** het gebruik van een antistof tegen Ly-6G (1A8) met hetzelfde variabele gebied als de oorspronkelijke rat IgG2a anti-Ly-6G 1A8-antistof, maar van het muis IgG2a-isotype. Het muis IgG2a-isotype bindt aan zowel alle muizen FcγRs als C1q, en induceert daarom zowel ADCC en ADCP als complement-afhankelijke cytotoxiciteit (CDC). We tonen aan dat deze muis anti-Ly-6G antistof efficiënte, langdurige en nagenoeg volledige (>90%) depletie van neutrofielen geeft in het perifere bloed van C57BL6, BALB/c, NXG en SCID muizen gedurende ten minste vier weken. Bovendien laten we zien dat neutrofielen efficiënt worden gedepleteerd in het bloed en in het tumorweefsel van SCID muizen met een IMR32 neuroblastoom, tot minstens zes weken na het begin van de depletie.

DEEL II: IGA-ANTISTOFTHERAPIE VOOR NEUROBLASTOOM

In het tweede deel van dit proefschrift wordt IgA-immunotherapie bij neuroblastoom toegepast. **Hoofdstuk 4** beschrijft eerst uitgebreid het tumormilieu van hoog risiconeuroblastoom, met speciale aandacht voor de rol van myeloïde cellen, wat de belangrijkste effectorcellen zijn voor IgA-immunotherapie.

Hoofstuk 4 vat eerst de pro- en anti-tumorigene functies van myeloïde cellen, waaronder granulocyten, monocyten, macrofagen en myeloïde suppressorcellen (MDSC's), samen tijdens de ontwikkeling en voortgang van neuroblastoom. Net als bij andere solide tumoren lijken neutrofielen bij hoog risiconeuroblastoom geassocieerd te zijn met een slechtere prognose. Daarnaast is duidelijk aangetoond dat MDSC's in hoog risiconeuroblastoom immunosuppressief zijn. In muismodellen lijken M-MDSC's meer immunosuppressief zijn dan PMN-MDSC's, maar het is onzeker of dit ook het geval is bij neuroblastoompatiënten, omdat daar nog weinig onderzoek naar is gedaan. Wat betreft de rol van macrofagen lopen onderzoeksresultaten uiteen. Sommige studies zien vooral inductie van M2-macrofagen, maar anderen observeerden voornamelijk M1-macrofagen, waarbij beide typen mogelijk verband houden met slechte overlevingskansen. Deze tegenstrijdigheden komen waarschijnlijk voort uit de verschillende genetische profielen binnen neuroblastoom; tumoren met deletie van chromosoom 11q of amplificatie van *MYCN* bevatten vooral macrofagen met het M2-fenotype, terwijl tumoren zonder *MYCN*-amplificatie een meer M1-macrofagen bevatten.

In het tweede deel van **hoofdstuk 4** bespreken we hoe myeloïde cellen betrokken zijn bij het huidige behandelschema van neuroblastoom en onderzoeken we nieuwe therapeutische strategieën om deze cellen aan te pakken. Deze strategieën omvatten: (1) het activeren van myeloïde cellen als effectorcellen van immunotherapie, (2) het depleteren van myeloïde cellen of het blokkeren van de migratie van myeloïde cellen naar de tumor en (3) het herprogrammeren van immunosuppressieve myeloïde cellen. Ondanks hun immunosuppressieve eigenschappen kunnen myeloïde cellen nog steeds worden gestimuleerd om de tumor aan te vallen, zoals wordt geïllustreerd door neutrofielen die belangrijke effectorcellen blijken te zijn in anti-GD2-antistoftherapie. Hun volledige potentieel is echter nog niet bereikt en activatie van myeloïde cellen kan worden verbeterd, bijvoorbeeld door myeloïde checkpoints te blokkeren. Hoewel de depletie van myeloïde cellen of het blokkeren van de infiltratie van myeloïde cellen effectief kan zijn, depleteert deze strategie dus ook mogelijke effectorcellen voor immunotherapie uit de tumoromgeving. Het herprogrammeren van immunosuppressieve myeloïde cellen lijkt daarom de optimale strategie, omdat hierbij immunosuppressieve eigenschappen worden teruggedraaid en myeloïde cellen beschikbaar blijven als effectorcellen. Daarnaast worden door het opheffen van immunosuppressie door myeloïde cellen tumor-infiltrerende T-cellen gereactiveerd. Geneesmiddelen die zich op myeloïde cellen richten en T-cel

therapieën, zoals checkpointremmers en chimere antigeenreceptor (CAR) T-cellen lijken daarom een gouden combinatie om neuroblastoom te behandelen.

In **Hoofdstuk 5** ontwikkelen we het eerste concept van IgA-immunotherapie voor neuroblastoom, waarbij we het isotype van de anti-GD2-antistof dinutuximab (ch14.18) omzetten van IgG1 naar IgA1. Allereerst hebben we IgA1 ch14.18 gezuiverd en bevestigd dat IgA1 ch14.18 met dezelfde affiniteit aan GD2 bindt als IgG1 ch14.18. IgA1 is superieur ten opzichte van IgG1 ch14.18 in het opwekken van neutrofiel-gemedieerde ADCC en dit kan worden verder worden verbeterd door toevoeging van GM-CSF en *13-cis*-retinoïnezuur. We stellen vast dat zowel *in vitro* als *in vivo* IgA1 ch14.18 geen complementdepositie induceert. Von Frey pijntesten in muismodellen laten zien dat injectie van IgG1 ch14.18 binnen 3 uur pijn opwekt, terwijl muizen geïnjecteerd met IgA1 ch14.18 geen pijn vertonen. In overeenstemming hiermee werd complementdepositie gevonden op de nervus ischiadicus na toediening van IgG1 in muizen, maar niet na een vergelijkbare dosis IgA1. **Hoofdstuk 5** laat zien dat het gebruik van het IgA-isotype voor anti-GD2 immunotherapie twee belangrijke voordelen heeft: het geeft geen neuropathische pijn en activeert neutrofielen om neuroblastoomcellen te elimineren.

Niettemin wordt de klinische toepassing van IgA-antistoftherapie belemmerd door enkele eigenschappen van het IgA-isotype. Allereerst hebben IgA-antistoffen een korte halfwaardetijd, onder andere omdat IgA-antistoffen snel weggevangen worden door hun omvangrijke glycosylering, die herkend wordt door de asialoglycoproteïne- en mannosereceptoren. Daarnaast zorgt de glycosylering voor heterogeniteit tussen productiebatches. Ten derde is het zuiveren van monomeer IgA ingewikkeld vanwege de vorming van aggregaten en de noodzaak om grootte-uitsluitingschromatografie als extra stap toe te voegen. Om IgA-antistoffen geschikt te maken voor klinische toepassing, hebben we in **hoofdstuk 6** het IgA3.0-molecuul ontwikkeld, waarbij door mutaties 3 van de 4 glycosyleringsplaatsen zijn verwijderd en de stabiliteit is verbeterd. Daarnaast is de IgA3.0-antistof afgeleid van het IgA2-isotype, omdat IgA1-antistoffen een rol spelen bij de ontwikkeling van IgA-nefropathie (Berger's ziekte).

Hoofdstuk 6 beschrijft de preklinische ontwikkeling van IgA3.0 ch14.18 voor toepassing bij neuroblastoom. Allereerst karakteriseren we de nieuwe IgA3.0 ch14.18-antistof en vergelijken we deze met het oorspronkelijke IgG1-isotype en de natuurlijk voorkomende IgA1- en IgA2-isotypen. GD2-binding van alle antistofvarianten is vergelijkbaar. Echter, de monomere binding van de Fc staart van IgA3.0 aan de FcαRI is licht verbeterd ten opzichte van IgA1 en IgA2. Opnieuw zijn in ADCC- en ADCP-experimenten met name neutrofielen en macrofagen efficiënt in het doden neuroblastoomcellen via IgA3.0 ch14.18. Niet alleen neutrofielen van gezonde donoren zijn hiertoe in staat na IgA3.0 stimulatie, maar ook neutrofielen van neuroblastoompatiënten.

Daarnaast heeft IgA3.0 ch14.18 een gunstiger glycosyleringspatroon in vergelijking met IgA1 en IgA2. De algehele mate van glycosylering is verminderd door de verwijdering van 3

van de 4 glycosyleringsplaatsen, maar daarnaast heeft ook de overgebleven glycosylering een gunstiger patroon, namelijk meer terminale sialylgroepen en minder vrije mannose- en galactosestructuren. Dit glycosyleringspatroon komt overeen met een verlengde halfwaardetijd van IgA3.0 ten opzichte van IgA1 en IgA2 in muismodellen.
Tot slot laten biodistributieproeven in muizen zien dat IgA3.0 ch14.18 de tumor bereikt en tumorcellen – zelfs in het centrum – opsoniseert. IgA3.0 ch14.18 therapie remt de tumorgroei in twee verschillende, lange-termijn neuroblastoommodellen in muizen, in zowel immuuncompetente muizen als in xenograft modellen. Ook neutrofielen van cynomolgus apen laten ADCC zien na stimulatie met IgA3.0 ch14.18, dus dit lijkt een goed model voor de allerlaatste preklinische testen in de toekomst. Met de studie in **hoofdstuk 6** lijken de belangrijkste hordes voor klinische toepassing van IgA3.0 ch14.18 genomen.
Ten slotte wordt in **hoofdstuk 7** voor het eerst een combinatietherapie met IgA3.0 ch14.18 bestudeerd om de therapie nog effectiever te maken. De activatiestatus van myeloïde cellen, zoals neutrofielen en macrofagen, is een balans tussen stimulerende en remmende signalen en in tumoren hebben de remmende signalen vaak de overhand. Veel tumoren, inclusief neuroblastoom, brengen CD47 tot overexpressie, ook wel het 'eet-me-niet-op' signaal genoemd. CD47 bindt aan de SIRPα receptor op myeloïde cellen, waardoor activatie tegen de tumor geremd wordt. In **hoofdstuk 7** onderzoeken we het effect van het blokkeren van CD47 op de werkzaamheid van IgA3.0 ch14.18, omdat we verwachten dat CD47 blokkade de IgA antistoftherapie zal versterken.
De eerste experimenten in **hoofdstuk 7** tonen aan dat neutrofiel-gemedieerde ADCC door IgA3.0 ch14.18 wordt versterkt door CD47-blokkade, in zowel neuroblastoomcellijnen als organoïden. Niet alleen de effectiviteit van IgA3.0, maar ook die van IgG1 ch14.18 wordt verbeterd door de CD47-blokkade, hoewel de combinatie met IgA3.0 ch14.18 resulteert in de grootste verbetering van ADCC. In muizen met een subcutaan neuroblastoom, blokkeren we CD47 met een SIRPα-fusie-eiwit en vergelijken we IgA3.0 ch14.18 met IgG1 ch14.18. *In vivo* remt CD47-blokkade in combinatie met IgA3.0 ch14.18 therapie de tumorgroei effectief en verlengt de tumor-specifieke overleving, meer dan IgA3.0 therapie alleen en ook meer dan in combinatie met IgG1 ch14.18. Bovendien induceert (alleen) de IgA3.0-combinatiestrategie een massale influx van neutrofielen in de tumor. De resultaten uit **hoofdstuk 7** benadrukken het belang van het ontwikkelen van combinatietherapieën met IgA3.0 ch14.18 om myeloïde cellen optimaal te activeren.

CONCLUSIE

In dit proefschrift wordt de ontwikkeling van anti-GD2 IgA-immunotherapie voor neuroblastoom beschreven vanaf de ontwikkeling van het eerste concept tot aan de preklinische toepassing. Met behulp van *in vitro* experimenten en muismodellen

hebben we gezien dat anti-GD2 IgA-antistoffen effectief zijn tegen neuroblastoom en verschillende voordelen hebben ten opzichte van de originele IgG1 antistof dinutuximab. Er zijn nog enkele laatste stappen nodig voordat de klinische toepassing van anti-GD2 IgA-antistoftherapie mogelijk is, zoals beschreven in **hoofdstuk 8**. Ik geloof dat de toepassing van anti-GD2 IgA-antistoftherapie voor neuroblastoom niet ver weg is en ik hoop dat dit proefschrift zal bijdragen aan een verbetering van de zorg voor neuroblastoompatiënten in de nabije toekomst.

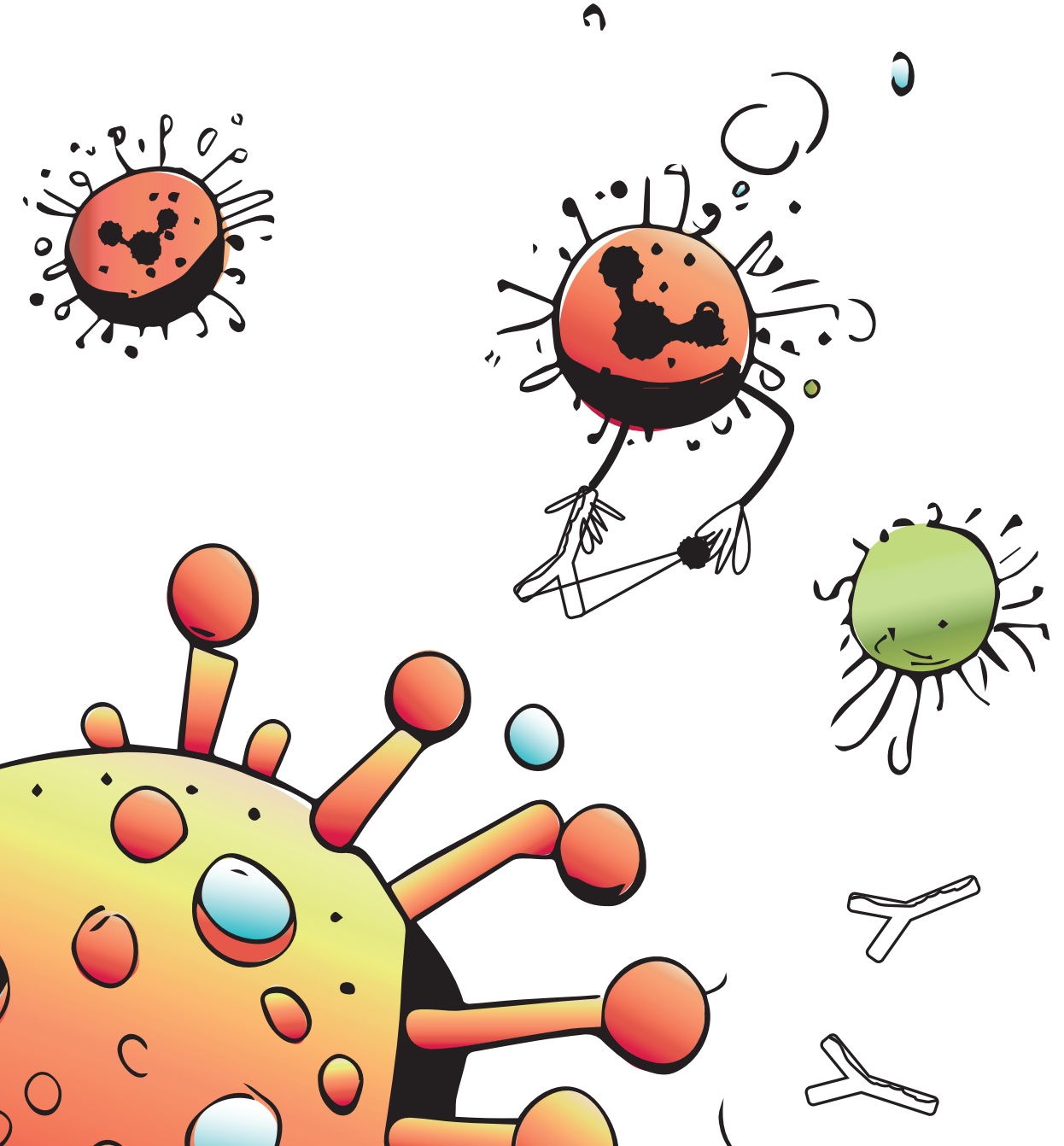

Appendices

Abbreviations

Ab Antibody
ADC Antibody-drug conjugate
ADCC Antibody-dependent cellular cytotoxicity
ADCP Antibody-dependent cellular phagocytosis
ADNR Adrenergic noradrenergic cells
ANOVA Analysis of variance
Arg-1 Arginase 1
ASCT Autologous stem cell transplantation
ASGPR Asialoglycoprotein receptor
ATCC American Type Culture Collection
ATP Adenosine triphosphate
ATRA All-*trans*-retinoic acid
AUC Area under the curve
BLI Bioluminescence imaging
BM Bone marrow
BMP-9 Bone morphogenic protein-9
BNC2 Basonuclin 2
BSA Bovine serum albumin
BTK Bruton's tyrosine kinase
CAFs Cancer-associated fibroblasts
CAR Chimeric antigen receptor
Cas9 CRISPR-associated protein 9
CCL C-C motif chemokine ligand
CDC Complement-dependent cytotoxicity
CHO Chinese hamster ovarian
COJEC Cisplatin [C], vincristine [O], carboplatin [J], etoposide [E] and cyclophosphamide [C]
COX Cyclooxygenase
CpG CpG-containing oligodeoxynucleotides
CR3 Complement receptor 3
CRISPR Clustered regularly interspaced short palindromic repeats
CSF-1R Colony stimulating factor 1 receptor
CTV Cell-trace violet
CXCR C-X-C motif chemokine receptor
DAPI 4',6-diamidino-2-phenylindole
DC Dendritic cell

DiO Dioctadecyloxacarbocyanine
DMSO Dimethylsulfoxide
DOX Doxorubicin
DTT Dithiothreitol
E-MDSC Early myeloid-derived suppressor cell
E:T Effector:target
EFS Event-free survival
EGFR Epidermal growth factor receptor
ELISA Enzyme-linked immunosorbent assay
EMA European medicines agency
Fab Antigen binding fragment
Fc Crystallizable fragment
FcαRI Fc alpha receptor I
FcγR Fc gamma receptor
FACS Fluorescence-activated cell sorting
FcRn Neonatal Fc receptor
FCS Fetal calf serum
FDA Food & Drug Administration
FITC Fluorescein isothiocyanate
FSC Forward scatter
G-CSF Granulocyte-colony stimulating factor
GD2 Disialoganglioside
GEMM Genetically engineered mouse model
GM-CSF Granulocyte/macrophage-colony stimulating factor
gMFI Geometric mean fluorescence intensity
GPI Glycosylphosphatidylinositol
HAMA Human anti-mouse antibody
HC Heavy chain
HDAC Histone deacetylase
HIF-2α Hypoxia inducible factor 2α
HLA Human leukocyte antigen
HRP Horseradish peroxidase
HSCT Hematopoietic stem cell transplantation
ICAM-1 Intercellular adhesion molecule-1
IFNγ Interferon gamma
Ig Immunoglobulin
IGF-2 Insulin-like growth factor 2
IL Interleukin
IMGT ImMunoGeneTics

INRG International Neuroblastoma Risk Group
i.p. Intraperitoneally
iTLC Instant thin-layer chromatography
i.v. Intravenously
IVIG Human intravenous immunoglobulin
κLC Kappa light chain
L-NAME *N*-nitro-L-arginine
LFA-1 Lymphocyte function-associated antigen 1
LMR Leukocyte-to-monocyte ratio
LysM Lysozyme M
mϕ Macrophage
M-CSF Macrophage-colony stimulating factor
M-MDSC Monocytic myeloid-derived suppressor cells
Mac-1 Membrane-activated complex 1
MDK Midkine
MES Mesenchymal-like cell
METTL Methyltransferase-like 3
MDSC Myeloid-derived suppressor cells
MIF Macrophage migration inhibitory factor
mPGES-1 Prostaglandin E synthase-1
MR Mannose receptor
MSC Mesenchymal stromal cells
NA-NB MYCN non-amplified neuroblastoma
NAP Neutrophil-activating protein
NEAA Non-essential amino acids
NECA 5'-*N*-Ethylcarboxamidoadenosine
NET Neutrophil extracellular traps
NHP Non-human primates
NHS *N*-hydroxy-succimidyl
NK Natural killer
NKT Natural killer T
NLR Neutrophil-to-lymphocyte ratio
NO Nitric oxide
ns Non-significant
NSG NOD SCID gamma
nTg Non-transgenic
NXG NOD Xenograft Gamma
OS Overall survival
PAD Peptide arginine deiminase

PBMC Peripheral blood mononuclear cells
PBS Phosphate-buffered saline
PCR Polymerase chain reaction
PD-1 Programmed cell death-protein 1
PD-L1 Programmed cell death-ligand 1
PDX Patient-derived xenograft
PE Phycoerythrin
Pen/Strep Penicillin/streptomycin
PFA Paraformaldehyde
pIgR Polymeric immunoglobulin receptor
PK Pharmacokinetic
PMN Polymorphonuclear cells
PMN-MDSC Polymorphonuclear myeloid-derived suppressor cells
QIFIKIT Quantitative Immunofluorescence Kit
ROS Reactive oxygen species
S1P Lipid sphingosine-1
s.c. Subcutaneous
SD Standard deviation
SEC Size-exclusion chromatography
SEM Standard error of mean
sgRNA Single guide RNA
SIRPα Signal regulatory protein alpha
SPECT Single-photon emission computed tomography
SSC Side scatter
STR Short-tandem repeat
TAM Tumor-associated macrophage
Tg Transgenic
TGF-β Transforming growth factor beta
TIL Tumor-infiltrating lymphocyte
TLA Targeted Locus Amplification
TLR Toll-like receptor
TME Tumor microenvironment
TNFα Tumor necrosis factor alpha
Unst Unstained
VEGF Vascular endothelial growth factor
W(B)L Whole (blood) leukocytes
Wt Wildtype

List of publications

1. Chan C, **Stip MC**, Nederend M, Jansen JHM, Passchier EM, van den Ham F, Wienke J, van Tetering G & Leusen JHW. Enhancing IgA-mediated neutrophil cytotoxicity against neuroblastoma by CD47 blockade. *Submitted to J. Immunother. Cancer*, 2024.
2. **Stip MC**, Teeuwen L, Dierselhuis MP, Leusen JHW & Krijgsman D. Targeting the myeloid microenvironment in neuroblastoma. *J Exp Clin Cancer Res*. **42**, 337 (2023).
3. **Stip MC**, Jansen JHM, Nederend M, Tsioumpekou M, Evers M, Olofsen PA, Meyer-Wentrup F & Leusen, JHW. Characterization of human Fc alpha receptor transgenic mice: comparison of CD89 expression and antibody-dependent tumor killing between mouse strains. *Cancer Immunol Immunother.* **72**, 3063-3077 (2023).
4. **Stip MC**, Evers M, Nederend M, Chan C, Reiding KR, Damen MJ, Heck AJR, Koustoulidou S, Ramakers R, Krijger GC, de Roos R, Souteyrand E, Cornel AM, Dierselhuis MP, Jansen M, de Boer M, Valerius T, van Tetering G, Leusen JHW & Meyer-Wentrup F. IgA antibody immunotherapy targeting GD2 is effective in preclinical neuroblastoma models. *J. Immunother. Cancer.* **11**, e006948 (2023).
5. Olofsen PA, **Stip MC**, Jansen JHM, Chan C, Nederend M, Tieland RG, Tsioumpekou M & Leusen JHW. Effective, Long-Term Neutrophil Depletion Using a Murinized Anti-Ly-6G 1A8 Antibody. *Cells*. **11**, 3406 (2022).
6. Evers M, **Stip MC**, Keller K, Willemen H, Nederend M, Jansen M, Chan C, Budding K, Nierkens S, Valerius T, Meyer-Wentrup F, Eijkelkamp N, & Leusen JHW. Anti-GD2 IgA kills tumors by neutrophils without antibody-associated pain in the preclinical treatment of high-risk neuroblastoma. *J Immunother Cancer.* **9**, e003163 (2021).
7. van Tetering G, Evers M, Chan C, **Stip MC**, Leusen JHW. Fc engineering strategies to advance IgA antibodies as therapeutic agents. *Antibodies (Basel).* **15**, 70 (2020).

Curriculum Vitae

Marjolein Stip was born on the 28th of July in 1994 in Sliedrecht, The Netherlands. She attended gymnasium at the Wartburg College in Rotterdam in 2012, after which she moved to Leiden to study Biomedical Sciences at the Leiden University Medical Center. During her bachelor, her interest in immunology and oncology was raised during courses and an internship at the Karolinska Institutet in Stockholm. In her master, she studied the role of mesenchymal stromal cells (MSC) and MSC-derived exosomes in the hematopoietic stem cell niche under the supervision of dr. Melissa van Pel at the Leiden University Medical Center. During a second internship, she worked on a transgenic mouse model for neutrophil depletion in the context of breast cancer under the supervision of dr. Camilla Salvagno and prof. dr. Karin de Visser at the Netherlands Cancer Institute in Amsterdam. Especially this final internship motivated her to find a PhD position in the field of tumor immunology, which she found in the lab of prof. dr. Jeanette Leusen (promotor) at the Center for Translational Immunology in the Utrecht University Medical Center. She was further supervised by dr. Friederike Meyer-Wentrup (copromotor), pediatric oncologist in the Princess Máxima Center in Utrecht. During her PhD project, Marjolein worked on IgA antibody immunotherapy as a treatment for high-risk neuroblastoma, which is described in this thesis. Currently, she is working as a postdoctoral fellow in the lab of Jørgen de Jonge at the RIVM on broadly reactive immunity in infectious diseases. Marjolein is currently living in Bilthoven with her husband Matthijs Zoutendijk and daughter Mirte.